Atomic Structure of Ferroelectric Domain Walls, Free Surfaces and Steps

Thesis by

Arash Yavari

In Partial Fulfillment of the Requirements

for the Degree of

Doctor of Philosophy

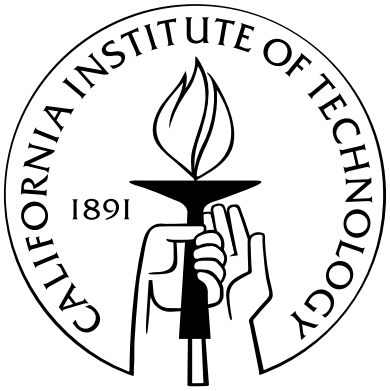

California Institute of Technology

Pasadena, California

2004

(Defended November 24, 2004)

To my father and the memory of my mother

Acknowledgements

I have been privileged to work with my advisors, Michael Ortiz and Kaushik Bhattacharya, in the last four years at Caltech and have learned a great deal through our interactions. I am grateful for their support, guidance and insight. They have influenced me by their knowledge, commitment, vision, discipline and love for mechanics. I should thank Michael for showing me the possibility of working in different fields and investigating different possibilities for solving new problems of mechanics. Kaushik has made me realize the value of experiments and the necessity of appreciating experimental work as a theoretician. I believe the influence of Michael and Kaushik on my scientific life is beyond this thesis and I hope I can have a similar effect on my future students.

I have been lucky to collaborate with Jerry Marsden in the last couple of years. I started interacting with him in the two courses I took with him. His special and unique understanding of mechanics has encouraged me to see mechanics from a new perspective. I have learned a lot from him through the interactions we have had, especially in the last one and a half years in the course of our joint work on configurational forces. His systematic way of thinking and his writing style have influenced my approach of attacking problems and my writing significantly.

I met G. Ravichandran the first few days I arrived at Caltech and since then he has been a mentor and friend for me. I had many instructive discussions with him in his fracture mechanics class and later on on some other problems. I have always found his advice invaluable and am very grateful to him. He is always an example for me to follow in teaching and advising students.

I would like to thank Jim Knowles for the many discussions we have had in the past four years, especially in the discussions we have had on configurational forces. His unique way of looking at solid mechanics problems and his vision has always been impressive and helpful. I thank him for his encouragement and support.

I would also like to thank Marino Arroyo, Anil Hirani, Melvin Leok, Igor Belegradek, Piere Suquet, Johannes Zimmer, Eugene Heifets, Rongjing Zhang, Yu Xiao, Qingsong Zhang, Tahir Cagin, Sofia Akber, Julian Gale and Ron Cohen for the interesting and helpful discussions I have had with them.

I have made several friends in the last four years at Caltech and they have all influenced me positively and have had a significant impact on the quality of my life. Special thanks go to Arash

Kheradvar, Maziar Motahari, Amir Sadjadpour, Aydin Babakhani, Olga Schneider, Jeffery Scruggs and Bill Klug.

Abstract

The goal of this thesis is to develop a general framework for lattice statics analysis of defects in ferroelectric Perovskites. The techniques presented here are general and can be easily applied to other systems as well. We present all the calculations and numerical examples for two technologically important ferroelectric materials, namely, PbTiO3 and BaTiO3. We use shell potentials, that are derived using quantum mechanics calculations, and analyze three types of defects: (i) 180° and 90° domain walls, (ii) free surfaces and (iii) steps in 180° domain walls. Our formulation assumes that an interatomic potential is given. In other words, there is no need to have the force constants or restrict the number of nearest neighbor interactions a priori. Depending on the defect and symmetry, the discrete governing equations are reduced to those for representatives of some equivalence classes. The idea of symmetry reduction in lattice statics calculations is one of the contributions of this thesis. We call our formulation of lattice statics 'inhomogeneous lattice statics' as we consider the fact that close to defects force constants (stiffness matrices) change. For defects with one-dimensional symmetry reduction we solve the discrete governing equations directly using a novel method in the setting of the theory of difference equations. This will be compared with the solutions obtained using discrete Fourier transform. For defects with two-dimensional symmetry reduction we solve the discrete governing equations using discrete Fourier transform. We calculate the fully nonlinear solutions using modified Newton-Raphson iterations and call the method 'inhomogeneous anharmonic lattice statics'. This work is aimed to fill the gap between quantum mechanics ab initio calculations and continuum models (based on Landau-Ginzberg-Devonshire theory) of ferroelectric domain walls.

Contents

List of Figures

List of Tables

Chapter 1

Introduction

In this chapter we review the previous attempts in understanding the structure of ferroelectric domain walls. Following that the method of lattice statics will be reviewed. We reformulate lattice statics in a form analogous to continuum mechanics. Restrictions put on the form of interatomic potentials by material frame indifference and a discrete version of Green-Naghdi-Rivilin theorem are contributions of this chapter.

1.1 Ferroelectrics

Piezoelectrics are those materials that can be polarized by applying mechanical stress. Piezoelectricity is a linear phenomenon, i.e., the relation between Cauchy stress tensor σ and the electric displacement $\mathbf{D}$ is linear.

$$\mathbf{D} = \mathbf{d}\sigma \qquad \text{or} \qquad D_i = d_{ijk}\sigma_{jk} \tag{1.1}$$

where $\mathbf{d}$ is the tensor of piezoelectric coefficients. Pyroelectric (polar) materials are those materials that are polarized even in the absence of an external electric field or external mechanical stress. Ferroelectrics are polar crystals whose spontaneous polarization vector can be switched by an applied electric field or an external mechanical stress (see Fig. 1.1). These materials have many potential applications in micro-actuators and micro-sensors. The phenomenon of ferroelectricity was discovered in 1921 (Valasek, 1921) and since then has been the subject of many theoretical and experimental investigations. Ferroelectricity is a result of the fairly complicated competition of short-range repulsive forces that favor the paraelectric state (high symmetry cubic phase) and long-range Coulombic forces that favor the ferroelectric state (low symmetry phase) (Cohen and Krakauer, 1992). Recent applications of ferroelectrics, especially MEMS applications, have attracted much attention in understanding the fundamentals of ferroelectrics. For recent reviews see Damjanovic (1998) and Kamlah (2001). It is known that many properties of ferroelectrics are controlled by the motion of domain walls, which are two-dimensional defects in ferroelectrics. This is not surprising as most of

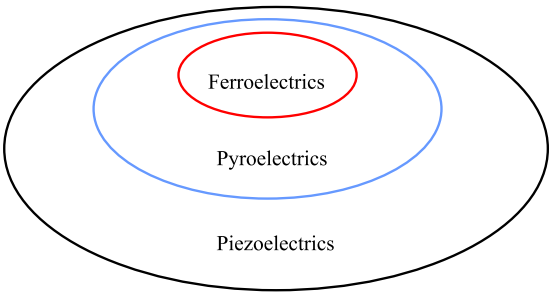

Figure 1.1: Piezoelectrics, pyroelectrics and ferroelectrics.

the interesting properties of solids, in general, are controlled by defects and their evolution. Macroscopically, a domain wall can be understood as a surface of discontinuity in polarization (polarization per unit volume) and deformation gradient. In the framework of continuum mechanics, motion of such a surface of discontinuity is caused by the driving (configurational) force on the domain wall and the normal velocity of the wall is related to the driving force through a (phenomenological) kinetic equation. Ideally, such a phenomenological kinetic equation should be based on an atomistic model of the domain wall. Therefore, understanding the atomic structure of ferroelectric domain walls and their energetics can play an important role in understanding the motion of domain walls and developing physically sound continuum models for them.

Ferroelectric crystals undergo a phase transition at the Curie temperature from a high temperature high symmetry to a low temperature lower symmetry configuration. In the case of $BaTiO_3$ and $PbTiO_3$ the phase transition is from cubic (high symmetry) at high temperature to tetragonal (low symmetry) at the room temperature. In this latter phase, there are six energetically equivalent polarization directions. There is no reason to expect a uniform polarization in a ferroelectric solid. Instead, polarization is not uniform but only uniform locally, i.e., it is uniform in subdomains of the body. Each of these regions is called a *domain*. The boundaries between domains are called *domain walls* (see Fig. 1.2). It has been experimentally observed that a ferroelectric solid usually has a complicated microstructure which consists of regions of different shapes with different orientations of (uniform) spontaneous polarization. Domains are formed to reduce the total free energy of the ferroelectric solid. Formation of domain walls is a result of competition between several energies, namely electric field energy, elastic energy and domain wall energy. Having domains with different uniform polarization reduces the energy of the electric field in the expense of domain wall energy. The equilibrium configuration can be obtained by minimizing the total energy.

Characteristics of domain boundaries (domain walls) have important effects on the performance of ferroelectric devices, like their fatigue, etc. The thickness of domain walls and the interfacial energy of ferroelectric domain walls are important in studying fatigue and switching kinetics of ferroelectric

solids. Domain wall characteristics such as profile of polarization across the domain wall, energetics and mobility can be determined after having the atomic structure of the ferroelectric domain wall.

It is known that one mechanism of polarization switching in $BaTiO_3$ and $PbTiO_3$ are motion of 180° domain walls (antiparallel domains). This means that a thorough theoretical understanding of ferroelectricity of $BaTiO_3$ and $PbTiO_3$ requires a detailed analysis of domain wall structure, energy of the domain walls and their dynamics. Ferroelectric domain walls have been studied in different scales by different researchers. $BaTiO_3$ and $PbTiO_3$ are two well-known and well-studied ferroelectric materials. $BaTiO_3$ has a Curie temperature of 120°C and undergoes a cubic to tetragonal phase transformation below its Curie temperature. $BaTiO_3$ belongs to the class of Perovskite-type structures ABO_3. Fig. 1.3 shows the displacements of atoms of a unit cell of $BaTiO_3$ from the cubic reference configuration. Actually, $BaTiO_3$ undergoes a series of phase transitions: cubic to tetragonal at 120°C, tetragonal to orthorhombic at 5°C and finally orthorhombic to rhombohedral at -90°C. For the bulk crystal, spontaneous polarization is measured as dipole moment per unit volume. The value of spontaneous polarization is $26 \times 10^{-6} C/cm^2$ for $BaTiO_3$ at room temperature. $PbTiO_3$ is cubic above its Curie temperature $T_c = 490°C$ and tetragonal below the Curie temperature. The value of spontaneous polarization is $75 \times 10^{-6} C/cm^2$. For early works on domain walls in $BaTiO_3$ the reader should see (Merz, 1952),(Merz, 1954), (Little, 1955), (Kinase, 1955). The early experimental studies of domain walls in $BaTiO_3$ were done by Merz (1952, 1954) and Little (1955). There are two types of domain walls in the tetragonal ABO_3: 90° and 180° domain walls. Examples are shown in Fig. 1.2. Note that the 90° domain walls shown in this figure are head-to-tail. This means that the domain wall is free of surface charges. In this thesis, we study only head-to-tail 90° domain walls as they have a lower energy compared to other types of 90° domain walls. For more details on different properties of $BaTiO_3$ the reader may refer to Jona and Shirane (1993) and Kanzig (1957).

The structure of ferroelectric domain walls in the continuum scale has been investigated using Landau-Ginzburg-Devonshire theory (LGD) (see Cao and Cross (1991), Zhirnov (1959), Huang et al. (1997) and references therein). In LGD theory, the free energy is a function of the order parameter (usually macroscopic polarization in the case of ferroelectrics), gradient of the order parameter, lattice strain and dipole-dipole interactions. The free energy usually has a polynomial form. The coefficients of the polynomial have to be given to the continuum theory. Most of these coefficients can be determined from the knowledge of bulk properties like elastic, dielectric and electrostrictive bulk properties. However, the coefficients of the gradient terms are related to the domain wall energy and thickness and have to be determined from the knowledge of structure and energetics of domain walls. It turns out that in the LGD theory, the polarization and the strain across a domain wall can be described by soliton-type solutions, e.g. Cao and Cross (1991). Zhirnov (1959) estimated the thickness of 180° and 90° domain walls for $BaTiO_3$ to be $5 - 20$ $\mathring{A}$ and $50 - 100$ $\mathring{A}$, respectively.

Huang et al. (1997), utilizing LGD theory, showed that in tetragonal $BaTiO_3$ there are two types of 180° domain walls: Ising-type and Bloch-type domain walls. They observed that the width of the Bloch walls are much larger than those of Ising walls. They showed that at low temperatures, the Bloch walls are stable while at high temperatures, the Ising walls are stable. They also observed that the Bloch domain walls are more mobile than the Ising domain walls. LGD theory has also been used in modelling the evolution of 180° and 90° domain walls (see Hu and Chen (1997), Hu and Chen (1998) and Yang and Chen (1995)). Hu and Chen (1998), using the LGD theory, numerically studied the evolution of 180° and 90° ferroelectric domain walls. Hu and Chen (1998) in their numerical examples observed that the depolarization energy is responsible for formation of 180° domain walls as a configuration with vanishing average polarization is energetically favorable and dipole-dipole interactions favor head to tail domain walls.

Phase field models, though useful for keeping track of the evolution of domain walls, are questionable in capturing the structure of ferroelectric domain walls if ferroelectric domain walls are atomically sharp. This implies that one should have more physics in their model and the atomic interactions should somehow be taken into account. The other problem with phase field models is that their macroscopic parameters are not easy to find using the available experimental data.

Lawless (1968) performed an atomistic analysis of 180° domain walls in $BaTiO_3$ using a point-dipole model by making a series of simplifying assumptions. It was assumed that the elastic energy (due to changes in lattice parameters) is negligible. Only Ti-O_a (O_a in Slater's notation*) bonds are considered as they have the dominant energy. Finally it is assumed that across the domain wall only the magnitude of the polarization vector varies and polarization vectors do not rotate.†. He considered the 180° domain walls perpendicular to the experimentally observed $\langle 100 \rangle$ and $\langle 110 \rangle$ directions. He analyzed four possible domain walls two of which are Ba-centered and the other two are Ti-centered. Finally, he showed that the Ba-centered wall (100) has the minimum energy.

First-principles (ab initio) calculations are on the other extreme side of the spectrum of modelling ferroelectric domain walls. To date there have been several ab initio analyses of ferroelectric domain walls (see Meyer and Vanderbilt (2001), Padilla et al. (1996), Pöykkö and Chadi (1999), Pöykkö and Chadi (2000) and references therein). For a recent review of different first-principle simulations of ferroelectrics see Resta (2003). Recently, Meyer and Vanderbilt (2001) performed an interesting first-principle calculation of 180° and 90° domain walls in the tetragonal $PbTiO_3$. They showed that these domain walls have comparable widths and that energy barrier for movement of 90° domain walls is extremely small. They discussed different possibilities for 180° and 90° domain walls. There are two types of 180° domain walls: Pb-centered and Ti-centered, which result from twinning on PbO- and TiO_2-planes, respectively. They showed that a Pb-centered domain wall has a lower

*O_a is O_3 in our notation.

†Our model does not have such restrictive assumptions and everything will come out of the energy minimization.

energy than a Ti-centered domain wall and hence it is the preferred wall structure.[‡] For 90° domain walls there are two possibilities: Pb-Ti-O- or O-O-centered domain walls. Here by an O-O-centered domain wall we mean that the reference (starting) configuration is obtained by twinning on an O-O type (101) plane. Meyer and Vanderbilt observed that the relaxed configuration lies between these two limits. They obtained the profiles of polarization change across the domain wall and calculated the domain wall energies. They also observed that the energy of a 90° domain wall is one-forth of that of a 180° domain wall. In their computations, Meyer and Vanderbilt had to consider a completely periodic system in order to be able to perform their quantum mechanical calculations. This is a serious drawback of these types of computations. The same superficial periodicity is assumed in all the existing molecular dynamics simulations of ferroelectrics. It is well known that in any mechanical system, constraints, in general, introduce forces of constraint and these forces might introduce artifacts that do not reflect the true physical properties of the system. What one should analyze is a single domain wall in an infinite solid body.

Among the recent experimental studies of ferroelectric domain walls in $PbTiO_3$ and $BaTiO_3$ we can mention Shilo et al. (2004), Burcsu et al. (2000), Burcsu et al. (2004), Stemmer et al. (1995), Floquet et al. (1997), Li et al. (1992), and Krishnan et al. (2000). Burcsu et al. (2000) using a suitable coupled electromechanical loading showed that $BaTiO_3$ can generate strains as high as 0.8% (see Fig. 1.4 in which domain wall patterns in $BaTiO_3$ measured using polarized light microscopy are shown). This shows the potential of $BaTiO_3$ and similar ferroelectrics in applications that need large actuation strains. Fig. 1.5 shows 90° domain patterns in the ferroelectric $PbTiO_3$ obtained by using polarized light microscopy (this is view from the top) in Professor Ravichandran's laboratory at Caltech. The area imaged is about $2.5\ mm \times 1.2\ mm$. Stemmer et al. (1995) measured the width of 90° domain walls in tetragonal $PbTiO_3$ to be 1.0 ± 0.3 nm and the energy per unit area of the wall to be 50 mJm^{-2}. Floquet et al. (1997) measured the width of 90° domain walls in tetragonal $BaTiO_3$ to be $4-6$ nm. Foeth et al. (1999) measured the thickness of 90° domain walls in $PbTiO_3$ to be $1.5 \pm 0.3\ nm$ and $2.1 \pm 0.7\ nm$ using HREM and WBTEM, respectively. For other experimental results on domain walls in $BaTiO_3$ see Arlt and Sasko (1980) and Hu et al. (1986). Krishnan et al. (2000) discussed the possibility of having domain walls with free charges. One reason for this is the existence of curved domain walls, for example, around the intersection point (line) of three or more 90° domain walls. They also mentioned that 'the precise wall structure in virtually all ferroelectric materials in still unknown'. This thesis aims to at least partially clarify this problem. It seems that there is not an agreement on the thickness of ferroelectric domain walls in the literature. The reason is believed to be the presence of other defects and in particular point defects (Shilo et al., 2004). Recently, Shilo et al. (2004) used an interesting technique to experimentally study the structure of 90° domain walls in $PbTiO_3$. Their idea is to use atomic force microscopy data and fit the thickness

[‡]Our lattice statics calculations are in agreement with this.

parameter of the soliton-type solution of LGD theory. Using this technique they observed that the domain wall thickness is about 1.5 nm but with a wide scatter. They associated this scatter to point defects.

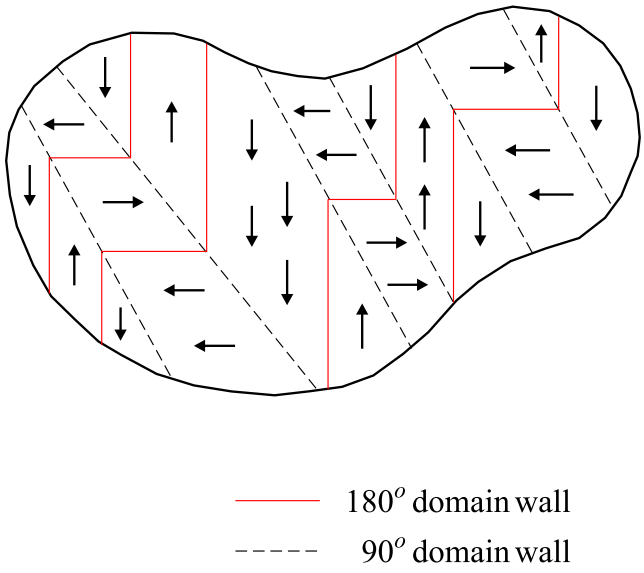

Figure 1.2: 180° and 90° domain walls.

1.2 Theory and Applications of Harmonic Lattice Statics

In this section we review the theory of harmonic lattice statics and some of its applications. The method of lattice statics was introduced by Matsubara (1952) and Kanazaki (1957). This method was used for point defects by Flocken and Hardy (1969) and Flocken (1972) for cracks by Hsieh and Thomson (1973) and Esterling (1978) and for dislocations by Maradudin (1958), Boyer and Hardy (1971), Esterling (1978), Esterling and Moriarty (1978), Shenoy et al. (1999) and Tewary (2000). For more details and history the reader may refer to Born and Huang (1988), Flocken and Hardy (1970) Boyer and Hardy (1971), Tewary (1973), Bullough and Tewary (1979), Flocken and Hardy (1969), Maradudin et al. (1971), Ortiz and Phillips (1999), Shenoy et al. (1999) and references therein. We present this in a language as close to continuum mechanics as possible.

Consider a collection of atoms $\mathcal{L}$ interacting with one another through some interatomic potential. The simplest possible interaction is when the effective potential is pairwise and quadratic, i.e., the force between atoms depends on their pairwise distances and has a linear relation with the corresponding displacements. This means that the collection of atoms can be modelled as a collection of point masses connected to each other with some linear springs. This would be a discrete analogue

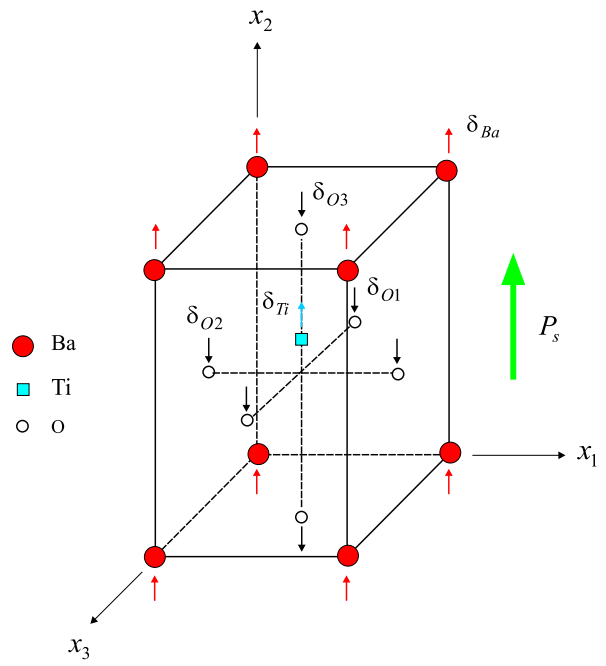

Figure 1.3: Tetragonal $BaTiO_3$ and its distortion from the cubic phase. $PbTiO_3$ has a similar tetragonal structure

of a linear elastic solid.[§] The advantage of having such a model is that it would be possible to solve the resulting system of linear difference equations analytically. One might object to the harmonic approximation for problems that are highly nonlinear. Although this is a reasonable objection, harmonic approximation is a fine approximation as long as the reference configuration is close to a local minimum of the energy. This is of course problem dependent and one has to be careful with such a simplifying assumption. This approximation has proved useful for studying many problems in solid state physics, e.g., studying dislocation core structure (Ortiz and Phillips (1999), Shenoy et al. (1999)). As an example the force-free reference configuration[¶] could be a Bravais lattice $\mathcal{L}$, i.e.,

$$\mathcal{L} = \left\{ \mathbf{X} \in \mathbb{R}^3 \mid \mathbf{X} = l^1\mathbf{e}_1 + l^2\mathbf{e}_2 + l^3\mathbf{e}_3,\ l^1, l^2, l^3 \in \mathbb{Z} \right\} \tag{1.2}$$

where $\mathbf{e}_i$ are lattice vectors.[‖] Deformation of a crystal is a discrete mapping $\varphi : \mathcal{L} \to \mathbb{R}^3$ (see Fig. 1.6). Here, we have assumed that the ambient space is $\mathbb{R}^3$ and this seems to be general enough for the applications we have in mind. In terms of the atom position vectors in the deformed and undeformed configurations, $\mathbf{x} = \varphi(\mathbf{X})$. We assume that the total energy of the lattice has the following forms,

[§]Note that linear elasticity is richer than pairwise interactions.

[¶]The problem we will study for ferroelectric crystals will require us to start from a reference configuration that is not force-free (not relaxed).

[‖]Note that, from an abstract algebra point of view, a lattice is a module over the ring $(\mathbb{Z}, +, .)$.

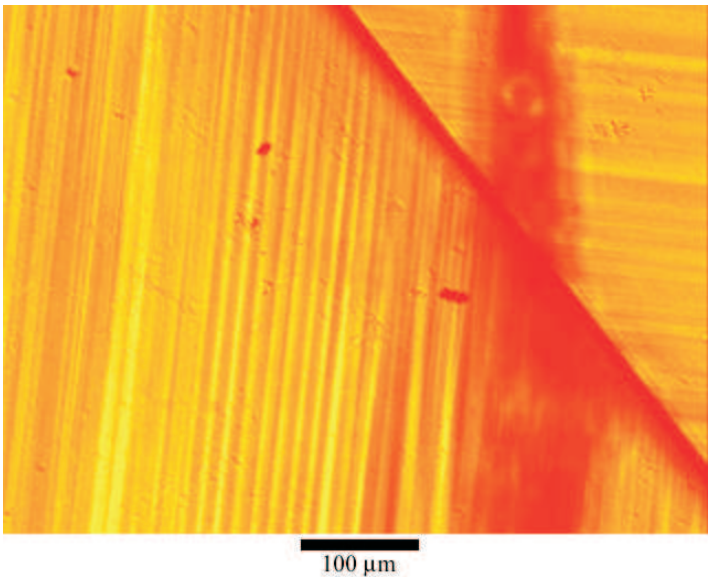

Figure 1.4: Domain walls in Tetragonal $BaTiO_3$.

$$\mathcal{E}^{\text{tot}} = \mathcal{E}^{\text{tot}}[\varphi] = \mathcal{E}^{\text{tot}}\left(\{\mathbf{x}^{\mathbf{i}}\}_{\mathbf{i}\in\mathcal{L}}\right) \tag{1.3}$$

where $\mathbf{x}^{\mathbf{i}}$ is the position of atom $\mathbf{i}$ after relaxation. In other words, energy is a functional on the space of discrete deformation mappings. Note that this is not the most general form of energy. For example, for a ferroelectric crystal the total energy depends on the atomic charges as well. But the form expressed in Eq. (1.3) would be general enough for the purposes of illustration of the main ideas.** Note that $\mathbf{i} \in \mathcal{L}$ is a material point (atom). Here $\mathcal{L}$ is the discrete material manifold and $\{\mathbf{X}^{\mathbf{i}}\}_{\mathbf{i}\in\mathcal{L}}$ is an embedding of the discrete material body and is called the reference configuration. Similar to continuum mechanics, material points (atoms) can be identified with their position vectors in the reference configuration. Suppose there is a discrete vector filed of body forces,

$$\mathbf{F} : \mathcal{L} \to \mathbb{R}^3. \tag{1.4}$$

Discrete body forces could be due to external fields like an external electric field or may represent a distribution of defects. Euler-Lagrange equations governing the equilibrium of the crystal are

**Another example is a system of unit cells with their position vectors and polarization vectors as independent variables. In this case, $\mathcal{E}^{\text{tot}} = \mathcal{E}^{\text{tot}}\left(\{\mathbf{x}^{\mathbf{i}}, \mathbf{p}^{\mathbf{i}}\}_{\mathbf{i}\in\mathcal{L}}\right)$.

Figure 1.5: 90° domain patterns in $PbTiO_3$ obtained by using polarized light microscopy. The area imaged is about 2.5 mm $\times$ 1.2 mm.

(ignoring the dynamic effects),[††]

$$-\frac{\partial \mathcal{E}^{\text{tot}}}{\partial \mathbf{x}^{\mathbf{i}}} + \mathbf{F}^{\mathbf{i}} = \mathbf{0} \qquad \forall\, \mathbf{i} \in \mathcal{L}. \tag{1.5}$$

Any given crystal has a symmetry group $\mathcal{S}$ which is a group of rotations that map the lattice back into itself. The total energy of the crystal should be invariant under the symmetry group. Here we assume that $\mathcal{E}^{\text{tot}}$ has such a property, i.e.,

$$\mathcal{E}^{\text{tot}}\left(\{\varphi(\mathbf{R}\mathbf{X}^{\mathbf{i}})\}_{\mathbf{i}\in\mathcal{L}}\right) = \mathcal{E}^{\text{tot}}\left(\{\varphi(\mathbf{X}^{\mathbf{i}})\}_{\mathbf{i}\in\mathcal{L}}\right) \qquad \forall\, \mathbf{R} \in \mathcal{S}. \tag{1.6}$$

A crystal is the discrete analogue of a homogenous solid. For an arbitrary collection of atoms $\mathcal{L}$, energies of two atoms $\mathbf{i} \neq \mathbf{j}$ are different, in general. This is similar to Eshelby's idea of assuming explicit dependence of strain energy density on $\mathbf{X}$ to describe material inhomogeneities (defects) in his theory of force on a defect (Eshelby, 1951), (Eshelby, 1975).

The other requirement is material-frame-indifference, which means that the energy of the crystal should be invariant under isometries of $\mathbb{R}^3$, i.e., rigid rotations and rigid translations. In other words,

$$\mathcal{E}^{\text{tot}}\left(\{\mathbf{x}^{\mathbf{i}}\}_{\mathbf{i}\in\mathcal{L}}\right) = \mathcal{E}^{\text{tot}}\left(\{\mathbf{Q}\mathbf{x}^{\mathbf{i}} + \mathbf{c}\}_{\mathbf{i}\in\mathcal{L}}\right) \qquad \forall\, \mathbf{Q} \in SO(3), \mathbf{c} \in \mathbb{R}^3. \tag{1.7}$$

[††]This is the balance of linear momentum in the absence of inertial forces. It will be shown in the sequel that if balance of linear momentum is satisfied for a system governed by pairwise interactions then balance of angular momentum would be satisfied trivially. This is similar to analysis of a truss in structural mechanics where one does not need to worry about equilibrium of moments.

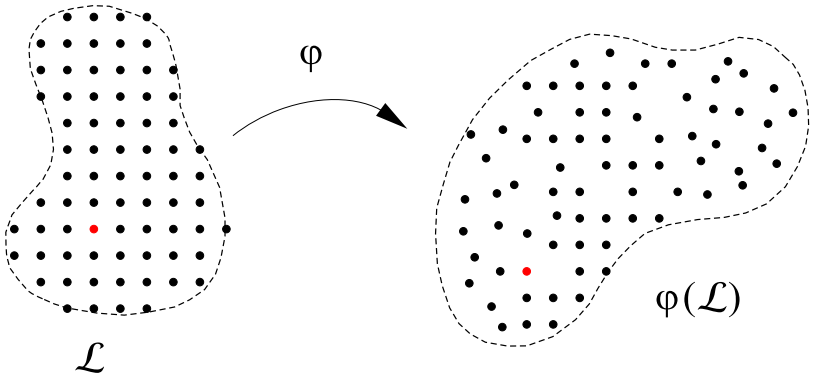

Figure 1.6: Deformation of a collection of atoms viewed as a discrete mapping between two configurations.

Similar to the arguments used in continuum mechanics, it is easy to show that this implies that

$$\mathcal{E}^{\text{tot}}\left(\{\mathbf{x}^{\mathbf{i}}\}_{\mathbf{i}\in\mathcal{L}}\right) = \hat{\mathcal{E}}\left(\{\left(\mathbf{x}^{\mathbf{i}}-\mathbf{x}^{\mathbf{j}}\right)\cdot\left(\mathbf{x}^{\mathbf{k}}-\mathbf{x}^{\mathbf{l}}\right)\}_{\mathbf{i},\mathbf{j},\mathbf{k},\mathbf{l}\in\mathcal{L}}\right) \tag{1.8}$$

where $\{\left(\mathbf{x}^{\mathbf{i}}-\mathbf{x}^{\mathbf{j}}\right)\cdot\left(\mathbf{x}^{\mathbf{k}}-\mathbf{x}^{\mathbf{l}}\right)\}_{\mathbf{i},\mathbf{j},\mathbf{k},\mathbf{l}\in\mathcal{L}}$ is the discrete analogue of the right Cauchy-Green strain tensor. Note also that a pairwise potential satisfies the requirement of material-frame-indifference.

What we are interested in is the discrete deformation mapping that maps the reference configuration to the equilibrium configuration. This is the discrete analogue of the deformation mapping in continuum mechanics. Let,

$$\mathbf{x}^{\mathbf{i}} = \mathbf{X}^{\mathbf{i}} + \mathbf{u}^{\mathbf{i}} \qquad \mathbf{i}\in\mathcal{L} \tag{1.9}$$

where $\mathbf{u}^{\mathbf{i}}$ is the displacement of atom $\mathbf{i}$ from its position in the reference configuration, i.e., $\mathbf{u}$ is the discrete vector field of displacements. Now let us expand $\frac{\partial\mathcal{E}^{\text{tot}}}{\partial\mathbf{x}^{\mathbf{i}}}$ in a Taylor series about the reference configuration.

$$\frac{\partial\mathcal{E}^{\text{tot}}}{\partial\mathbf{x}^{\mathbf{i}}} = \frac{\partial\mathcal{E}^{\text{tot}}}{\partial\mathbf{x}^{\mathbf{i}}}(\mathbf{X}) + \sum_{\mathbf{j}\in\mathcal{L}}\frac{\partial^2\mathcal{E}^{\text{tot}}}{\partial\mathbf{x}^{\mathbf{i}}\partial\mathbf{x}^{\mathbf{j}}}(\mathbf{X})\ \left(\mathbf{x}^{\mathbf{j}}-\mathbf{X}^{\mathbf{j}}\right) + ... \tag{1.10}$$

Substituting (1.10) into (1.5) and taking only the first two terms yields

$$-\frac{\partial\mathcal{E}^{\text{tot}}}{\partial\mathbf{x}^{\mathbf{i}}}(\mathbf{X}) - \sum_{\mathbf{j}\in\mathcal{L}}\frac{\partial^2\mathcal{E}^{\text{tot}}}{\partial\mathbf{x}^{\mathbf{i}}\partial\mathbf{x}^{\mathbf{j}}}(\mathbf{X})\ \mathbf{u}^{\mathbf{j}} + \mathbf{F}^{\mathbf{i}} = \mathbf{0}. \tag{1.11}$$

Note that for a force-free reference configuration,

$$\frac{\partial\mathcal{E}^{\text{tot}}}{\partial\mathbf{x}^{\mathbf{i}}}(\mathbf{X}) = \mathbf{0}. \tag{1.12}$$

However, if the reference configuration is not force-free this term would be a part of the forcing term. We call this term the discrete field of *unbalanced forces*. In this thesis we consider three types of defects in ferroelectrics: (i) domain walls, (ii) free surfaces, and (iii) steps. The nominal configurations of these defects are schematically shown in terms of macroscopic polarization in Figs.1.7, 1.8 and 1.9. Our interatomic potentials are explicit functions of some position vectors (core and shell position vectors) and thus one needs to interpret these reference configurations carefully. This will be discussed in subsequent chapters. To see the connection of our formulation with the

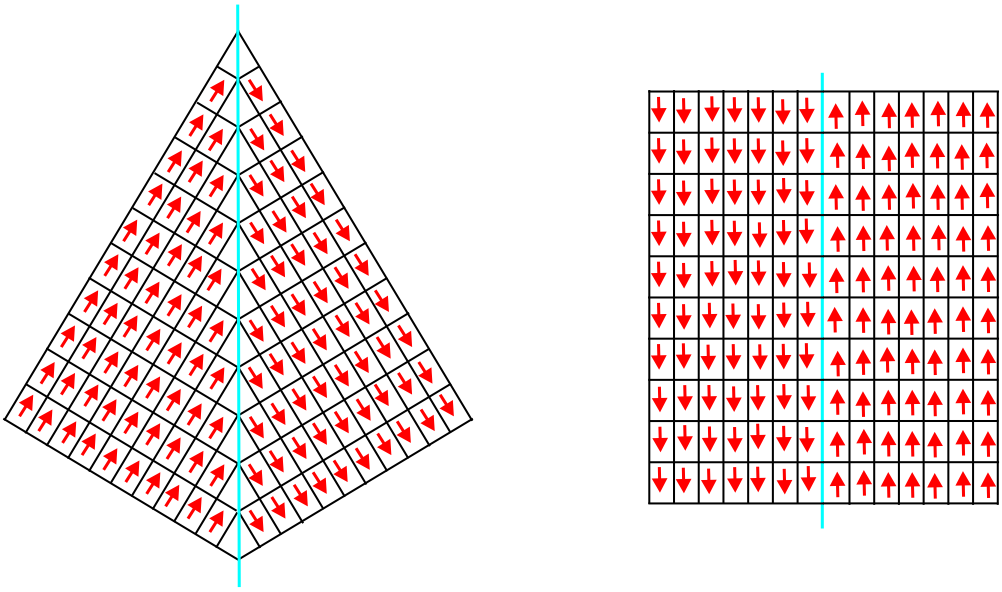

(a) (b)

Figure 1.7: Nominal 90° and 180° domain walls in the tetragonal phase.

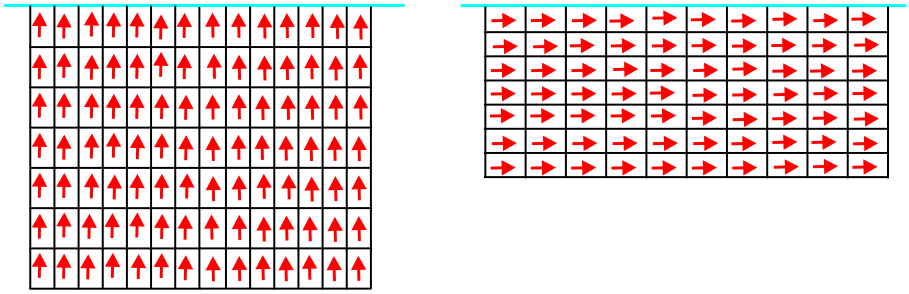

Figure 1.8: Nominal free surfaces in the tetragonal phase.

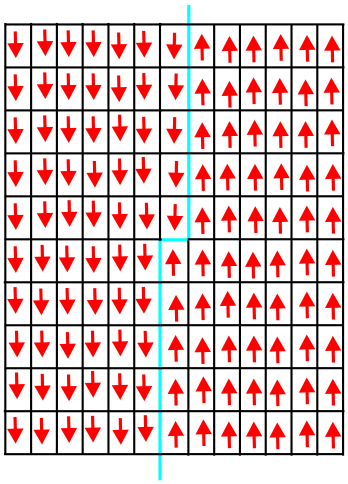

Figure 1.9: Nominal 180° step in the tetragonal phase.

classical treatments, the linearized equilibrium equations are now written as

$$\sum_{\mathbf{j}\in\mathcal{L}} \mathbf{\Phi}(\mathbf{i},\mathbf{j};\mathbf{X})\ \mathbf{u}^{\mathbf{j}} = \mathbf{f}^{\mathbf{i}} \qquad \forall\ \mathbf{i}\in\mathcal{L} \tag{1.13}$$

where

$$\mathbf{f}^{\mathbf{i}} = \mathbf{F}^{\mathbf{i}} - \frac{\partial \mathcal{E}^{\text{tot}}}{\partial \mathbf{x}^{\mathbf{i}}}(\mathbf{X}), \quad \mathbf{\Phi}(\mathbf{i},\mathbf{j};\mathbf{X}) = \frac{\partial^2 \mathcal{E}^{\text{tot}}}{\partial \mathbf{x}^{\mathbf{i}}\partial \mathbf{x}^{\mathbf{j}}}(\mathbf{X}). \tag{1.14}$$

Here $\mathbf{\Phi}(\mathbf{i},\mathbf{j};\mathbf{X}) \in \mathbb{R}^{3\times 3}$ are called the stiffness constants. These constants have the following properties for a bulk crystal (Ortiz and Phillips, 1999),

$$\mathbf{\Phi}(\mathbf{i},\mathbf{j};\mathbf{X})_{rs} = \mathbf{\Phi}(\mathbf{j},\mathbf{i};\mathbf{X})_{sr}, \tag{1.15}$$

$$\mathbf{\Phi}(\mathbf{i}+\mathbf{k},\mathbf{j}+\mathbf{k};\mathbf{X}) = \mathbf{\Phi}(\mathbf{i},\mathbf{j};\mathbf{X}) \qquad \forall\ \mathbf{k}\in\mathcal{L}, \tag{1.16}$$

$$\mathbf{\Phi}(\mathbf{I},\mathbf{J};\mathbf{X}) = \mathbf{Q}\mathbf{\Phi}(\mathbf{i},\mathbf{j};\mathbf{X})\mathbf{Q}^T, \quad \mathbf{x}^{\mathbf{I}} = \mathbf{Q}\mathbf{x}^{\mathbf{i}}, \quad \mathbf{x}^{\mathbf{J}} = \mathbf{Q}\mathbf{x}^{\mathbf{j}}, \ \mathbf{Q}\in\mathcal{S}, \tag{1.17}$$

$$\sum_{\mathbf{j}\in\mathcal{L}} \mathbf{\Phi}(\mathbf{i},\mathbf{j};\mathbf{X}) = \mathbf{0}, \tag{1.18}$$

$$\sum_{\mathbf{j}\in\mathcal{L}} \left(\mathbf{\Phi}(\mathbf{i},\mathbf{j};\mathbf{X})_{rs}\mathbf{x}^{\mathbf{j}}{}_p - \mathbf{\Phi}(\mathbf{i},\mathbf{j};\mathbf{X})_{rp}\mathbf{x}^{\mathbf{j}}{}_s \right) = \mathbf{0}. \tag{1.19}$$

where (1.15) is a direct consequence of the definition of $\mathbf{\Phi}(\mathbf{i},\mathbf{j};\mathbf{X})$, (1.16) is a consequence of translation invariance of the crystal, (1.17) is the restriction imposed on stiffness constants by the symmetry group, and (1.18) and (1.19) follow from the invariance of the energy under rigid body translations and rotations of the lattice. The property (1.18) implies that

$$\mathbf{\Phi}(\mathbf{i},\mathbf{j};\mathbf{X}) = \tilde{\mathbf{\Phi}}(\mathbf{i}-\mathbf{j};\mathbf{X}). \tag{1.20}$$

The total energy in the harmonic approximation can now be written as

$$\mathcal{E}^{\text{tot}}_{\text{harm}} = \frac{1}{2}\sum_{\mathbf{i},\mathbf{j}\in\mathcal{L}} \tilde{\mathbf{\Phi}}(\mathbf{i}-\mathbf{j};\mathbf{X})\mathbf{u}^{\mathbf{i}}\cdot\mathbf{u}^{\mathbf{j}} = -\frac{1}{4}\sum_{\mathbf{i},\mathbf{j}\in\mathcal{L}} \tilde{\mathbf{\Phi}}(\mathbf{i}-\mathbf{j};\mathbf{X})(\mathbf{u}^{\mathbf{i}}-\mathbf{u}^{\mathbf{j}})\cdot(\mathbf{u}^{\mathbf{i}}-\mathbf{u}^{\mathbf{j}}). \tag{1.21}$$

In some applications, the problem is solved by starting from the most general possible form of force constants for a given crystal and a given number of nearest neighbor interactions that come from the abovementioned properties (see Ortiz and Phillips (1999) and Shenoy et al. (1999) and references therein). In this work, we choose a more general approach and start from a potential and find the governing equations directly. This means that we will not need to worry about the symmetries of the stiffness constants, i.e., starting from a potential that respects the crystal symmetries and material-frame-indifference, stiffness constants will all have the abovementioned properties. We will verify this statement in the sequel.

It is seen that the harmonic energy (1.21) is convex and not able to model defective crystals. One way to go around this is to introduce eigendistortions (Mura, 1977), (King and Mura, 1991a) and (Gallego and Ortiz, 1993; Ortiz and Phillips, 1999). The idea is very similar to that of defining eigenstrains and eigenstresses in the continuum theory of defects (Mura, 1982). The main idea is to replace the problem of a defective crystal in the harmonic approximation to that of a perfect lattice with a distribution of forces that represent the effect of the defect(s)(see Mura (1977) and King and Mura (1991b)).[‡‡] Similar to what is common in elasticity, one can define a discrete field of strains $\mathsf{B} : \mathcal{L}\times\mathcal{L} \to \mathbb{R}^{3\times 3}$ such that

$$\mathbf{u}^{\mathbf{i}} - \mathbf{u}^{\mathbf{j}} = \mathsf{B}(\mathbf{i},\mathbf{j})(\mathbf{x}^{\mathbf{i}} - \mathbf{x}^{\mathbf{j}}). \tag{1.22}$$

Note that

$$\mathbf{u}^{\mathbf{j}} - \mathbf{u}^{\mathbf{i}} = \mathsf{B}(\mathbf{j},\mathbf{i})(\mathbf{x}^{\mathbf{j}} - \mathbf{x}^{\mathbf{i}}) = -\mathsf{B}(\mathbf{i},\mathbf{j})(\mathbf{x}^{\mathbf{i}} - \mathbf{x}^{\mathbf{j}}). \tag{1.23}$$

Thus

$$\mathsf{B}(\mathbf{j},\mathbf{i}) = \mathsf{B}(\mathbf{i},\mathbf{j}). \tag{1.24}$$

Now let us call $\beta(\mathbf{i},\mathbf{j}) = \mathsf{B}(\mathbf{i},\mathbf{j})(\mathbf{x}^{\mathbf{i}} - \mathbf{x}^{\mathbf{j}})$ the total distortion field. Part of this distortion field is elastic. A distortion field β is called compatible if there is a discrete displacement field $\mathbf{u}$ such that

$$\beta(\mathbf{i},\mathbf{j}) = \mathbf{u}^{\mathbf{i}} - \mathbf{u}^{\mathbf{j}}. \tag{1.25}$$

It is easy to show that a discrete distortion field is compatible if and only if

$$\beta(\mathbf{i},\mathbf{j}) + \beta(\mathbf{j},\mathbf{k}) + \beta(\mathbf{k},\mathbf{i}) = \mathbf{0} \qquad \forall\ \mathbf{i},\mathbf{j},\mathbf{k}\in\mathcal{L}. \tag{1.26}$$

[‡‡]We will numerically compare the harmonic solutions obtained using this approximation with the harmonic solutions obtained from our inhomogeneous lattice statics for 180° domain walls in Chapter 4.

Obviously the elastic and non-elastic distortions need not be compatible in general. This is very similar to incompatibility of elastic and plastic deformation gradients in finite plasticity. Having incompatible distortions the harmonic energy of the lattice can be written as

$$\mathcal{E}^{\text{tot}}_{\text{harm}} = -\frac{1}{4}\sum_{\mathbf{i},\mathbf{j}\in\mathcal{L}} \tilde{\mathbf{\Phi}}(\mathbf{i}-\mathbf{j};\mathbf{X})\left[\beta(\mathbf{i},\mathbf{j}) - \beta^E(\mathbf{i},\mathbf{j})\right]\cdot\left[\beta(\mathbf{i},\mathbf{j}) - \beta^E(\mathbf{i},\mathbf{j})\right], \tag{1.27}$$

where $\beta(\mathbf{i},\mathbf{j}) - \beta^E(\mathbf{i},\mathbf{j})$ is the discrete elastic distortion and $\beta^E(\mathbf{i},\mathbf{j})$ is the discrete eigendistortion field. It should be noted that the eigendistortions leave the energy of the lattice unchanged. Now the harmonic energy can be written in terms of eigendistortions and the discrete displacement field as (Ortiz and Phillips, 1999),

$$\mathcal{E}^{\text{tot}}_{\text{harm}} = -\frac{1}{4}\sum_{\mathbf{i},\mathbf{j}\in\mathcal{L}} \tilde{\mathbf{\Phi}}(\mathbf{i}-\mathbf{j};\mathbf{X})\left[\mathbf{u}^{\mathbf{i}} - \mathbf{u}^{\mathbf{j}} - \beta^E(\mathbf{i},\mathbf{j})\right]\cdot\left[\mathbf{u}^{\mathbf{i}} - \mathbf{u}^{\mathbf{j}} - \beta^E(\mathbf{i},\mathbf{j})\right]. \tag{1.28}$$

This energy is now nonconvex in the discrete displacement field. Eigendistortions represent defects and minimizing the above energy with respect to discrete displacements yields the following governing equations for the defective lattice,

$$\sum_{\mathbf{j}\in\mathcal{L}} \tilde{\mathbf{\Phi}}(\mathbf{i}-\mathbf{j};\mathbf{X})\mathbf{u}^{\mathbf{j}} = \mathbf{F}^E_{\mathbf{i}} \qquad \forall\ \mathbf{i}\in\mathcal{L}, \tag{1.29}$$

where

$$\mathbf{F}^E_{\mathbf{i}} = \sum_{\mathbf{j}\in\mathcal{L}} \tilde{\mathbf{\Phi}}(\mathbf{i}-\mathbf{j};\mathbf{X})\beta^E(\mathbf{j},\mathbf{i}) \qquad \forall\ \mathbf{i}\in\mathcal{L}. \tag{1.30}$$

It is seen that problem of analysis of a defective crystal is transformed to that of a perfect lattice with a distribution of forces.

We will not use this approach in this work as we start from an interatomic potential and not the force constants. As we will see in our formulation the defect forces are calculated exactly. Let us briefly explain how our approach is related to the idea of eigendistortions. In the method of eigendistortions there are two approximations: (i) it is assumed that force constants close to the defect are equal to the bulk force constants, (ii) unbalanced forces are approximately calculated using force constants. We will take a more general approach in this work. We assume that we are given a set of interatomic potentials that describe the interactions between different atoms. This way we will be able to find the unbalanced forces exactly. For domain walls (which have a 1-D symmetry reduction as we will see in the sequel) we can take into account the fact that force constants close to the defect are different from the bulk force constants. However, for more complicated defects like steps, we will have to homogenize the force constants.

1.2.1 Discrete Balance of Energy

In this subsection we look at balance of energy for an arbitrary collection of atoms $\mathcal{L}$ and prove a discrete version of Green-Naghdi-Rivilin (GNR) Theorem. For the sake of simplicity, ignoring thermal effects the balance of energy for $\mathcal{L}$ can be written as

$$\frac{d}{dt}\sum_{\mathbf{i}\in\mathcal{L}}\left(\mathcal{E}^{\mathbf{i}}+\frac{1}{2}m_{\mathbf{i}}\dot{\mathbf{x}}^{\mathbf{i}}\cdot\dot{\mathbf{x}}^{\mathbf{i}}\right)=\sum_{\mathbf{i}\in\mathcal{L}}\mathbf{F}_{\mathbf{i}}\cdot\dot{\mathbf{x}}^{\mathbf{i}}. \tag{1.31}$$

Assuming two-body interactions the first term in the left hand side of Eq. (1.31) can be written as

$$\begin{aligned}\frac{d}{dt}\sum_{\mathbf{i}\in\mathcal{L}}\mathcal{E}^{\mathbf{i}}\left(\{\mathbf{x}^{\mathbf{i}}\}_{\mathbf{i}\in\mathcal{L}}\right) &= \frac{1}{2}\frac{d}{dt}\sum_{\substack{\mathbf{i},\mathbf{j}\in\mathcal{L}\\ \mathbf{j}\neq\mathbf{i}}}\Phi\left(|\mathbf{x}^{\mathbf{i}}-\mathbf{x}^{\mathbf{j}}|\right)\\ &= \frac{1}{2}\sum_{\substack{\mathbf{i},\mathbf{j}\in\mathcal{L}\\ \mathbf{j}\neq\mathbf{i}}}\Phi'\left(|\mathbf{x}^{\mathbf{i}}-\mathbf{x}^{\mathbf{j}}|\right)\frac{\mathbf{x}^{\mathbf{i}}-\mathbf{x}^{\mathbf{j}}}{|\mathbf{x}^{\mathbf{i}}-\mathbf{x}^{\mathbf{j}}|}\cdot\left(\dot{\mathbf{x}}^{\mathbf{i}}-\dot{\mathbf{x}}^{\mathbf{j}}\right)\\ &= \frac{1}{2}\sum_{\substack{\mathbf{i},\mathbf{j}\in\mathcal{L}\\ \mathbf{j}\neq\mathbf{i}}}\mathbf{f}_{\mathbf{ij}}\cdot\left(\dot{\mathbf{x}}^{\mathbf{i}}-\dot{\mathbf{x}}^{\mathbf{j}}\right)\end{aligned} \tag{1.32}$$

where

$$\mathbf{f}_{\mathbf{ij}}=\Phi'\left(|\mathbf{x}^{\mathbf{i}}-\mathbf{x}^{\mathbf{j}}|\right)\frac{\mathbf{x}^{\mathbf{i}}-\mathbf{x}^{\mathbf{j}}}{|\mathbf{x}^{\mathbf{i}}-\mathbf{x}^{\mathbf{j}}|}. \tag{1.33}$$

Note that

$$\mathbf{f}_{\mathbf{ji}}=-\mathbf{f}_{\mathbf{ij}}. \tag{1.34}$$

Using this property, it can be easily shown that

$$\frac{d}{dt}\sum_{\mathbf{i}\in\mathcal{L}}\mathcal{E}^{\mathbf{i}}\left(\{\mathbf{x}^{\mathbf{i}}\}_{\mathbf{i}\in\mathcal{L}}\right)=-\sum_{\substack{\mathbf{i},\mathbf{j}\in\mathcal{L}\\ \mathbf{j}\neq\mathbf{i}}}\mathbf{f}_{\mathbf{ij}}\cdot\dot{\mathbf{x}}^{\mathbf{i}}. \tag{1.35}$$

Therefore the balance of energy for $\mathcal{L}$ can be written as

$$-\sum_{\substack{\mathbf{i},\mathbf{j}\in\mathcal{L}\\ \mathbf{j}\neq\mathbf{i}}}\mathbf{f}_{\mathbf{ij}}\cdot\dot{\mathbf{x}}^{\mathbf{i}}+\sum_{\mathbf{i}\in\mathcal{L}}m_{\mathbf{i}}\ddot{\mathbf{x}}^{\mathbf{i}}\cdot\dot{\mathbf{x}}^{\mathbf{i}}=\sum_{\mathbf{i}\in\mathcal{L}}\mathbf{F}_{\mathbf{i}}\cdot\dot{\mathbf{x}}^{\mathbf{i}}. \tag{1.36}$$

Now let us try to write the balance of energy for an arbitrary subset $\mathcal{M}\subset\mathcal{L}$. We start with the following definition.

Definition 1. *Atom energy $\mathcal{E}^i$ for $\mathbf{i}\in\mathcal{M}$ is defined to be one half of the sum of the energies of atomic bonds between $\mathbf{i}$ and all the other atoms in $\mathcal{M}$.*

Balance of energy for $\mathcal{M}$ is written as

$$\frac{d}{dt}\sum_{\mathbf{i}\in\mathcal{M}}\left(\mathcal{E}^{\mathbf{i}}+\frac{1}{2}m_{\mathbf{i}}\dot{\mathbf{x}}^{\mathbf{i}}\cdot\dot{\mathbf{x}}^{\mathbf{i}}\right)=\sum_{\mathbf{i}\in\mathcal{M}}\mathbf{F}_{\mathbf{i}}\cdot\dot{\mathbf{x}}^{\mathbf{i}}+\sum_{\mathbf{i}\in\mathcal{M}}\sum_{\mathbf{j}\in\mathcal{L}\setminus\mathcal{M}}\mathbf{f}_{\mathbf{ij}}\cdot\dot{\mathbf{x}}^{\mathbf{i}}. \tag{1.37}$$

This can be rewritten as

$$\frac{d}{dt}\sum_{\mathbf{i}\in\mathcal{M}}\left(\mathcal{E}^{\mathbf{i}}+\frac{1}{2}m_{\mathbf{i}}\dot{\mathbf{x}}^{\mathbf{i}}\cdot\dot{\mathbf{x}}^{\mathbf{i}}\right)=\sum_{\mathbf{i}\in\mathcal{M}}\mathbf{F}_{\mathbf{i}}\cdot\dot{\mathbf{x}}^{\mathbf{i}}+\sum_{\mathbf{i}\in\mathcal{M}}\mathbf{t}_{\mathbf{i}}\cdot\dot{\mathbf{x}}^{\mathbf{i}} \tag{1.38}$$

where

$$\mathbf{t}_{\mathbf{i}}=\sum_{\mathbf{j}\in\mathcal{L}\setminus\mathcal{M}}\mathbf{f}_{\mathbf{ij}} \tag{1.39}$$

is a 'discrete traction' for atom $\mathbf{i}$. Balance of energy is now simplified to

$$-\sum_{\substack{\mathbf{i},\mathbf{j}\in\mathcal{M}\\ \mathbf{j}\neq\mathbf{i}}}\mathbf{f}_{\mathbf{ij}}\cdot\dot{\mathbf{x}}^{\mathbf{i}}+\sum_{\mathbf{i}\in\mathcal{M}}m_{\mathbf{i}}\ddot{\mathbf{x}}^{\mathbf{i}}\cdot\dot{\mathbf{x}}^{\mathbf{i}}=\sum_{\mathbf{i}\in\mathcal{M}}\mathbf{F}_{\mathbf{i}}\cdot\dot{\mathbf{x}}^{\mathbf{i}}+\sum_{\mathbf{i}\in\mathcal{M}}\mathbf{t}_{\mathbf{i}}\cdot\dot{\mathbf{x}}^{\mathbf{i}}. \tag{1.40}$$

A very special subset would be the set $\mathcal{M}=\{\mathbf{i}\}$ for which the balance of energy simplifies to

$$m_{\mathbf{i}}\ddot{\mathbf{x}}^{\mathbf{i}}\cdot\dot{\mathbf{x}}^{\mathbf{i}}=(\mathbf{F}_{\mathbf{i}}+\mathbf{t}_{\mathbf{i}})\cdot\dot{\mathbf{x}}^{\mathbf{i}}\qquad\forall\mathbf{i}\in\mathcal{L} \tag{1.41}$$

where

$$\mathbf{t}_{\mathbf{i}}=\sum_{\substack{\mathbf{i},\mathbf{j}\in\mathcal{M}\\ \mathbf{j}\neq\mathbf{i}}}\mathbf{f}_{\mathbf{ij}}\qquad\forall\mathbf{i}\in\mathcal{L}. \tag{1.42}$$

Note that for this discrete system conservation of mass states that

$$\sum_{\mathbf{i}\in\mathcal{M}}m_{\mathbf{i}}=\text{constant}\qquad\forall\mathcal{M}\subset\mathcal{L}. \tag{1.43}$$

Choosing $\mathcal{M}=\{\mathbf{i}\}$ this reads

$$m_{\mathbf{i}}=\text{constant}\qquad\forall\mathbf{i}\in\mathcal{L}. \tag{1.44}$$

Here we have implicitly assumed that no chemical reactions are involved in the process of deformation.

1.2.1.1 Discrete Green-Naghdi-Rivilin Theorem

Green, Naghdi and Rivilin (Green and Rivilin, 1964) realized that conservation of mass and balance of linear and angular momenta can be obtained by postulating balance of energy under isometries of $\mathbb{R}^3$. Here we present a discrete version of this theorem. Consider a discrete collection of atoms $\mathcal{L}$ and suppose it deforms under the discrete deformation mapping φ and the balance of energy holds

for any subset $\mathcal{M} \subset \mathcal{L}$. First, let us consider a rigid translation of the deformed configuration, i.e., $\varphi'_t = \xi_t \circ \varphi_t$, where

$$\xi_t(\mathbf{x^i}) = \mathbf{x^i} + (t - t_0)\mathbf{c} \tag{1.45}$$

where $\mathbf{c}$ is a time independent vector. Let us postulate that discrete energy balance is invariant under ξ_t, i.e.,

$$-\sum_{\substack{\mathbf{i},\mathbf{j}\in\mathcal{M}\\ \mathbf{j}\neq\mathbf{i}}} \mathbf{f'_{ij}} \cdot \dot{\mathbf{x}'}^{\mathbf{i}} + \sum_{\mathbf{i}\in\mathcal{M}} m'_{\mathbf{i}} \ddot{\mathbf{x}'}^{\mathbf{i}} \cdot \dot{\mathbf{x}'}^{\mathbf{i}} = \sum_{\mathbf{i}\in\mathcal{M}} \mathbf{F'_i} \cdot \dot{\mathbf{x}'}^{\mathbf{i}} + \sum_{\mathbf{i}\in\mathcal{M}} \mathbf{t'_i} \cdot \dot{\mathbf{x}'}^{\mathbf{i}}. \tag{1.46}$$

Note that at $t = t_0$

$$\mathbf{f'_{ij}} = \mathbf{f_{ij}},\ \mathbf{t'_i} = \mathbf{t_i},\ \dot{\mathbf{x}'}^{\mathbf{i}} = \dot{\mathbf{x}}^{\mathbf{i}} + \mathbf{c},\ m'_{\mathbf{i}} = m_{\mathbf{i}} \tag{1.47}$$

and (see Marsden and Hughes (1983))

$$\mathbf{F'_i} - m'_{\mathbf{i}} \ddot{\mathbf{x}'}^{\mathbf{i}} = \mathbf{F_i} - m_{\mathbf{i}} \ddot{\mathbf{x}}^{\mathbf{i}}. \tag{1.48}$$

Thus subtracting the balance of energy for $\mathcal{M}$ from that of $\xi_t(\mathcal{M})$ at time $t = t_0$ we obtain

$$-\sum_{\substack{\mathbf{i},\mathbf{j}\in\mathcal{M}\\ \mathbf{j}\neq\mathbf{i}}} \mathbf{f_{ij}} \cdot \mathbf{c} + \sum_{\mathbf{i}\in\mathcal{M}} m_{\mathbf{i}} \ddot{\mathbf{x}}^{\mathbf{i}} \cdot \mathbf{c} = \sum_{\mathbf{i}\in\mathcal{M}} \mathbf{F_i} \cdot \mathbf{c} + \sum_{\mathbf{i}\in\mathcal{M}} \mathbf{t_i} \cdot \mathbf{c}. \tag{1.49}$$

Since $\mathbf{c}$ is arbitrary we have

$$-\sum_{\substack{\mathbf{i},\mathbf{j}\in\mathcal{M}\\ \mathbf{j}\neq\mathbf{i}}} \mathbf{f_{ij}} + \sum_{\mathbf{i}\in\mathcal{M}} m_{\mathbf{i}} \ddot{\mathbf{x}}^{\mathbf{i}} = \sum_{\mathbf{i}\in\mathcal{M}} \mathbf{F_i} + \sum_{\mathbf{i}\in\mathcal{M}} \mathbf{t_i}. \tag{1.50}$$

Or

$$\sum_{\mathbf{i}\in\mathcal{M}} \left(\mathbf{F_i} - m_{\mathbf{i}} \ddot{\mathbf{x}}^{\mathbf{i}} + \sum_{\substack{\mathbf{j}\in\mathcal{M}\\ \mathbf{j}\neq\mathbf{i}}} \mathbf{f_{ij}} \right) = \mathbf{0}. \tag{1.51}$$

This is the discrete balance of linear momentum. In particular when $\mathcal{M} = \{\mathbf{i}\}$ we have

$$m_{\mathbf{i}} \ddot{\mathbf{x}}^{\mathbf{i}} = \mathbf{F_i} + \mathbf{t_i} \qquad \forall \mathbf{i} \in \mathcal{L}. \tag{1.52}$$

Or

$$m_{\mathbf{i}} \ddot{\mathbf{x}}^{\mathbf{i}} = \mathbf{F_i} + \sum_{\substack{\mathbf{i},\mathbf{j}\in\mathcal{L}\\ \mathbf{j}\neq\mathbf{i}}} \mathbf{f_{ij}} \qquad \forall \mathbf{i} \in \mathcal{L}. \tag{1.53}$$

Now let us consider a time-dependent rigid rotation in the ambient space, i.e.,

$$\xi_t(\mathbf{x^i}) = e^{(t-t_0)\mathbf{\Omega}} \mathbf{x^i} \tag{1.54}$$

for some skew-symmetric matrix $\mathbf{\Omega}$. Note that at $t = t_0$

$$\dot{\mathbf{x}'}^{\mathbf{i}} = \dot{\mathbf{x}}^{\mathbf{i}} + \mathbf{\Omega}\mathbf{x}^{\mathbf{i}} \tag{1.55}$$

and

$$\mathbf{F}'_{\mathbf{i}} - m'_{\mathbf{i}}\ddot{\mathbf{x}'}^{\mathbf{i}} = \mathbf{F}_{\mathbf{i}} - m_{\mathbf{i}}\ddot{\mathbf{x}}^{\mathbf{i}}. \tag{1.56}$$

Let us now postulate that the discrete balance of energy is invariant under the spatial isometry ξ_t, i.e.,

$$-\sum_{\substack{\mathbf{i},\mathbf{j}\in\mathcal{M}\\ \mathbf{j}\neq\mathbf{i}}} \mathbf{f}'_{\mathbf{ij}} \cdot \dot{\mathbf{x}'}^{\mathbf{i}} + \sum_{\mathbf{i}\in\mathcal{M}} m'_{\mathbf{i}}\ddot{\mathbf{x}'}^{\mathbf{i}} \cdot \dot{\mathbf{x}'}^{\mathbf{i}} = \sum_{\mathbf{i}\in\mathcal{M}} \mathbf{F}'_{\mathbf{i}} \cdot \dot{\mathbf{x}'}^{\mathbf{i}} + \sum_{\mathbf{i}\in\mathcal{M}} \mathbf{t}'_{\mathbf{i}} \cdot \dot{\mathbf{x}'}^{\mathbf{i}}. \tag{1.57}$$

Note that at $t = t_0$

$$\mathbf{f}'_{\mathbf{ij}} = \mathbf{f}_{\mathbf{ij}},\ \mathbf{t}'_{\mathbf{i}} = \mathbf{t}_{\mathbf{i}},\ m'_{\mathbf{i}} = m_{\mathbf{i}}. \tag{1.58}$$

Subtracting the balance of energy for $\mathcal{M}$ from that of $\xi_t(\mathcal{M})$ at $t = t_0$ we obtain

$$-\sum_{\substack{\mathbf{i},\mathbf{j}\in\mathcal{M}\\ \mathbf{j}\neq\mathbf{i}}} \mathbf{f}_{\mathbf{ij}} \cdot \mathbf{\Omega}\mathbf{x}^{\mathbf{i}} - \sum_{\mathbf{i}\in\mathcal{M}} \left(\mathbf{F}_{\mathbf{i}} - m_{\mathbf{i}}\ddot{\mathbf{x}}^{\mathbf{i}}\right) \cdot \mathbf{\Omega}\mathbf{x}^{\mathbf{i}} = \sum_{\mathbf{i}\in\mathcal{M}} \mathbf{t}_{\mathbf{i}} \cdot \mathbf{\Omega}\mathbf{x}^{\mathbf{i}}. \tag{1.59}$$

Or

$$\sum_{\mathbf{i}\in\mathcal{M}} \left[\sum_{\substack{\mathbf{j}\in\mathcal{M}\\ \mathbf{j}\neq\mathbf{i}}} \mathbf{f}_{\mathbf{ij}} + \left(\mathbf{F}_{\mathbf{i}} - m_{\mathbf{i}}\ddot{\mathbf{x}}^{\mathbf{i}}\right) + \mathbf{t}_{\mathbf{i}} \right] \cdot \mathbf{\Omega}\mathbf{x}^{\mathbf{i}} = 0. \tag{1.60}$$

But the expression inside the bracket can be simplified to

$$\sum_{\substack{\mathbf{j}\in\mathcal{L}\\ \mathbf{j}\neq\mathbf{i}}} \mathbf{f}_{\mathbf{ij}} + \left(\mathbf{F}_{\mathbf{i}} - m_{\mathbf{i}}\ddot{\mathbf{x}}^{\mathbf{i}}\right) = \mathbf{0}. \tag{1.61}$$

This shows that the balance of angular momentum is satisfied trivially when atomic interactions are pairwise.

1.2.2 Harmonic/Anharmonic Energy Partition Method

In harmonic lattice statics one assumes that energy can be approximated by the first two terms of its Taylor series expansion. In other words, it is assumed that the lattice is lightly distorted and the energy can be approximated by a quadratic potential. However, harmonic approximation cannot be valid in regions of the lattice where displacements are large. This can happen in regions very close to defects, for example, near dislocation cores. This also applies to our model of a ferroelectric domain wall, which is an example of a planar defect. This means that the harmonic approximation may not

capture the correct structure of the domain wall. Anharmonic lattice statics is a natural modification of harmonic lattice statics in which one uses harmonic lattice statics far from defects and uses the full nonlinear potential in localized regions around the defects. This idea was first proposed by Flocken (1972) and Esterling (1978) and was later used by Gallego and Ortiz (1993) in the analysis of dislocations. We now briefly explain how this method should be implemented in our formulation of lattice statics. This method is in fact nothing but a modified Newton-Raphson iteration. We first start from the harmonic lattice statics with the forces that reflect the nonequilibrium nature of the reference configuration. The linear solution is obtained by solving the discrete governing equations. We can then calculate the forces on the distorted lattice and apply these new forces to the original harmonic lattice, i.e., we keep the stiffness matrices constant in all the steps. This is not as fast as the usual Newton-Raphson (actually it has linear convergence) but is very simple to use. As we will observe, the relaxed lattice is distorted in a highly localized region close to a domain wall and a few lattice spacings away from the domain displacements are zero (or a constant rigid translation). This means that the nonlinear effects are highly localized.

1.2.3 Motivation for Lattice Static Analysis of Ferroelectric Defects

As was mentioned in the Introduction, there have been theoretical, numerical and experimental studies of ferroelectric domain walls in the literature. Theoretical works are in the continuum scale and do not give one any information regarding the detailed structure of the domain walls and other defects. Quantum mechanics calculations are valuable and give us a lot of information about the structure and energetics of domain walls. However, these analyses are purely numerical in nature. The other problem with these methods is that they cannot be used for more complicated defects, e.g., steps. What is missing in the literature is a semi-analytical analysis of ferroelectric domain walls. There are several recent works on analysis of solids in the lattice scale. Most of these models are highly idealized and their results are only qualitatively valuable. The other drawback of almost all the existing theoretical lattice-scale calculations is the fact that they are restricted to one and two dimensions. In this work, we start from a physically realistic potential that is derived from quantum mechanics calculations. This potential is used for analysis of a single ferroelectric domain wall in an infinite solid (and some other defects). Our semi-analytical technique enables us to freely work with the parameter space and study the effect of, for example, different potentials on the domain wall structure. The potentials used in this work are examples and given similar potentials many relevant problems can be studied in the lattice scale. We reformulate lattice statics and will try to exploit the similarities with continuum mechanics. We hope that this work give some structure to lattice scale calculations and helps us in doing analytic atomistic calculations more systematically. We can summarize our motivation for the lattice statics calculations of ferroelectric defects as follows.

- To have an analytic tool for comparing different interatomic potentials in terms of the defect structure and energy that they predict.
- To have an analytic verification tool for numerical techniques like quasi-continuum method.
- To develop a systematic theory for lattice-scale calculations.

1.3 Organization of The Thesis

This thesis is organized as follows. Chapter 2 reviews shell potentials and the linearized governing equations for an arbitrary collection of atoms are obtained. Formulations are made as abstract as possible in order to be applicable to other similar systems. Multi-lattice of ABO_3 Perovskites are treated abstractly and some issues like defining polarization in the lattice scale are discussed. This follows by a detailed discussion on long-range forces and a careful numerical study of Wolf et al. (1999)'s summation method for shell potentials of $BaTiO_3$ and $PbTiO_3$. The chapter is ended by a discussion on structure optimization of tetragonal $PbTiO_3$ and stability of local minima of the energy surface.

Chapter 3 presents a formal method of obtaining discrete governing equations for an arbitrary collection of atoms. The main contribution of this chapter is the systematic derivation of governing equations for defective crystals and the idea of 1-D and 2-D symmetry reductions. Another contribution of this chapter is putting the discrete governing equations in a form familiar in the theory of difference equations. This is very useful as one can see the discrete governing equations in a structured form for any given system.

Chapter 4 presents a systematic lattice statics analysis of 180° domain walls. The discrete governing equations are reduced to a vector-valued ordinary difference equation (ODE) on $\mathbb{Z}$. Because of a symmetry relation between the right and left sides of the domain wall, the governing ODE is further reduced to an ODE on $\mathbb{N}$. A novel solution technique taking into account the variability of the stiffness matrices close to the domain wall is developed for solving the governing ODE. The chapter ends with a formulation of anharmonic lattice statics and some numerical examples for $BaTiO_3$ and $PbTiO_3$. Chapters 5 and 6 extend the calculations of Chapter 4 to 90° domain walls and free surfaces.

Chapter 7 presents a lattice statics analysis of steps in 180° domain walls in $PbTiO_3$. We first reduce the discrete governing equations to a vector-valued partial difference equation in two discrete independent variables and then solve the governing equations using discrete Fourier transform. In obtaining anharmonic solutions use is made of the fully-nonlinear solutions of 180° domain walls. Conclusions and future directions are given in Chapter 8.

Appendix A presents a detailed review and discussion on summing conditionally convergent lattice sums and in particular the mathematical foundations of Ewald method. Appendix B contains several independent topics. Theory of ordinary and partial difference equations is briefly reviewed. Discrete Fourier transform and its application in solving linear difference equations is explained. A novel method for solving a general class of partial difference equations is presented. We end the appendix by solving a simple 2-D lattice problem under two loading systems. We found this simple example helpful in developing intuition for solving the more complicated problems studied in this thesis.

Chapter 2

Total Energy of a Ferroelectric Solid

2.1 Shell Models and Polarizability

The Coulomb energy is the leading term in a series of different moments of charge density. The second term represents the dipole (first moment of charge densities), and the tendency of the electronic charge to poses a dipole is called polarizability. One way of taking into account the polarizability is to use shell models. The classical shell model was originally developed by Dick and Overhauser (1964). Ferroelectric materials are now usually modelled by shell models in molecular dynamics simulations. It should be noted that modelling ionic interactions by two-body Coulombic potentials is just an approximation (rigid ion approximation). To correct this approximation and take into account the many-body interaction nature of electrostatic interactions, usually shell models are used. Shell models are more accurate models as they assume a uniform distribution of electrons on a sphere that can move independently of the core. Such a model is used in modelling ferroelectrics in this work. In these models it is assumed that an atom is composed of a core which consists of the nucleus and the inner electrons and a shell, which consists of the valence electrons. A classical shell potential has the following three parts,

$$\mathcal{E} = \mathcal{E}_{\text{long-range}} + \mathcal{E}_{\text{short-range}} + \mathcal{E}_{\text{core-shell}} \tag{2.1}$$

The long-range energy is the classical Coulombic electrostatic energy between cores and shells excluding the core-shell interaction in the same atom. Fig. 2.1 shows the interaction graph for cores and shells of atoms i and j. The short-range interactions are between the massless shells and in general not all shells contribute to this energy. The third part of the energy is the energy of interaction of core and shell of the same atom. The core-shell coupling is anharmonic but isotropic with

the following form,

$$V_I(\mathbf{x}I_c^i, \mathbf{x}I_s^i) = \frac{1}{2}c_{2I}|\mathbf{x}I_c^i - \mathbf{x}I_s^i|^2 + \frac{1}{24}c_{4I}|\mathbf{x}I_c^i - \mathbf{x}I_s^i|^4 \tag{2.2}$$

where I refers to the atom type and i is the unit cell index.

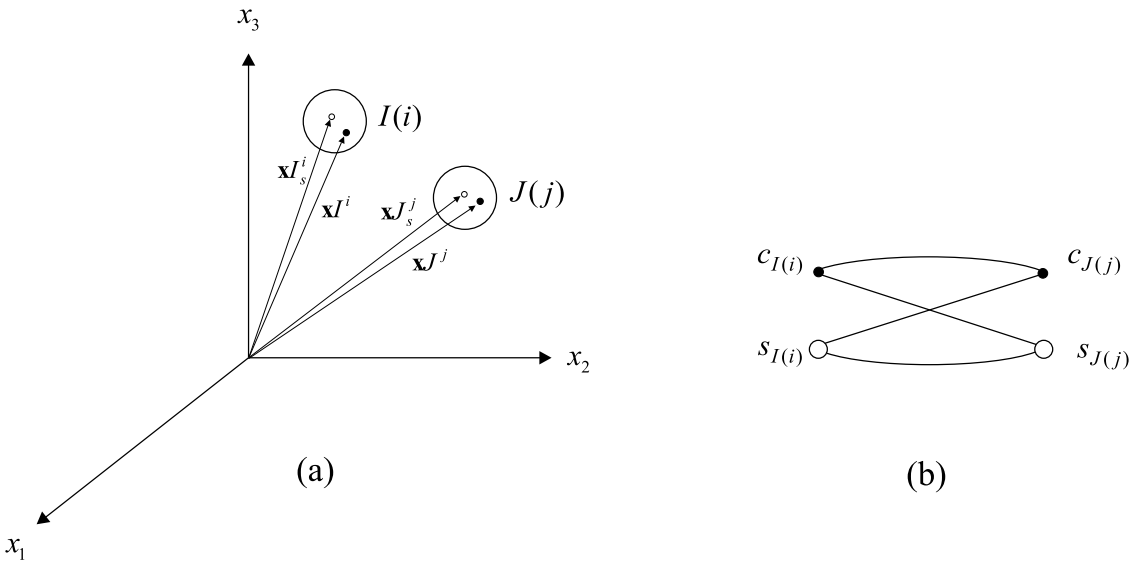

Figure 2.1: (a) Core and shell position vectors for atoms i and j, (b) the interaction graph.

The potential we use for $PbTiO_3$ is a classical shell model developed by Sepliarsky and Cohen (2002) and Sepliarsky et al. (2004). In Sepliarsky et al. (2004)'s potential (we call it SC potential from now on) the short-range interactions are between shells of pairs Pb-O, Pb-Ti and O-O, with the following forms,

$$Pb-Ti, Pb-O, Ti-O \quad : \quad V_{IJ}(r) = (a_{IJ} + b_{IJ}r)\, e^{-\frac{r}{\rho_{IJ}}} \tag{2.3}$$

$$O-O \quad : \quad V_{33}(r) = a_{33}e^{-\frac{r}{\rho_{33}}} + \frac{c_{33}}{r^6} \tag{2.4}$$

The first potential is called Rydberg potential and the second one is Buckingham's potential. The parameters of these potentials are given in Table 2.1. The short-range energy is usually chosen such that it contains terms that describe both the Pauli repulsion at short distances and dispersive interaction at longer distances. In ionic crystals the most long-ranged part of energy is due to Coulombic interactions. The second most long-ranged part is the dispersion term. Dispersion energy is the result of interaction of fluctuating electron charge moments of different orders. This part of energy can be written as

$$\mathcal{E}_{\text{dispersion}} = -\sum_{i,j\in\mathcal{L}}\sum_{n=3}^{\infty} C_{2n}|\mathbf{x}_i - \mathbf{x}_j|^{-2n} \tag{2.5}$$

Table 2.1: Parameters of short-range energy in SC potential.

I	J	$a(eV)$	$b(\mathring{A}^{-1}eV)$	$c(\mathring{A}^{6}eV)$	$\rho(\mathring{A})$
1	2	0.096	-12.5665		2.420131
1	3	6766.270	127.7793		0.273805
2	3	1130.010	-160.8363		0.359723
3	3	3634.861		331.6058	0.314424

Table 2.2: Core and shell charges and masses for $PbTiO_3$ in SC potential.

I	$Q_c(e)$	$Q_s(e)$	m_c
1	4.9580	-2.7850	207.2000
2	8.8200	-5.1580	47.9000
3	0.5630	-2.5080	16.0000

The first term represents the interaction of instantaneous dipole-instantaneous dipole energy, for example (Gale and Rohl, 2003). Usually, only the first term is considered as is seen in the form of the Buckingham potential above. The core and shell charges for different atom types are given in Table 2.2. Finally the parameters of core-shell interaction is given in Table 2.3. The optimized structure is given in Table 2.9. For this structure polarization is $P_s = 76.2336 \times 10^{-6} C/cm^2$ which is very close to the experimental value of $P_s = 75 \times 10^{-6} C/cm^2$.The ground state is tetragonal and we do all the calculations at $T = 0$.

After an extensive literature review and studying different interatomic potentials for ferroelectrics, we discovered that all the existing potentials are stable only under some constraints. We used both GULP (Gale, 1997), (Gale and Rohl, 2003) and our Mathematica code for stability analysis of the optimized structure and in all the tests they agreed. SC potential is stable under the constraint that all the perturbations are in the tetragonal c-direction (for fixed values of lattice parameters $a = 3.9053\mathring{A}$, $c = 4.1514\mathring{A}$). We studied other possibilities like allowing perturbations to be in ac plane. In all these cases the ground state was unstable. Therefore, we had to do all the numerical calculations by constraining core and shell displacements to be in the c-direction. However, the techniques developed here and all the implementations are general and can handle stable potentials in three dimensions. We have been unable to find a completely stable interatomic potential but if there is one we could repeat all the calculations with no constraints.

Table 2.3: Parameters of core-shell interaction energy for $PbTiO_3$ in SC potential.

Elm	$c_2(\mathring{A}^{-2}eV)$	$c_4(\mathring{A}^{-4}eV)$
Pb	119.48	17968.50
Ti	1428.59	36411.00
O	23.29	4514.70

Table 2.4: Parameters of the van der Waals energy.

I	J	D_{IJ}	α_{IJ}	$R_{IJ}(\mathring{A})$
3	3	0.0905	7.1579	3.9975
1	2	0.9777	7.8754	3.3868

Table 2.5: Parameters of the pure repulsion energy.

I	J	A_{IJ}	m_{IJ}
3	1	2.5841	6.2615
3	2	1.6163	8.4430

2.1.1 Polarizable Charge Equilibrium Force Field

Another potential that we use in this thesis is a modified shell potential that is derived from quantum mechanics ab initio calculations of $BaTiO_3$ performed by Goddard and his co-workers (Goddard et al., 2003) and it is called Polarizable Charge Equilibrium Force Field (PCEFF). From now on we will refer to this potential as PCEFF potential. In the so-called ReaxFF (Goddard et al., 2003), each atom has a fixed core charge and a variable shell charge both with Gaussian distributions. This potential reflects the fact that in every atom the shell charge can move with respect to the core and variability of shell charges represents the charge transfer between atoms. In this section we briefly explain the structure and parameters of this potential.

The short-range part of the potential for a pair of two anions or two cations is a van der Waals energy which is modelled by a Morse potential. This potential has exponential repulsion for short distances and exponential attraction for long distances. The form of this energy is shown below,

$$\mathcal{E}^{vdw}_{I(i)J(j)} = D_{IJ}\Big\{exp\Big[\frac{\alpha_{IJ}}{2}\ (1-\frac{r_{ij}}{R_{IJ}})\Big]-1\Big\}^2 - D_{IJ} \tag{2.6}$$

where $r_{ij} = |\mathbf{x}I^i - \mathbf{x}J^j|$. The parameters of this part of the energy are given in Table 2.4. For a pair of an anion and a cation, the short-range energy has a power repulsive form and describes the Pauli repulsion. This potential has the following form,

$$\mathcal{E}^{pr}_{I(i)J(j)} = (A_{IJ})^m_{IJ} r_{ij}^{-m_{IJ}} \tag{2.7}$$

The parameters of this potential are given in Table 2.5. Self energy has the following form,

$$\mathcal{E}I^{self}_i = E_I + \chi_I(QI_c + QI^i_s) + \frac{J_I}{2}(QI_c + QI^i_s)^2 \tag{2.8}$$

where χ is electronegativity (V) and J is electronegativity hardness (V/e). Parameters of self-energy for different species are given in Table 2.6. Note that the values of E_I do not affect the governing equilibrium equations. The core and shell charges are assumed to have the following Gaussian

Table 2.6: Parameters of the self energy.

I	$\chi_I(V)$	$J_I(V/e)$	$QI_c(e)$
1	-5.0992	12.7457	2.0000
2	2.0369	11.3415	4.0000
3	9.3877	15.9439	2.0000

Table 2.7: Parameters of the interaction energy.

Elm	$R_c(\mathring{A})$	$R_s(\mathring{A})$
Ba	0.1632	0.8021
Ti	0.4255	0.5404
O	0.2618	0.4238

distributions (see Fig. 2.2),

$$\rho I_c^i = \left(\frac{\eta_c^I}{\pi}\right)^{\frac{3}{2}} QI_c \; exp(-\eta_c^I|\mathbf{x}-\mathbf{x}I^i|^2), \quad \rho I_s^i = \left(\frac{\eta_s^I}{\pi}\right)^{\frac{3}{2}} QI_s^i \; exp(-\eta_s^I|\mathbf{x}-\mathbf{x}I_s^i|^2) \tag{2.9}$$

where,

$$\eta_c^I = \frac{1}{4RI_c^2}, \quad \eta_s^I = \frac{1}{4RI_s^2}$$

and where RI_c and RI_s are core and shell radii for specie I and are given in Table 2.7. There is a

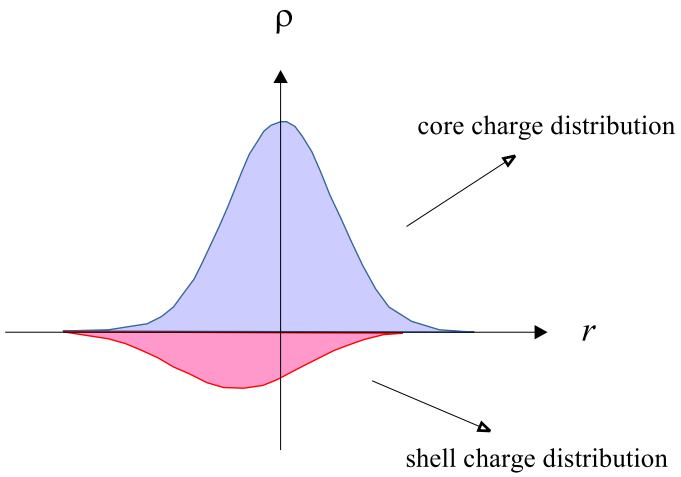

Figure 2.2: Core and shell charge distributions.

fourth-order correction term that has the following form,

$$\mathcal{E}_{I(i)J(j)}^{correction} = K_I(r_{ij})^4 \tag{2.10}$$

where $K_{Ba} = K_{Ti} = 1.0 \; eV\mathring{A}^{-4}$ and $K_O = 2000.0 \; eV\mathring{A}^{-4}$. The interaction part of the Coulombic

energy has the following form,

$$\Psi\Big(|\mathbf{x}I^i - \mathbf{x}J_s^j|, QI_c, QJ_s^j\Big) = \frac{QI_c\ QJ_s^j}{|\mathbf{x}I^i - \mathbf{x}J_s^j|}\ \mathrm{erf}\left(\sqrt{\frac{\eta_c^I \eta_s^J}{\eta_c^I + \eta_s^J}}|\mathbf{x}I^i - \mathbf{x}J_s^j|\right) \tag{2.11}$$

where erf(.) is the error function and is defined as

$$\mathrm{erf}(x) = \frac{2}{\sqrt{\pi}}\int_0^x e^{-t^2}dt$$

All the other five terms of the interaction energy are defined similar to Eq. (2.11). This is nothing but the Coulombic interaction between two distributed charges with the Gaussian distributions shown in Fig. 2.2.

2.1.2 Discrete Governing Equations for an Abstract Shell Potential

Consider the ith I atom in a multi-lattice $\mathcal{L}$ with three species, where $i \in \{1, 2, 3, ...\}$ is the unit cell index and $I \in \{1, 2, 3, 4, 5\}$ refers to the sublattice number. Here, without loss of generality, we have assumed that $\mathcal{L}$ has five sublattices. Suppose this atom has core position vector $\mathbf{x}I^i$, shell position vector $\mathbf{x}I_s^i$ and core and shell charges QI_c^i and QI_s^i, respectively. It is assumed that all the core charges for species I are the same. The total energy of the system is assumed to have the following form,

$$\mathcal{E} = \mathcal{E}_{short-range} + \mathcal{E}_{long-range}. \tag{2.12}$$

It is assumed that the short-range energy is pairwise and is equal to $\Phi(|\mathbf{x}I^i - \mathbf{x}J^j|)$ for atoms $I(i)$ and $J(j)$ for some given scaler-valued function Φ. Thus, the total short-range energy of the system can be written as

$$\mathcal{E}_{short-range} = \frac{1}{4}\sum_{I,J=1}^{5}\sum_{i,j}\Phi(|\mathbf{x}I^i - \mathbf{x}J^j|). \tag{2.13}$$

Note that because of the short-range nature of the above energy i and j belong to a finite index set.

The long-range energy is assumed to have two parts, self-energy and interaction energy, i.e,

$$\mathcal{E}_{long-range} = \mathcal{E}_{self} + \mathcal{E}_{interaction} \tag{2.14}$$

where self-energy is only a function of core and shell charges and the interaction energy is Coulombic energy and is a function of both charges and core positions (see Fig. 2.3). Thus

$$\mathcal{E}_{self} = \sum_{I=1}^{5}\sum_{i}\Upsilon(QI_c, QI_s^i). \tag{2.15}$$

And,

$$\begin{aligned}\mathcal{E}_{interaction} &= \frac{1}{4}\sum_{I,J=1}^{3}\sum_{i,j}\{\mathcal{C}(c_{I(i)},s_{I(i)})+\mathcal{C}(c_{I(i)},c_{J(j)})+\mathcal{C}(c_{I(i)},s_{J(j)}) \\ &\qquad +\mathcal{C}(s_{I(i)},c_{J(j)})+\mathcal{C}(s_{I(i)},s_{J(j)})+\mathcal{C}(c_{J(j)},s_{J(j)})\} \\ &= \frac{1}{4}\sum_{I,J=1}^{3}\sum_{i,j}\{\Psi(|\mathbf{x}I^i-\mathbf{x}J_s^j|,QI_c,QJ_s^j)+\Psi(|\mathbf{x}I^i-\mathbf{x}I^j|,QI_c,QJ_c) \\ &\qquad +\Psi(|\mathbf{x}I^i-\mathbf{x}I_s^j|,QI_c,QJ_s^j)+\Psi(|\mathbf{x}I_s^i-\mathbf{x}I^j|,QI_s^i,QJ_c) \\ &\qquad +\Psi(|\mathbf{x}I_s^i-\mathbf{x}I_s^j|,QI_s^i,QJ_s^j)+\Psi(|\mathbf{x}J^i-\mathbf{x}I_s^j|,QJ_c,QJ_s^j)\} \quad (2.16)\end{aligned}$$

Therefore, the total energy can be written as

$$\begin{aligned}\mathcal{E} &= \frac{1}{4}\sum_{I,J=1}^{3}\sum_{i,j}\Phi(|\mathbf{x}I^i-\mathbf{x}J^j|)+\sum_{I=1}^{3}\sum_{i}\Upsilon(QI_c,QI_s^i) \\ &\quad +\frac{1}{4}\sum_{I,J=1}^{3}\sum_{i,j}\Big\{\Psi(|\mathbf{x}I^i-\mathbf{x}J_s^j|,QI_c,QJ_s^j)+\Psi(|\mathbf{x}I^i-\mathbf{x}J^j|,QI_c,QI_c)+\Psi(|\mathbf{x}I^i-\mathbf{x}I_s^j|,QI_c,QI_s^j) \\ &\qquad +\Psi(|\mathbf{x}I_s^i-\mathbf{x}J^j|,QI_s^i,QJ_c)+\Psi(|\mathbf{x}I_s^i-\mathbf{x}J_s^j|,QI_s^i,QJ_s^j)+\Psi(|\mathbf{x}J^i-\mathbf{x}J_s^j|,QJ_c,QJ_s^j)\Big\}\end{aligned}$$

The graph of interaction of PCEFF potential is shown in Fig. 2.3. Note that this energy should be minimized subject to charge conservation constraint, which reads,

$$\sum_{I}\sum_{i}\big(QI_c+Q_s^i\big)=0. \quad (2.17)$$

Throughout this work we assume that all charges are fixed.

2.1.2.1 Governing Equilibrium Equations

Here, we obtain the governing equilibrium equations for $\mathbf{x}I^i$, $\mathbf{x}I_s^i$ and QI_s^i. This is done by minimizing the energy with respect to these two (vector and scalar) variables. Our governing equilibrium equations are

$$\delta E\big(\{\mathbf{x}I^i,\mathbf{x}I_s^i,QI_s^i\}\big)=0 \quad \Rightarrow \quad \mathbf{D}_1E=\mathbf{D}_2E=\mathbf{0}, \quad (2.18)$$

Or,

$$\mathbf{f}(\mathbf{x}I^i,\mathbf{x}I_s^i,QI_s^i)=\mathbf{0} \qquad \forall\ i=1,2,...,\ I=1,2,3 \quad (2.19)$$

$$\mathbf{g}(\mathbf{x}I^i,\mathbf{x}I_s^i,QI_s^i)=\mathbf{0} \qquad \forall\ i=1,2,...,\ I=1,2,3 \quad (2.20)$$

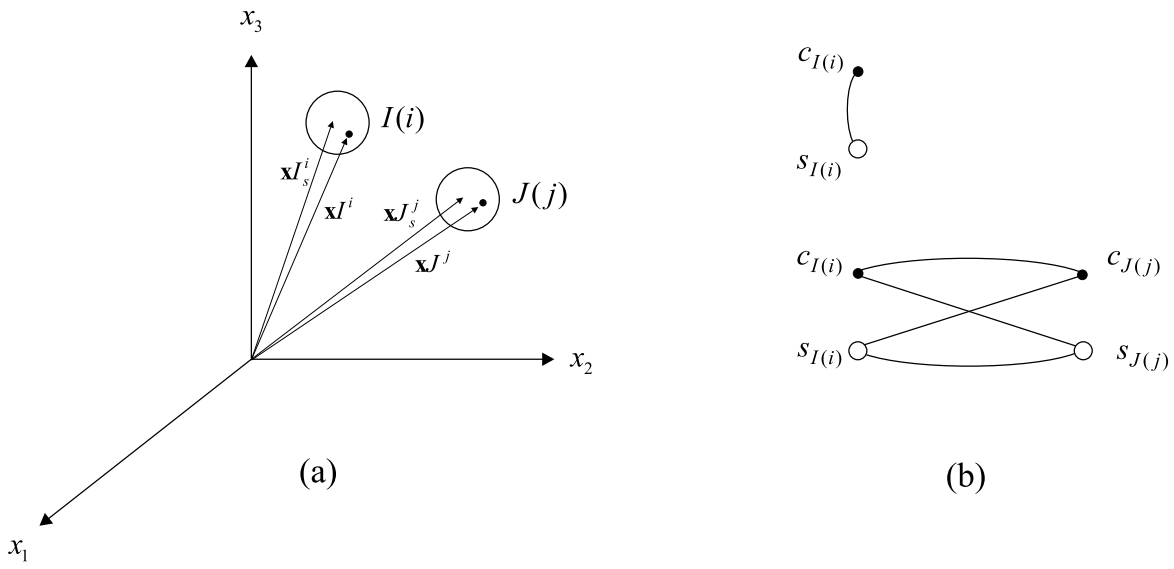

Figure 2.3: (a) Atoms I(i) and J(j) and their position vectors, (b) Four Coulombic interactions between atoms I(i) and J(j). Note that $c_{I(i)} - s_{I(i)}$ interaction should not be counted more than once.

where

$$\begin{aligned} \mathbf{f}(\mathbf{x}I^i, \mathbf{x}I_s^i, QI_s^i) &= \mathbf{D}_1\tilde{E}(\mathbf{x}I^i, \mathbf{x}I_s^i, QI_s^i), \\ \mathbf{g}(\mathbf{x}I^i, \mathbf{x}I_s^i, QI_s^i) &= \mathbf{D}_2\tilde{E}(\mathbf{x}I^i, \mathbf{x}I_s^i, QI_s^i). \end{aligned}$$

2.1.2.2 Linearized Equilibrium Equations

We now linearize the governing equations (2.19) about a reference configuration $\mathcal{B}_0 = (\mathbf{x}I_0^i, \mathbf{x}I_{s0}^i, QI_{s_0}^i)$ as follows,

$$\begin{aligned} \mathbf{f}(\mathbf{x}I_0^i, \mathbf{x}I_{s0}^i, QI_{s_0}^i) &+ \mathbf{D}_1\mathbf{f}(\mathbf{x}I_0^i, \mathbf{x}I_{s0}^i, QI_{s_0}^i) \cdot (\mathbf{x}I^i - \mathbf{x}I_0^i) \\ &+ \mathbf{D}_2\mathbf{f}(\mathbf{x}I_0^i, \mathbf{x}I_{s0}^i, QI_{s_0}^i) \cdot (\mathbf{x}I^i - \mathbf{x}I_0^i) \\ &+ o\left(\|\mathbf{x}I^i - \mathbf{x}I_0^i\|, \|\mathbf{x}I_s^i - \mathbf{x}I_{s0}^i\|, |QI_s^i - QI_{s_0}^i|\right) = 0. \end{aligned} \tag{2.21}$$

Thus

$$\mathbf{D}_1\mathbf{f}(\mathbf{x}I_0^i, \mathbf{x}I_{s0}^i, QI_{s_0}^i) \cdot \mathbf{u}I^i + \mathbf{D}_2\mathbf{f}(\mathbf{x}I_0^i, \mathbf{x}I_{s0}^i, QI_{s_0}^i) \cdot \mathbf{u}I_s^i = -\mathbf{F}(\mathbf{x}I_0^i, \mathbf{x}I_{s0}^i, QI_{s_0}^i) \tag{2.22}$$

where

$$\mathbf{u}I^i = \mathbf{x}I^i - \mathbf{x}I^i_0, \quad \mathbf{u}I^i_s = \mathbf{x}I^i_s - \mathbf{x}I^i_{s0}. \tag{2.23}$$

Similarly,

$$\mathbf{D}_1\mathbf{g}(\mathbf{x}I^i_0, \mathbf{x}I^i_{s0}, QI^i_{s_0}) \cdot \mathbf{u}I^i + \mathbf{D}_2\mathbf{g}(\mathbf{x}I^i_0, \mathbf{x}I^i_{s0}, QI^i_{s_0}) \cdot \mathbf{u}I^i_s = -\mathbf{G}(\mathbf{x}I^i_0, \mathbf{x}I^i_{s0}, QI^i_{s_0}) \tag{2.24}$$

and

$$\mathbf{D}_1 h(\mathbf{x}I^i_0, \mathbf{x}I^i_{s0}, QI^i_{s_0}) \cdot \mathbf{u}I^i + \mathbf{D}_2 h(\mathbf{x}I^i_0, \mathbf{x}I^i_{s0}, QI^i_{s_0}) \cdot \mathbf{u}I^i_s = -H(\mathbf{x}I^i_0, \mathbf{x}I^i_{s0}, QI^i_{s_0}). \tag{2.25}$$

For a given reference configuration, the above equations give a system of linear difference equations for the discrete fields of core and shell position vectors. In the sequel, we will simplify the above equations for a given potential. It will be seen that for a given geometry there are many important details in deriving the governing system of difference equations.

2.2 Energy and Force in Systems Governed by Pairwise Interactions

In this section we explicitly explain some facts about calculating energy and force in a collection of atoms and study the effect of periodicity in calculation of force. In a system governed by pairwise interactions, the potential between two atoms with position vectors $\mathbf{X}_i$ and $\mathbf{X}_j$ is $\Phi(|\mathbf{X}_i - \mathbf{X}_j|)$. The atom energy is defined formally by

$$\mathcal{E}_i = \frac{1}{2} \sum_{\substack{j \in \mathcal{L} \\ j \neq i}} \Phi(|\mathbf{X}_i - \mathbf{X}_j|). \tag{2.26}$$

Note that the $\frac{1}{2}$ factor shows up because each atomic bond is shared by two atoms in the lattice. For now let us assume that the potential is short-ranged and hence all the lattice sums are absolutely convergent.* Consider two systems: (i) A non-periodic system, i.e., an arbitrary collection of atoms $\mathcal{L}$. We are interested in having an expression giving the force on atom $i \in \mathcal{L}$, (ii) We assume that the system is periodic, i.e., one can group the atoms into unit cells with N atoms in each unit cell and repeat the unit cell periodically. In this case we want to have an expression for force on atom i in the unit cell $\mathbf{n} = \mathbf{0} \in \mathcal{L}$. We consider the above two cases separately.

*In Appendix A we review some known results on convergence of lattice sums as we need to have a good understanding of different types of convergence for lattice sums in this thesis.

(i) (***Non-periodic System***) Energy is defined as

$$\mathcal{E}^{\mathsf{np}} = \frac{1}{2} \sum_{\substack{k,j\in\mathcal{L} \\ k\neq j}} \Phi(|\mathbf{X}_j - \mathbf{X}_k|). \tag{2.27}$$

Thus

$$\mathbf{f}_i^{\mathsf{np}} = -\frac{\partial}{\partial \mathbf{X}_i}\mathcal{E}^{\mathsf{np}} = -\frac{1}{2} \sum_{\substack{k,j\in\mathcal{L} \\ k\neq j}} \frac{\partial}{\partial \mathbf{X}_i}\Phi(|\mathbf{X}_j - \mathbf{X}_k|). \tag{2.28}$$

Note that

$$\frac{\partial}{\partial \mathbf{X}_i}\Phi(|\mathbf{X}_j - \mathbf{X}_k|) = \Phi'(|\mathbf{X}_j - \mathbf{X}_k|)\frac{\mathbf{X}_j - \mathbf{X}_k}{|\mathbf{X}_j - \mathbf{X}_k|}(\delta_{ij} - \delta_{ik}) \qquad \text{(no summation)} \tag{2.29}$$

Therefore,

$$\begin{aligned}
\mathbf{f}_i^{\mathsf{np}} &= -\frac{1}{2} \sum_{\substack{k,j\in\mathcal{L} \\ k\neq j}} \Phi'(|\mathbf{X}_j - \mathbf{X}_k|)\frac{\mathbf{X}_j - \mathbf{X}_k}{|\mathbf{X}_j - \mathbf{X}_k|}\ \delta_{ij} + \frac{1}{2} \sum_{\substack{k,j\in\mathcal{L} \\ k\neq j}} \Phi'(|\mathbf{X}_j - \mathbf{X}_k|)\frac{\mathbf{X}_j - \mathbf{X}_k}{|\mathbf{X}_j - \mathbf{X}_k|}\ \delta_{ik} \\
&= -\frac{1}{2} \sum_{\substack{k\in\mathcal{L} \\ k\neq i}} \Phi'(|\mathbf{X}_i - \mathbf{X}_k|)\frac{\mathbf{X}_i - \mathbf{X}_k}{|\mathbf{X}_j - \mathbf{X}_k|} + \frac{1}{2} \sum_{\substack{j\in\mathcal{L} \\ j\neq i}} \Phi'(|\mathbf{X}_j - \mathbf{X}_i|)\frac{\mathbf{X}_j - \mathbf{X}_i}{|\mathbf{X}_j - \mathbf{X}_i|} \\
&= \sum_{\substack{j\in\mathcal{L} \\ j\neq i}} \Phi'(|\mathbf{X}_j - \mathbf{X}_i|)\frac{\mathbf{X}_j - \mathbf{X}_i}{|\mathbf{X}_j - \mathbf{X}_i|}.
\end{aligned} \tag{2.30}$$

(ii) (***Periodic System***) In this case energy can be written as

$$\mathcal{E}^{\mathsf{p}} = \frac{1}{2} \sum_{j,k=1}^{N} {\sum_{\mathbf{n}\in\mathcal{L}}}' \Phi(|\mathbf{r}_j - \mathbf{r}_k + \mathbf{n}|). \tag{2.31}$$

Thus

$$\mathbf{f}_i^{\mathsf{p}} = -\frac{\partial}{\partial \mathbf{r}_i}\mathcal{E}^{\mathsf{p}} = -\frac{1}{2} \sum_{j,k=1}^{N} {\sum_{\mathbf{n}\in\mathcal{L}}}' \frac{\partial}{\partial \mathbf{r}_i}\Phi(|\mathbf{r}_j - \mathbf{r}_k + \mathbf{n}|). \tag{2.32}$$

But,

$$\frac{\partial}{\partial \mathbf{r}_i}\Phi(|\mathbf{r}_j - \mathbf{r}_k + \mathbf{n}|) = \Phi'(|\mathbf{r}_j - \mathbf{r}_k + \mathbf{n}|)\frac{\mathbf{r}_j - \mathbf{r}_k + \mathbf{n}}{|\mathbf{r}_j - \mathbf{r}_k + \mathbf{n}|}(\delta_{ij} - \delta_{ik}) \qquad \text{(no summation)}. \tag{2.33}$$

Therefore,

$$\begin{aligned}
\mathbf{f}_i^{\mathsf{p}} &= -\frac{1}{2} \sum_{j,k=1}^{N} {\sum_{\mathbf{n}\in\mathcal{L}}}' \Phi'(|\mathbf{r}_{jk} + \mathbf{n}|)\frac{\mathbf{r}_{jk} + \mathbf{n}}{|\mathbf{r}_{jk} + \mathbf{n}|}\ \delta_{ij} + \frac{1}{2} \sum_{j,k=1}^{N} {\sum_{\mathbf{n}\in\mathcal{L}}}' \Phi'(|\mathbf{r}_{jk} + \mathbf{n}|)\frac{\mathbf{r}_{jk} + \mathbf{n}}{|\mathbf{r}_{jk} + \mathbf{n}|}\ \delta_{ik} \\
&= -\frac{1}{2} \sum_{k=1}^{N} {\sum_{\mathbf{n}\in\mathcal{L}}}' \Phi'(|\mathbf{r}_{ik} + \mathbf{n}|)\frac{\mathbf{r}_{ik} + \mathbf{n}}{|\mathbf{r}_{ik} + \mathbf{n}|} + \frac{1}{2} \sum_{j=1}^{N} {\sum_{\mathbf{n}\in\mathcal{L}}}' \Phi'(|\mathbf{r}_{ji} + \mathbf{n}|)\frac{\mathbf{r}_{ji} + \mathbf{n}}{|\mathbf{r}_{ji} + \mathbf{n}|}.
\end{aligned} \tag{2.34}$$

Note that

$$-\sum_{k=1}^{N}{\sum_{\mathbf{n}\in\mathcal{L}}}' \Phi'(|\mathbf{r}_{ik}+\mathbf{n}|)\frac{\mathbf{r}_{ik}+\mathbf{n}}{|\mathbf{r}_{ik}+\mathbf{n}|} = \sum_{k=1}^{N}{\sum_{\mathbf{n}\in\mathcal{L}}}' \Phi'(|\mathbf{r}_{ki}-\mathbf{n}|)\frac{\mathbf{r}_{ki}-\mathbf{n}}{|\mathbf{r}_{ki}-\mathbf{n}|}$$
$$= \sum_{k=1}^{N}{\sum_{\mathbf{n}\in\mathcal{L}}}' \Phi'(|\mathbf{r}_{ki}+\mathbf{n}|)\frac{\mathbf{r}_{ki}+\mathbf{n}}{|\mathbf{r}_{ki}+\mathbf{n}|}. \tag{2.35}$$

where use has been made of the fact that if $\mathbf{m}\in\mathcal{L}$ then $-\mathbf{m}\in\mathcal{L}$ by definition of a Bravais lattice. Therefore,

$$\mathbf{f}_i^{\mathsf{p}} = \sum_{j=1}^{N}{\sum_{\mathbf{n}\in\mathcal{L}}}' \Phi'(|\mathbf{r}_{ji}+\mathbf{n}|)\frac{\mathbf{r}_{ji}+\mathbf{n}}{|\mathbf{r}_{ji}+\mathbf{n}|}. \tag{2.36}$$

Note that

$$\sum_{\substack{\mathbf{n}\in\mathcal{L}\\ \mathbf{n}\neq\mathbf{0}}} \Phi'(|\mathbf{n}|)\frac{\mathbf{n}}{|\mathbf{n}|} = \mathbf{0}. \tag{2.37}$$

Thus

$$\mathbf{f}_i^{\mathsf{p}} = \sum_{\substack{j=1\\ j\neq i}}^{N}\sum_{\mathbf{n}\in\mathcal{L}} \Phi'(|\mathbf{r}_{ji}+\mathbf{n}|)\frac{\mathbf{r}_{ji}+\mathbf{n}}{|\mathbf{r}_{ji}+\mathbf{n}|}. \tag{2.38}$$

Lemma 2. *For a collection of atoms governed by a pairwise potential,*

$$\mathbf{f}_i^{np} = \mathbf{f}_i^{p}. \tag{2.39}$$

Proof: Noting that $\mathbf{r}_{ji}+\mathbf{n} = (\mathbf{r}_j+\mathbf{n})-\mathbf{r}_i = \mathbf{X}_j - \mathbf{X}_i$ *one can rewrite (2.36) as*

$$\mathbf{f}_i^{p} = \sum_{\substack{j\in\mathcal{L}\\ j\neq i}} \Phi'(|\mathbf{X}_j-\mathbf{X}_i|)\frac{\mathbf{X}_j-\mathbf{X}_i}{|\mathbf{X}_j-\mathbf{X}_i|} \qquad \square \tag{2.40}$$

Physically this is because the only difference in the definition of the two forces is in that in the periodic case all the atoms equivalent to i move with it and hence do not contribute to the force. In the nonperiodic case each equivalent atom exerts a force on i but because the collection of all the equivalent atoms is a Bravais lattice the sum of these forces is zero.

2.3 Multi-Lattices of ABO_3 Perovskites

In an ABO_3 crystal there are three species. ABO_3 multi-lattice has five simple sublattices. Throughout this analysis we adopt the following identification,

$$\mathrm{A}=1,\ \mathrm{B}=2,\ \mathrm{O1}=3,\ \mathrm{O2}=4,\ \mathrm{O3}=5$$

Table 2.8: Relative position vectors and charges for $\mathfrak{L}^-$ half lattice of $BaTiO_3$.

ID	Elm	$core/shell$	x_1	x_3	x_2	$q(e)$
1	Ba	c	0.0000	0.0000	0.0000	2.0000
1	Ba	s	0.0000	0.0000	-0.0032	-0.3746
1	Ti	c	1.9952	1.9952	2.1197	4.0000
1	Ti	s	1.9952	1.9952	2.0846	-2.2702
1	O	c	1.9952	0.0000	1.9610	2.00000
1	O	s	1.9952	0.0000	1.9592	-3.1025
2	O	c	0.0000	1.9952	1.9610	2.00000
2	O	s	0.0000	1.9952	1.9592	-3.1025
3	O	c	1.9952	1.9952	-0.1596	2.00000
3	O	s	1.9952	1.9952	-0.2317	-3.1503

where O1, O2 and O3 are the three simple lattices of Oxygen. $BaTiO_3$ and $PbTiO_3$ are studied in their tetragonal phases with lattice parameters a = b = 3.9904 Å , c = 4.1030 Å and a = b = 3.9053 Å , c = 4.1514 Å, respectively. The coordinates of atoms in a unit cell and atomic charges in the tetragonal phase are given in Table 2.8 for $BaTiO_3$ and in Table 2.9 (see also Fig. 1.3). Note that this unit cell has $\mathbf{P} = (0, 0, -P_s)$.[†] For a tetragonal unit cell with $\mathbf{P} = (0, 0, P_s)$ the relative displacements of cores and shells in the x_3 for $BaTiO_3$ are,

$$\delta Ba_c = 0.0000\ \mathring{A},\ \delta Ti_c = 0.0682\ \mathring{A},\ \delta O3_c = -0.1596\ \mathring{A},\ \delta O1_c = \delta O2_c = -0.0905\ \mathring{A}$$
$$\delta Ba_s = -0.0032\ \mathring{A},\ \delta Ti_s = 0.0331\ \mathring{A},\ \delta O3_s = -0.2317\ \mathring{A},\ \delta O1_s = \delta O2_s = -0.0923\ \mathring{A}$$

and for $PbTiO_3$,

$$\delta Pb_c = 0.0000\ \mathring{A},\ \delta Ti_c = 0.185696\ \mathring{A},\ \delta O3_c = 0.455469\ \mathring{A},\ \delta O1_c = \delta O2_c = 0.552926\ \mathring{A}$$
$$\delta Pb_s = 0.0826173\ \mathring{A},\ \delta Ti_s = 0.207228\ \mathring{A},\ \delta O3_s = 0.577246\ \mathring{A},\ \delta O1_s = \delta O2_s = 0.535008\ \mathring{A}$$

Note that the above tetragonal structures have been obtained for $T = 0$ and these are just local minima for energies with multiple wells. The multi-lattice of ABO_3 can be defined as

$$\mathcal{L} = \left\{ \mathbf{x} = \nu^1 \mathbf{e}_1 + \nu^2 \mathbf{e}_2 + \nu^3 \mathbf{e}_3 + \mathbf{p}_i, \quad \nu^1, \nu^2, \nu^3 \in \mathbb{Z},\ i = 1, ..., 5 \right\} \tag{2.41}$$

where $\mathbf{e}_i,\ \mathbf{p}_i$ are lattice and shift vectors, respectively. For tetragonal ABO_3,

$$\mathbf{e}_1 = \begin{pmatrix} a \\ 0 \\ 0 \end{pmatrix}, \quad \mathbf{e}_2 = \begin{pmatrix} 0 \\ c \\ 0 \end{pmatrix}, \quad \mathbf{e}_3 = \begin{pmatrix} 0 \\ 0 \\ a \end{pmatrix} \tag{2.42}$$

[†]At the end of this section we will explain how one can calculate P_s for a given unit cell configuration.

and,

$$\mathbf{p}_1 = \begin{pmatrix} 0 \\ 0 \\ 0 \end{pmatrix}, \quad \mathbf{p}_2 = \begin{pmatrix} \frac{a}{2} \\ \frac{c}{2} \\ \frac{a}{2} \end{pmatrix}, \quad \mathbf{p}_3 = \begin{pmatrix} \frac{a}{2} \\ \frac{c}{2} \\ 0 \end{pmatrix}, \quad \mathbf{p}_4 = \begin{pmatrix} 0 \\ \frac{c}{2} \\ \frac{a}{2} \end{pmatrix}, \quad \mathbf{p}_5 = \begin{pmatrix} \frac{a}{2} \\ 0 \\ \frac{a}{2} \end{pmatrix}. \tag{2.43}$$

Fig. 2.4 shows a unit cell with its shift vectors and atom numbers. In this work we will use a shell

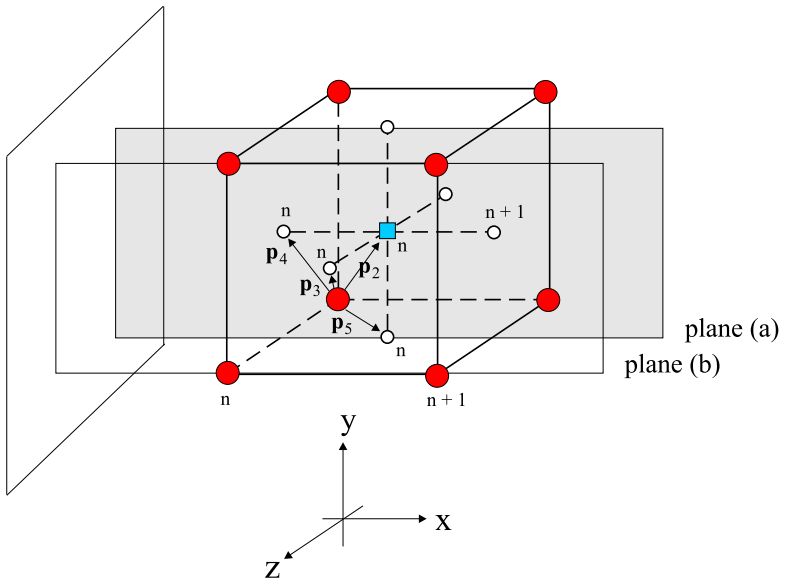

Figure 2.4: A unit cell of ABO_3 with its shift vectors and atom numbers.

model, in which every atom has a core and a shell of electrons that can move independently. This means that for defining the multilattice of cores and shells one needs ten shift vectors. We use the following identification,

$$\{A^c, A^s, ..., O3^c, O3^s\} = \{1, 2, ..., 9, 10\}. \tag{2.44}$$

Table 2.9: Fractional coordinates and core and shell charges for $\mathfrak{L}^-$ half lattice of $PbTiO_3$.

ID	*Elm*	*core/shell*	x_1/a	x_3/a	x_2/c
1	Pb	c	0.0000	0.0000	0.0000
1	Pb	s	0.0000	0.0000	0.0199
1	Ti	c	0.5000	0.5000	0.5447
1	Ti	s	0.5000	0.5000	0.5499
1	O	c	0.5000	0.0000	0.6332
1	O	s	0.5000	0.0000	0.6289
2	O	c	0.0000	0.5000	0.6332
2	O	s	0.0000	0.5000	0.6289
3	O	c	0.5000	0.5000	0.1097
3	O	s	0.5000	0.5000	0.1390

Thus considering an A core site as the origin the shift vectors are,

$$\mathbf{p}_1 = \begin{pmatrix} 0 \\ 0 \\ 0 \end{pmatrix},\ \mathbf{p}_2 = \begin{pmatrix} 0 \\ \delta A_s - \delta A_c \\ 0 \end{pmatrix},\ \mathbf{p}_3 = \begin{pmatrix} \frac{a}{2} \\ \frac{c}{2} + \delta B_c - \delta A_c \\ \frac{a}{2} \end{pmatrix},\ \mathbf{p}_4 = \begin{pmatrix} \frac{a}{2} \\ \frac{c}{2} + \delta B_s - \delta A_c \\ \frac{a}{2} \end{pmatrix},$$
$$\mathbf{p}_5 = \begin{pmatrix} \frac{a}{2} + \delta O1_c - \delta A_c \\ \frac{c}{2} \\ 0 \end{pmatrix},\ \mathbf{p}_6 = \begin{pmatrix} \frac{a}{2} \\ \frac{c}{2} + \delta O1_s - \delta A_c \\ \frac{a}{2} \end{pmatrix},\ \mathbf{p}_7 = \begin{pmatrix} 0 \\ \frac{c}{2} + \delta O2_c - \delta A_c \\ \frac{a}{2} \end{pmatrix}, \quad (2.45)$$
$$\mathbf{p}_8 = \begin{pmatrix} 0 \\ \frac{c}{2} + \delta O2_s - \delta A_c \\ \frac{a}{2} \end{pmatrix},\ \mathbf{p}_9 = \begin{pmatrix} 0 \\ \delta O3_c - \delta A_c \\ \frac{a}{2} \end{pmatrix},\ \mathbf{p}_{10} = \begin{pmatrix} 0 \\ \delta O3_s - \delta A_c \\ \frac{a}{2} \end{pmatrix}.$$

When origin is at a B site one would have similar shift vectors.

2.3.1 Nearest Neighbors in a Multi-Lattice

A given simple Bravais lattice $\mathcal{L}$ is in a one-to-one correspondence with the unit cubic lattice $\mathcal{L}_0$, i.e., $\varphi : \mathcal{L} \to \mathcal{L}_0$, where φ is a bijection. Points of the unit cubic lattice lie on a sequence of spheres with radii $\{R_k\}_{k=1}^{\infty} = \{1, \sqrt{2}, \sqrt{3}, 2, \sqrt{5}, \sqrt{6}, \sqrt{8}, 3, ...\}$. The set of k$th$ nearest neighbors of $\mathbf{x}_0 \in \mathcal{L}_0$ is defined by

$$\mathcal{N}_0^k(\mathbf{x}_0) = \{\mathbf{y} \in \mathcal{L}_0 :\ |\mathbf{y}| = R_k\}. \quad (2.46)$$

The set of kth nearest neighbors of a point $\mathbf{x} \in \mathcal{L}$ can be defined by

$$\mathcal{N}^k(\mathbf{x}) = \mathcal{N}_0^k(\varphi(\mathbf{x})). \quad (2.47)$$

Consider a multilattice $\mathcal{L}$ composed of m simple lattices. This lattice is the disjoint union of m translates of a simple lattice $\mathcal{L}^1$, i.e.,

$$\mathcal{L} = \bigcup_{j=1}^{m} \mathcal{L}^j = \bigcup_{j=1}^{m} (\mathcal{L}^1 + \mathbf{p}_j) \tag{2.48}$$

where $\mathbf{p}_s$'s are the shift vectors and $\mathbf{p}_1 = \mathbf{0}$. The set of k$th$ nearest neighbors of $\mathbf{x} \in \mathcal{L}^i$ is defined by

$$i = 1 \quad : \quad \mathcal{N}_i^k(\mathbf{x}) = \bigcup_{j=1}^{m} \mathcal{N}^k\big(\mathbf{x} + \mathbf{p}_j - \mathbf{p}_i; \mathcal{L}^j\big) \bigcup \big\{\mathbf{x} + \mathbf{p}_1 - \mathbf{p}_i, ..., \hat{\mathbf{x}}, ..., \mathbf{x} + \mathbf{p}_m - \mathbf{p}_i\big\} \tag{2.49}$$

$$i > 1 \quad : \quad \mathcal{N}_i^k(\mathbf{x}) = \bigcup_{j=1}^{m} \mathcal{N}^k\big(\mathbf{x} + \mathbf{p}_j - \mathbf{p}_i; \mathcal{L}^j\big) \tag{2.50}$$

where $\mathcal{N}^k\big(\mathbf{x} + \mathbf{p}_j - \mathbf{p}_i; \mathcal{L}^j\big)$ is the set of kth nearest neighbors of the point $\mathbf{x} + \mathbf{p}_j - \mathbf{p}_i$ in the simple lattice $\mathcal{L}^j$ and the hat in $\hat{\mathbf{x}}$ means that $\mathbf{x}$ is not considered in the union. Fig. 2.5 shows the set of first three nearest neighbors for point $\mathbf{x}$ in a two-dimensional multi-lattice with $m = 2$. We will see in the sequel that because of the discrete translation symmetry in defect-free 180° and 90° domain walls (and also free surfaces and steps) one may reduce the governing equations. For the reduced system, there will not be any ambiguity in defining nearest neighbors.

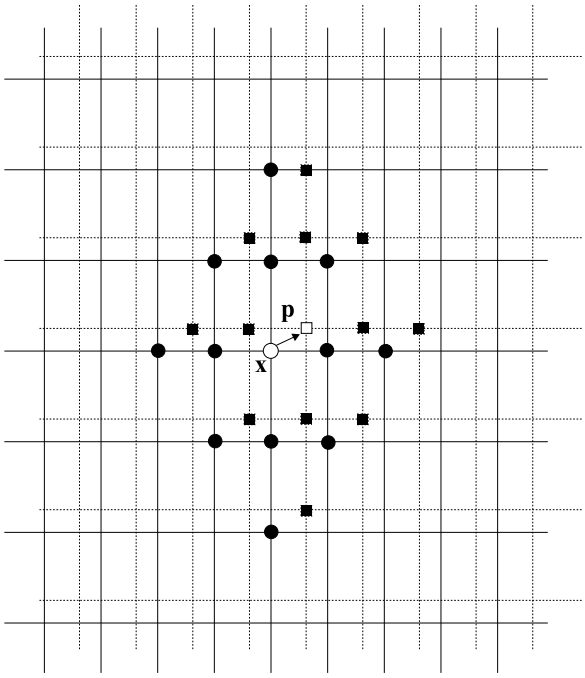

Figure 2.5: The set of first three neighbors for the atom $\mathbf{x}$.

2.3.2 Macroscopic Polarization

Macroscopic polarization is an important quantity that is directly seen in Maxwell's equations. This quantity is not well-defined for an infinite crystal. Macroscopic polarization cannot be defined as the dipole moment of the unit cell. The reason is that infinitely many unit cells can define the same lattice and, in general, the dipole moments of different unit cells of the same crystal are different.

Example 3. *Let us consider a simple 1-D periodic distribution of electric charge with the following charge distribution,*

$$q(x) = q_0 \sin \frac{2\pi x}{a} \tag{2.51}$$

We can have the following one-parameter family of unit cells,

$$[\epsilon, \epsilon + a) \qquad \epsilon \in [0, a] \tag{2.52}$$

The unit cell dipole is

$$p = \int_{\epsilon}^{\epsilon+a} xq(x)dx \tag{2.53}$$

It can be easily shown that

$$\frac{dp}{d\epsilon} = q_0 a \sin \frac{2\pi x_0}{a} \neq 0 \tag{2.54}$$

This means that the unit cell dipole depends on ϵ, i.e., the unit cell dipole explicitly depends on the unit cell.

It turns out that macroscopic polarization has a quantum mechanical nature (see King-Smith and Vanderbilt (1989) and Resta (2003)). The well-defined macroscopic quantity is $\Delta\mathbf{P}$, i.e., difference of $\mathbf{P}$ for two given states of the crystal and only this difference is an observable (can be measured). Saying that macroscopic polarization in the cubic phase of ABO_3 is zero is just a convention because the absolute bulk polarization has never been experimentally measured (Resta, 1994). The macroscopic polarization of the tetragonal phase is defined as the difference of macroscopic polarizations of the tetragonal and cubic phases. For the tetragonal ABO_3 in the bulk polarization is defined as

$$\mathbf{P} := \Delta\mathbf{P}\,(\text{cubic}, \text{tetragonal}) = \sum_{i=1}^{10} Q_i(\mathbf{r}_i - \mathbf{r}_i^0) \tag{2.55}$$

where $\mathbf{r}_i$ is the position vector of the charge Q_i in the tetragonal unit cell (for example, the Ba-centered tetragonal unit cell given in Table. 2.8). $\mathbf{r}_i^0$ is the corresponding position vector in the symmetric tetragonal configuration. Using the identification $\{A_c, A_s, B_c, B_s, O1_c, O1_s, O2_c, O2_s, O3_c, O3_s\} =$

$\{1, ..., 10\}$ we have

$$\begin{aligned}
\mathbf{r}_1^0 &= \mathbf{r}_2^0 = \{0, 0, 0\} \\
\mathbf{r}_3^0 &= \mathbf{r}_4^0 = \left\{\frac{a}{2}, \frac{c}{2}, \frac{a}{2}\right\} \\
\mathbf{r}_5^0 &= \mathbf{r}_6^0 = \left\{\frac{a}{2}, \frac{c}{2}, 0\right\} \\
\mathbf{r}_7^0 &= \mathbf{r}_8^0 = \left\{0, \frac{c}{2}, \frac{a}{2}\right\} \\
\mathbf{r}_9^0 &= \mathbf{r}_{10}^0 = \left\{\frac{a}{2}, 0, \frac{a}{2}\right\}
\end{aligned} \tag{2.56}$$

Defining polarization near a domain wall (or any other defect) in the lattice scale is always ambiguous and there are different possibilities for choosing the unit cells that support the polarization. We will come back to this when we solve the 180° and 90° domain wall problems.

2.4 Long-Range Forces

These are forces that come from Coulombic interactions. The usual practice is to first assume a periodic system and find an expression for energy of a unit cell using Ewald summation technique and then find the force vectors by taking the appropriate partial derivatives. We are interested in energy (and forces) of the reference configuration (forces that push the unrelaxed reference configuration to relax). It is known that the unit cell should be charge neutral to get a finite energy (de Leeuw et al., 1980). We choose a unit cell centered at an A core site and containing N=10 charges (five cores and five charges). This unit cell is charge neutral as can be directly checked from the data in Table 2.8, for example. Assuming that each unit cell is a lattice site, we will have a simple tetragonal lattice of unit cells and denote it by $\mathfrak{L}$. It should be noted that, for a 180° domain wall, this lattice has three types of unit cells in terms of internal coordinates $\mathbf{r}_{ij}$ of charges in each unit cell. These are unit cells on the right side of the domain wall, unit cell on the domain wall and unit cells on the left side of the domain wall. This can be expressed by the following partitioning of $\mathfrak{L}$,

$$\mathfrak{L} = \mathfrak{L}^+ \sqcup \mathfrak{L}^0 \sqcup \mathfrak{L}^- \tag{2.57}$$

We are interested in calculating $\mathbf{f}^i = -\frac{\partial \mathcal{E}}{\partial \mathbf{x}^i}(\mathcal{B}_0)$, where $\mathcal{E}$ is the electrostatic energy of the unit cell containing the atom i. We know that

$$\text{SC potetial} \quad : \quad \mathcal{E} = \frac{1}{2} \sum_{\mathbf{n} \in \mathfrak{L}} {}' \sum_{j,k=1}^{N} \frac{Q_j Q_k}{|\mathbf{r}_{jk}(\mathbf{n}) + \mathbf{n}|} \tag{2.58}$$

$$\text{PCEFF potebtial} \quad : \quad \mathcal{E} = \frac{1}{2} \sum_{\mathbf{n} \in \mathfrak{L}} {}' \sum_{j,k=1}^{N} \frac{Q_j Q_k \text{erf}(\beta_{jk} |\mathbf{r}_{jk}(\mathbf{n}) + \mathbf{n}|)}{|\mathbf{r}_{jk}(\mathbf{n}) + \mathbf{n}|} \tag{2.59}$$

Thus

$$\text{SC potetial} \quad : \quad \frac{\partial \mathcal{E}}{\partial \mathbf{x}^i} = \frac{1}{2} \sum_{\mathbf{n} \in \mathfrak{L}} {}' \sum_{j=1}^{N} Q_i Q_j \frac{\partial}{\partial \mathbf{x}^i} \frac{Q_j Q_k}{|\mathbf{r}_{ij}(\mathbf{n}) + \mathbf{n}|} \tag{2.60}$$

$$\text{PCEFF potebtial} \quad : \quad \frac{\partial \mathcal{E}}{\partial \mathbf{x}^i} = \frac{1}{2} \sum_{\mathbf{n} \in \mathfrak{L}} {}' \sum_{j=1}^{N} Q_i Q_j \frac{\partial}{\partial \mathbf{x}^i} \frac{Q_j Q_k \text{erf}(\beta_{jk} |\mathbf{r}_{jk}(\mathbf{n}) + \mathbf{n}|)}{|\mathbf{r}_{ij}(\mathbf{n}) + \mathbf{n}|} \tag{2.61}$$

Note that the unit-cell energy as defined above does not make sense. In other words, the lattice sums defining the unit-cell energy are conditionally convergent. This means that some information is missing and simply having the position of charges in an indefinite system is not enough for calculating the unit-cell energy unambiguously. The appearance of conditionally convergent lattice sums in energy calculations is due to surface charges.

2.4.1 Wolf's Method for PCEFF-Potential

In a recent paper, Wolf et al. (Wolf et al., 1999) studied the Madelung problem by direct summation. Earlier Wolf (Wolf, 1992),(Wolf, 1995) had observed that the effective Coulombic potential of ions in condensed systems is short-ranged and falls off as r^{-5}. Based on this and similar observations by others, Wolf et al. (1999) developed a numerical method for calculating the Madelung energy by direct summation in direct space. Their idea is to consider spherical shells of increasing radii and calculate the electrostatic energy of corresponding neutralized spherical balls. It is assumed that the total charge of a given spherical ball is concentrated on its boundary sphere instead of in a layer of thickness equal to the length of the shift vector (for a multilattice of two simple lattices like NaCl). For NaCl lattice, they numerically show that the sequence of energies of the neutralized spherical balls approaches to the Madelung energy of the infinite lattice in an oscillatory way. They show that neutralizing a spherical ball is equivalent to radially projecting every charge inside the ball on the boundary sphere with the opposite charge. However, they do not mention the fact that their projection is not unique and putting the neutralizing charges anywhere on the sphere gives the same Madelung energy. The important thing to note is that forces (and higher derivatives of energy) depend on the position of neutralizing charges and it is not clear to us why Wolf's projection should give the correct forces.[‡] This method is very attractive as it does not assume any (artificial) periodicity. However, this method ignores the effect of surface charge distribution.

The shortcoming of Wolf et al.'s (Wolf et al., 1999) work is that it is tested only for simple multi-lattices like NaCl and only for spherical geometry. It is not clear if this method can be used for an arbitrary multilattice of charges and for other geometries. It would also be interesting to know what happens if one considers cubic shells instead of spherical shells, for example. The most

[‡]The numerical tests show that this projection gives the correct forces but the convergence is very poor. This will be numerically shown for $BaTiO_3$ and $PbTiO_3$ in this chapter.

serious problem is the lack of a rigorous proof of energy convergence in this method.

Let us first briefly review this method for PCEFF potential. We will compare the results with full Ewald summation later. Consider a charge i with position vector $\mathbf{x}^i$ (this could be a core or a shell charge) and a spherical shell with radius R_c. We consider only those charges that lie inside the sphere. In general, the collection of charges inside the sphere is not charge neutral. The energy of ion i for the cut-off radius R_c is

$$\mathcal{E}_i(R_c) = \frac{1}{2} \sum_{\substack{j \neq i \\ |\mathbf{x}_{ij}| < R_c}} \frac{Q_i Q_j \ \mathrm{erf}(\beta_{ij} |\mathbf{x}_{ij}|)}{|\mathbf{x}_{ij}|} \tag{2.62}$$

where $\mathbf{x}_{ij} = \mathbf{x}_i - \mathbf{x}_j$ is the relative position vector. It should be noted that this energy does not converge to the correct Madelung energy as $R_c \to \infty$ because of the lack of charge neutrality. Wolf et al. (1999) resolve this by considering a sequence of charge-neutralized spheres. It is assumed that the net charge is concentrated on the boundary of the sphere. The neutralized potential can be written as

$$\mathcal{E}_i^{\mathrm{neut.}}(R_c) = \frac{1}{2} \sum_{\substack{j \\ |\mathbf{x}_{ij}| < R_c}} \frac{Q_i Q_j \ \mathrm{erf}(\beta_{ij} R_c)}{R_c} \tag{2.63}$$

Note that this includes the term $i = j$. Also note that

$$\Delta Q_i(R_c) = \sum_{\substack{j \\ |\mathbf{x}_{ij}| < R_c}} Q_j \tag{2.64}$$

and each Q_j interacts with Q_i by a different potential (because of different charge distributions for different species). Neutralizing a given sphere is equivalent to radially projecting each charge on the sphere with the opposite sign. To be able to calculate the forces due to the neutralizing potential, the neutralizing potential should be rewritten as

$$\mathcal{E}_i^{\mathrm{neut.}}(R_c) = \lim_{|\mathbf{x}_{ij}| \to R_c} \frac{1}{2} \sum_{\substack{j \neq i \\ |\mathbf{x}_{ij}| < R_c}} \frac{Q_i Q_j \ \mathrm{erf}(\beta_{ij} |\mathbf{x}_{ij}|)}{|\mathbf{x}_{ij}|} + \frac{Q_i^2 \ \mathrm{erf}(\beta_{ij} R_c)}{2R_c}$$

Therefore the electrostatic energy of the charge i is

$$\mathcal{E}_i^{\mathrm{tot.}}(R_c) = \frac{1}{2} \sum_{\substack{j \neq i \\ |\mathbf{x}_{ij}| < R_c}} \frac{Q_i Q_j \ \mathrm{erf}(\beta_{ij} |\mathbf{x}_{ij}|)}{|\mathbf{x}_{ij}|} - \lim_{|\mathbf{x}_{ij}| \to R_c} \frac{1}{2} \sum_{\substack{j \neq i \\ |\mathbf{x}_{ij}| < R_c}} \frac{Q_i Q_j \ \mathrm{erf}(\beta_{ij} |\mathbf{x}_{ij}|)}{|\mathbf{x}_{ij}|} - \frac{Q_i^2 \ \mathrm{erf}(\beta_{ij} R_c)}{2R_c}$$

Now, for example, force on charge i can be written as

$$\mathbf{f}^i = -\frac{1}{2} \sum_{\substack{j\neq i \\ |\mathbf{x}_{ij}|<R_c}} \frac{\partial}{\partial \mathbf{x}^i} \frac{Q_i Q_j \ \mathrm{erf}(\beta_{ij}|\mathbf{x}_{ij}|)}{|\mathbf{x}_{ij}|} + \lim_{|\mathbf{x}_{ij}|\to R_c} \frac{1}{2} \sum_{\substack{j\neq i \\ |\mathbf{x}_{ij}|<R_c}} \frac{\partial}{\partial \mathbf{x}^i} \frac{Q_i Q_j \ \mathrm{erf}(\beta_{ij}|\mathbf{x}_{ij}|)}{|\mathbf{x}_{ij}|}$$

2.4.2 Damped Wolf's Method

We first explain the damped Wolf's method for the classical Coulombic potential and then generalize it for PCEFF potential and numerically investigate its validity. We also numerically study the energy and force convergence for $PbTiO_3$ lattice using the SC classical shell potential. In this method the complementary error function is used as the damping function. The only reason for choosing this function, besides the required properties it has, is that this is the same damping function used in the classical Ewald summation method. The energy of the i*th* charge can be written as

$$\mathcal{E}^i = \frac{1}{2} \sum_{j\neq i} \frac{Q_i Q_j \ \mathrm{erfc}(\alpha|\mathbf{x}_{ij}|)}{|\mathbf{x}_{ij}|} + \frac{1}{2} \sum_{j\neq i} \frac{Q_i Q_j \ \mathrm{erf}(\alpha|\mathbf{x}_{ij}|)}{|\mathbf{x}_{ij}|} \tag{2.65}$$

where α is a damping parameter. Now the idea is to decompose the energy into two parts such that one part is negligible. The above decomposition does not have this property because the second term becomes very large for large values of α. However adding the term corresponding to $i = j$ and subtracting it from the first term would make (2.67) what we need. Thus

$$\mathcal{E}^i_{\mathrm{sphere}}(R_c) \approx \frac{1}{2} \sum_{\substack{j\neq i \\ |\mathbf{x}_{ij}|<R_c}} \frac{Q_i Q_j \ \mathrm{erfc}(\alpha|\mathbf{x}_{ij}|)}{|\mathbf{x}_{ij}|} - \frac{\alpha}{\sqrt{\pi}} Q_i^2 \tag{2.66}$$

The neutralizing energy is

$$\mathcal{E}^i_{\mathrm{neut}}(R_c) = \frac{1}{2} \frac{Q_i \Delta Q_i(R_c) \mathrm{erfc}(\alpha R_c)}{R_c} = \frac{1}{2} \lim_{|\mathbf{x}_{ij}|\to R_c} \sum_{\substack{j\neq i \\ |\mathbf{x}_{ij}|<R_c}} \frac{Q_i Q_j \ \mathrm{erfc}(\alpha|\mathbf{x}_{ij}|)}{|\mathbf{x}_{ij}|} + \frac{\mathrm{erfc}(\alpha R_c)}{2R_c} Q_i^2$$

Therefore, the energy for a cut-off radius R_c is

$$\mathcal{E}^i(R_c) = \frac{1}{2} \sum_{\substack{j\neq i \\ |\mathbf{x}_{ij}|<R_c}} \Big[\frac{Q_i Q_j \ \mathrm{erfc}(\alpha|\mathbf{x}_{ij}|)}{|\mathbf{x}_{ij}|} - \lim_{|\mathbf{x}_{ij}|\to R_c} \frac{Q_i Q_j \ \mathrm{erfc}(\alpha|\mathbf{x}_{ij}|)}{|\mathbf{x}_{ij}|} \Big] - \Big(\frac{\mathrm{erfc}(\alpha R_c)}{2R_c} + \frac{\alpha}{\sqrt{\pi}} \Big) Q_i^2$$

Similarly for PCEFF-potential we have

$$\mathcal{E}^i = \frac{1}{2} \sum_{j\neq i} \frac{Q_i Q_j \ \big[\mathrm{erfc}(\alpha|\mathbf{x}_{ij}|) - \mathrm{erfc}(\beta_{ij}|\mathbf{x}_{ij}|)\big]}{|\mathbf{x}_{ij}|} + \frac{1}{2} \sum_{j\neq i} \frac{Q_i Q_j \ \mathrm{erf}(\alpha|\mathbf{x}_{ij}|)}{|\mathbf{x}_{ij}|} \tag{2.67}$$

The neutralizing energy for PCEFF potential is

$$\mathcal{E}^i_{\text{neut}}(R_c) = \frac{1}{2} \lim_{|\mathbf{x}_{ij}|\to R_c} \sum_{\substack{j\neq i \\ |\mathbf{x}_{ij}|<R_c}} \frac{Q_iQ_j\ [\text{erfc}(\alpha|\mathbf{x}_{ij}|) - \text{erfc}(\beta_{ij}R_c)]}{|\mathbf{x}_{ij}|} + \frac{\text{erfc}(\alpha R_c) - \text{erfc}(\beta_{ii}R_c)}{2R_c} Q_i^2 \tag{2.68}$$

Thus

$$\mathcal{E}^i(R_c) = \frac{1}{2} \sum_{\substack{j\neq i \\ |\mathbf{x}_{ij}|<R_c}} \Big[\frac{Q_iQ_j\ \big[\text{erfc}(\alpha|\mathbf{x}_{ij}|) - \text{erfc}(\beta_{ij}|\mathbf{x}_{ij}|)\big]}{|\mathbf{x}_{ij}|} - \lim_{|\mathbf{x}_{ij}|\to R_c} \frac{Q_iQ_j\big[\text{erfc}(\alpha|\mathbf{x}_{ij}|) - \text{erfc}(\beta_{ij}|\mathbf{x}_{ij}|)\big]}{|\mathbf{x}_{ij}|}\Big]$$
$$- \Big(\frac{\text{erfc}(\alpha R_c) - \text{erfc}(\beta_{ii}R_c)}{2R_c} + \frac{\alpha}{\sqrt{\pi}}\Big) Q_i^2 \tag{2.69}$$

2.4.3 Comparison Between Wolf and Ewald Methods

It is not clear if Wolf's method agrees with Ewald summation technique for an arbitrary crystal. Wolf et al. (1999) studied their method carefully for NaCl and a few other simple crystals. We repeated the same calculations for NaCl and were able to reproduce the same results. To see the effect of the number of sulattices in a multi-lattice of charges, we calculated the Madelung's constant of CaF_2 using Wolf and Ewald methods and obtained the same results. It should be noted that in Ewald's method the dipole energy is ignored for centrosymmetric crystals (see Deem et al. (1990) for a theoretical justification). In all our numerical tests (even for the noncentrosymmetric $BaTiO_3$ with shifted shells) Wolf's method converges to Ewald energy without the dipole energy term. However, the convergence is very poor as will be seen shortly.

Assuming that the surrounding medium is a conductor the dipole energy part of Ewald can be ignored. All the calculations for fitting the energy parameters of $BaTiO_3$ are based on this assumption (Goddard et al., 2003). It is known that Ewald method corresponds to summing the conditionally convergent lattice by shells which have zero dipole (Harris, 1975). But it is not clear to us how this relates to Wolf charge-neutralized spheres. Wolf's method in its present form makes every spherical shell charge neutral but not dipole free, in general. One should note that for neutralizing a given sphere for each charge q inside the sphere a charge $-q$ should be put on the sphere. The position of the charge $-q$ is immaterial in calculating the Madelung energy. However, position of the neutralizing charge affects the force values. It is not clear to us why the projection proposed by Wolf et al. (Wolf et al., 1999) should be the right one.[§]

Now we present a simple modification of Wolf's method that makes a spherical shell both charge neutral and dipole free. Consider a given lattice point with charge q_0. We like to calculate the energy of this charge (half of the energy of all the bonds that are incident to this charge). Consider

[§]A rigorous proof is missing here.

a spherical shell of radius R_c centered at q_0. It is again assumed that the net charge is distributed on the boundary of the sphere. The projection proposed by Wolf et al. (1999) is shown in Fig. 2.6a. As was explained before, every charge inside the sphere is projected radially on the sphere boundary and is given the opposite sign. A charge $-q_0$ is also put on an arbitrary point of the boundary of the sphere. This transformation makes the sphere charge neutral but, in general, not dipole free. Our modified projection is shown in Fig. 2.6b. Instead of projecting a given charge on one point on the sphere boundary, we project it to two antipodal points corresponding to the position of the charge q_i and assume that there are two charges αq_i and βq_i at these two points and find α and β such that

$$(\alpha+\beta)q_i + q_i = 0, \qquad q_i\mathbf{x}_i + \alpha q_i \frac{R_c}{|\mathbf{x}_i|}\mathbf{x}_i - \beta q_i \frac{R_c}{|\mathbf{x}_i|}\mathbf{x}_i = \mathbf{0} \tag{2.70}$$

This gives us

$$\alpha = -\frac{1}{2}\Big(\frac{|\mathbf{x}_i|}{R_c}+1\Big), \qquad \beta = \frac{1}{2}\Big(\frac{|\mathbf{x}_i|}{R_c}-1\Big) \tag{2.71}$$

Two charges of magnitude $-\frac{q_0}{2}$ are put on two arbitrary antipodal points. Now, it is clear that the transformed system of charges is both charge neutral and dipole free. Our numerical tests show that for a centrosymmetric crystal this modified method gives the same force values as Wolf et al.'s give. But, for noncentrosymmetric crystals, our modified method does not give the correct forces.¶

We have performed the following numerical tests for tetragonal $BaTiO_3$ and $PbTiO_3$.

- ***$BaTiO_3$***: The convergence of the unit cell energy in the bulk tetragonal phase using Ewald, Wolf and damped Wolf is shown in Fig. 2.7. The convergence of energy for the usual Wolf method, i.e., taking charge neutralized spheres is very poor; the cut-off radius should be about 15 lattice spacings to get reasonable results. The damped method (for $\alpha < 0.4$) converges very nicely but for $\alpha > 0.6$ or 0.8, the energy converges to a wrong value. Ewald's idea is to add and subtract a distributed charge for each charge in the lattice. Adding a Gaussian distribution of opposite charge leads to a lattice sum of complementary error functions which can be easily calculated in the real (direct) space (as it is absolutely convergent with a very good rate of convergence). The other charge distribution, which has the same sign as the point charges, is another absolutely convergent lattice sum that is summed in the reciprocal lattice because of its poor rate of convergence. If α is very small, i.e., if the distributed charges are very flat, the part in the reciprocal lattice is extremely small and can be ignored. We believe damped Wolf method is nothing but Ewald without the reciprocal space part. The dependence on α shows that this method is not robust and should be carefully tested for a given crystal system. We compared damped Wolf with Ewald without Fourier part and they are almost the same for cut-off radii larger than $3a$. We think the reason is that the contribution of neutralizing

¶This is interesting and should be studied more carefully. One would be interested to see if there is a relation between this and the Ewald clusters in the direct space.

charges to energy is $O(1/R_c)$ and becomes very small for large R_c. So, we do not believe there is anything profound about damped Wolf method but still it can be a useful method if used carefully. The other thing that we should not forget is that in Ewald method there is a shape-dependent term that reflects the long-range nature of interactions and also depends on boundary conditions. Wolf's method, in its present form, does not have any shape-dependent and/or boundary condition-dependent terms. An interesting thing to be noted is the fact that unlike NaCl lattice (that was the case study in Wolf's papers), convergence is not oscillatory. This could mean that geometry of the lattice has some effects. A detailed study of electrostatic

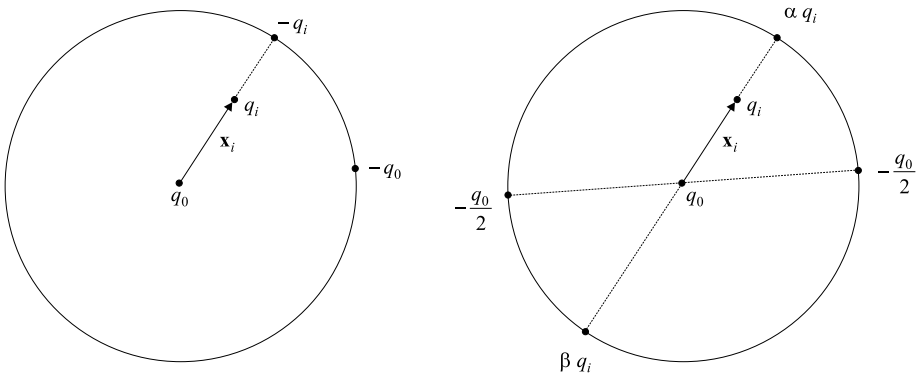

Figure 2.6: (a) Wolf projection of charges inside a sphere of radius R_c. (b) A modified projection.

forces in the bulk tetragonal using Ewald and the usual Wolf are shown in Fig. 2.8. All the shell and core forces are shown. Note that two of the oxygens have the same forces in the bulk due to symmetry. Again, Wolf's method has a very poor convergence behavior and even after taking the cut-off radius of $R_c = 16a$, forces do not converge to the correct values. The same study for damped Wolf ($\alpha = 0.2$) is shown in Fig 2.9. This time convergence is excellent and taking $R_c = 5a$ is enough. Again, large values of α will lead to incorrect force values.

- ***PbTiO*$_3$**: We performed similar numerical tests for $PbTiO_3$. The calculated unit-cell energy using Wold's method, Ewald and damped Wolf's method for different values of the damping parameter are compared in Fig. 2.10. It is interesting that in damped Wolf's method energy is very sensitive to the damping parameter and there is a very small interval of α that gives the correct energy. The optimum values is $\alpha \simeq 0.01$. Similar to $BaTiO_3$, Wolf's method does not have a good convergence as the calculated energy does not converge to its correct values even for $R_c = 14a$. The other thing to note is that convergence is not oscillatory.

  Pb core forces calculated using Wolf, Ewald and damped Wolf are compared in Fig. 2.11. Here a larger interval of α is acceptable and the optimum value is $\alpha \simeq 0.2$. Wolf's method is very slowly convergent and hence not practically useful.

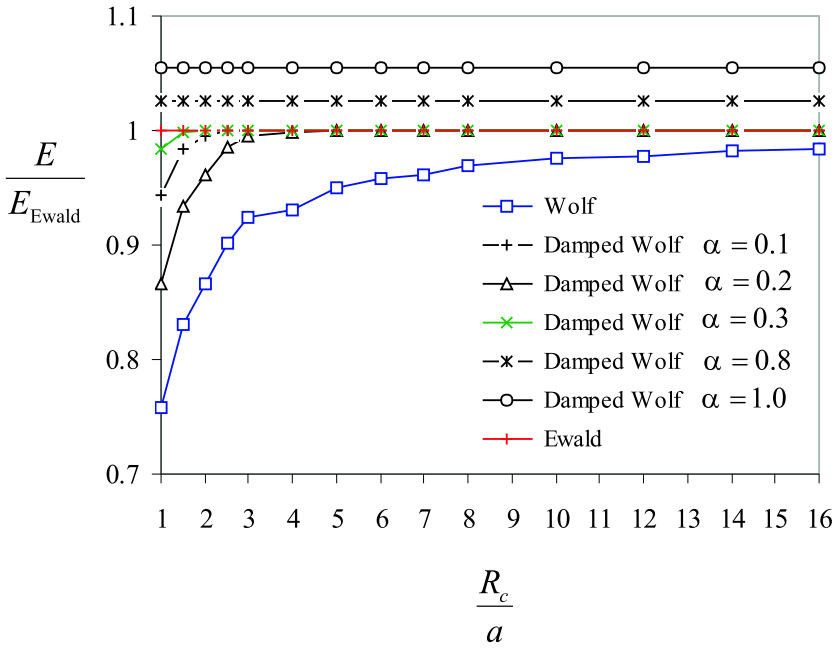

Figure 2.7: Wolf energy convergence for $BaTiO_3$ unit cell.

2.5 Structure Optimization

In this section we explain in some detail how we optimized the structure of tetragonal $PbTiO_3$ given the shell potential parameters. We also discuss the stability check of the optimized structure.

2.5.1 Molecular Mechanics

Born-Oppenheimer (BO) approximation is implicitly used in molecular mechanics. BO approximation states that for a molecule the Schrodinger equation can be separated into two parts, one describing the motion of electrons and one describing the motion of nuclei and that these two sets of motions can be studied independently. In molecular mechanics electrons are not explicitly examined and only the motion of nuclei is studied; it is assumed that electrons find an optimum distribution about the nuclei. The potential energy surface (or Born-Oppenheimer surface) is a manifold that describes the energy of the molecule in terms of the position of nuclei. In the case of shell models some average position of electrons is considered too. In molecular mechanics one starts from a set of empirically derived functions for the potential energy function. This set of potential functions are called force fields that contain some adjustable parameters, which are optimized to obtain the best fit of experimental (or quantum-mechanically calculated) properties of the molecules, like structure, heat of formation, lattice parameters, etc. (see Carlsson (1990) and Gale (1996) for more details).

Many problems are tractable with interatomic potentials but too complex to be treated with

quantum-mechanical methods. One application of an empirical potential energy function is in finding the geometry of a molecule that corresponds to a local minimum of the potential energy. The process of finding local minima of an empirical potential energy function is called *molecular mechanics*. It should be noted that the potential energy function refers to a ground state of the molecule. This means that the potential energy function does not explicitly deal with the electronic structure. Given a potential energy function, one usually looks for local minima which make sense physically, e.g., the ones that are close to the experimental data. In general the energy landscape could be very complicated and finding the global minimum may be very difficult. Unless the potential energy has one well, the optimized geometry obtained depends on the starting configuration. Most optimization codes find the local minima. In some applications one would be even more interested in some local minima that are not the global minimum. This may be the case in understanding metastable states or energy barrier for moving from one equilibrium state to another one. For more details on molecular mechanics and different issues in structure optimization see Burkert and Allinger (1982) and Wales (2003).

In general the energy of a given collection of atoms $\mathcal{L}$ has the following form,

$$\mathcal{E}\left(\{\mathbf{x}^i\}\right) = \sum_{i\in\mathcal{L}} \phi_1(\mathbf{x}^i) + \frac{1}{2}\sum_{i,j\in\mathcal{L}} \phi_2(\mathbf{x}^i,\mathbf{x}^j) + \frac{1}{6}\sum_{i,j,k\in\mathcal{L}} \phi_3(\mathbf{x}^i,\mathbf{x}^j,\mathbf{x}^k) + ... \tag{2.72}$$

Considering only the first two terms the resulting potential is called a pair potential. Considering three-body interactions (or higher interactions) the potential is called a cluster potential (Carlsson, 1990). Note that a cluster potential is not the most general form of the total configurational energy. One could use environment-dependent potentials in some application (Carlsson, 1990). For many molecules considering two body interactions is enough. In shell models all the potential functions are pairwise (two-body) and also isotropic (i.e., explicitly depend on the relative distance between cores and shells). However, each atom is composed of a core and a shell that interact with other cores and shells independently. This is somehow a correction for the many body nature of interactions of charges.

Given a shell model one needs to find the optimized structure of the ground state. We briefly explain this process for $PbTiO_3$ using the SC potential. For fixed experimental lattice parameters $a = b = 3.9053\mathring{A}$ and $c = 4.1514\mathring{A}$, the unit cell energy is a function of the variable $\mathbf{x} \in \mathbb{R}^7$ defined as

$$\mathbf{x} = \{\delta_s Pb, \delta Ti, \delta_s Ti, \delta O1, \delta_s O1, \delta O3, \delta_s O3\} \tag{2.73}$$

where the origin is the Pb core and the symmetries $\delta O1 = \delta O2$ and $\delta_s O1 = \delta_s O2$ have been used. Thus

$$E_{\text{cell}} = E_{\text{cell}}(\mathbf{x}) \tag{2.74}$$

The unit cell energy E_{cell} has a short-range part and a long-range part. The long-range part is calculated using the Ewald method. The unit cell force is defined as

$$\mathbf{f}_{\text{cell}} = -\frac{\partial E_{\text{cell}}}{\partial \mathbf{x}} \tag{2.75}$$

In the optimized structure $\mathbf{f}_{\text{cell}} = \mathbf{0}$. We use the Newton-Raphson iteration method for finding the optimized structure. Starting from an initial guess $\mathbf{x}_0$[‖],

$$\mathbf{x}_{k+1} = \mathbf{x}_k - \mathbf{H}_k^{-1}\mathbf{f}_k \qquad k \geq 0 \tag{2.76}$$

where $\mathbf{H}_k$ is the Hessian matrix in the kth iteration and is defined as

$$\mathbf{H} = \frac{\partial^2 E_{\text{cell}}}{\partial \mathbf{x} \partial \mathbf{y}} \in \mathbb{R}^{7\times 7} \tag{2.77}$$

The expressions and the method of derivation of force and Hessian in electrostatic systems are given in Appendix A. The optimized structure is given in Table 2.9 and agrees with what GULP (Gale, 1997),(Gale and Rohl, 2003) predicts. The Hessian of the optimized structure is positive-definite with the following eigenvalues (in units of $\frac{eV}{\mathring{A}^2}$),

$$\text{Eigenvalues}(\mathbf{H}) = \{2853.000, 202.402, 133.276, 63.8607, 20.467, 10.849, 0.896\} \tag{2.78}$$

This is the same structure that Sirpiensky et al. (private communication) obtained. The structure optimization was performed under the tetragonal constraint. We observed that Hessian of the optimized structure is not positive-definite if arbitrary perturbations are allowed (i.e., when $\mathbf{H} \in \mathbb{R}^{27\times 27}$). This means that we have to do all the calculations under the constraint that all the displacements are in the tetragonal c-direction. We have not been able to find an interatomic potential that is completely stable. However, all the formulations and implementations are general and do not need any constraints.

[‖]In molecular calculations this initial guess is chosen to be close to experimental data if there is any. The reason is that the energy landscape might be extremely complicated. For $PbTiO_3$ we chose different initial guesses and did not see any sensitivity to the initial guess.

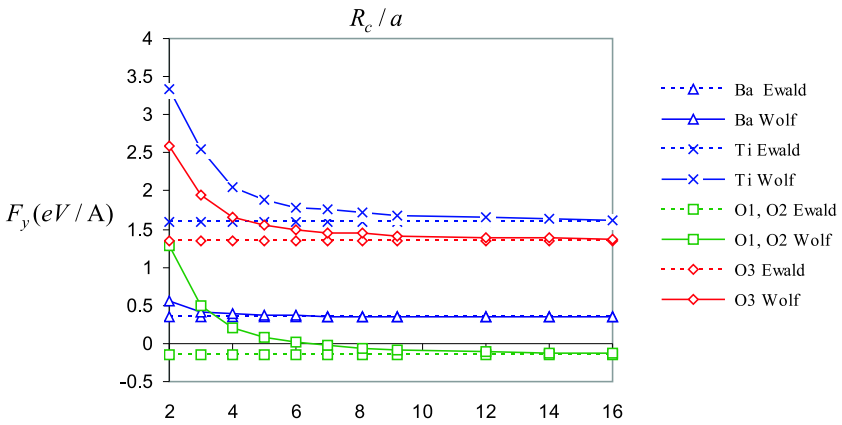

(a)

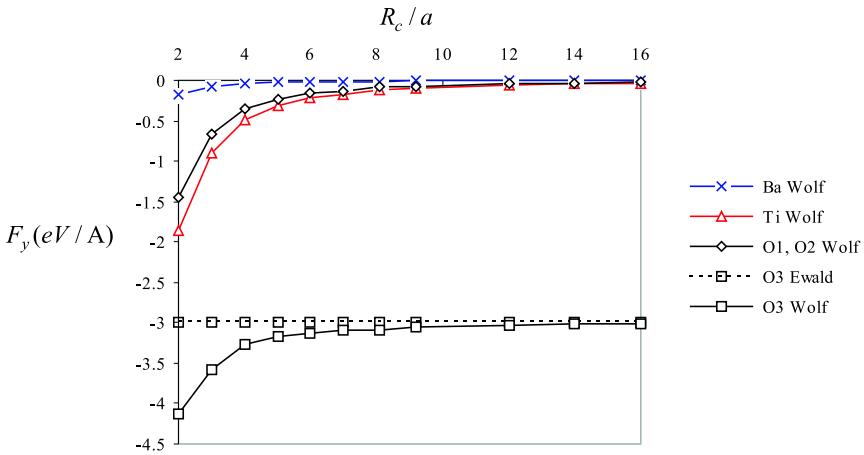

(b)

Figure 2.8: (a) Ewald and Wolf core electrostatic forces in $BaTiO_3$, (b) Ewald and Wolf shell electrostatic forces in $BaTiO_3$.

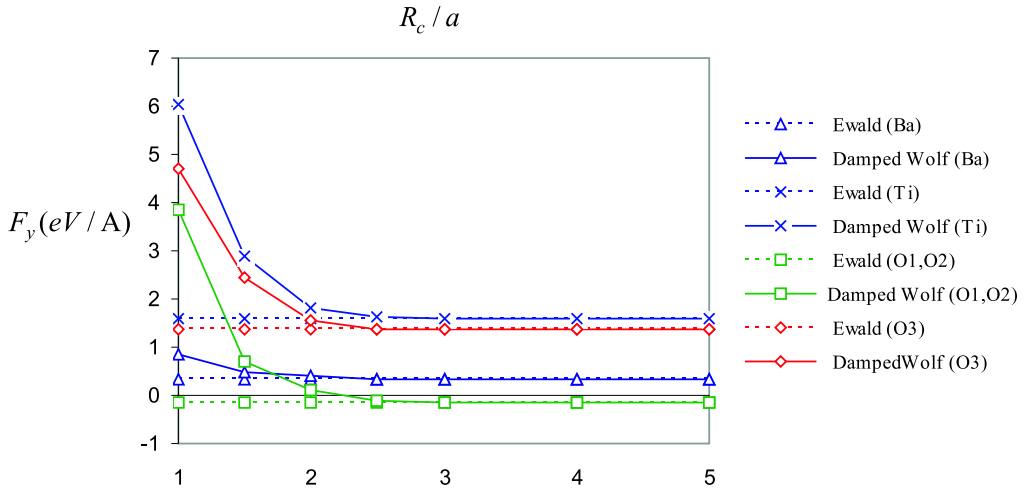

(a)

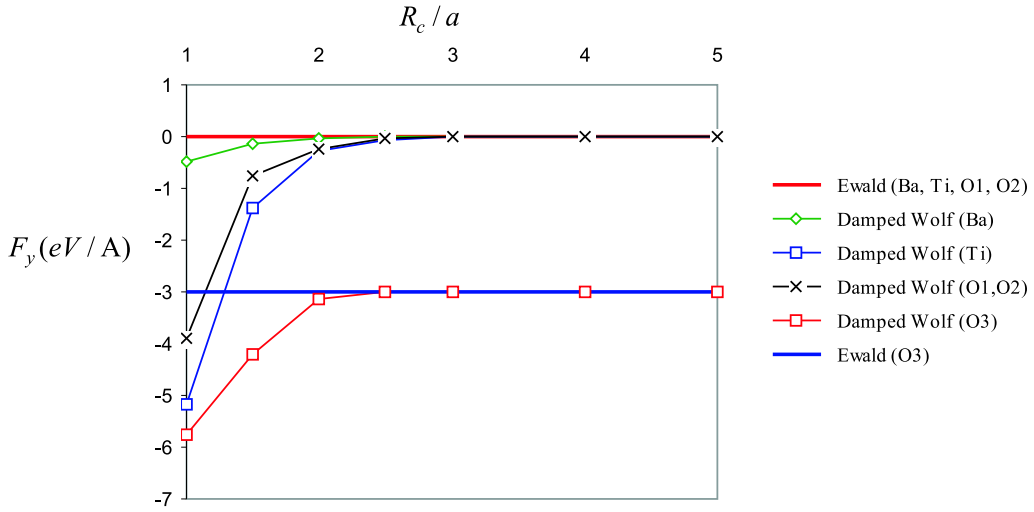

(b)

Figure 2.9: (a) Ewald and damped Wolf ($\alpha = 0.2$) core electrostatic forces, (b) Ewald and Wolf ($\alpha = 0.2$) shell electrostatic forces.

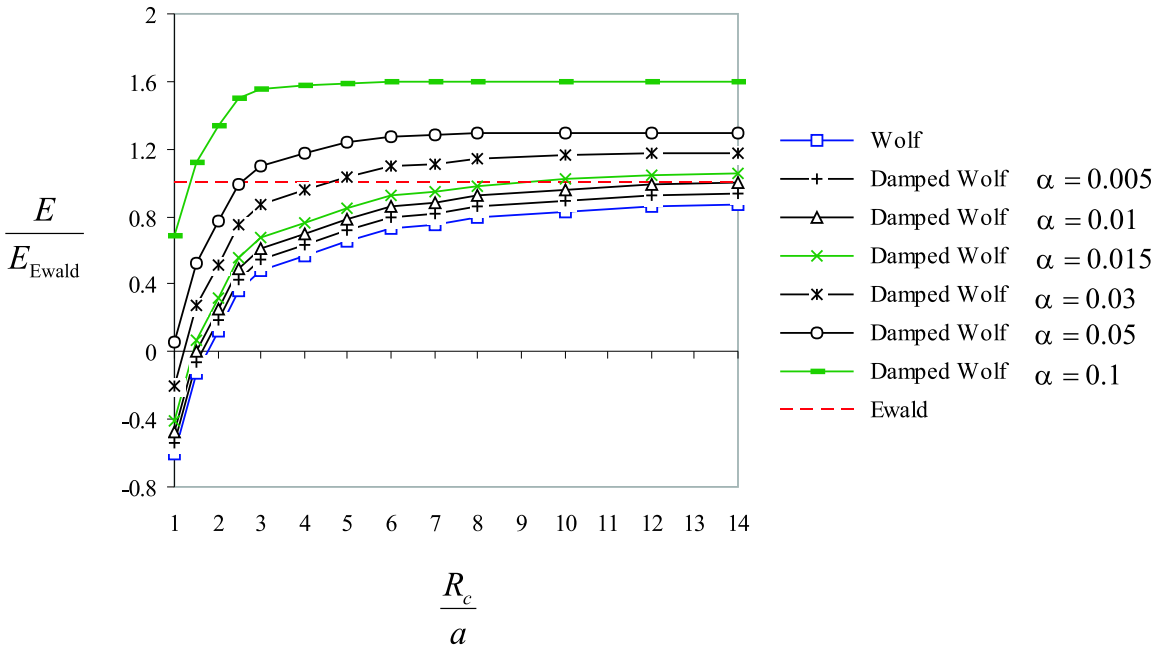

Figure 2.10: Unit cell electrostatic energy in $PbTiO_3$ using Ewald, Wolf and damped Wolf methods.

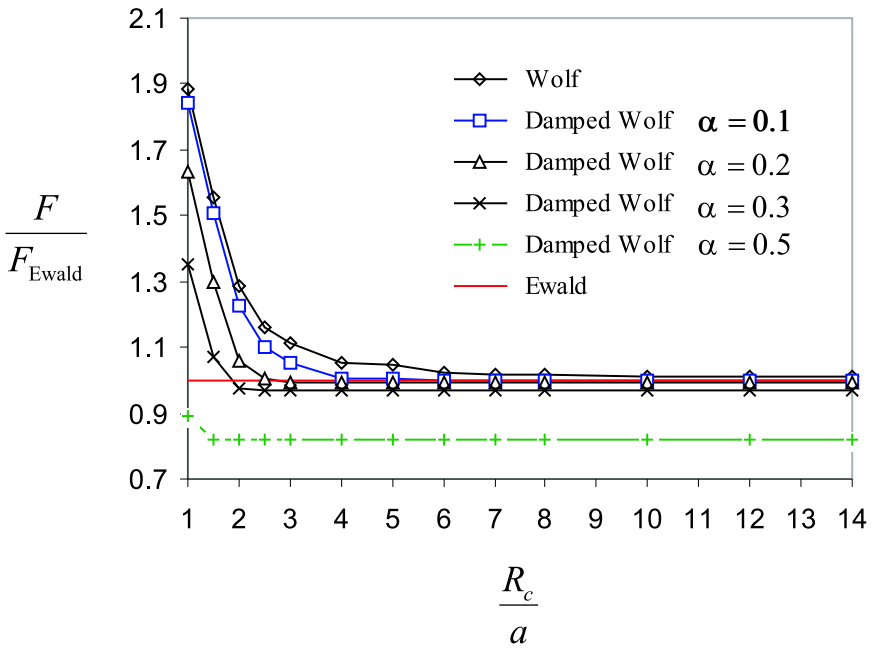

Figure 2.11: Pb core force in tetragonal direction in $PbTi_3$.

Chapter 3

Discrete Governing Equations

In this chapter we discuss the method of construction of the discrete governing equations. We use Mathematica for the symbolic and numerical calculations. First we find the coefficients of the governing difference equations for an atom which is far enough from the domain wall (or any other defect) such that all the interacting neighbors are on one side of the wall. This will give us all the global governing difference equations. We will find the boundary equations later. Suppose we are given a collection of atoms $\mathcal{L}$.

Definition 4. *Atom energy $\mathcal{E}^i$ for a given atom $i \in \mathcal{L}$ is one half of the energy of all those atomic bonds that are incident to i.*

Definition 5. *For an atom $i \in \mathcal{L}$ the neighboring set $\mathcal{S}_i$ is the set of all the atoms in $\mathcal{L}$ that interact with i. Note that $i \notin \mathcal{S}_i$, i.e., there are no self interactions.*

Note that

$$\mathcal{E}^i = \mathcal{E}^i \left(\mathbf{x}^i, \{\mathbf{x}^j\}_{j\in\mathcal{S}_i}\right) \tag{3.1}$$

The total energy is a function of the atomic positions (for now we are looking only at short-range interactions),

$$\mathcal{E} = \mathcal{E} \left(\{\mathbf{x}^j\}_{j\in\mathcal{L}}\right) \tag{3.2}$$

Suppose the position of a given atom is $\mathbf{x}^i$. Assuming that there are no discrete body forces, equilibrium of this atom is equivalent to minimizing the total energy with respect to its position, i.e,

$$\frac{\partial \mathcal{E}}{\partial \mathbf{x}^i} = \mathbf{0} \qquad \forall i \in \mathcal{L} \tag{3.3}$$

It can be easily shown that this is equivalent to minimizing the energy of the atom $\mathcal{E}^i$ with respect to $\mathbf{x}^i$, i.e.,

$$\frac{\partial \mathcal{E}^i}{\partial \mathbf{x}^i} \left(\mathbf{x}^i, \{\mathbf{x}^j\}_{j\in\mathcal{S}_i}\right) = \mathbf{0} \tag{3.4}$$

Suppose we are given a defective crystal for which the reference configuration $\mathcal{L}$ can be partitioned

into some equivalence classes. We assume that for our two-dimensional defect (a domain wall for example) $\mathcal{L}$ can be partitioned into two-dimensional equivalence classes, i.e., infinite sets of atoms that lie on some planes. This is not the only possibility but is general enough for now.* The neighboring set $\mathcal{S}_i$ can be partitioned as

$$\mathcal{S}_i = \bigcup_{\alpha=-m}^{m} \bigcup_{I=1}^{5} \mathcal{S}_{I\alpha} \tag{3.5}$$

where $\mathcal{S}_{I\alpha}$ is the subset of all the atoms of the same type and index, $I \in \{1,2,3,4,5\}$ represents the atom type and $\alpha \in \{-m,...,m\}$ represents the nearest neighbor index. For the sake of clarity, we work with $m = 2$ and then generalize the results. Taylor expansion of the governing equations for atom i about the reference configuration $\mathcal{B}_0 = \left(\mathbf{x}_0^i, \{\mathbf{x}_0^j\}_{i\in\mathcal{L}}\right)$, Eq. (3.3) reads,

$$\frac{\partial \mathcal{E}}{\partial \mathbf{x}^i} = \frac{\partial \mathcal{E}}{\partial \mathbf{x}^i}(\mathcal{B}_0) + \frac{\partial^2 \mathcal{E}^i}{\partial \mathbf{x}^i \partial \mathbf{x}^i}(\mathcal{B}_0)(\mathbf{x}^i - \mathbf{x}_0^i) + \sum_{j\in\mathcal{S}_i} \frac{\partial^2 \mathcal{E}^i}{\partial \mathbf{x}^i \partial \mathbf{x}^j}(\mathcal{B}_0)(\mathbf{x}^j - \mathbf{x}_0^j) + ... = \mathbf{0} \tag{3.6}$$

Note that

$$\sum_{j\in\mathcal{S}_i} \frac{\partial^2 \mathcal{E}^i}{\partial \mathbf{x}^i \partial \mathbf{x}^j}(\mathcal{B}_0)(\mathbf{x}^j - \mathbf{x}_0^j) = \sum_{\alpha=-2}^{2}{}' \sum_{I=1}^{5} \sum_{J\beta\in\mathcal{S}_{I\alpha}} \frac{\partial^2 \mathcal{E}^i}{\partial \mathbf{x}^i \partial \mathbf{x}^{J\beta}}(\mathcal{B}_0)\left(\mathbf{x}^{J\beta} - \mathbf{x}_0^{J\beta}\right) \tag{3.7}$$

where the prime on the first sum means that the term $\alpha = 0, I = i$ is excluded because by definition $i \notin \mathcal{S}_i$, i.e., there are no self interactions. Also note that in the above sum each mixed partial derivative of the energy $\mathcal{E}^i$ represents only one term, which is nothing but the derivative of the pair potential representing the interaction of atoms i and j.

Lemma 6. *For a system governed by pairwise interactions,*

$$\frac{\partial^2 \mathcal{E}^i}{\partial \mathbf{x}^i \partial \mathbf{x}^i}(\mathcal{B}_0) = -\sum_{j\in\mathcal{S}_i} \frac{\partial^2 \mathcal{E}^i}{\partial \mathbf{x}^i \partial \mathbf{x}^j}(\mathcal{B}_0) \tag{3.8}$$

Proof: Note that

$$\frac{\partial \mathcal{E}}{\partial \mathbf{x}^i} = \sum_{j\in\mathcal{S}_i} \mathbf{\Psi}(\mathbf{x}^i, \mathbf{x}^j) \tag{3.9}$$

where

$$\mathbf{\Psi}(\mathbf{x}^i, \mathbf{x}^j) = \Phi'(|\mathbf{x}^i - \mathbf{x}^j|)\frac{\mathbf{x}^i - \mathbf{x}^j}{|\mathbf{x}^i - \mathbf{x}^j|} \tag{3.10}$$

*Later we will have a 2-D symmetry reduction for a 180° step in $PbTiO_3$.

Thus

$$\frac{\partial^2 \mathcal{E}}{\partial \mathbf{x}^i \partial \mathbf{x}^i} = \sum_{j \in \mathcal{S}_i} \frac{\partial}{\partial \mathbf{x}^i} \mathbf{\Psi}(\mathbf{x}^i, \mathbf{x}^j) \tag{3.11}$$

$$\frac{\partial^2 \mathcal{E}}{\partial \mathbf{x}^i \partial \mathbf{x}^j} = \sum_{j \in \mathcal{S}_i} \frac{\partial}{\partial \mathbf{x}^j} \mathbf{\Psi}(\mathbf{x}^i, \mathbf{x}^j) \tag{3.12}$$

But,

$$\begin{aligned} \frac{\partial}{\partial \mathbf{x}^i} \mathbf{\Psi}(\mathbf{x}^i, \mathbf{x}^j) &= \Phi''(|\mathbf{x}^i - \mathbf{x}^j|) \frac{(\mathbf{x}^i - \mathbf{x}^j) \otimes (\mathbf{x}^i - \mathbf{x}^j)}{|\mathbf{x}^i - \mathbf{x}^j|^2} + \frac{\Phi'(|\mathbf{x}^i - \mathbf{x}^j|)\ \mathbf{1}}{|\mathbf{x}^i - \mathbf{x}^j|} \\ &\quad -\Phi'(|\mathbf{x}^i - \mathbf{x}^j|) \frac{(\mathbf{x}^i - \mathbf{x}^j) \otimes (\mathbf{x}^i - \mathbf{x}^j)}{|\mathbf{x}^i - \mathbf{x}^j|^3} \end{aligned} \tag{3.13}$$

And,

$$\frac{\partial}{\partial \mathbf{x}^j} \mathbf{\Psi}(\mathbf{x}^i, \mathbf{x}^j) = -\frac{\partial}{\partial \mathbf{x}^i} \mathbf{\Psi}(\mathbf{x}^i, \mathbf{x}^j) \qquad \square \tag{3.14}$$

Linearization of the discrete governing equations about the reference configuration $\mathcal{B}_0$ means that only terms up to quadratic should be kept. This gives us the following system of linear difference equations,

$$\sum_{\alpha=-2}^{2}{}' \sum_{I=1}^{5} \mathbf{K}_{iI\alpha} \mathbf{u}^{I\alpha} + \left(- \sum_{\alpha=-2}^{2}{}' \sum_{I=1}^{5} \mathbf{K}_{iI\alpha} \right) \mathbf{u}^i = \mathbf{f}_i \tag{3.15}$$

where

$$\begin{aligned} \mathbf{K}_{iI\alpha} &= \sum_{J\beta \in \mathcal{S}_{I\alpha}} \frac{\partial^2 \mathcal{E}^i}{\partial \mathbf{x}^i \partial \mathbf{x}^{J\beta}} (\mathcal{B}_0) \\ \mathbf{f}_i &= -\frac{\partial \mathcal{E}^i}{\partial \mathbf{x}^i} (\mathcal{B}_0) \\ \mathbf{u}^{I\alpha} &= \mathbf{x}^{I\alpha} - \mathbf{x}_0^{I\alpha} = \mathbf{x}^{J\beta} - \mathbf{x}_0^{J\beta} \qquad \forall\ J\beta \in \mathcal{S}_{I\alpha} \end{aligned} \tag{3.16}$$

Prime on the second sum in (3.15) means that the term $\alpha = 0, I = i$ is omitted. Note that the symmetry of 180° and 90° domain walls implies that atoms of the same type that lie on a plane parallel to the domain wall are all equivalent. In other words, a planar defect (a 180° or 90° here) leaves the translation invariance of the lattice in y and z directions (yz is the plane of the defect) unchanged. This means that there is a discrete group of translations that partitions the lattice into equivalence classes. This implies that atoms in the same equivalence class contribute to the same stiffness matrix. Note also that to calculate $\mathbf{K}_{iI\alpha}$, contributions from atoms of the same type and index will add up. That is why two summations appear in the Taylor expansion. Also note that considering first and second nearest neighbors in the reduced 1-D system (for $m = 2$), there are twenty five $\mathbf{K}_{iI\alpha}$ and twenty five $\mathbf{u}^{I\alpha}$ and that $\mathbf{u}^i, \mathbf{u}^{I\alpha}, \mathbf{f}_i \in \mathbb{R}^3$ and $\mathbf{K}_{iI\alpha} \in \mathbb{R}^{3\times 3}$. In general, for interactions of order m, there are $5(2m+1)$ submatrices and five force vectors.

Let us define a vector $\mathbf{X}_n \in \mathbb{R}^{15}$,

$$\mathbf{X}_n = \begin{pmatrix} \mathbf{x}1_n & ... & \mathbf{x}5_n \end{pmatrix}^{\mathsf{T}} \tag{3.17}$$

where n is the atomic index (unit cell number) defined above. In the end, we will need to solve a system of linear difference equations with constant coefficients with the following form.

$$\sum_{\alpha=-m}^{\alpha=m} \mathcal{A}_\alpha \mathbf{X}_{n+\alpha} = \mathbf{F}_n \qquad , |n| \geq m+2 \tag{3.18}$$

where $\mathcal{A}_\alpha \in \mathbb{R}^{15\times 15},\ \alpha = -m, ..., m$ and $\mathbf{F}_n \in \mathbb{R}^{15},\ \ \forall n \in \mathbb{N}$. Note that, in general, $\mathcal{A}_\alpha$ need not be symmetric as will be explained shortly. The above system of difference equations is a Volterra system of difference equations (see Elaydi (1996))[†].

The relation between $\mathbf{K}_{iI\alpha}$ and, for example, $\mathcal{A}_{-1}$ and $\mathcal{A}_0$ of Eq. (3.18) is[‡]

$$\mathcal{A}_{-2}^{\text{short}} = \begin{pmatrix} \mathbf{K}_{11\text{-}2} & \mathbf{K}_{12\text{-}2} & \mathbf{K}_{13\text{-}2} & \mathbf{K}_{14\text{-}2} & \mathbf{K}_{15\text{-}2} \\ \mathbf{K}_{21\text{-}2} & \mathbf{K}_{22\text{-}2} & \mathbf{K}_{23\text{-}2} & \mathbf{K}_{24\text{-}2} & \mathbf{K}_{25\text{-}2} \\ \mathbf{K}_{31\text{-}2} & \mathbf{K}_{32\text{-}2} & \mathbf{K}_{33\text{-}2} & \mathbf{K}_{34\text{-}2} & \mathbf{K}_{35\text{-}2} \\ \mathbf{K}_{41\text{-}2} & \mathbf{K}_{42\text{-}2} & \mathbf{K}_{43\text{-}2} & \mathbf{K}_{44\text{-}2} & \mathbf{K}_{45\text{-}2} \\ \mathbf{K}_{51\text{-}2} & \mathbf{K}_{52\text{-}2} & \mathbf{K}_{53\text{-}2} & \mathbf{K}_{54\text{-}2} & \mathbf{K}_{55\text{-}2} \end{pmatrix}$$

$$\mathcal{A}_0^{\text{short}} = \begin{pmatrix} \mathbf{K}_{110} & \mathbf{K}_{120} & \mathbf{K}_{130} & \mathbf{K}_{140} & \mathbf{K}_{150} \\ \mathbf{K}_{210} & \mathbf{K}_{220} & \mathbf{K}_{230} & \mathbf{K}_{240} & \mathbf{K}_{250} \\ \mathbf{K}_{310} & \mathbf{K}_{320} & \mathbf{K}_{330} & \mathbf{K}_{340} & \mathbf{K}_{350} \\ \mathbf{K}_{410} & \mathbf{K}_{420} & \mathbf{K}_{430} & \mathbf{K}_{440} & \mathbf{K}_{450} \\ \mathbf{K}_{510} & \mathbf{K}_{520} & \mathbf{K}_{530} & \mathbf{K}_{540} & \mathbf{K}_{550} \end{pmatrix}$$

This can be verified by direct expansion of Eq. (3.15). Also,

$$\mathbf{F}_n = \begin{pmatrix} -\mathbf{f}_A \\ -\mathbf{f}_B \\ -\mathbf{f}_{O1} \\ -\mathbf{f}_{O2} \\ -\mathbf{f}_{O3} \end{pmatrix} \tag{3.19}$$

[†]As will become clearer in the sequel, lattice statics analysis of ferroelectric domain walls will lead to the solution of vector-valued ordinary difference equations with variable coefficient matrices. Inhomogeneities are localized and the idea is to treat the inhomogeneous region as boundary and transition regions. This will result in two vector-valued difference equations with constant coefficient matrices one forward and one backward. In the end, the original difference equation will be solved by matching the solutions of these two ordinary difference equations.

[‡]Construction of these stiffness matrices is very much like what is called direct stiffness assembly in structural mechanics.

There are some subtleties in calculating the $\mathcal{A}_\alpha$ matrices. Some interactions should be ignored. One is the interaction of an atom of type I and index n with all atoms of type I and index n, i.e., there are no interactions within a given equivalence class (this is nothing but a restatement of $i \notin \mathcal{S}_i$). This means that $\mathcal{A}_0^{\text{short}}$ has a special structure. When position of atom i of type I changes, all its equivalent atoms, i.e., those with $\alpha = 0$ undergo the same perturbation. Atoms of the same type as i do not contribute to energy of i because the potential is pairwise and their relative distances from the atom i are always the same. This means that

$$\mathbf{K}_{II0} = -\sum_{\alpha=-2}^{2}{}' \sum_{\substack{J=1 \\ J\neq I}}^{5} \mathbf{K}_{IJ\alpha} \tag{3.20}$$

The same thing is true for forcing terms. The reason for this is that the distance between the equivalent atoms is fixed and the equivalent atoms of i do not contribute to $-\frac{\partial \mathcal{E}^i}{\partial \mathbf{x}^i}$ and its derivatives. The other subtlety is the following. Consider atoms with index n and project the whole crystal (with a domain wall) on a line perpendicular to the domain wall (parallel to x axis). We have the picture shown in Fig. 3.1 for A and O2 atoms. We consider the interaction of A and O2 atoms with other

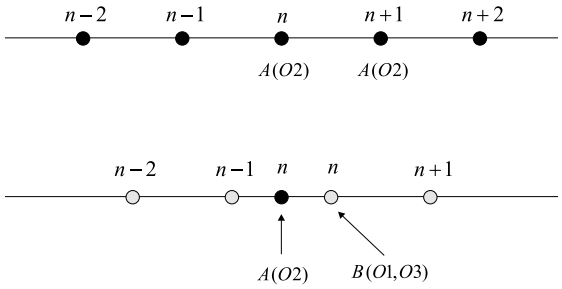

Figure 3.1: Nearest neighbors of A and O2 atoms and their indices.

A and O2 atoms of indices $\{n-m, ..., n+m\}$ (except the one that have already been excluded). Looking at Fig. 3.1, one can see that symmetry of interactions dictates that interactions of A and O2 atoms with O1, O2 and O3 atoms with index $n+m$ should be ignored. Similarly, consider atoms B, O2 or O3 with index n and their nearest neighbors as shown in Fig. 3.2. Every atom B (O1 or O3) interacts with B, O1 and O3 atoms with index $\{n-m, ..., n+m\}$ (except the one that have already been excluded). Again, symmetry implies that the interactions of B, O1 and O3 atoms with A and O2 atoms with index $n-m$ should be ignored. The other interesting subtlety is the symmetry of $\mathcal{A}_\alpha$ matrices. It should be noted that each $\mathbf{K}_{iI\alpha}$ is symmetric but the matrices $\mathcal{A}_\alpha$ ($\alpha = -m, ..., m$) are not symmetric. This can be seen more clearly in a simple 2-D model. Consider a 2-D rectangular multi-lattice composed of two simple lattices each with lattice parameters a and c and the shift vector $\mathbf{p} = (p_1, p_2)$. This system has three coefficient matrices $\mathcal{A}_{-1}, \mathcal{A}_0, \mathcal{A}_1 \in \mathbb{R}^{4\times 4}$. We now compare

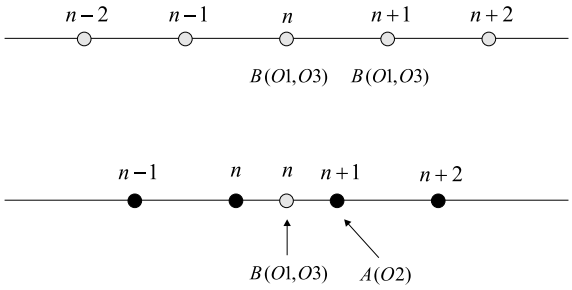

Figure 3.2: Nearest neighbors of B, O1 and O3 atoms and their indices.

$\mathbf{K}_{12\text{-}1}$ and $\mathbf{K}_{21\text{-}1}$ to see if $\mathcal{A}_{\text{-}1}$ is symmetric. It can be easily shown that

$$\mathbf{K}_{12\text{-}1} = \sum_{Y\{n-1\}} \frac{\partial^2 E}{\partial \mathbf{x}_{n-1} \partial \mathbf{y}_{n-1}}(\mathcal{B}_0) \tag{3.21}$$

$$\mathbf{K}_{21\text{-}1} = \sum_{X\{n-1\}} \frac{\partial^2 E}{\partial \mathbf{y}_{n-1} \partial \mathbf{x}_{n-1}}(\mathcal{B}_0) \tag{3.22}$$

where $X\{n-1\}$ is the set of atoms of type 1 which have index $n-1$ relative to the atom n of type 2 (these are the black circles in Fig. 3.3). Similarly, $Y\{n-1\}$ is the set of atoms of type 2 which have index $n-1$ relative to the atom n of type 1 (these are the black squares in Fig. 3.3). $\mathbf{x}_{n-1}$ and $\mathbf{y}_{n-1}$ are position vectors of atoms of types 1 and 2 with index $n-1$, respectively. As it is seen in Fig. 3.3, these two matrices are not equal as the length of the corresponding relative position vectors are not equal. It should be noted that the lose of symmetry in the reduced 1-D system is just a consequence of symmetry reduction and still the underlying 3-D physical system is symmetric.

As was mentioned earlier, starting from an interatomic potential one does not need to worry about the symmetries of the force constants. Here we check one of the symmetries. Suppose all the atoms in the lattice have the same displacements, i.e.,

$$\mathbf{X}_n = \mathbf{C} = \begin{pmatrix} \mathbf{c} & \mathbf{c} & \mathbf{c} & \mathbf{c} & \mathbf{c} \end{pmatrix}^{\mathsf{T}}, \qquad \mathbf{c} \in \mathbb{R}^3 \tag{3.23}$$

Using Eq. (3.20), it can be easily shown that

$$\sum_{\alpha=-m}^{\alpha=m} \mathcal{A}_\alpha \mathbf{C} = \mathbf{0} \qquad \forall \mathbf{c} \in \mathbb{R}^3 \tag{3.24}$$

i.e.,

$$\text{Nullity}\Big(\sum_{\alpha=-m}^{\alpha=m} \mathcal{A}_\alpha \Big) = 3 \tag{3.25}$$

as was expected.

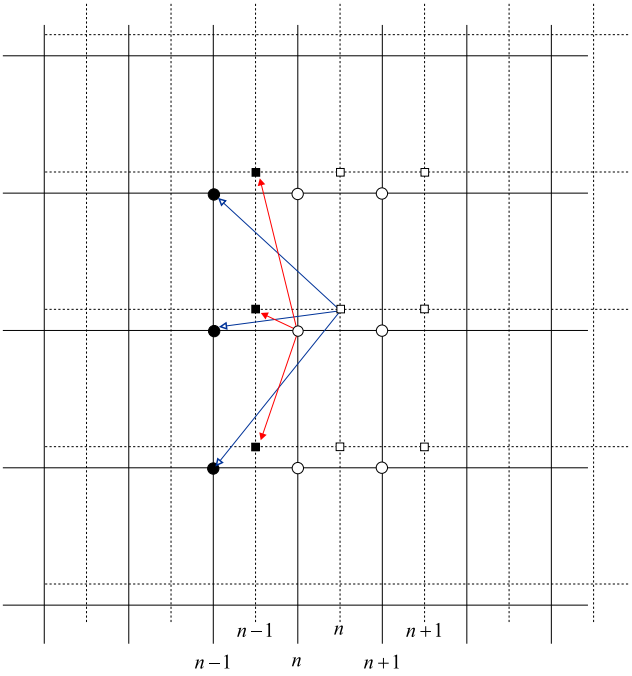

Figure 3.3: Non-symmetry of $\mathcal{A}_i$ matrices.

Long-range interactions can be treated similarly. Given an atom i, we want to calculate all the relevant stiffnesses that come from the interaction energy. In the interaction of atom i with atom j, four separate interactions should be considered as is schematically shown in Fig. 2.3. In this case the total energy has the following form,

$$\mathcal{E} = \mathcal{E}\big(\{\mathbf{x}^j\}, \{\mathbf{x}_s^j\}\big) \tag{3.26}$$

Considering shell charges as variables, stiffness matrices will be of orders $O\big(\frac{1}{r^2}\big)$ and $O\big(\frac{1}{r^3}\big)$ and this one order of magnitude difference will lead to extremely ill-conditioned stiffness matrices. In our lattice statics model, we assume that core and shell charges are fixed. Assuming that there are no discrete body forces, the system is in equilibrium if and only if

$$\frac{\partial \mathcal{E}}{\partial \mathbf{x}^i} = \mathbf{0}, \quad \frac{\partial \mathcal{E}}{\partial \mathbf{x}_s^i} = \mathbf{0} \qquad \forall\ i \in \mathcal{L} \tag{3.27}$$

This is equivalent to,

$$\frac{\partial \mathcal{E}^i}{\partial \mathbf{x}^i} = \mathbf{0}, \quad \frac{\partial \mathcal{E}^i}{\partial \mathbf{x}_s^i} = \mathbf{0} \qquad \forall\ i \in \mathcal{L} \tag{3.28}$$

where $\mathcal{E}^i$ is the energy of the atom i, which is one half of the energy of all the atomic bonds that are incident to i. Note that the Coulombic energy is $O(\frac{1}{r})$ and this means that electrostatic force is $O(\frac{1}{r^2})$ and the electrostatic stiffness coefficients are $O(\frac{1}{r^3})$. In our calculations, we consider a finite

range of interaction for stiffness coefficients in order to have a system of difference equations of finite order.[§] However, electrostatic forces are calculated exactly using Ewald summation technique or direct summation in direct space following Wolf et al. (Wolf et al., 1999). We will have a discussion on energy and force calculations shortly. Note that each atom should interact with atoms on finitely many planes (of atoms) in order to have a system of governing difference equations of finite order. Consider an atom of type i interacting with atoms of type I lying on a plane with index $n+1$. The submatrix $\mathbf{K}_{iI1}$ representing this interaction is defined by summing different contributions of equivalent atoms on the plane $n+1$. This lattice sum is absolutely convergent as the stiffness coefficients are $O(\frac{1}{r^3})$ and the summation is on a plane with dimension 2[¶]. This means there is no ambiguity in calculating electrostatic stiffnesses.[‖] The second alternative is to use Ewald's expression for energy and then minimize it. The nice thing would be the fact that in this case the energy can be calculated with a good accuracy taking into account a small number of nearest neighbors (in real and Fourier spaces). The problem with this method is that Ewald's energy is valid only for a completely periodic system. By minimizing Ewald's energy we would implicitly look for local energy minimizers only in the class of periodic solutions. This is why we choose not to use this method.[**]

Linearizing equations (3.28) about a reference configuration $\mathcal{B}_0 = \big(\{\mathbf{x}_0^j\}, \{\mathbf{x}_{s0}^j\}\big)$ gives us the following system of linear equations,

$$\frac{\partial^2 \mathcal{E}^i}{\partial \mathbf{x}^i \partial \mathbf{x}^i}(\mathcal{B}_0)\mathbf{u}^i + \sum_{\alpha=\text{-}2}^{2}{}' \sum_{I=1}^{5} \sum_{J\beta \in \mathcal{S}_{I\alpha}} \frac{\partial^2 \mathcal{E}^i}{\partial \mathbf{x}^i \partial \mathbf{x}^{J\beta}}(\mathcal{B}_0)\mathbf{u}^{I\alpha} + \sum_{\alpha=\text{-}2}^{2}{}' \sum_{I=1}^{5} \sum_{J\beta \in \mathcal{S}_{I\alpha}} \frac{\partial^2 \mathcal{E}^i}{\partial \mathbf{x}^i \partial \mathbf{x}_s^{J\beta}}(\mathcal{B}_0)\mathbf{u}_s^{I\alpha} = -\frac{\partial \mathcal{E}}{\partial \mathbf{x}^i}(\mathcal{B}_0)$$

$$\frac{\partial^2 \mathcal{E}^i}{\partial \mathbf{x}_s^i \partial \mathbf{x}_s^i}(\mathcal{B}_0)\mathbf{u}_s^i + \sum_{\alpha=\text{-}2}^{2}{}' \sum_{I=1}^{5} \sum_{J\beta \in \mathcal{S}_{I\alpha}} \frac{\partial^2 \mathcal{E}^i}{\partial \mathbf{x}_s^i \partial \mathbf{x}^{J\beta}}(\mathcal{B}_0)\mathbf{u}^{I\alpha} + \sum_{\alpha=\text{-}2}^{2}{}' \sum_{I=1}^{5} \sum_{J\beta \in \mathcal{S}_{I\alpha}} \frac{\partial^2 \mathcal{E}^i}{\partial \mathbf{x}_s^i \partial \mathbf{x}_s^{J\beta}}(\mathcal{B}_0)\mathbf{u}_s^{I\alpha} = -\frac{\partial \mathcal{E}}{\partial \mathbf{x}_s^i}(\mathcal{B}_0)$$

This can be written as

$$\sum_{\alpha=\text{-}2}^{2}{}' \sum_{I=1}^{5} \mathbf{K}_{iI\alpha}^{cc}\mathbf{u}^{I\alpha} + \sum_{\alpha=\text{-}2}^{2}{}' \sum_{I=1}^{5} \mathbf{K}_{iI\alpha}^{cs}\mathbf{u}_s^{I\alpha} + \Big(- \sum_{\alpha=\text{-}2}^{2}{}' \sum_{I=1}^{5} \big[\mathbf{K}_{iI\alpha}^{cc} + \mathbf{K}_{iI\alpha}^{cs}\big]\Big)\mathbf{u}^i = \mathbf{f}_i^c \quad (3.29)$$

$$\sum_{\alpha=\text{-}2}^{2}{}' \sum_{I=1}^{5} \mathbf{K}_{iI\alpha}^{sc}\mathbf{u}^{I\alpha} + \sum_{\alpha=\text{-}2}^{2}{}' \sum_{I=1}^{5} \mathbf{K}_{iI\alpha}^{ss}\mathbf{u}_s^{I\alpha} + \Big(- \sum_{\alpha=\text{-}2}^{2}{}' \sum_{I=1}^{5} \big[\mathbf{K}_{iI\alpha}^{sc} + \mathbf{K}_{iI\alpha}^{ss}\big]\Big)\mathbf{u}_s^i = \mathbf{f}_i^s \quad (3.30)$$

[§]The effect of range of interaction will be numerically studied in the sequel.

[¶]Note that any lattice sum in $\mathbb{R}^p$ with terms $O(\frac{1}{r^{p+1}})$ is absolutely convergent.

[‖]However, these absolutely convergent lattice sums converge slowly and one should be careful and take enough number of lattice points for calculating the substiffness matrices. Our numerical tests show that taking 50^2 lattice points in a given plane is enough for accurate calculation of the corresponding substiffness matrix.

[**]In Appendix A we will discuss some issues on convergence of lattice sums.

where

$$\mathbf{K}^{cc}_{iI\alpha} = \sum_{J\beta\in\mathcal{S}_{I\alpha}} \frac{\partial^2\mathcal{E}^i}{\partial\mathbf{x}^i\partial\mathbf{x}^{J\beta}}(\mathcal{B}_0) \in \mathbb{R}^{3\times3},\ \mathbf{K}^{cs}_{iI\alpha} = \sum_{J\beta\in\mathcal{S}_{I\alpha}} \frac{\partial^2\mathcal{E}^i}{\partial\mathbf{x}^i\partial\mathbf{x}_s^{J\beta}}(\mathcal{B}_0) \in \mathbb{R}^{3\times3}$$
$$\mathbf{K}^{sc}_{iI\alpha} = \sum_{J\beta\in\mathcal{S}_{I\alpha}} \frac{\partial^2\mathcal{E}^i}{\partial\mathbf{x}_s^i\partial\mathbf{x}^{J\beta}}(\mathcal{B}_0) \in \mathbb{R}^{3\times3},\ \mathbf{K}^{ss}_{iI\alpha} = \sum_{J\beta\in\mathcal{S}_{I\alpha}} \frac{\partial^2\mathcal{E}^i}{\partial\mathbf{x}_s^i\partial\mathbf{x}_s^{J\beta}}(\mathcal{B}_0) \in \mathbb{R}^{3\times3}$$
$$\mathbf{f}^c_i = -\frac{\partial\mathcal{E}}{\partial\mathbf{x}^i}(\mathcal{B}_0) \in \mathbb{R}^{3\times1},\ \mathbf{f}^s_i = -\frac{\partial\mathcal{E}}{\partial\mathbf{x}_s^i}(\mathcal{B}_0) \in \mathbb{R}^{3\times1}$$

Let us define a vector $\mathbf{X}_n \in \mathbb{R}^{30}$,

$$\mathbf{X}_n = \begin{pmatrix} \mathbf{x}1_n & ... & \mathbf{x}5_n & \mathbf{x}1_{sn} & ... & \mathbf{x}5_{sn} \end{pmatrix}^{\mathsf{T}} \tag{3.31}$$

where n is the atomic index (unit cell number) defined above. In the end, we will need to solve a system of linear difference equations with the following form.

$$\sum_{\alpha=-m}^{\alpha=m} \mathcal{A}_\alpha \mathbf{X}_{n+\alpha} = \mathbf{F}_n \qquad , |n| \geq m+2 \tag{3.32}$$

where $\mathcal{A}_\alpha \in \mathbb{R}^{30\times30},\ \alpha = -m, ..., m$ and $\mathbf{F}_n \in \mathbb{R}^{30},\ \ \forall n \in \mathbb{N}$. The above governing equations can be written in terms of a discrete convolution operator as,[††]

$$\mathsf{AX} = \mathsf{F} \tag{3.33}$$

where $\mathsf{X} = \{\mathbf{X}_n\}$, $\mathsf{F} = \{\mathbf{F}_n\}$ and the discrete convolution operator is defined as

$$\mathsf{AX} = \left\{ \left(\mathsf{AX}\right)_n \right\} \tag{3.34}$$

and,

$$\left(\mathsf{AX}\right)_n = \sum_{m=0}^{\infty} \mathsf{A}_{n-m}\mathbf{X}_m \tag{3.35}$$

[††]This is the approach that Babŭska (1959) chooses in his treatment of difference equations. We do not use this notation in this thesis but it would be useful to know that the discrete governing equations have a discrete convolution form.

Matrices $\mathcal{A}_{\text{-}2}$ and $\mathcal{A}_0$, for example, have the following relation with the substiffness matrices $\mathbf{K}_{iI\alpha}$,

$$\mathcal{A}_{\text{-}2}^{\text{int}} = \begin{pmatrix} \mathbf{K}^{cc}_{11\text{-}2} & \mathbf{K}^{cc}_{12\text{-}2} & \mathbf{K}^{cc}_{13\text{-}2} & \mathbf{K}^{cc}_{14\text{-}2} & \mathbf{K}^{cc}_{15\text{-}2} & \mathbf{K}^{cs}_{11\text{-}2} & \mathbf{K}^{cs}_{12\text{-}2} & \mathbf{K}^{cs}_{13\text{-}2} & \mathbf{K}^{cs}_{14\text{-}2} & \mathbf{K}^{cs}_{15\text{-}2} \\ \mathbf{K}^{cc}_{21\text{-}2} & \mathbf{K}^{cc}_{22\text{-}2} & \mathbf{K}^{cc}_{23\text{-}2} & \mathbf{K}^{cc}_{24\text{-}2} & \mathbf{K}^{cc}_{25\text{-}2} & \mathbf{K}^{cs}_{21\text{-}2} & \mathbf{K}^{cs}_{22\text{-}2} & \mathbf{K}^{cs}_{23\text{-}2} & \mathbf{K}^{cs}_{24\text{-}2} & \mathbf{K}^{cs}_{25\text{-}2} \\ \mathbf{K}^{cc}_{31\text{-}2} & \mathbf{K}^{cc}_{32\text{-}2} & \mathbf{K}^{cc}_{33\text{-}2} & \mathbf{K}^{cc}_{34\text{-}2} & \mathbf{K}^{cc}_{35\text{-}2} & \mathbf{K}^{cs}_{31\text{-}2} & \mathbf{K}^{cs}_{32\text{-}2} & \mathbf{K}^{cs}_{33\text{-}2} & \mathbf{K}^{cs}_{34\text{-}2} & \mathbf{K}^{cs}_{35\text{-}2} \\ \mathbf{K}^{cc}_{41\text{-}2} & \mathbf{K}^{cc}_{42\text{-}2} & \mathbf{K}^{cc}_{43\text{-}2} & \mathbf{K}^{cc}_{44\text{-}2} & \mathbf{K}^{cc}_{45\text{-}2} & \mathbf{K}^{cs}_{41\text{-}2} & \mathbf{K}^{cs}_{42\text{-}2} & \mathbf{K}^{cs}_{43\text{-}2} & \mathbf{K}^{cs}_{44\text{-}2} & \mathbf{K}^{cs}_{45\text{-}2} \\ \mathbf{K}^{cc}_{51\text{-}2} & \mathbf{K}^{cc}_{52\text{-}2} & \mathbf{K}^{cc}_{53\text{-}2} & \mathbf{K}^{cc}_{54\text{-}2} & \mathbf{K}^{cc}_{55\text{-}2} & \mathbf{K}^{cs}_{51\text{-}2} & \mathbf{K}^{cs}_{52\text{-}2} & \mathbf{K}^{cs}_{53\text{-}2} & \mathbf{K}^{cs}_{54\text{-}2} & \mathbf{K}^{cs}_{55\text{-}2} \\ \mathbf{K}^{sc}_{11\text{-}2} & \mathbf{K}^{sc}_{12\text{-}2} & \mathbf{K}^{sc}_{13\text{-}2} & \mathbf{K}^{sc}_{14\text{-}2} & \mathbf{K}^{sc}_{15\text{-}2} & \mathbf{K}^{ss}_{11\text{-}2} & \mathbf{K}^{ss}_{12\text{-}2} & \mathbf{K}^{ss}_{13\text{-}2} & \mathbf{K}^{ss}_{14\text{-}2} & \mathbf{K}^{ss}_{15\text{-}2} \\ \mathbf{K}^{sc}_{21\text{-}2} & \mathbf{K}^{sc}_{22\text{-}2} & \mathbf{K}^{sc}_{23\text{-}2} & \mathbf{K}^{sc}_{24\text{-}2} & \mathbf{K}^{sc}_{25\text{-}2} & \mathbf{K}^{ss}_{21\text{-}2} & \mathbf{K}^{ss}_{22\text{-}2} & \mathbf{K}^{ss}_{23\text{-}2} & \mathbf{K}^{ss}_{24\text{-}2} & \mathbf{K}^{ss}_{25\text{-}2} \\ \mathbf{K}^{sc}_{31\text{-}2} & \mathbf{K}^{sc}_{32\text{-}2} & \mathbf{K}^{sc}_{33\text{-}2} & \mathbf{K}^{sc}_{34\text{-}2} & \mathbf{K}^{sc}_{35\text{-}2} & \mathbf{K}^{ss}_{31\text{-}2} & \mathbf{K}^{ss}_{32\text{-}2} & \mathbf{K}^{ss}_{33\text{-}2} & \mathbf{K}^{ss}_{34\text{-}2} & \mathbf{K}^{ss}_{35\text{-}2} \\ \mathbf{K}^{sc}_{41\text{-}2} & \mathbf{K}^{sc}_{42\text{-}2} & \mathbf{K}^{sc}_{43\text{-}2} & \mathbf{K}^{sc}_{44\text{-}2} & \mathbf{K}^{sc}_{45\text{-}2} & \mathbf{K}^{ss}_{41\text{-}2} & \mathbf{K}^{ss}_{42\text{-}2} & \mathbf{K}^{ss}_{43\text{-}2} & \mathbf{K}^{ss}_{44\text{-}2} & \mathbf{K}^{ss}_{45\text{-}2} \\ \mathbf{K}^{sc}_{51\text{-}2} & \mathbf{K}^{sc}_{52\text{-}2} & \mathbf{K}^{sc}_{53\text{-}2} & \mathbf{K}^{sc}_{54\text{-}2} & \mathbf{K}^{sc}_{55\text{-}2} & \mathbf{K}^{ss}_{51\text{-}2} & \mathbf{K}^{ss}_{52\text{-}2} & \mathbf{K}^{ss}_{53\text{-}2} & \mathbf{K}^{ss}_{54\text{-}2} & \mathbf{K}^{ss}_{55\text{-}2} \end{pmatrix}$$

$$\mathcal{A}_0^{\text{int}} = \begin{pmatrix} \mathbf{K}^{cc}_{110} & \mathbf{K}^{cc}_{120} & \mathbf{K}^{cc}_{130} & \mathbf{K}^{cc}_{140} & \mathbf{K}^{cc}_{150} & \mathbf{K}^{cs}_{110} & \mathbf{K}^{cs}_{120} & \mathbf{K}^{cs}_{130} & \mathbf{K}^{cs}_{140} & \mathbf{K}^{cs}_{150} \\ \mathbf{K}^{cc}_{210} & \mathbf{K}^{cc}_{220} & \mathbf{K}^{cc}_{230} & \mathbf{K}^{cc}_{240} & \mathbf{K}^{cc}_{250} & \mathbf{K}^{cs}_{210} & \mathbf{K}^{cs}_{220} & \mathbf{K}^{cs}_{230} & \mathbf{K}^{cs}_{240} & \mathbf{K}^{cs}_{250} \\ \mathbf{K}^{cc}_{310} & \mathbf{K}^{cc}_{320} & \mathbf{K}^{cc}_{330} & \mathbf{K}^{cc}_{340} & \mathbf{K}^{cc}_{350} & \mathbf{K}^{cs}_{310} & \mathbf{K}^{cs}_{320} & \mathbf{K}^{cs}_{330} & \mathbf{K}^{cs}_{340} & \mathbf{K}^{cs}_{350} \\ \mathbf{K}^{cc}_{410} & \mathbf{K}^{cc}_{420} & \mathbf{K}^{cc}_{430} & \mathbf{K}^{cc}_{440} & \mathbf{K}^{cc}_{450} & \mathbf{K}^{cs}_{410} & \mathbf{K}^{cs}_{420} & \mathbf{K}^{cs}_{430} & \mathbf{K}^{cs}_{440} & \mathbf{K}^{cs}_{450} \\ \mathbf{K}^{cc}_{510} & \mathbf{K}^{cc}_{520} & \mathbf{K}^{cc}_{530} & \mathbf{K}^{cc}_{540} & \mathbf{K}^{cc}_{550} & \mathbf{K}^{cs}_{510} & \mathbf{K}^{cs}_{520} & \mathbf{K}^{cs}_{530} & \mathbf{K}^{cs}_{540} & \mathbf{K}^{cs}_{550} \\ \mathbf{K}^{sc}_{110} & \mathbf{K}^{sc}_{120} & \mathbf{K}^{sc}_{130} & \mathbf{K}^{sc}_{140} & \mathbf{K}^{sc}_{150} & \mathbf{K}^{ss}_{110} & \mathbf{K}^{ss}_{120} & \mathbf{K}^{ss}_{130} & \mathbf{K}^{ss}_{140} & \mathbf{K}^{ss}_{150} \\ \mathbf{K}^{sc}_{210} & \mathbf{K}^{sc}_{220} & \mathbf{K}^{sc}_{230} & \mathbf{K}^{sc}_{240} & \mathbf{K}^{sc}_{250} & \mathbf{K}^{ss}_{210} & \mathbf{K}^{ss}_{220} & \mathbf{K}^{ss}_{230} & \mathbf{K}^{ss}_{240} & \mathbf{K}^{ss}_{250} \\ \mathbf{K}^{sc}_{310} & \mathbf{K}^{sc}_{320} & \mathbf{K}^{sc}_{330} & \mathbf{K}^{sc}_{340} & \mathbf{K}^{sc}_{350} & \mathbf{K}^{ss}_{310} & \mathbf{K}^{ss}_{320} & \mathbf{K}^{ss}_{330} & \mathbf{K}^{ss}_{340} & \mathbf{K}^{ss}_{350} \\ \mathbf{K}^{sc}_{410} & \mathbf{K}^{sc}_{420} & \mathbf{K}^{sc}_{430} & \mathbf{K}^{sc}_{440} & \mathbf{K}^{sc}_{450} & \mathbf{K}^{ss}_{410} & \mathbf{K}^{ss}_{420} & \mathbf{K}^{ss}_{430} & \mathbf{K}^{ss}_{440} & \mathbf{K}^{ss}_{450} \\ \mathbf{K}^{sc}_{510} & \mathbf{K}^{sc}_{520} & \mathbf{K}^{sc}_{530} & \mathbf{K}^{sc}_{540} & \mathbf{K}^{sc}_{550} & \mathbf{K}^{ss}_{510} & \mathbf{K}^{ss}_{520} & \mathbf{K}^{ss}_{530} & \mathbf{K}^{ss}_{540} & \mathbf{K}^{ss}_{550} \end{pmatrix}$$

Similar to the case of short-range interactions, the $\mathcal{A}_0^{\text{int}}$ has the following extra structure.

$$\mathbf{K}^{cc}_{II0} = -\sum_{\alpha=\text{-}2}^{2}{}' \sum_{\substack{J=1 \\ J\neq I}}^{5} \left[\mathbf{K}^{cc}_{IJ\alpha} + \mathbf{K}^{cs}_{IJ\alpha}\right] \qquad \text{and} \qquad \mathbf{K}^{ss}_{II0} = -\sum_{\alpha=\text{-}2}^{2}{}' \sum_{\substack{J=1 \\ J\neq I}}^{5} \left[\mathbf{K}^{sc}_{IJ\alpha} + \mathbf{K}^{ss}_{IJ\alpha}\right] \tag{3.36}$$

Finally, $\mathcal{A}_{\text{-}2}, ..., \mathcal{A}_2$ are obtained by assembling all the stiffness matrices that come from short-range energy, interaction energy and self energy. Again, it can be easily shown that

$$\text{Nullity}\Big(\sum_{\alpha=\text{-}\mathsf{m}}^{\mathsf{m}} \mathcal{A}_\alpha\Big) = 3 \tag{3.37}$$

i.e., the governing equations are invariant under a rigid translation as expected. Now let us check the other force constant properties. Each substiffness matrix is symmetric by definition and hence (1.15) is satisfied. Property (1.16) is satisfied because the substiffness matrices are independent of the index n. This is of course only true for bulk unit cells. Property (1.17) is satisfied because

substiffness matrices are calculated using the relative position of core and shells. Property (1.18) has already been discussed. Property (1.19) needs the following discussion. Suppose the whole multi-lattice is rotated by a rotation $\mathbf{Q}$. This means that each $\mathbf{X}_n$ is transformed to $\mathbf{X}'_n$ which is related to $\mathbf{X}_n$ by

$$\mathbf{X}'_n = \widetilde{\mathbf{Q}}\mathbf{X}_n, \qquad \widetilde{\mathbf{Q}} = \begin{pmatrix} \mathbf{Q} & & \\ & \ddots & \\ & & \mathbf{Q} \end{pmatrix} \in \mathbb{R}^{30\times 30} \tag{3.38}$$

Now let us left multiply Eq. (3.32) by $\widetilde{\mathbf{Q}}$.

$$\sum_{\alpha=-m}^{\alpha=m} \widetilde{\mathbf{Q}}\mathcal{A}_\alpha \mathbf{X}_{n+\alpha} = \widetilde{\mathbf{Q}}\mathbf{F}_n \tag{3.39}$$

But note that because of the special form of $\widetilde{\mathbf{Q}}$, $\widetilde{\mathbf{Q}}\mathcal{A}_\alpha = \mathcal{A}_\alpha\widetilde{\mathbf{Q}}$. Thus

$$\sum_{\alpha=-m}^{\alpha=m} \mathcal{A}_\alpha\Big(\widetilde{\mathbf{Q}}\mathbf{X}_{n+\alpha}\Big) = \Big(\widetilde{\mathbf{Q}}\mathbf{F}_n\Big) \tag{3.40}$$

i.e., the governing equations are invariant under rigid rotations in the deformed configuration (material frame indifference).

There is another symmetry relating $\mathcal{A}_{-\gamma}$ to $\mathcal{A}_\gamma$. It can be easily shown that reciprocity implies that

$$\mathbf{K}_{IJ-\gamma} = \mathbf{K}_{JI\gamma} \tag{3.41}$$

The following are the steps needed for constructing the discrete governing equations:

- Construct the multi-lattice.
- Modify the bulk multi-lattice close to the defect(s).
- For a given unit cell partition the neighboring unit cells into equivalent classes.
- For the given interatomic potential calculate the stiffness and force expressions.
- Calculate stiffness matrices by some appropriate assembling algorithm.
- Calculate the unbalanced forces.
- Solve for the discrete displacement field.

3.1 Hessian Matrix for the Bulk Crystal

Let us briefly explain how one should calculate the Hessian matrix of a bulk crystal for checking stability. In the bulk all the unit cells are equivalent. Now an equivalence class is a Bravais lattice. For ABO_3 there are $N = 10$ equivalence classes. Consider the governing equations for the charge I in the unit cell $\mathbf{n} = \mathbf{0}$.

$$\frac{\partial \mathcal{E}}{\partial \mathbf{x}^I} = \mathbf{0} \qquad I = 1, ..., 10 \tag{3.42}$$

Linearization about $\mathcal{B}_0 = \{\mathbf{X}_I\}$ yields

$$\frac{\partial^2 \mathcal{E}}{\partial \mathbf{x}^I \partial \mathbf{x}^I}(\mathcal{B}_0)(\mathbf{x}^I - \mathbf{X}^I) + \sum_{j \in \mathcal{S}_I} \frac{\partial^2 \mathcal{E}}{\partial \mathbf{x}^I \partial \mathbf{x}^j}(\mathcal{B}_0)(\mathbf{x}^j - \mathbf{X}^j) + ... = -\frac{\partial \mathcal{E}}{\partial \mathbf{x}^I}(\mathcal{B}_0) \tag{3.43}$$

Note that

$$\mathcal{S}_I = \bigcup_{\substack{J=1 \\ J \neq I}}^{10} \mathcal{L}_J \tag{3.44}$$

Thus

$$\sum_{j \in \mathcal{S}_I} \frac{\partial^2 \mathcal{E}}{\partial \mathbf{x}^I \partial \mathbf{x}^j}(\mathcal{B}_0)(\mathbf{x}^j - \mathbf{X}^j) = \sum_{\substack{J=1 \\ J \neq I}}^{10} \sum_{j \in \mathcal{L}_J} \frac{\partial^2 \mathcal{E}}{\partial \mathbf{x}^I \partial \mathbf{x}^j}(\mathcal{B}_0)(\mathbf{x}^J - \mathbf{X}^J) \tag{3.45}$$

Note that because of pairwise nature of interactions,

$$\frac{\partial^2 \mathcal{E}}{\partial \mathbf{x}^I \partial \mathbf{x}^I}(\mathcal{B}_0) = -\sum_{j \in \mathcal{S}_I} \frac{\partial^2 \mathcal{E}}{\partial \mathbf{x}^I \partial \mathbf{x}^j}(\mathcal{B}_0) \tag{3.46}$$

Therefore the linearized governing equations may be written as

$$\sum_{\substack{J=1 \\ J \neq I}}^{10} \mathbf{K}_{IJ} \mathbf{u}^J + \left(-\sum_{\substack{J=1 \\ J \neq I}}^{10} \mathbf{K}_{IJ} \right) \mathbf{u}^I = \mathbf{f}^I \qquad I = 1, ..., 10 \tag{3.47}$$

where

$$\begin{aligned} \mathbf{K}_{IJ} &= \sum_{j \in \mathcal{L}_J} \frac{\partial^2 \mathcal{E}}{\partial \mathbf{x}^I \partial \mathbf{x}^j}(\mathcal{B}_0) \\ \mathbf{f}^I &= -\frac{\partial \mathcal{E}}{\partial \mathbf{x}^I}(\mathcal{B}_0) \\ \mathbf{u}^J &= \mathbf{x}^J - \mathbf{X}^J = \mathbf{x}^j - \mathbf{X}^j \qquad \forall\ j \in \mathcal{L}_J \end{aligned} \tag{3.48}$$

The Hessian matrix of the bulk crystal is

$$\mathbf{H} = \begin{pmatrix} \mathbf{K}_{11} & \mathbf{K}_{12} & \dots & \mathbf{K}_{19} & \mathbf{K}_{110} \\ \mathbf{K}_{21} & \mathbf{K}_{22} & \dots & \mathbf{K}_{29} & \mathbf{K}_{210} \\ \vdots & \vdots & \ddots & \vdots & \vdots \\ \mathbf{K}_{91} & \mathbf{K}_{92} & \dots & \mathbf{K}_{93} & \mathbf{K}_{910} \\ \mathbf{K}_{101} & \mathbf{K}_{102} & \dots & \mathbf{K}_{109} & \mathbf{K}_{1010} \end{pmatrix} \tag{3.49}$$

It is important to note that for electrostatic energy, the lattice sum defining $\mathbf{K}_{IJ}$ is conditionally convergent. These substiffness matrices are calculated using Ewald method. The details are given in Appendix A. Note that because of translation invariance $\mathbf{H}$ has a zero eigenvalue with multiplicity three. Note also that because $\mathcal{L}_I,\ I = 1, ..., 10$ is a Bravais lattice,

$$\forall\ j \in \mathcal{L}_I\ \exists\ j' \in \mathcal{L}_J \quad \text{s.t.} \quad \mathbf{r}_I - \mathbf{x}_j = \mathbf{r}_J - \mathbf{x}_{j'} \tag{3.50}$$

Thus

$$\sum_{j \in \mathcal{L}_J} \frac{\partial^2 \mathcal{E}}{\partial \mathbf{x}^I \partial \mathbf{x}^j}(\mathcal{B}_0) = \sum_{j \in \mathcal{L}_I} \frac{\partial^2 \mathcal{E}}{\partial \mathbf{x}^J \partial \mathbf{x}^j}(\mathcal{B}_0), \qquad , i.e., \qquad \mathbf{K}_{IJ} = \mathbf{K}_{JI} \tag{3.51}$$

Note that the Hessian matrix $\mathbf{H}$ always has an eigenvalue $\lambda = 0$ with multiplicity three. This eigenvalue represents the translation invariance of the governing equations in $\mathbb{R}^3$.

Chapter 4

180° Domain Walls in $BaTiO_3$ and $PbTiO_3$

Ferroelectric domain walls are boundaries between regions of uniform polarization. Depending on the crystalline structure there are different types of domain walls. In the tetragonal phase there are two types of domain walls: 180° and 90° domain walls. There is a well established continuum theory that explains why ferroelectric domain walls exist (Shu and Bhattacharya, 2001). Basically domain walls lower the total energy. Ferroelectric domain walls have been modelled in different scales. We can classify these models into the following three groups:

i) *Quantum mechanics ab initio calculations* are first principle calculations for perfect domain walls. There are several such calculations in the literature as was explained in the Introduction. The shortcoming of these calculations is that only systems with at most a few hundred atoms can be treated quantum mechanically to this date. Thus, only a completely periodic array of domain walls can be analyzed. However, numerical studies show that the calculations are insensitive to the supercell size with more than six to eight unit cells for $PbTiO_3$ (Meyer and Vanderbilt, 2001). More complicated defects are beyond the reach of quantum mechanics at this time.

ii) *Continuum models based on Landau-Ginzberg-Devonshire theory* (Devonshire, 1949a), (Devonshire, 1949b), (Devonshire, 1954) are attractive models capable of keeping track of the evolution of domain walls. These phase field theories have been implemented by several groups as was explained in the Introduction. The problem with these models is that there are several parameters that need to be fitted to the experimental data. It is also questionable to model an atomically sharp domain wall by a continuum model. Thus these models cannot be useful for understanding the structure of ferroelectric domain walls. It should be noted that in these models a domain wall has a finite thickness across which polarization changes continuously.

iii) *Continuum mechanics modelling of ferroelectric domain walls.* In continuum mechanics an

interface is a surface across which some fields have jump discontinuities. A ferroelectric domain wall is a surface of discontinuity in both deformation gradient $\mathbf{F}$ and polarization $\mathbf{p}$. Denoting a ferroelectric domain wall by $\mathfrak{s}_f$ and $\mathfrak{S}_f$ in the deformed and undeformed configurations, respectively, the following compatibility equations should be satisfied,

$$[\![\mathbf{F}]\!] = \mathbf{a} \otimes \mathbf{N} \tag{4.1}$$

$$[\![\mathbf{p}]\!] \cdot \mathbf{n} = 0 \tag{4.2}$$

where Eq. (4.1) is Hadamard's compatibility equation and Eq. (4.2) is a consequence of Maxwell's equations for a charge-free domain wall. Here $\mathbf{n}$ and $\mathbf{N}$ are the unit normals on $\mathfrak{s}_f$ and $\mathfrak{S}_f$, respectively. A sharp domain wall is nothing but an idealization of what happens in smaller scales. For modelling the motion of a domain wall one needs to calculate the configurational force (normal component of Eshelby's energy-momentum tensor) and assume a kinetic equation,

$$V_n = \Phi(f) \tag{4.3}$$

where f is the configurational (driving) force and V_n is the normal component of the velocity of the domain wall (the only intrinsic component of the velocity vector). James (2002) has recently obtained an expression for the configurational force on a ferromagnetic domain wall. This can immediately be used for a charge-free ferroelectric domain wall. However, this would not be the correct configurational force for a charged ferroelectric domain wall.

In the lattice scale one can no longer think of the macroscopic fields. What one has in this scale is the position vector of the nuclei and the electronic distributions. Using the Born-Oppenheimer approximation one can simplify the electronic effects. In particular, in a shell model the independent kinematical variables are core and shell position vectors. In shell models there are two contributions to polarization, one that comes from the relative core-shell displacements in the same atom and one that comes from the distortion of unit cells. The bulk spontaneous polarization $(0, P_s, 0)$, for example, is a result of some relative core-shell displacements in the tetragonal c-direction (the direction $(0, 1, 0)$). In the lattice scale discontinuity has no meaning as all the fields are discrete. Discontinuity of macroscopic polarization is a result of sudden changes of sign of the relative core-shell displacements across a plane, for example.

4.1 Symmetry Reduction in 180° Domain Walls

The reference configuration and idea of symmetry reduction is schematically shown in Fig. 4.1 for a 180° domain wall. Because of symmetry, it is enough to obtain the atomic displacements only in the

two planes (a) and (b) as shown in Fig. 4.2. A more detailed structure of reference configuration in planes (a) and (b) is shown in Fig. 4.3. Governing equilibrium equations for domain walls can

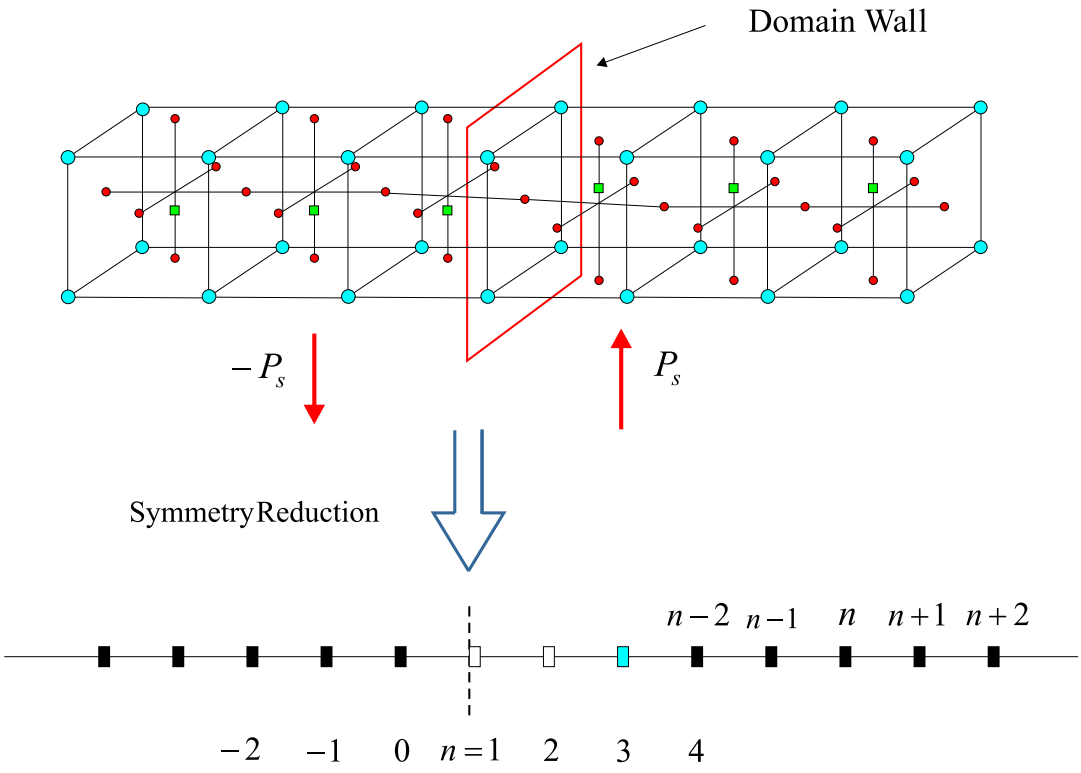

Figure 4.1: Reference configuration used in analysis of a 180° domain wall.

be obtained by minimizing the total energy of the crystal. These (nonlinear) governing equations will be linearized later about different reference configurations. Because of symmetry in both 180° and 90° domain problems all the atoms of the same type that lie on the same plane parallel to the domain wall have the same displacements. For a 180° domain wall because of symmetry we can look at only $\mathcal{L}^r = \mathcal{L}^0 \sqcup \mathcal{L}^+$, the half lattice of ABO_3, i.e., the half space of atoms that lie on the right side of the domain wall including the atoms that lie on the wall. $\mathcal{L}^r$ can be partitioned into ten pairwise disjoint sublattices, i.e.,

$$\mathcal{L}^r = \bigcup_{I=1}^{10} \mathcal{L}_I \tag{4.4}$$

Each $\mathcal{L}_I$ is partitioned into subsets according to their distance from the domain wall.

$$\mathcal{L}_I = \bigcup_{n=0}^{\infty} \mathcal{L}_I(n) \tag{4.5}$$

where

$$\mathcal{L}_I(n) = \left\{ \mathbf{x} \in \mathcal{L}_I \;\middle|\; (\mathbf{x} - \mathbf{p}_I) \cdot \hat{\mathbf{e}}_x = na',\ n \in \mathbb{N} \cup \{0\} \right\} \tag{4.6}$$

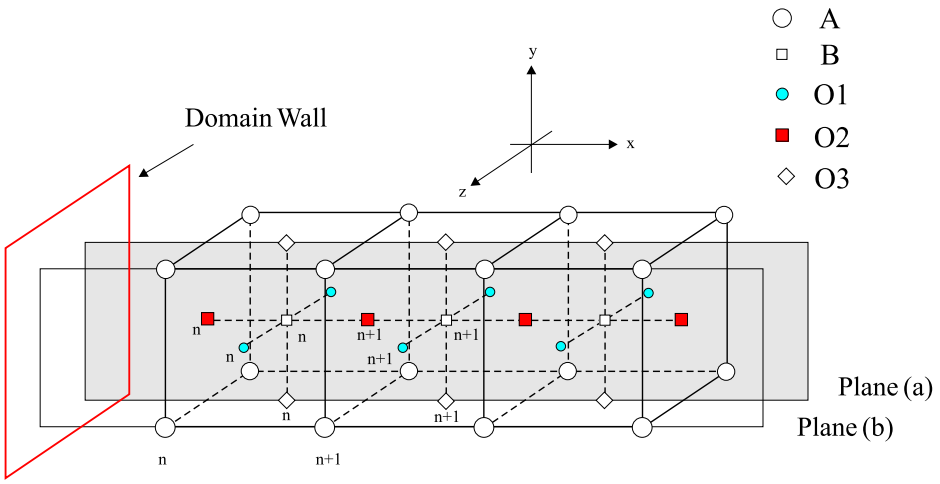

Figure 4.2: Two planes perpendicular to the domain wall and the atomic numbering used in the lattice static analysis.

where $a' = a$ and $(\mathbf{x} - \mathbf{p}_I) \cdot \hat{\mathbf{e}}_x$ is the component of $\mathbf{x} - \mathbf{p}_I$ perpendicular to the domain wall. For a 90° domain wall one has to consider the whole multi-lattice. In this case,

$$\mathcal{L}_I = \bigcup_{n=-\infty}^{\infty} \mathcal{L}_I(n) \tag{4.7}$$

where

$$\mathcal{L}_I(n) = \left\{ \mathbf{x} \in \mathcal{L}_I \;\middle|\; (\mathbf{x} - \mathbf{p}_I) \cdot \hat{\mathbf{e}}_x = na',\ n \in \mathbb{Z} \right\} \tag{4.8}$$

and $a' = \frac{ac}{\sqrt{a^2+c^2}}$. Using this symmetry, for each atom type, finding the displacement of atoms on a half line (or a line in the case of a 90° domain wall) perpendicular to the wall would give us the complete structure of the domain wall. This is why our lattice statics model for domain walls leads to a system of ordinary (and not partial) difference equations. The system of difference equations (3.18) can be easily transformed to a first-order equation. For the sake of clarity let us consider the two cases $m = 1$ and $m = 2$ separately and then generalizing the results for an arbitrary range of interaction m would be straightforward. For those atoms that lie on the domain wall, i.e., for A and O2 atoms (for an A-centered 180° domain wall), the relative shifts of core and shell are assumed to be zero in the reference configuration.

i) $\mathbf{m = 1}$: The bulk governing equations are,

$$\mathcal{A}_{-1}\mathbf{X}_{n-1} + \mathcal{A}_0\mathbf{X}_n + \mathcal{A}_1\mathbf{X}_{n+1} = \mathbf{F}_n \qquad n \geq 3 \tag{4.9}$$

Boundary equations are the governing equations for the boundary atoms. In this problem, a

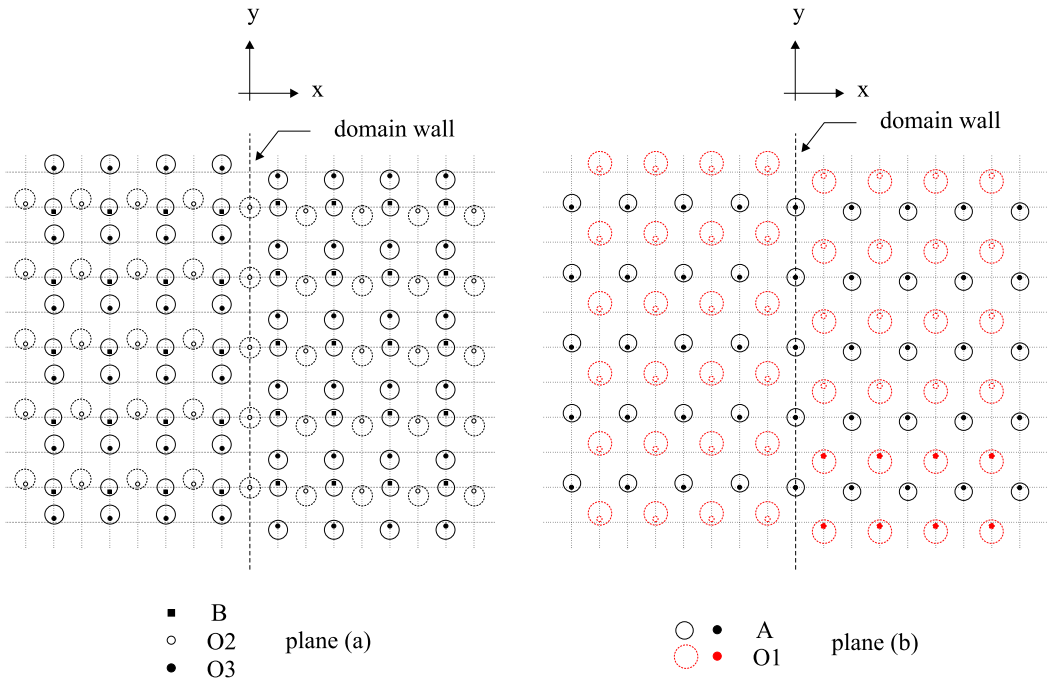

Figure 4.3: Reference configuration for an A-centered 180° domain wall shown in the two planes (a) and (b). Note that the reference configuration is invariant under the transformation $x \to -x, y \to -y, z \to z(\text{or } -z)$.

bulk atom is an atom that does not interact with any atom on the wall or on the left side of the wall. All the other atoms are boundary and transition atoms. For interactions of order m, boundary atoms are atoms with indices $n \in \{1, 2, ..., m\}$ and transition atoms are atoms with index $n = m + 1$. For the interaction range $m = 2$, atoms with atomic indices $n = 1, 2$ are boundary atoms and transition atoms have index $n = 3$. Note that for a 180° domain wall, boundary atoms have the same neighbors as the interior atoms do. The only difference is that atoms on the left side of the domain wall have different reference coordinates. The unit cells $n = 1, 2$ should be treated separately as the stiffness matrices close to the domain wall are not constant. These are the boundary and transition equations and can be expressed as

$$n = 1 \quad : \quad \mathcal{A}_{-1}^{(1)}\mathbf{X}_0 + \mathcal{A}_0^{(1)}\mathbf{X}_1 + \mathcal{A}_1^{(1)}\mathbf{X}_2 = \mathbf{F}_1 \tag{4.10}$$

$$n = 2 \quad : \quad \mathcal{A}_{-1}^{(2)}\mathbf{X}_1 + \mathcal{A}_0^{(2)}\mathbf{X}_2 + \mathcal{A}_1^{(2)}\mathbf{X}_3 = \mathbf{F}_2 \tag{4.11}$$

Treating the boundary unit cells separately is one of the main features of our inhomogeneous lattice statics. It should also be noted that displacements of the atoms on the left side of the wall are related to those of their corresponding atoms on the right side of the domain wall. The form of this dependence is governed by the symmetry of the problem and is discussed in

the sequel for both A-centered and B-centered 180° domain walls.* Consider an atom n and

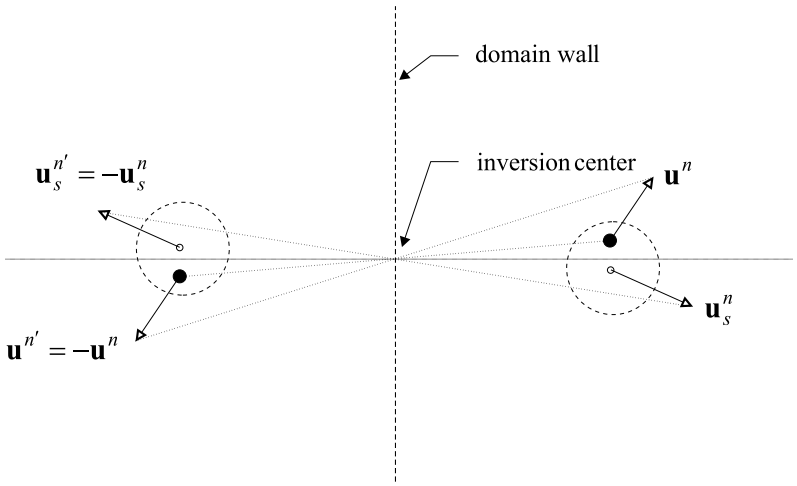

Figure 4.4: Inversion symmetry for displacements in a 180° domain wall.

its image on the other side of the wall (see Fig. 4.4). Each such pair of atoms are related by an inversion symmetry. As it is seen in the figure, all the inversion centers lie on the domain wall. One possibility is the following symmetry,

$$\mathbf{u}^{n'} = -\mathbf{u}^n, \quad \mathbf{u}_s^{n'} = -\mathbf{u}_s^n \tag{4.12}$$

where for A and O2 (atoms that lie on the domain wall) $n' = -n + 2$ and for other atoms $n' = -n+1$. We assume that the unit cell index $n = 1$ corresponds to those unit cells with cores and shells lying on the domain wall. The other possibilities for core and shell displacements are the following,

$$\left(\mathbf{u}^{n'}\right)_x = -\left(\mathbf{u}^n\right)_x \ , \ \left(\mathbf{u}_s^{n'}\right)_x = -\left(\mathbf{u}_s^n\right)_x \tag{4.13}$$

$$\left(\mathbf{u}^{n'}\right)_y = \left(\mathbf{u}^n\right)_y \ , \ \left(\mathbf{u}_s^{n'}\right)_y = \left(\mathbf{u}_s^n\right)_y \ , \ \left(\mathbf{u}^{n'}\right)_z = -\left(\mathbf{u}^n\right)_z \ , \ \left(\mathbf{u}_s^{n'}\right)_z = -\left(\mathbf{u}_s^n\right)_z \tag{4.14}$$

And,

$$\left(\mathbf{u}^{n'}\right)_x = -\left(\mathbf{u}^n\right)_x \ , \ \left(\mathbf{u}_s^{n'}\right)_x = -\left(\mathbf{u}_s^n\right)_x \tag{4.15}$$

$$\left(\mathbf{u}^{n'}\right)_y = \left(\mathbf{u}^n\right)_y \ , \ \left(\mathbf{u}_s^{n'}\right)_y = \left(\mathbf{u}_s^n\right)_y \ , \ \left(\mathbf{u}^{n'}\right)_z = \left(\mathbf{u}^n\right)_z \ , \ \left(\mathbf{u}_s^{n'}\right)_z = \left(\mathbf{u}_s^n\right)_z \tag{4.16}$$

We call these three symmetries, Type I, Type II and Type III symmetries, respectively. Note

*Exploiting this symmetry makes the calculations more efficient. However, one can solve the governing difference equations on $\mathbb{Z}$. The two methods should give the same results and our numerical results confirm this. The method of solution of governing discrete equations on the whole $\mathbb{Z}$ will be discussed in the next chapter for 90° domain walls.

that there are other possibilities but these three seem to be the most reasonable. Our numerical tests show that Type II and Type III symmetries are equivalent (note that all forces have zero z-components) and that the energy minimizing configuration is Type I symmetry. We have the following relation,

$$\mathbf{X}_0 = \mathbf{R}\mathbf{X}_1 + \mathbf{R}'\mathbf{X}_2 \tag{4.17}$$

where the matrices $\mathcal{R}$ and $\mathbf{R}'$ have the following forms,

$$\mathbf{R} = \begin{pmatrix} \widetilde{\mathbf{R}} & \\ & \widetilde{\mathbf{R}} \end{pmatrix}, \qquad \mathbf{R}' = \begin{pmatrix} \widetilde{\mathbf{R}'} & \\ & \widetilde{\mathbf{R}'} \end{pmatrix} \tag{4.18}$$

where for Type I symmetry,

$$\widetilde{\mathbf{R}} = \mathrm{diag}\{\mathbf{0}, -\mathbf{I}, -\mathbf{I}, \mathbf{0}, -\mathbf{I}\}, \qquad \widetilde{\mathbf{R}'} = \mathrm{diag}\{-\mathbf{I}, \mathbf{0}, \mathbf{0}, -\mathbf{I}, \mathbf{0}\}, \qquad \mathbf{I} = \mathrm{diag}\{1, 1, 1\} \tag{4.19}$$

and for Type II symmetry,

$$\widetilde{\mathbf{R}} = \mathrm{diag}\{\mathbf{0}, \bar{\mathbf{I}}, \bar{\mathbf{I}}, \mathbf{0}, \bar{\mathbf{I}}\}, \qquad \widetilde{\mathbf{R}'} = \mathrm{diag}\{\bar{\mathbf{I}}, \mathbf{0}, \mathbf{0}, \bar{\mathbf{I}}, \mathbf{0}\}, \qquad \bar{\mathbf{I}} = \mathrm{diag}\{-1, 1, -1\} \tag{4.20}$$

and for Type III symmetry,

$$\widetilde{\mathbf{R}} = \mathrm{diag}\{\mathbf{0}, \bar{\mathbf{I}}, \bar{\mathbf{I}}, \mathbf{0}, \bar{\mathbf{I}}\}, \qquad \widetilde{\mathbf{R}'} = \mathrm{diag}\{\bar{\mathbf{I}}, \mathbf{0}, \mathbf{0}, \bar{\mathbf{I}}, \mathbf{0}\}, \qquad \bar{\mathbf{I}} = \mathrm{diag}\{-1, 1, 1\} \tag{4.21}$$

For a B-centered 180° domain wall a similar symmetry relation holds,

$$\mathbf{X}_0 = \mathbf{R}'\mathbf{X}_1 + \mathbf{R}\mathbf{X}_2 \tag{4.22}$$

The expected displacements for an A-centered 180° domain walls is schematically shown in Fig. 4.5. The boundary and transition equations are now written as

$$\begin{pmatrix} \mathcal{A}_0^{(1)} + \mathcal{A}_{-1}^{(1)}\mathbf{R} & \mathcal{A}_1^{(1)} + \mathcal{A}_{-1}^{(1)}\mathbf{R}' & \mathbf{0} \\ \mathcal{A}_{-1}^{(2)} & \mathcal{A}_0^{(2)} & \mathcal{A}_1^{(2)} \end{pmatrix} \begin{pmatrix} \mathbf{X}_1 \\ \mathbf{X}_2 \\ \mathbf{X}_3 \end{pmatrix} = \begin{pmatrix} \mathbf{F}_1 \\ \mathbf{F}_2 \end{pmatrix} \tag{4.23}$$

Let us now transform the bulk governing equations to an auxiliary system of first-order difference equations by defining,

$$\mathbf{Y}_n = \begin{pmatrix} \mathbf{X}_{n-1} \\ \mathbf{X}_n \end{pmatrix} \qquad n \geq 3 \tag{4.24}$$

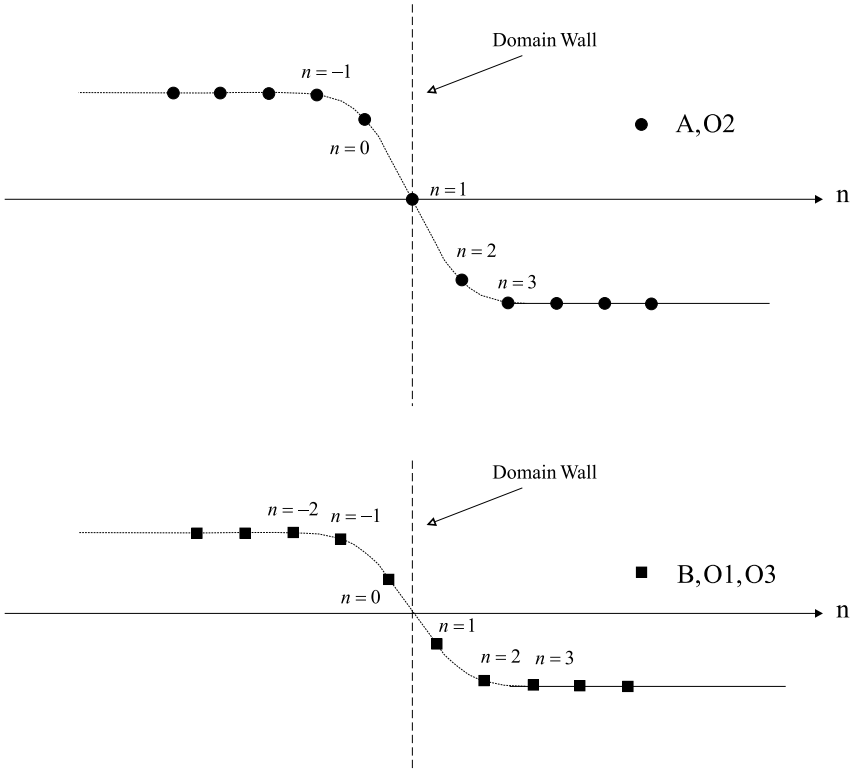

Figure 4.5: Expected displacements for an A-centered 180° domain wall.

Now the governing equations for $\mathbf{Y}_n$ would be,

$$\mathbf{Y}_{n+1} = \mathcal{A}\mathbf{Y}_n + \mathbf{G}_n \qquad n \geq 3 \tag{4.25}$$

where

$$\mathcal{A} = \begin{pmatrix} \mathbf{0} & \mathbf{1} \\ -\mathcal{A}_1^{-1}\mathcal{A}_{-1} & -\mathcal{A}_1^{-1}\mathcal{A}_0 \end{pmatrix} \in \mathbb{R}^{60\times 60} \quad \text{and} \quad \mathbf{G}_n = \begin{pmatrix} \mathbf{0} \\ \mathcal{A}_1^{-1}\mathbf{F}_n \end{pmatrix} \in \mathbb{R}^{60} \tag{4.26}$$

Note that here we have assumed that $\mathcal{A}_1$ is invertible. This is not necessarily the case and should be checked. In our numerical results this matrix is always invertible as roughly speaking we use 'enough' number of nearest neighbors. At the end of Appendix B we study the possible degeneracy in a difference equation for a simplified 2-D model. One can easily show by induction that the solution has the following explicit form,

$$\mathbf{Y}_n = \mathcal{A}^{n-3}\mathbf{c} + \sum_{j=3}^{n-1} \mathcal{A}^{n-j-1}\mathbf{G}_j \qquad n \geq 3 \tag{4.27}$$

where

$$\mathbf{c} = \mathbf{Y}_3 = \begin{pmatrix} \mathbf{X}_2 \\ \mathbf{X}_3 \end{pmatrix} \tag{4.28}$$

It is difficult to impose the boundedness equations at infinity to the above explicit solution. However, we can simplify the solution by exploiting the property that unbalanced forces are nonzero only in a localized region close to the domain wall. Suppose $\mathbf{G}_n = \mathbf{0}$ for $|n| > N$. As we will see later, for the shell potentials modelling $BaTiO_3$ and $PbTiO_3$, N is a small integer. In the case of localized forces the solution is rewritten as

$$\begin{aligned}
&\mathbf{Y}_4 = \mathcal{A}\mathbf{c} + \mathbf{G}_3 \\
&\mathbf{Y}_5 = \mathcal{A}^2\mathbf{c} + \mathcal{A}\mathbf{G}_3 + \mathbf{G}_4 \\
&\vdots \\
&\mathbf{Y}_{N+1} = \mathcal{A}^{N-2}\mathbf{c} + \mathcal{A}^{N-3}\mathbf{G}_3 + ... + \mathbf{G}_N = \mathcal{A}^{N-2}\mathbf{c} + \mathbf{d} \\
&\mathbf{Y}_{N+2} = \mathcal{A}\left(\mathcal{A}^{N-2}\mathbf{c} + \mathbf{d}\right) \\
&\vdots \\
&\mathbf{Y}_n = \mathcal{A}^{n-(N+1)}\left(\mathcal{A}^{N-2}\mathbf{c} + \mathbf{d}\right) \qquad n \geq N+1
\end{aligned} \tag{4.29}$$

A physically meaningful solution should be bounded at infinity. The matrix $\mathcal{A}$ is not diagonalizable because of translation invariance of the governing equations. However, it has the following Jordan decomposition,

$$\mathcal{A} = \mathbf{X}\mathbf{\Lambda}\mathbf{X}^{-1} \tag{4.30}$$

where $\mathbf{X}$ is the matrix of generalized eigenvectors and $\mathbf{\Lambda}$ has the following form,

$$\mathbf{\Lambda} = \begin{pmatrix} \mathbf{\Lambda}_1 & & \\ & \mathbf{J} & \\ & & \mathbf{\Lambda}_2 \end{pmatrix} \in \mathbb{R}^{60}, \quad \mathbf{\Lambda}_1, \mathbf{\Lambda}_2 \in \mathbb{R}^{27} \tag{4.31}$$

Here $\mathbf{\Lambda}_1$ and $\mathbf{\Lambda}_2$ are diagonal matrices of eigenvalues of modulus greater than and smaller than 1, respectively and $\mathbf{J} \in \mathbb{R}^{6\times 6}$ is the Jordan block corresponding to the eigenvalue $\lambda = 1$ with multiplicity six. It is interesting that we see this beautiful structure for both $BaTiO_3$ and $PbTiO_3$ shell potentials. Now for $n \geq N+1$,

$$\mathbf{Y}_n = \mathbf{X}\mathbf{\Lambda}^{n-(N+1)}\left(\mathbf{\Lambda}^{N-2}\mathbf{X}^{-1}\mathbf{c} + \mathbf{X}^{-1}\mathbf{d}\right) \tag{4.32}$$

Boundedness equations can be written as

$$\left(\mathbf{\Lambda}^{N-2}\mathbf{X}^{-1}\mathbf{c}\right)_{\{1,\ldots,30\}} = \left(-\mathbf{X}^{-1}\mathbf{d}\right)_{\{1,\ldots,30\}} \tag{4.33}$$

where $(.)_{\{1,\ldots,30\}}$ means the first thirty rows of the matrix (.). The boundedness and boundary/transition equations can be rewritten as

$$\begin{pmatrix} \mathcal{A}_{-1}^{(1)}\mathbf{R} + \mathcal{A}_{0}^{(1)} & \mathcal{A}_{-1}^{(1)}\mathbf{R}' + \mathcal{A}_{1}^{(1)} & \mathbf{0} \\ \mathcal{A}_{-1}^{(2)} & \mathcal{A}_{0}^{(2)} & \mathcal{A}_{1}^{(2)} \\ \mathbf{0} & \mathbf{D}_1 & \mathbf{D}_2 \end{pmatrix} \begin{pmatrix} \mathbf{X}_1 \\ \mathbf{X}_2 \\ \mathbf{X}_3 \end{pmatrix} = \begin{pmatrix} \mathbf{F}_1 \\ \mathbf{F}_2 \\ \mathbf{F}_D \end{pmatrix} \tag{4.34}$$

Note that for a translationally-invariant system the above system of equations may not have a solution. In other words, the coefficient matrix may not be full rank. Here, there is no such problem as we used the symmetry of the 180° domain wall and A and O2 (for an A-centered domain wall) cores and shells on the domain wall will be fixed. The numerical results confirm this. It turns out that the matrix $\mathcal{A}$ is highly ill-conditioned. The reason is that the stiffness coefficients fall off as $O(\frac{1}{r^3})$ and this results in a wide spectrum for $\mathcal{A}$. Our direct solution involves several high-order powers of this matrix which result in serious numerical problems. This can be resolved as follows. Using the boundedness relations (4.33), the solution can be written as

$$\mathbf{Y}_n = \mathbf{X}\mathbf{\Lambda}^{n-(N+1)}\mathbf{e} \tag{4.35}$$

where

$$\mathbf{e} = \begin{pmatrix} \mathbf{0} \\ \mathbf{E} \end{pmatrix} \in \mathbb{R}^{60} \tag{4.36}$$

and

$$\mathbf{E} = \left(\mathbf{X}^{-1}\mathcal{A}^{N-3}\mathbf{c} + \mathbf{X}^{-1}\mathbf{d}\right)_{\{31,\ldots,60\}} \tag{4.37}$$

Thus

$$\mathbf{Y}_n = \mathbf{X}\begin{pmatrix} \mathbf{0} \\ \overline{\mathbf{\Lambda}}_2{}^{n-(N+1)}\mathbf{E} \end{pmatrix} = \begin{pmatrix} \mathbf{X}_{12}\overline{\mathbf{\Lambda}}_2{}^{n-(N+1)}\mathbf{E} \\ \mathbf{X}_{22}\overline{\mathbf{\Lambda}}_2{}^{n-(N+1)}\mathbf{E} \end{pmatrix} \tag{4.38}$$

where

$$\mathbf{\Lambda} = \begin{pmatrix} \overline{\mathbf{\Lambda}}_1 & \mathbf{0} \\ \mathbf{0} & \overline{\mathbf{\Lambda}}_2 \end{pmatrix}, \qquad \mathbf{X} = \begin{pmatrix} \mathbf{X}_{11} & \mathbf{X}_{12} \\ \mathbf{X}_{21} & \mathbf{X}_{22} \end{pmatrix} \tag{4.39}$$

i.e., $\overline{\mathbf{\Lambda}}_1$ is the part of $\mathbf{\Lambda}$ that corresponds to boundedness equations. Note that we assumed that all the necessary row permutations have been done for writing the above representation. The nice thing about the above modified solution is that those eigenvalues with modulus larger than one are automatically ignored and the effective condition number is reduced considerably. If N

is not a small number the following method for solving the difference equations may be more favorable as one does not like to see large matrix powers of $\mathbf{\Lambda}$ in the numerical calculations. Let us consider the representative unit cells $n = 1, ..., N$ as boundary cells with the following governing equations,

$$\mathcal{A}_{-1}^{(1)}\mathbf{X}_0 + \mathcal{A}_0^{(1)}\mathbf{X}_1 + \mathcal{A}_1^{(1)}\mathbf{X}_2 = \mathbf{F}_1 \tag{4.40}$$

$$\mathcal{A}_{-1}^{(2)}\mathbf{X}_1 + \mathcal{A}_0^{(2)}\mathbf{X}_2 + \mathcal{A}_1^{(2)}\mathbf{X}_3 = \mathbf{F}_2 \tag{4.41}$$

$$\mathcal{A}_{-1}\mathbf{X}_2 + \mathcal{A}_0\mathbf{X}_3 + \mathcal{A}_1\mathbf{X}_4 = \mathbf{F}_3 \tag{4.42}$$

$$\vdots$$

$$\mathcal{A}_{-1}\mathbf{X}_{N-1} + \mathcal{A}_0\mathbf{X}_N + \mathcal{A}_1\mathbf{X}_{N+1} = \mathbf{F}_N \tag{4.43}$$

We know that

$$\mathbf{Y}_{n+1} = \mathbf{A}\mathbf{X}_n \qquad n \geq N+1 \tag{4.44}$$

Thus

$$\mathbf{Y}_n = \mathbf{A}^{n-N}\mathbf{c}, \mathbf{c} = \mathbf{Y}_N \qquad n \geq N+1 \tag{4.45}$$

Boundedness equations can be written as

$$\left(\mathbf{X}^{-1}\mathbf{c}\right)_{\{1,...,30\}} = \mathbf{0} \tag{4.46}$$

There are $30 \times N$ boundary equations and 30 boundedness equations and solving these equations we obtain the $N+1$ unknown vectors $\mathbf{X}_1, ..., \mathbf{X}_{N+1}$.

ii) $\mathbf{m = 2}$: The bulk governing equations are,

$$\mathcal{A}_{-2}\mathbf{X}_{n-2} + \mathcal{A}_{-1}\mathbf{X}_{n-1} + \mathcal{A}_0\mathbf{X}_n + \mathcal{A}_1\mathbf{X}_{n+1} + \mathcal{A}_2\mathbf{X}_{n+2} = \mathbf{F}_n \qquad n \geq 4 \tag{4.47}$$

The boundary and transition equations are,

$$n = 1: \quad \mathcal{A}_{-2}^{(1)}\mathbf{X}_{n-2} + \mathcal{A}_{-1}^{(1)}\mathbf{X}_{n-1} + \mathcal{A}_0^{(1)}\mathbf{X}_n + \mathcal{A}_1^{(1)}\mathbf{X}_{n+1} + \mathcal{A}_2^{(1)}\mathbf{X}_{n+2} = \mathbf{F}_1 \tag{4.48}$$

$$n = 2: \quad \mathcal{A}_{-2}^{(2)}\mathbf{X}_{n-2} + \mathcal{A}_{-1}^{(2)}\mathbf{X}_{n-1} + \mathcal{A}_0^{(2)}\mathbf{X}_n + \mathcal{A}_1^{(2)}\mathbf{X}_{n+1} + \mathcal{A}_2^{(2)}\mathbf{X}_{n+2} = \mathbf{F}_2 \tag{4.49}$$

$$n = 3: \quad \mathcal{A}_{-2}^{(3)}\mathbf{X}_{n-2} + \mathcal{A}_{-1}^{(3)}\mathbf{X}_{n-1} + \mathcal{A}_0^{(3)}\mathbf{X}_n + \mathcal{A}_1^{(3)}\mathbf{X}_{n+1} + \mathcal{A}_2^{(3)}\mathbf{X}_{n+2} = \mathbf{F}_3 \tag{4.50}$$

where one has the following symmetries,

$$\text{A-centered}: \quad \mathbf{X}_0 = \mathbf{R}\mathbf{X}_1 + \mathbf{R}'\mathbf{X}_2, \ \mathbf{X}_{-1} = \mathbf{R}\mathbf{X}_2 + \mathbf{R}'\mathbf{X}_3 \tag{4.51}$$

$$\text{B-centered}: \quad \mathbf{X}_0 = \mathbf{R}'\mathbf{X}_1 + \mathbf{R}\mathbf{X}_2, \ \mathbf{X}_{-1} = \mathbf{R}'\mathbf{X}_2 + \mathbf{R}\mathbf{X}_3 \tag{4.52}$$

The bulk governing equations can be transformed into auxiliary first-order difference equations by defining,

$$\mathbf{Y}_n = \begin{pmatrix} \mathbf{X}_{n-2} \\ \mathbf{X}_{n-1} \\ \mathbf{X}_n \\ \mathbf{X}_{n+1} \end{pmatrix} \in \mathbb{R}^{120} \qquad n \geq 4 \tag{4.53}$$

The governing equations for $\mathbf{Y}_n$ are,

$$\mathbf{Y}_{n+1} = \mathcal{A}\mathbf{Y}_n + \mathbf{G}_n \qquad n \geq 4 \tag{4.54}$$

where

$$\mathcal{A} = \begin{pmatrix} \mathbf{0} & \mathbf{1} & \mathbf{0} & \mathbf{0} \\ \mathbf{0} & \mathbf{0} & \mathbf{1} & \mathbf{0} \\ \mathbf{0} & \mathbf{0} & \mathbf{0} & \mathbf{1} \\ -\mathcal{A}_2^{-1}\mathcal{A}_{-2} & -\mathcal{A}_2^{-1}\mathcal{A}_{-1} & -\mathcal{A}_2^{-1}\mathcal{A}_0 & -\mathcal{A}_2^{-1}\mathcal{A}_1 \end{pmatrix} \in \mathbb{R}^{120\times 120}, \quad \mathbf{G}_n = \begin{pmatrix} \mathbf{0} \\ \mathbf{0} \\ \mathbf{0} \\ \mathcal{A}_2^{-1}\mathbf{F}_n \end{pmatrix} \in \mathbb{R}^{120} \tag{4.55}$$

The general solution can be written as

$$\mathbf{Y}_n = \mathcal{A}^{n-4}\mathbf{c} + \sum_{j=4}^{n-1} \mathcal{A}^{n-j-1}\mathbf{G}_j \qquad n \geq 4 \tag{4.56}$$

where $\mathbf{c} = \mathbf{Y}_4 = (\mathbf{X}_2 \ \mathbf{X}_3 \ \mathbf{X}_4 \ \mathbf{X}_5)^\mathsf{T}$ is the vector of integration constants. In general for interactions of order m the solution of the auxiliary first-order equation can be written as

$$\mathbf{Y}_n = \mathcal{A}^{n-m-2}\mathbf{Y}_{m+2} + \sum_{j=m+2}^{n-1} \mathcal{A}^{n-j-1}\mathbf{G}_j \qquad n \geq m+2 \tag{4.57}$$

where

$$\mathbf{Y}_n = \left(\mathbf{X}_{n-m}, ..., \mathbf{X}_{n+m-1}\right)^\mathsf{T} \tag{4.58}$$

If $\mathbf{G}_n = \mathbf{0}$ for $|n| > N$, then,

$$\begin{aligned}
&\mathbf{Y}_5 = \mathcal{A}\mathbf{c} + \mathbf{G}_4 \\
&\mathbf{Y}_6 = \mathcal{A}^2\mathbf{c} + \mathcal{A}\mathbf{G}_4 + \mathbf{G}_5 \\
&\vdots \\
&\mathbf{Y}_{N+1} = \mathcal{A}^{N-3}\mathbf{c} + \mathcal{A}^{N-4}\mathbf{G}_4 + ... + \mathbf{G}_N = \mathcal{A}^{N-3}\mathbf{c} + \mathbf{d} \\
&\mathbf{Y}_{N+2} = \mathcal{A}\left(\mathcal{A}^{N-3}\mathbf{c} + \mathbf{d}\right) \\
&\vdots \\
&\mathbf{Y}_n = \mathcal{A}^{n-(N+1)}\left(\mathcal{A}^{N-3}\mathbf{c} + \mathbf{d}\right) \qquad n \geq N+1
\end{aligned} \tag{4.59}$$

Boundedness equations read,

$$\left(\mathbf{\Lambda}^{N-3}\mathbf{X}^{-1}\mathbf{c}\right)_{\{1,\ldots,60\}} = \left(-\mathbf{X}^{-1}\mathbf{d}\right)_{\{1,\ldots,60\}} \tag{4.60}$$

Or,

$$\begin{pmatrix} \mathbf{D}_{11} & \mathbf{D}_{12} & \mathbf{D}_{13} & \mathbf{D}_{14} \\ \mathbf{D}_{21} & \mathbf{D}_{22} & \mathbf{D}_{23} & \mathbf{D}_{24} \end{pmatrix} \begin{pmatrix} \mathbf{X}_2 \\ \mathbf{X}_3 \\ \mathbf{X}_4 \\ \mathbf{X}_5 \end{pmatrix} = \begin{pmatrix} \mathbf{F}_{D1} \\ \mathbf{F}_{D2} \end{pmatrix} \tag{4.61}$$

Thus the vector of unknowns can be obtained by solving the following system of linear equations,

$$\begin{pmatrix} \mathcal{A}_{-1}^{(1)}\mathbf{R} + \mathcal{A}_0^{(1)} & \mathcal{A}_{-2}^{(1)}\mathbf{R} + \mathcal{A}_{-1}^{(1)}\mathbf{R}' + \mathcal{A}_1^{(1)} & \mathcal{A}_{-2}^{(1)}\mathbf{R}' + \mathcal{A}_2^{(1)} & \mathbf{0} & \mathbf{0} \\ \mathcal{A}_{-2}^{(2)}\mathbf{R} + \mathcal{A}_{-1}^{(2)} & \mathcal{A}_{-2}^{(2)}\mathbf{R}' + \mathcal{A}_0^{(2)} & \mathcal{A}_1^{(2)} & \mathcal{A}_2^{(2)} & \mathbf{0} \\ \mathcal{A}_{-2}^{(3)} & \mathcal{A}_{-1}^{(3)} & \mathcal{A}_0^{(3)} & \mathcal{A}_1^{(3)} & \mathcal{A}_2^{(3)} \\ \mathbf{0} & \mathbf{D}_{11} & \mathbf{D}_{12} & \mathbf{D}_{13} & \mathbf{D}_{14} \\ \mathbf{0} & \mathbf{D}_{21} & \mathbf{D}_{22} & \mathbf{D}_{23} & \mathbf{D}_{24} \end{pmatrix} \begin{pmatrix} \mathbf{X}_1 \\ \mathbf{X}_2 \\ \mathbf{X}_3 \\ \mathbf{X}_4 \\ \mathbf{X}_5 \end{pmatrix} = \begin{pmatrix} \mathbf{F}_1 \\ \mathbf{F}_2 \\ \mathbf{F}_3 \\ \mathbf{F}_{D1} \\ \mathbf{F}_{D2} \end{pmatrix} \tag{4.62}$$

Because of symmetry, A and O2 cores and shells (for an A-centered 180° domain wall) on the domain wall will remain on the domain wall after deformation. Again, because of ill-conditioning of $\mathcal{A}$ the solution should be rewritten as

$$\mathbf{Y}_n = \mathbf{X}\mathbf{\Lambda}^{n-(N+1)}\mathbf{e}, \qquad \mathbf{e} = \begin{pmatrix} \mathbf{0} \\ \mathbf{E} \end{pmatrix} \in \mathbb{R}^{60} \tag{4.63}$$

where

$$\mathbf{E} = \left(\mathbf{X}^{-1}\mathbf{\Lambda}^{N-3}\mathbf{c} + \mathbf{X}^{-1}\mathbf{d}\right)_{\{61,\ldots,120\}} \tag{4.64}$$

Thus

$$\mathbf{Y}_n = \begin{pmatrix} \mathbf{X}_{12}\bar{\mathbf{\Lambda}}_1^{n-(N+1)}\mathbf{E} \\ \mathbf{X}_{22}\bar{\mathbf{\Lambda}}_2^{n-(N+1)}\mathbf{E} \end{pmatrix}, \quad \mathbf{X} = \begin{pmatrix} \mathbf{X}_{11} & \mathbf{X}_{12} \\ \mathbf{X}_{21} & \mathbf{X}_{22} \end{pmatrix} \in \mathbb{R}^{120\times 120}, \quad \mathbf{\Lambda} = \begin{pmatrix} \bar{\mathbf{\Lambda}}_1 & \mathbf{0} \\ \mathbf{0} & \bar{\mathbf{\Lambda}}_2 \end{pmatrix} \in \mathbb{R}^{120\times 120} \tag{4.65}$$

4.1.1 Domain Wall Energy

Domain wall energy is defined to be the difference between energies of a crystal with and without the domain wall. Because the distortions are localized[†] one can calculate the domain wall energy numerically by considering a finite region including the domain wall and calculating its energy. Energy is defined per unit of the wall area,

$$E_{\mathrm{DW}} = \lim_{N\to\infty} \frac{1}{ac}\left(\sum_{n=-N}^{N} E_n - 2NE_{\mathrm{cell}}\right)$$

where E_n is the energy of unit cell of index n and E_{cell} is the energy of the bulk tetragonal unit cell.

4.1.2 A Note on Stiffness Matrices on Left and Right Sides of the Domain Wall

A major difference of the problem of domain walls with other defects studied in the literature using the method of lattice statics is the inhomogeneity of the stiffness matrices. For the sake of clarity we explain this point for 180° domain walls in $PbTiO_3$. It would be enough to see the inhomogeneity of the stiffness matrices for the short-range interactions. Let us denote the multi-lattice with spontaneous polarization $\mathbf{P}^+ = \mathbf{P}_s\hat{\mathbf{e}}_2$ by $\mathcal{L}^+$ and the multi-lattice with spontaneous polarization $\mathbf{P}^- = -\mathbf{P}_s\hat{\mathbf{e}}_2$ by $\mathcal{L}^-$. The only difference between $\mathcal{L}^-$ and $\mathcal{L}^-$ is their shift vectors. For short-range interactions we only need to look at the Bravais lattices of shells. These have the following shift vectors for the two multi-lattices,

$$\mathbf{p}_1^+ = \begin{pmatrix} 0 \\ \delta_s Pb \\ 0 \end{pmatrix}, \mathbf{p}_2^+ = \begin{pmatrix} a/2 \\ \delta_s Ti \\ a/2 \end{pmatrix}, \mathbf{p}_3^+ = \begin{pmatrix} a/2 \\ c/2+\delta_s O1 \\ 0 \end{pmatrix}, \mathbf{p}_4^+ = \begin{pmatrix} 0 \\ c/2+\delta_s O2 \\ a/2 \end{pmatrix}, \mathbf{p}_5^+ = \begin{pmatrix} a/2 \\ \delta_s O3 \\ a/2 \end{pmatrix}$$

$$\mathbf{p}_1^- = \begin{pmatrix} 0 \\ -\delta_s Pb \\ 0 \end{pmatrix}, \mathbf{p}_2^- = \begin{pmatrix} a/2 \\ -\delta_s Ti \\ a/2 \end{pmatrix}, \mathbf{p}_3^- = \begin{pmatrix} a/2 \\ c/2-\delta_s O1 \\ 0 \end{pmatrix}, \mathbf{p}_4^- = \begin{pmatrix} 0 \\ c/2-\delta_s O2 \\ a/2 \end{pmatrix}, \mathbf{p}_5^- = \begin{pmatrix} a/2 \\ -\delta_s O3 \\ a/2 \end{pmatrix}$$

[†]This will be seen in the numerical examples.

We know that

$$\mathbf{K}^{+}_{iI\alpha} = \sum_{J\beta \in \mathcal{S}^{+}_{I\alpha}} \frac{\partial^2 E}{\partial \mathbf{x}^i \partial \mathbf{x}^{J\beta}}(\mathcal{B}^{+}_0) \tag{4.66}$$

$$\mathbf{K}^{-}_{iI\alpha} = \sum_{J\beta \in \mathcal{S}^{-}_{I\alpha}} \frac{\partial^2 E}{\partial \mathbf{x}^i \partial \mathbf{x}^{J\beta}}(\mathcal{B}^{-}_0) \tag{4.67}$$

It can be easily shown that

$$\mathbf{K}^{-}_{II\alpha} = \mathbf{K}^{+}_{II\alpha} \tag{4.68}$$

This can be clearly seen by looking at the example $I = 1, \alpha = 1$. In this case,

$$\mathcal{S}^{+}_{11} = \left\{(\nu^1 a, \nu^2 c + \delta_s Pb, \nu^a) \in \mathbb{R}^3 : (\nu^1, \nu^2, \nu^3) \in \mathbb{Z}^3\right\} \tag{4.69}$$

$$\mathcal{S}^{-}_{11} = \left\{(\nu^1 a, \nu^2 c - \delta_s Pb, \nu^3 a) \in \mathbb{R}^3 : (\nu^1, \nu^2, \nu^3) \in \mathbb{Z}^3\right\} \tag{4.70}$$

For calculating $\mathbf{K}^{+}_{111}$ the origin is $(0, \delta_s Pb, 0)$ and the following relative position vectors are used,

$$\mathcal{V} = \left\{(\nu^1 a, \nu^2 c, \nu^3 a) \in \mathbb{R}^3 : (\nu^1, \nu^2, \nu^3) \in \mathbb{Z}^3\right\} \tag{4.71}$$

For calculating $\mathbf{K}^{-}_{111}$ the origin is $(0, -\delta_s Pb, 0)$ and the set of relative position vectors would be identical to $\mathcal{V}$ and hence $\mathbf{K}^{-}_{111} = \mathbf{K}^{+}_{111}$. However, in general,

$$\mathbf{K}^{-}_{IJ\alpha} \neq \mathbf{K}^{+}_{IJ\alpha} \qquad I \neq J \tag{4.72}$$

To see this let us consider the case $I = 1, J = 2, \alpha = 1$. For calculating $\mathbf{K}^{+}_{121}$ the origin is $(0, \delta_s Pb, 0)$ and the following relative position vectors are used,

$$\mathcal{V}^{+} = \left\{(\nu^1 a, \nu^2 c + \delta_s Ti - \delta_s Pb, \nu^3 a) \in \mathbb{R}^3 : (\nu^1, \nu^2, \nu^3) \in \mathbb{Z}^3\right\} \tag{4.73}$$

and for calculating $\mathbf{K}^{-}_{121}$ the origin is $(0, -\delta_s Pb, 0)$ and the following relative position vectors are used,

$$\mathcal{V}^{-} = \left\{(\nu^1 a, \nu^2 c - (\delta_s Ti - \delta_s Pb), \nu^3 a) \in \mathbb{R}^3 : (\nu^1, \nu^2, \nu^3) \in \mathbb{Z}^3\right\} \tag{4.74}$$

Obviously $\mathcal{V}^{-} \neq \mathcal{V}^{+}$ and hence $\mathbf{K}^{-}_{121} \neq \mathbf{K}^{+}_{121}$.

4.1.3 An Approximate Solution of the 180° Domain Wall Problem

In this subsection we present an approximate solution for the analysis of 180° domain walls using discrete Fourier transform. This method will be used for the 180° step problem in the sequel. We know that on the two sides of the domain wall stiffnesses are different. Let us consider a homogenized

medium with the average stiffness matrices of the both sides of the domain wall, i.e.,

$$\mathbf{K}_{IJ\alpha} = \frac{1}{2}\left(\mathbf{K}^{+}_{IJ\alpha} + \mathbf{K}^{-}_{IJ\alpha}\right) \tag{4.75}$$

where $\mathbf{K}^{+}_{IJ\alpha}$ and $\mathbf{K}^{-}_{IJ\alpha}$ are the bulk stiffnesses for the multi-lattices $\mathcal{L}^{+}$ and $\mathcal{L}^{-}$, respectively. We also ignore the local inhomogeneity of the stiffness matrices close to the domain wall. Thus the following is the governing equations of the homogenized medium,

$$\sum_{\alpha=-m}^{\alpha=m} \mathcal{A}_{\alpha}\mathbf{X}_{n+\alpha} = \mathbf{F}_{n} \qquad n \in \mathbb{Z} \tag{4.76}$$

where $\mathbf{F}_n$ is the exact force vector calculated from the interatomic potential. Applying DFT to the above equation yields

$$\mathbf{B}(k)\widehat{\mathbf{X}_n}(k) = \widehat{\mathbf{F}_n}(k) \qquad k \in B = [-\pi, \pi] \tag{4.77}$$

where

$$\mathbf{B}(k) = \sum_{\alpha=-m}^{\alpha=m} e^{-i\alpha k}\mathcal{A}_{\alpha} \tag{4.78}$$

Note that $\mathbf{B}(k)$ is singular at $k = 0$ because of translation invariance of the governing equations. Taking the inverse DFT we obtain,

$$\mathbf{X}_n = \frac{1}{2\pi}\int_{-\pi}^{\pi} e^{-ink}\left[\mathbf{B}^{-1}(k) - e^{ink}\mathbf{D}(k)\right]\widehat{\mathbf{F}_n}(k)dk \tag{4.79}$$

where

$$\mathbf{D}(k) = \begin{pmatrix} \mathbf{U}(k) & \dots & \mathbf{U}(k) \\ \vdots & & \vdots \\ \mathbf{U}(k) & \dots & \mathbf{U}(k) \end{pmatrix}, \qquad \mathbf{U}(k) = \begin{pmatrix} d_1(k) & 0 & 0 \\ 0 & d_2(k) & 0 \\ 0 & 0 & d_3(k) \end{pmatrix},$$

$$d_1(k) = \left(\mathbf{B}^{-1}(k)\right)_{11}, d_2(k) = \left(\mathbf{B}^{-1}(k)\right)_{22}, d_3(k) = \left(\mathbf{B}^{-1}(k)\right)_{33}$$

Note that

$$-\frac{1}{2\pi}\int_{-\pi}^{\pi} \mathbf{D}(k)\widehat{\mathbf{F}_n}(k)dk \tag{4.80}$$

is a rigid translation that removes the singularity. We will compare the approximate DFT harmonic displacements with the exacts ones at the end of this chapter.

4.1.4 Effect of Range of Interaction

In our lattice statics model forces are always calculated exactly. However, to be able to solve the governing discrete equations for an infinite lattice we need to have a system of difference equations of finite order. It would be interesting to know how sensitive the solutions are to the range of interaction of representative unit cells. It will be seen shortly that the solutions for $m = 1$ and $m = 2$ are different by less than 2%. Let us remind ourselves that in a continuum one can have two displacement fields which are close in some norm but have strain fields that are not close in the same norm. This cannot happen in a discrete system as will be shown below. The following lemma shows that two discrete displacement fields that are close in some norm have close discrete strain fields in the same norm.

Consider a sequence $\{x_n\}_{n=-\infty}^{\infty} \subset \mathbb{R}$ and assume that

$$\inf_{n\in\mathbb{Z}} |x_{n+1} - x_n| = \ell > 0$$

Consider real-valued functions f and g defined on this sequence. Define,

$$(\Delta f)(x_n) = \frac{f(x_{n+1}) - f(x_n)}{x_{n+1} - x_n}, \qquad (\Delta g)(x_n) = \frac{g(x_{n+1}) - g(x_n)}{x_{n+1} - x_n} \tag{4.81}$$

We have the following lemma.

Lemma 7. *Suppose,*

$$\sup_{n\in\mathbb{Z}} |f(x_n) - g(x_n)| \leq \epsilon \qquad \textit{for some positive } \epsilon$$

Then,

$$\sup_{n\in\mathbb{Z}} |(\Delta f)(x_n) - (\Delta g)(x_n)| \leq \frac{2\epsilon}{\ell} \qquad \textit{for some positive } \epsilon$$

Proof:

$$\begin{aligned} |(\Delta f)(x_n) - (\Delta g)(x_n)| &= \left| \frac{f(x_{n+1}) - g(x_{n+1})}{x_{n+1} - x_n} - \frac{f(x_n) - g(x_n)}{x_{n+1} - x_n} \right| \\ &\leq \left| \frac{f(x_{n+1}) - g(x_{n+1})}{x_{n+1} - x_n} \right| + \left| \frac{f(x_n) - g(x_n)}{x_{n+1} - x_n} \right| \qquad (4.82) \\ &\leq \frac{|f(x_{n+1}) - g(x_{n+1})|}{\ell} + \frac{|f(x_n) - g(x_n)|}{\ell} \qquad (4.83) \end{aligned}$$

Thus

$$\sup_{n\in\mathbb{Z}} |(\Delta f)(x_n) - (\Delta g)(x_n)| \leq \frac{2\epsilon}{\ell} \qquad \square$$

We will numerically study the effect of range of interaction on discrete displacements at the end

of this chapter.

4.2 Inhomogeneous Anharmonic Lattice Statics Analysis of 180° Domain Walls

Anharmonic lattice statics is based on Newton-Raphson (NR) method for solving nonlinear equations. The basic idea of NR method is to look at a quadratic approximation to the nonlinear equations in each step. Suppose $\mathbf{f} : \mathbb{R}^n \to \mathbb{R}^n$ is continuously differentiable and that $\mathbf{f}(\mathbf{x}^*) = \mathbf{0}$ for some $\mathbf{x}^* \in \mathcal{D} \subset \mathbb{R}^n$. We know that derivative of $\mathbf{f}$ is a linear map defined as

$$\mathbf{f}(\mathbf{x} + \mathbf{u}) = \mathbf{f}(\mathbf{x}) + D\mathbf{f}(\mathbf{x})\mathbf{u} + o(\|\mathbf{u}\|) \tag{4.84}$$

Let us start from an initial guess $\mathbf{x}_0 \in \mathcal{D}$. The linear approximation of $\mathbf{f}$ about $\mathbf{x}_0$ calculated at a point $\mathbf{x}_1 \in \mathcal{D}$ is

$$\mathbf{f}(\mathbf{x}_1) \approx \mathbf{f}(\mathbf{x}_0) + D\mathbf{f}(\mathbf{x}_0)(\mathbf{x}_1 - \mathbf{x}_0) \tag{4.85}$$

Assuming that $\mathbf{f}(\mathbf{x}_1) \approx \mathbf{0}$,

$$\mathbf{x}_1 = \mathbf{x}_0 - D\mathbf{f}(\mathbf{x}_0)^{-1}\mathbf{f}(\mathbf{x}_0) \tag{4.86}$$

Similarly, in the kth step,

$$\mathbf{x}_{k+1} = \mathbf{x}_k - D\mathbf{f}(\mathbf{x}_k)^{-1}\mathbf{f}(\mathbf{x}_k) \tag{4.87}$$

It can be shown that this algorithm has a quadratic convergence (see Dennis and Schnabel (1996)), i.e.,

$$\|\mathbf{x}_{k+1} - \mathbf{x}^*\| \leq C\|\mathbf{x}_k - \mathbf{x}^*\|^2 \qquad \text{for some positive number } C \tag{4.88}$$

The modified NR method is based on a similar idea. In the kth iteration,

$$\mathbf{x}_{k+1} = \mathbf{x}_k - D\mathbf{f}(\mathbf{x}_0)^{-1}\mathbf{f}(\mathbf{x}_k) \tag{4.89}$$

i.e., the only difference is that in all the steps the derivative of the initial guess is used. This is slower than the usual NR iteration. By modifying the proof presented in (Dennis and Schnabel, 1996), it can be easily shown that the convergence of modified NR method is linear, i.e.,

$$\|\mathbf{x}_{k+1} - \mathbf{x}^*\| \leq C\|\mathbf{x}_k - \mathbf{x}^*\| \qquad \text{for some positive number } C \tag{4.90}$$

It is important to note that the Hessian at $\mathbf{x} = \mathbf{x}_0$ should be positive-definite for the modified NR to converge.

The idea of anharmonic lattice statics is to find the fully nonlinear solutions by a modified Newton-Raphson iteration. In modified Newton-Raphson method the Hessian matrix is not updated in each iteration and the initial Hessian is used. Modified Newton-Raphson is slowly and linearly convergent and a large number of iterations should be performed to get good results. In our lattice statics calculations this is an efficient method as the most expensive part of the calculations is the computation of substiffness matrices (very slowly converging lattice sums). The discrete governing boundary-value problem for a 180° domain wall is

$$\begin{cases} \sum_{\alpha=-m}^{m} \mathcal{A}_\alpha \mathbf{X}_{n+\alpha} = \mathbf{F}_n, & n \geq m+2 \ (m \in \mathbb{N}) \\ \sum_{\alpha=-m}^{m} \mathcal{A}_\alpha(n) \mathbf{X}_{n+\alpha} = \mathbf{F}_n, & n = 1, ..., m+1 \\ \|\mathbf{X}_n\| < \infty \quad \text{as } n \to \infty \end{cases} \tag{4.91}$$

with the following symmetry relations,

$$\mathbf{X}_k = \mathbf{R}\mathbf{X}_{-k+1} + \mathbf{R}'\mathbf{X}_{-k+2} \qquad k = -m+1, ..., 0 \tag{4.92}$$

In the governing equations $\mathcal{A}_\alpha(n)$ are the boundary stiffness matrices and explicitly depend on n. For the first iteration the discrete governing boundary-value problem determining $\mathbf{X}^1 = \left\{\mathbf{X}_n^1\right\}$ is

$$\begin{cases} \sum_{\alpha=-m}^{m} \mathcal{A}_\alpha \mathbf{X}_{n+\alpha}^1 = \mathbf{F}_n^0, & n \geq m+2 \ (m \in \mathbb{N}) \\ \sum_{\alpha=-m}^{m} \mathcal{A}_\alpha(n) \mathbf{X}_{n+\alpha}^1 = \mathbf{F}_n^0, & n = 1, ..., m+1 \\ \|\mathbf{X}_n^1\| < \infty \quad \text{as } n \to \infty \end{cases} \tag{4.93}$$

where

$$\mathbf{F}_n^0 = \mathbf{F}_n\left(\mathcal{B}_0\right) \tag{4.94}$$

and $\mathcal{B}_0$ is the starting configuration (reference configuration). For the next step,

$$\mathcal{B}_1 = \mathcal{B}_0 + \left\{\mathbf{X}_n^1\right\}, \qquad \mathbf{F}_n^1 = \mathbf{F}_n\left(\mathcal{B}_1\right) \tag{4.95}$$

Now the discrete governing boundary-value problem determining $\mathbf{X}^2 = \left\{\mathbf{X}_n^2\right\}$ is

$$\begin{cases} \sum_{\alpha=-m}^{m} \mathcal{A}_\alpha \mathbf{X}_{n+\alpha}^2 = \mathbf{F}_n^1, & n \geq m+2 \ (m \in \mathbb{N}) \\ \sum_{\alpha=-m}^{m} \mathcal{A}_\alpha(n) \mathbf{X}_{n+\alpha}^2 = \mathbf{F}_n^1, & n = 1, ..., m+1 \\ \|\mathbf{X}_n^2\| < \infty \quad \text{as } n \to \infty \end{cases} \tag{4.96}$$

Similarly, the discrete governing boundary-value problem determining $\mathbf{X}^{k+1} = \left\{\mathbf{X}_n^{k+1}\right\}$ is

$$\begin{cases} \sum_{\alpha=-m}^{m} \mathcal{A}_\alpha \mathbf{X}_{n+\alpha}^{k+1} = \mathbf{F}_n^k, & n \geq m+2 \ (m \in \mathbb{N}) \\ \sum_{\alpha=-m}^{m} \mathcal{A}_\alpha(n) \mathbf{X}_{n+\alpha}^{k+1} = \mathbf{F}_n^k, & n = 1, ..., m+1 \\ \|\mathbf{X}_n^{k+1}\| < \infty \quad \text{as } n \to \infty \end{cases} \tag{4.97}$$

where

$$\mathcal{B}_k = \mathcal{B}_{k-1} + \left\{\mathbf{X}_n^k\right\}, \qquad \mathbf{F}_n^k = \mathbf{F}_n\left(\mathcal{B}_k\right) \tag{4.98}$$

It is to be noted that the matrices $\mathcal{A}_\alpha$ and $\mathcal{A}_\alpha(n)$ are calculated with reference to $\mathcal{B}_0$ and remain fixed during all the iterations. As we do not have control on the reference configuration it may be reasonable to update the stiffness matrices to ensure positive-definiteness of the discrete convolution operator. Because we expect to see localized distortions, the matrices $\mathcal{A}_\alpha$ will not change and it would be enough to update the boundary stiffness matrices. Now the kth iteration would have the following form,

$$\begin{cases} \sum_{\alpha=-m}^{m} \mathcal{A}_\alpha \mathbf{X}_{n+\alpha}^{k+1} = \mathbf{F}_n^k, & n \geq m+2 \ (m \in \mathbb{N}) \\ \sum_{\alpha=-m}^{m} \mathcal{A}_\alpha^k(n) \mathbf{X}_{n+\alpha}^{k+1} = \mathbf{F}_n^k, & n = 1, ..., m+1 \\ \|\mathbf{X}_n^{k+1}\| < \infty \quad \text{as } n \to \infty \end{cases} \tag{4.99}$$

where

$$\mathcal{A}_\alpha^k(n) = \mathcal{A}_\alpha(n)\left(\mathcal{B}_k\right) \tag{4.100}$$

We will numerically compare the harmonic and anharmonic solutions in the next section.

4.3 Numerical Results

In this section, we report some numerical results for both $BaTiO_3$ and $PbTiO_3$.

i) ***$BaTiO_3$***: The distribution of forces close to a Ba-centered 180° domain wall is shown in Fig. 4.6. It is seen that only atoms which have index $n = 1$ (atoms that are on the wall or are half a lattice spacing away from the wall) have non-zero forces. This will most likely lead to a very narrow domain wall. Also note that the only nonzero forces are the ones parallel to the c-axis (y-components) and perpendicular to the domain wall (x-components). It is also seen that the x-component of forces are much smaller than the y-components. Similar results can be observed for Ti-centered 180° domain wall in Fig. 4.7. One conclusion here is that the effective potential is highly localized. Harmonic displacement components of Ba and Ti core and shells near a Ba-centered 180° domain wall are shown in Fig. 4.8. As can be seen all the displacements approach constant values very quickly and the thickness of the domain wall is

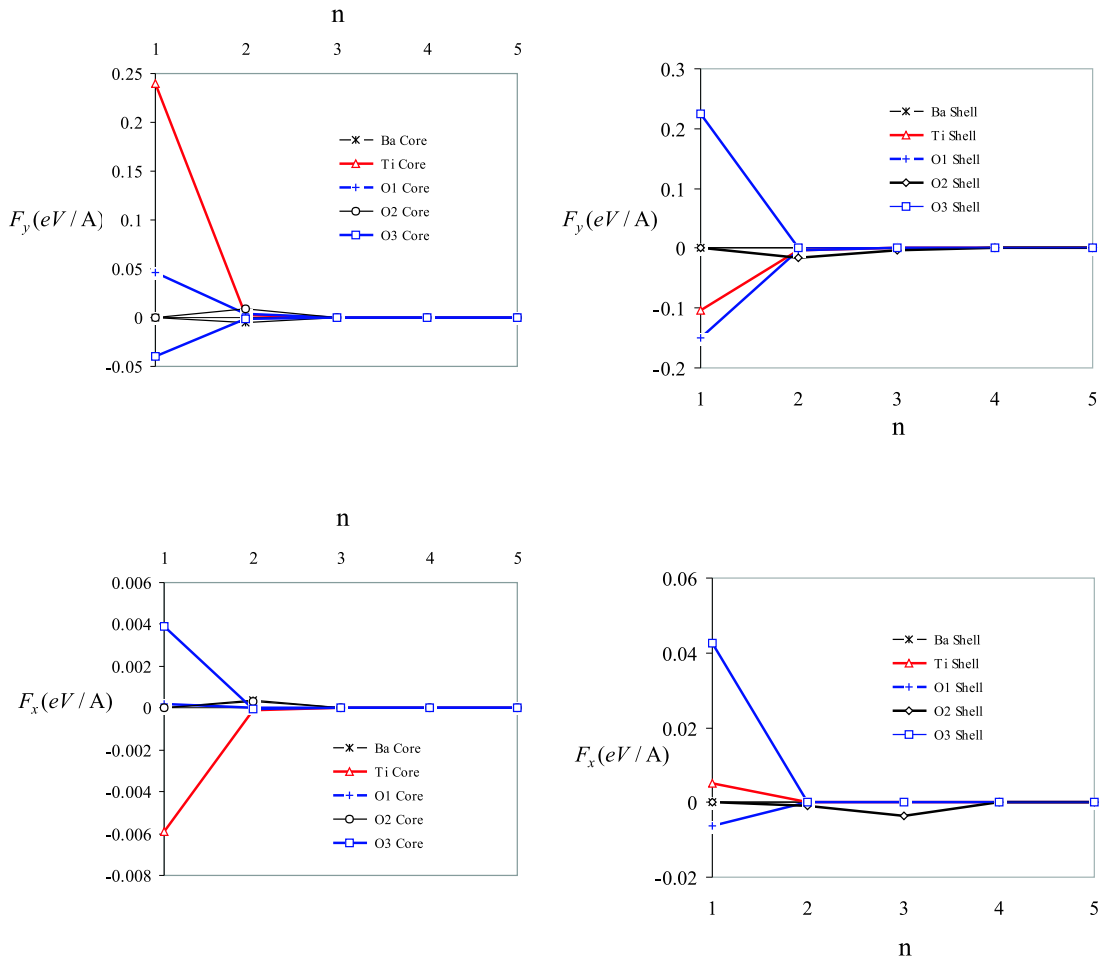

Figure 4.6: Unbalanced forces in the reference configuration of a Ba-centered 180° domain wall.

about 2 *nm*. It is seen that Ba does not contribute much to polarization in the tetragonal c-direction (y-component) as the cores and shells displace almost together. The harmonic displacements of O1, O2 and O3 core and shells are shown in Fig. 4.9. Again, the domain wall thickness is almost 2 *nm* and the O1 atoms do not contribute much to the polarization in the tetragonal c-direction. It is observed that for all the five lattices displacements perpendicular to the domain wall (x-component) are nonzero. The interesting thing is that (as we will see shortly) that x-component of displacements do not contribute to polarization and polarization vector is along the c-direction.

Figs. 4.10 and 4.11 show the distribution of discrete strains, which are defined to be the normalized backward differences of displacements, for all the five atoms. This gives one an idea on how thick a ferroelectric domain wall is. Fig. 4.12 shows the polarization distribution for Ba-centered and Ti-centered domain walls. It should be noted that in the lattice scale

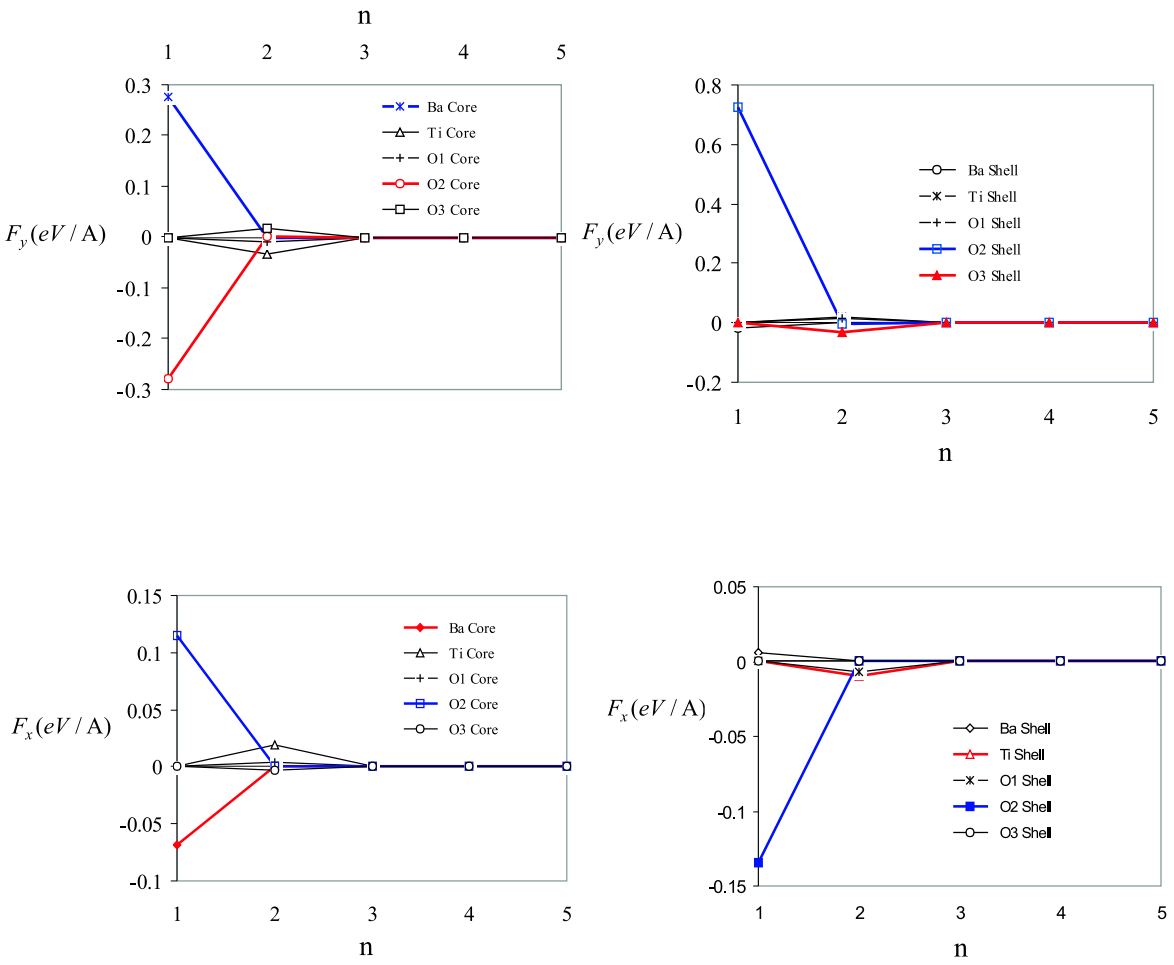

Figure 4.7: Unbalanced forces in the reference configuration of a Ti-centered 180° domain wall.

polarization (a macroscopic quantity) cannot be defined unambiguously. Here, we associate a polarization vector to each unit cell. For a Ba-centered domain wall, displacements of Ba and O2 on the two sides of each unit cell are averaged. For a Ti-centered 180° domain wall displacements of Ti, O1 and O3 are averaged.

To understand the effect of the range of interaction of equivalence classes the y-component of displacements of Ba cores and shells obtained from the second and fourth-order difference equations (m=1 and 2, respectively) are compared in Fig. 4.13. It is seen that the displacements are very close and this shows that considering the interactions $\{n-2, n-1, n, n+1, n+2\}$ should be enough for capturing the structure of the domain wall. This again shows that the effective potential is highly localized.

To study the effect of displacements perpendicular to the domain wall, we compare the con-

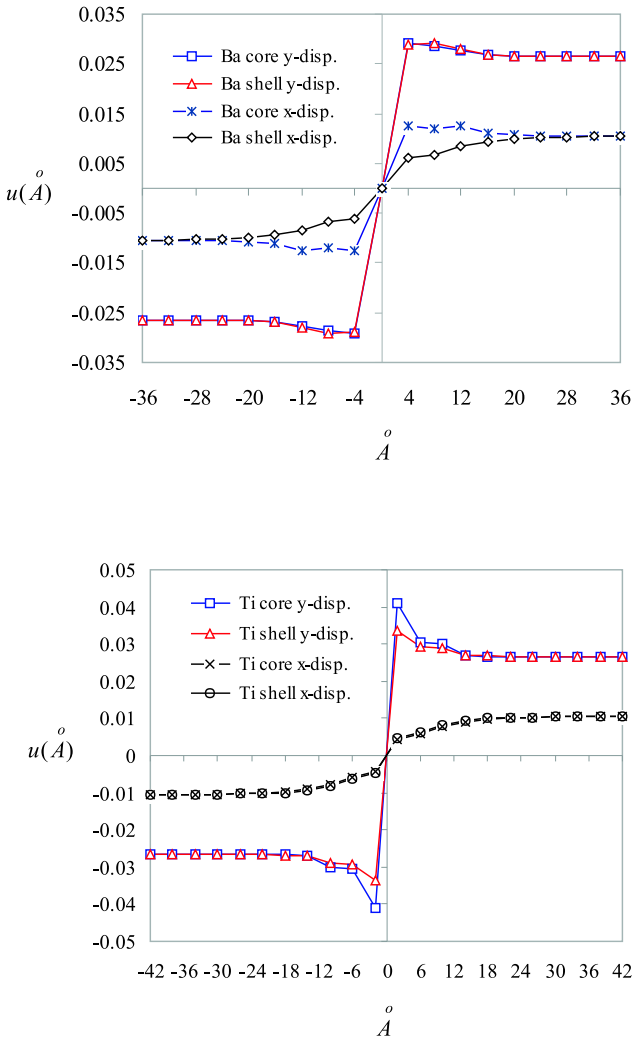

Figure 4.8: Displacements of Ba and Ti core and shells in a Ba-centered 180° domain wall.

strained and unconstrained solutions. By constrained we mean the domain wall in which only displacements in the tetragonal c-direction are allowed. The unconstrained system is completely three-dimensional. Fig. 4.14 compares the y-component of displacements for Ba and Ti atoms for the constrained and unconstrained domain walls. It is seen that the displacements are different. The same comparison for polarization component in the c-direction is shown in Fig. 4.15. Energy calculations show that a Ti-centered 180° has a lower energy and the energies are an order of magnitude larger than the energy values in the literature. This may be due to the fact that our calculations are for $T = 0$ and tetragonal phase is unstable at this temperature. This can also be an artifact of the potential.

ii) ***$PbTiO_3$***: Fig. 4.16 compares Pb core harmonic displacements in the homogenized lattice for

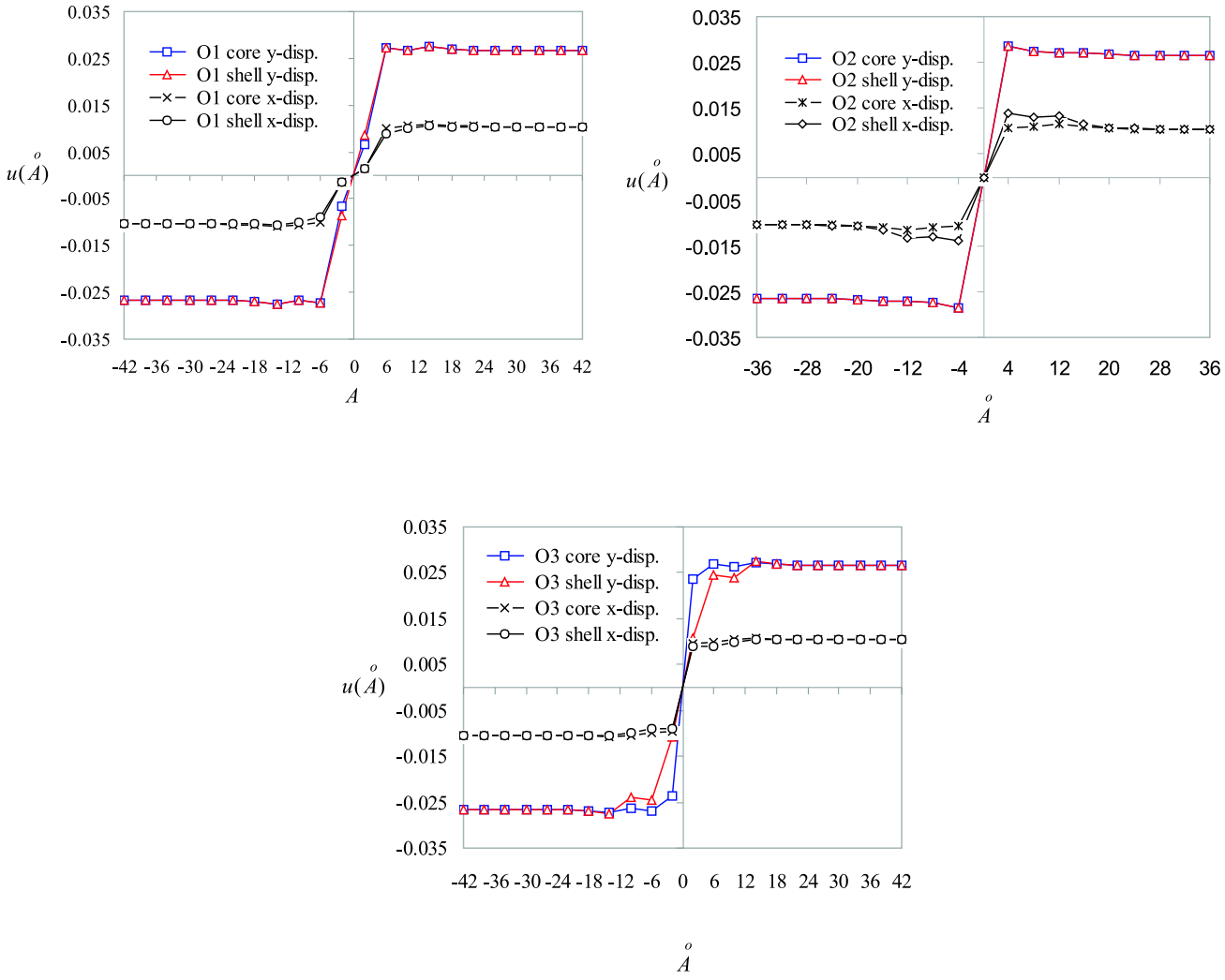

Figure 4.9: Displacements of O1, O2 and O3 cores and shells in a Ba-centered 180° domain wall.

different ranges of interaction of representative unit cells. It is seen that the shell potential is extremely localized. In all the numerical calculations we used $m = 2$. Fig. 4.17 shows the unbalanced force distribution for a Pb-centered 180° domain wall. It is seen that the unbalanced forces are highly localized. Unbalance force distribution in a Ti-centered 180° domain wall is given in Fig. 4.18. Again, the unbalanced forces are localized. Harmonic and anharmonic displacements of Pb, Ti, O1, O2 and O3 in a Pb-centered 180° domain wall are shown in Figs. 4.19 and 4.20. The anharmonic lattice statics iterations converged after fifteen iterations. It is seen that the domain wall thickness is about 2 nm in agreement with the ab initio calculations (Meyer and Vanderbilt, 2001). It is observed that O3 has the most contribution to polarization. Beyond two lattice spacings away from the domain wall all the

cores and shells move rigidly and with the same amount, i.e., away from the domain wall the displacement field is a rigid translation. The harmonic and anharmonic displacements of Pb, Ti, O1, O2 and O3 in a Ti-centered 180° domain wall are given in Figs. 4.21 and 4.22. Again, the domain wall is about 2 nm wide. We compared the anharmonic lattice statics solutions for $m = 1$ and $m = 2$ and observed that their nonlinear solutions are exactly the same.

Fig. 4.23 compares the approximate DFT displacements with the exact harmonic displacements for Pb cores and shells in a Pb-centered 180° domain wall. It is seen that the two differ by more than 40%. However, the anharmonic displacements obtained by using the DFT harmonic displacements in each step are exactly the same as the ones obtained using the exact harmonic displacements in each step.

Harmonic and anharmonic polarization profiles for Pb-centered and Ti-centered 180° domain walls are shown in Fig. 4.24. It is seen that the domain walls are atomically sharp. Of course, polarization is not defined unambiguously in this scale and we have associated a polarization to each unit cells. For a Pb-centered domain wall the Pb and O2 displacements are averaged for each unit cell. For a Ti-centered domain wall the Ti, O1 and O3 displacements are averaged for each unit cell. Energy calculations show that energies are three orders of magnitude larger than the ones ab initio calculations predict. A Ti-centered 180° domain wall has an energy about 40% higher than that of a Pb-centered domain wall. Note that ab initio calculations predict that energy of a Ti-centered domain wall is 30% higher than that of a Pb-centered domain wall.

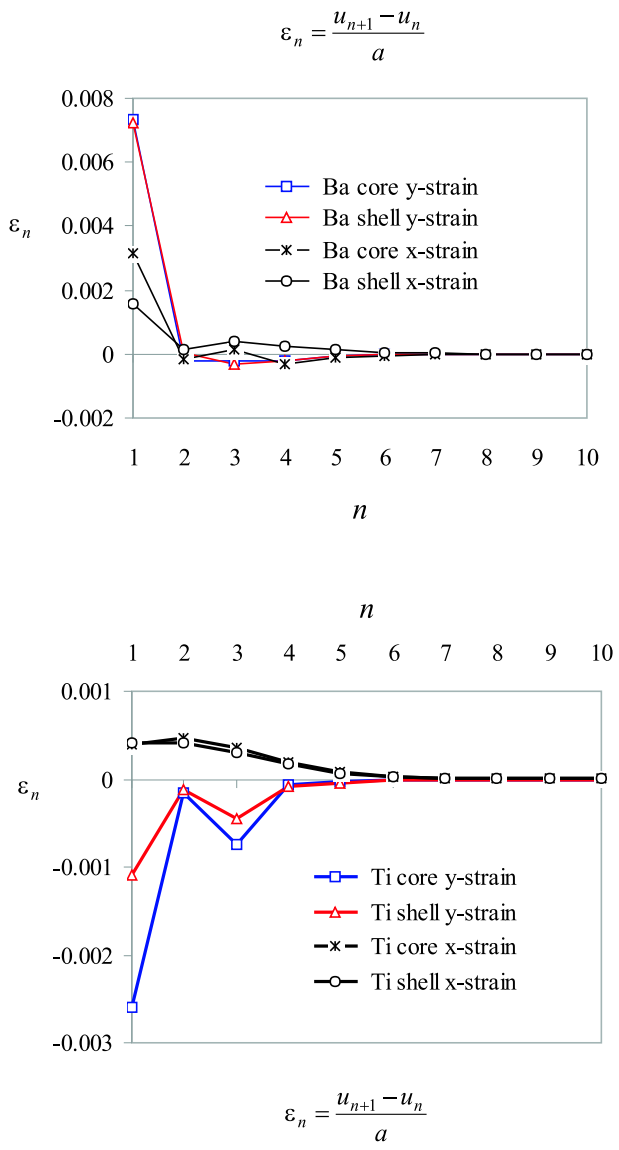

Figure 4.10: Discrete strains of Ba and Ti cores and shells in a Ba-centered 180° domain wall.

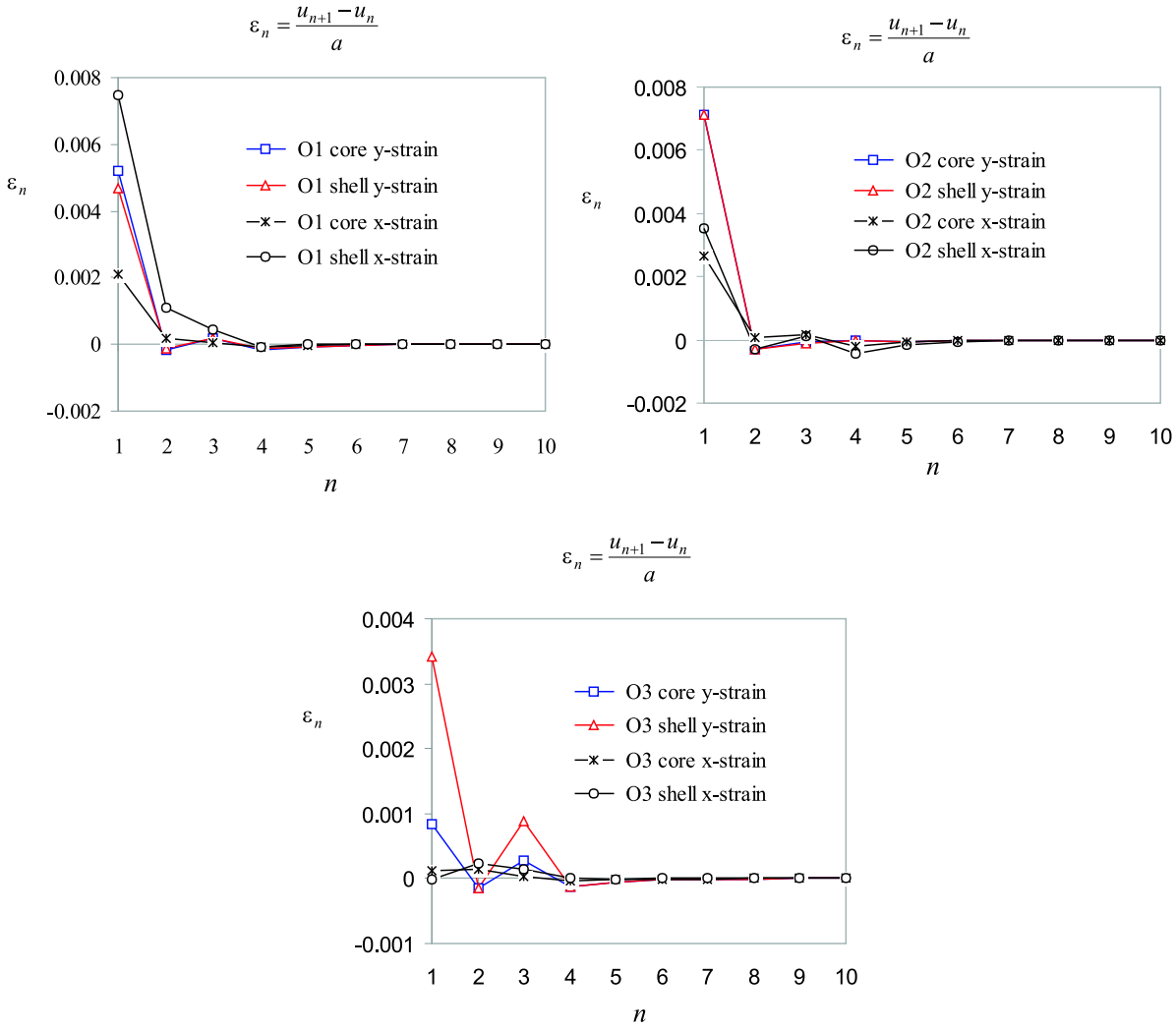

Figure 4.11: Discrete strains of O1, O2 and O3 cores and shells in a Ba-centered 180° domain wall.

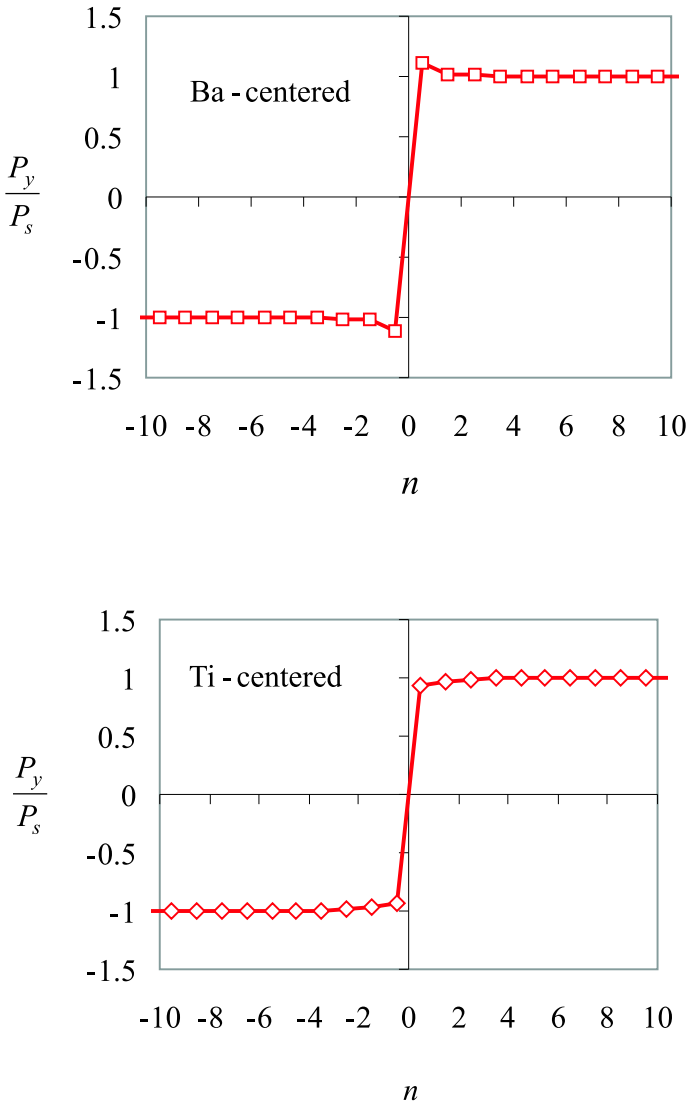

Figure 4.12: y-component of polarization profile for Ba-centered and Ti-centered 180° domain walls.

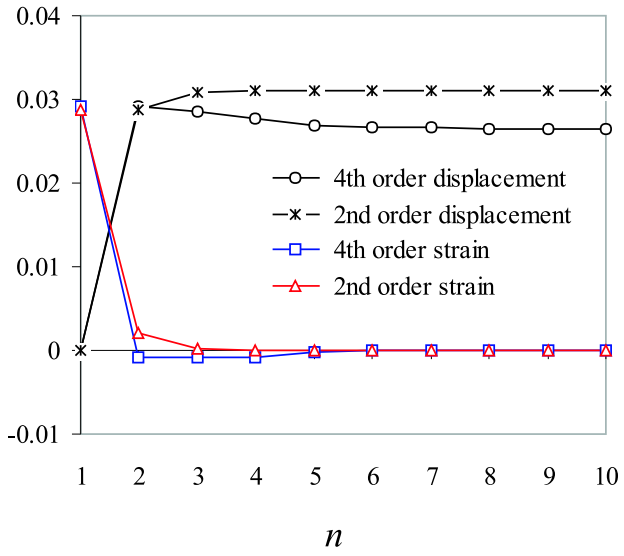

Figure 4.13: y-displacements of Ba atoms obtained by considering first nearest neighbor and first and second nearest neighbors interactions.

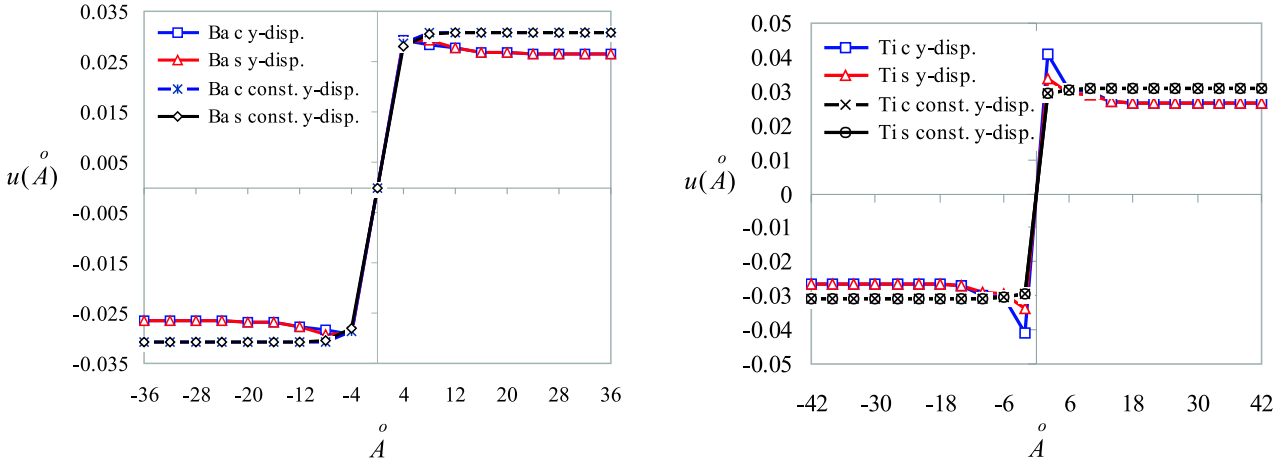

Figure 4.14: y-displacements of Ba and Ti cores and shells for constrained and unconstrained Ba-centered 180° domain walls.

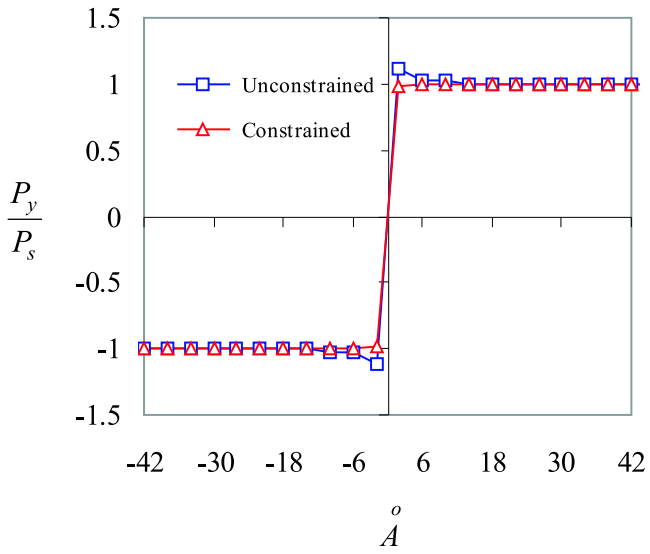

Figure 4.15: y-components of polarization for constrained and unconstrained Ba-centered 180° domain walls.

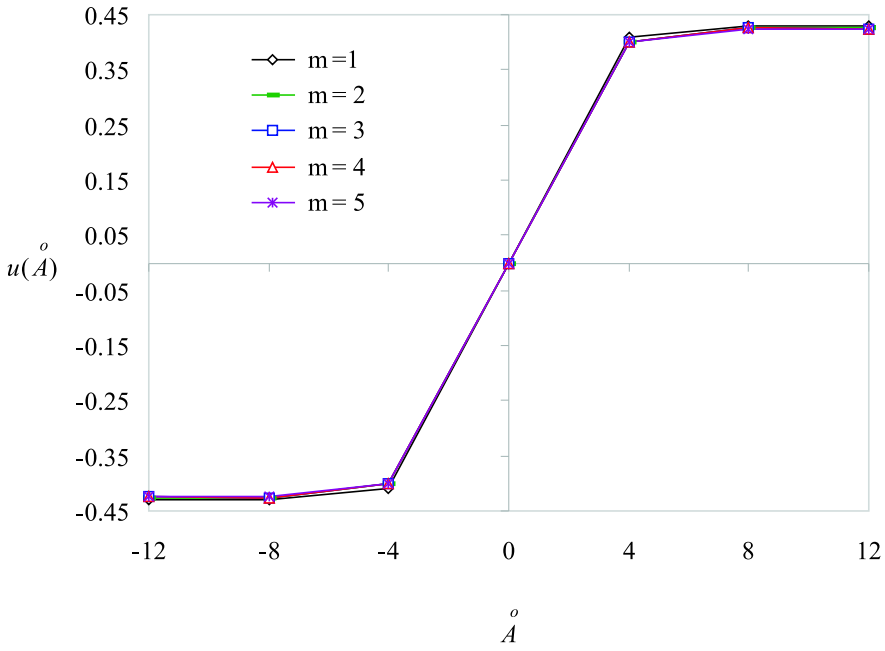

Figure 4.16: Comparison of harmonic displacements of Pb cores for different ranges of interactions for equivalent classes.

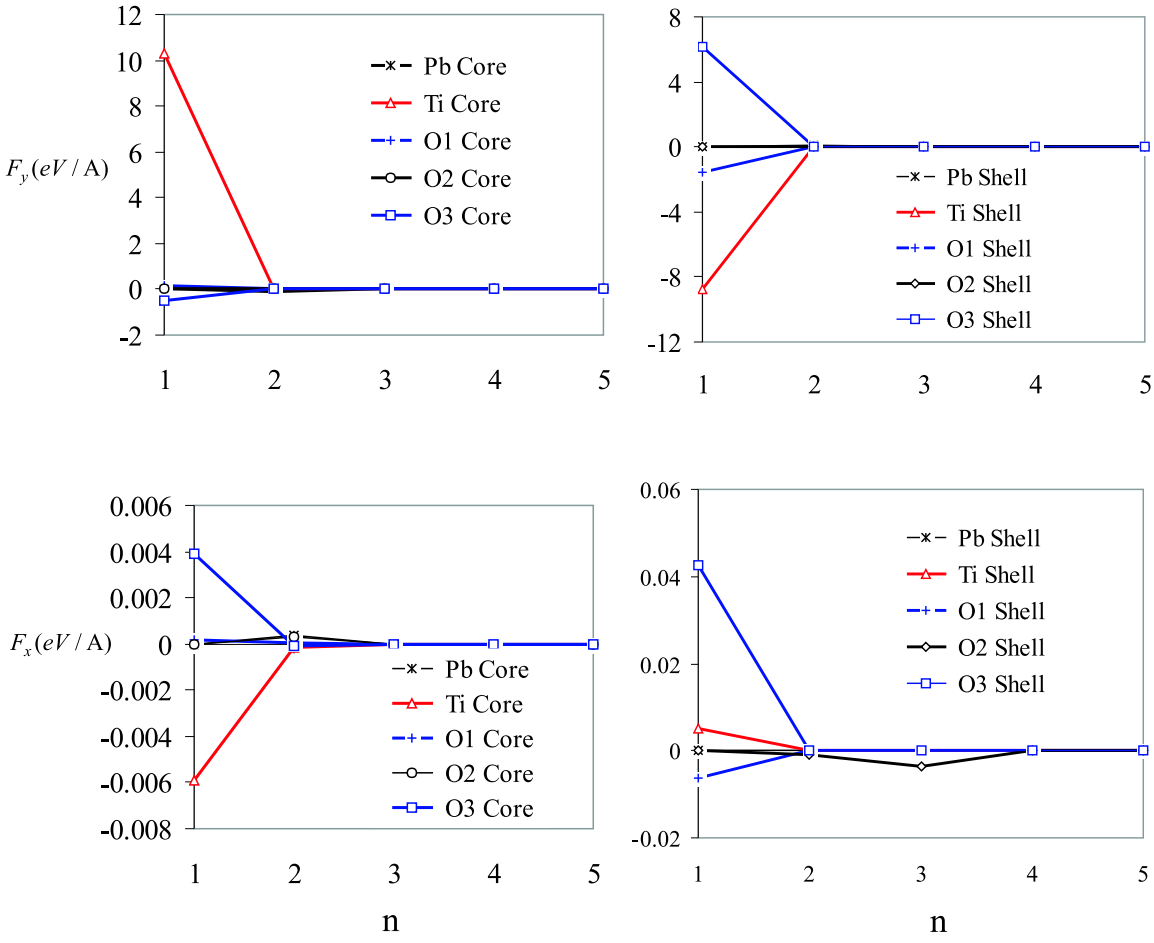

Figure 4.17: Unbalanced forces in the reference configuration of a Pb-centered 180° domain wall.

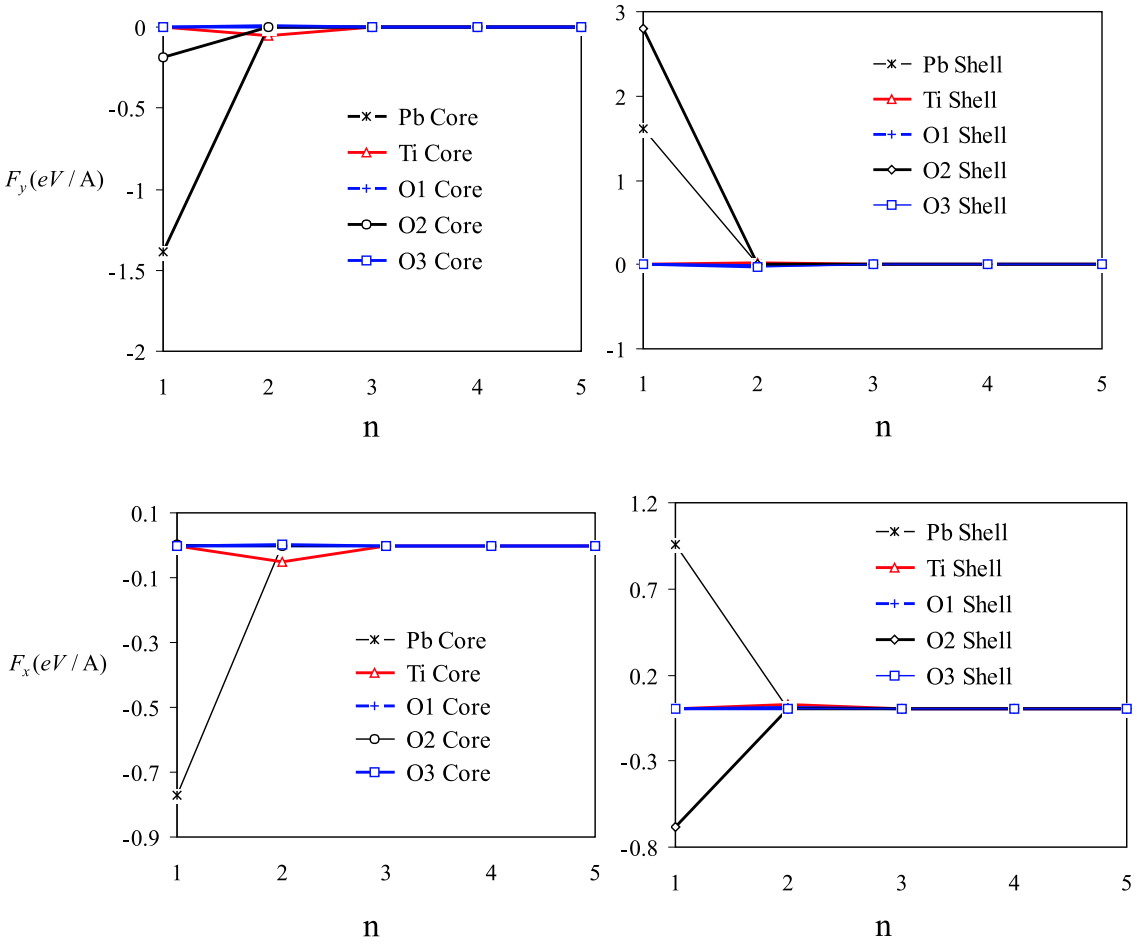

Figure 4.18: Unbalanced forces in the reference configuration of a Ti-centered 180° domain wall.

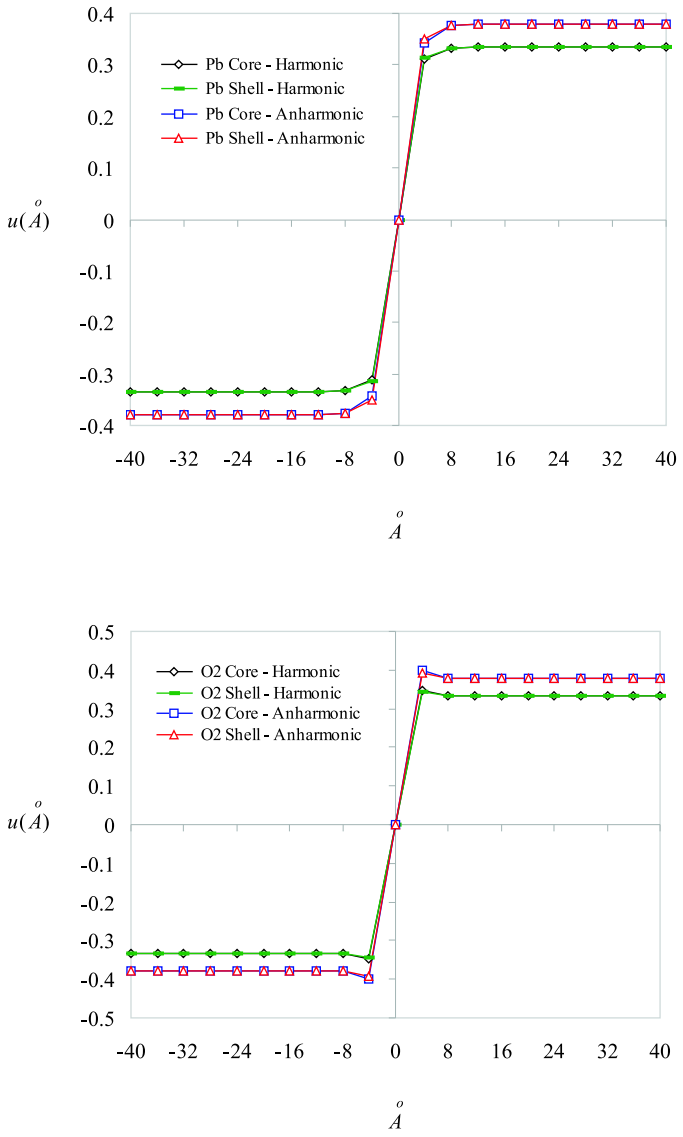

Figure 4.19: Harmonic and anharmonic displacements of Pb and O2 cores and shells for a Pb-centered 180° domain wall.

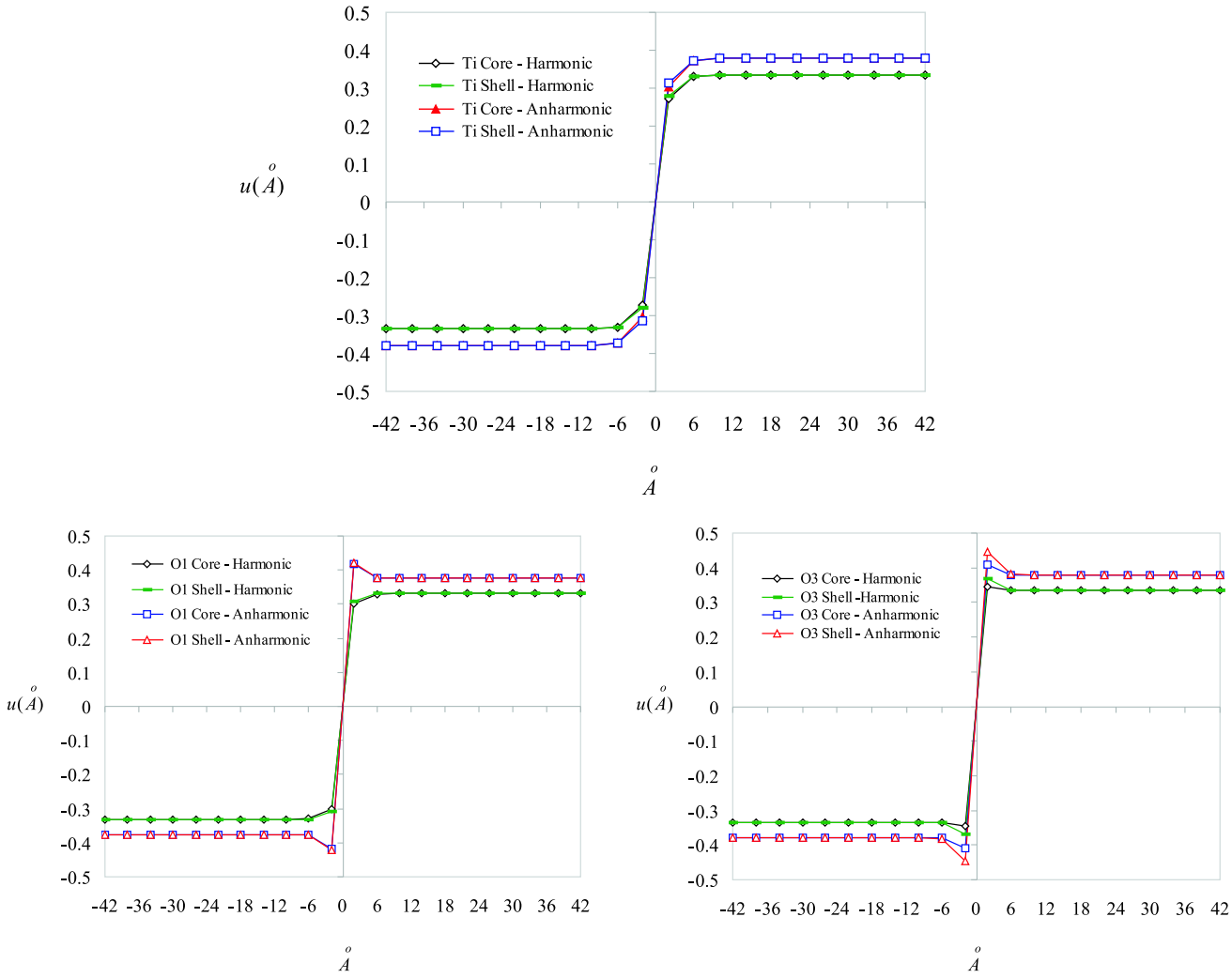

Figure 4.20: Harmonic and anharmonic displacements of Ti, O1 and O3 cores and shells for a Pb-centered 180° domain wall.

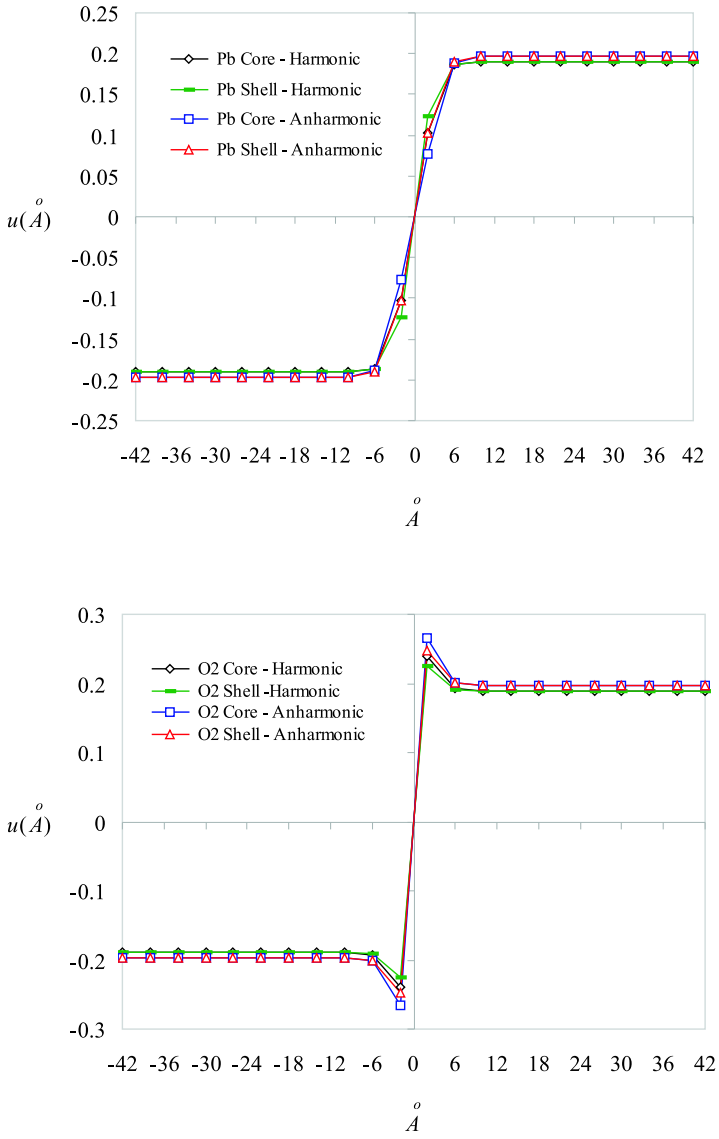

Figure 4.21: Harmonic and anharmonic displacements of Pb and O2 cores and shells for a Ti-centered 180° domain wall.

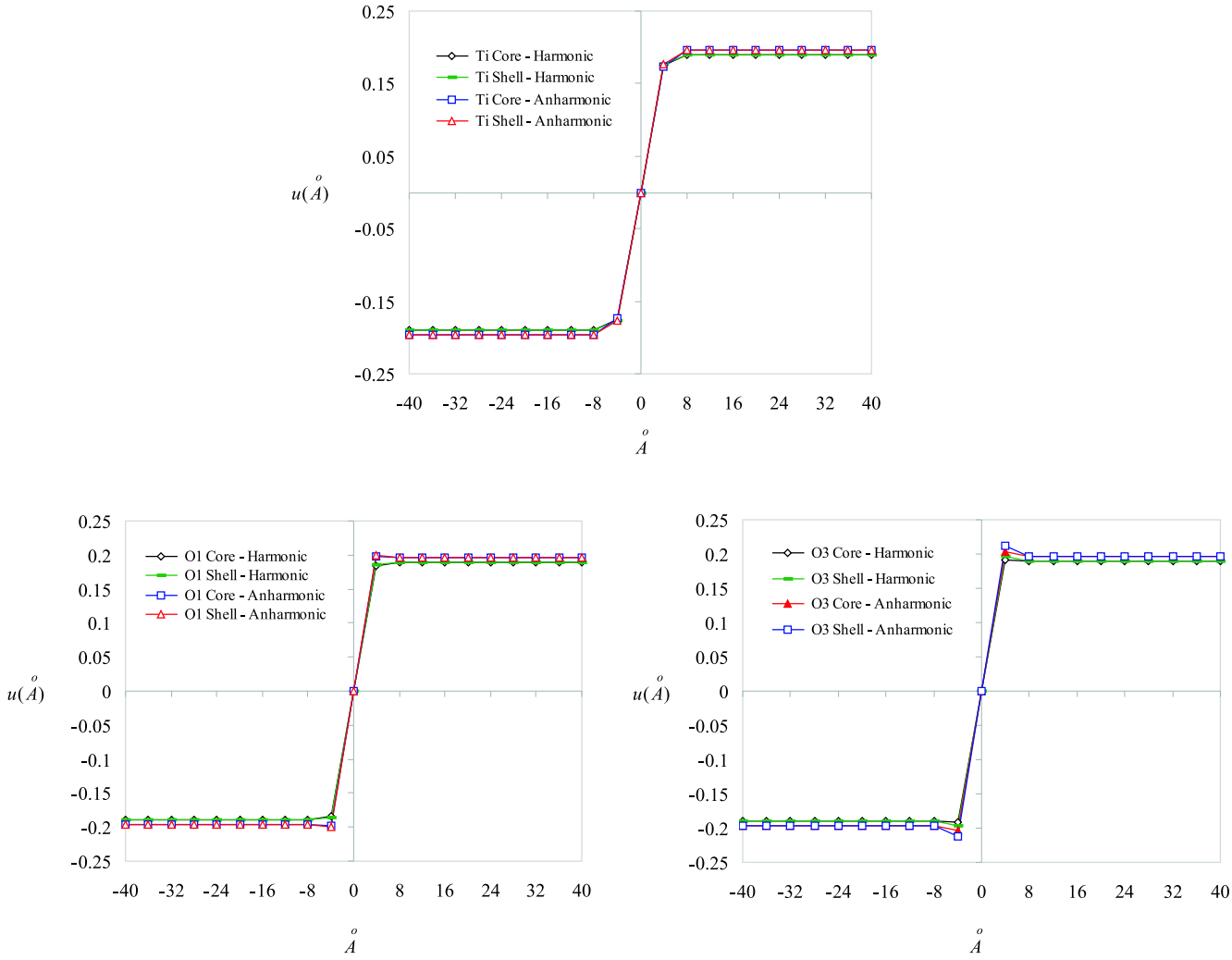

Figure 4.22: Harmonic and anharmonic displacements of Ti, O1 and O3 cores and shells for a Ti-centered 180° domain wall.

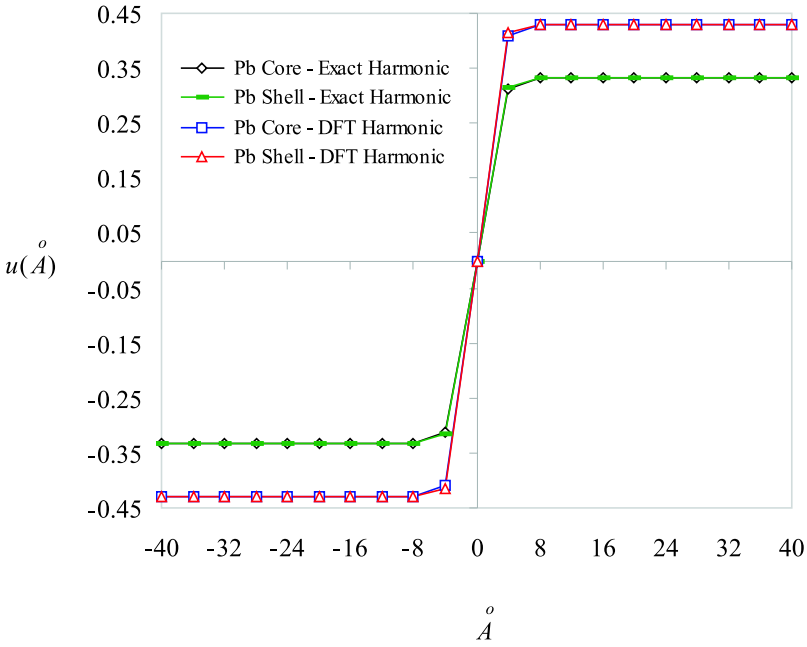

Figure 4.23: Comparison of harmonic displacements of Pb cores obtained from inhomogeneous harmonic lattice statics and homogeneous harmonic lattice statics (DFT solutions).

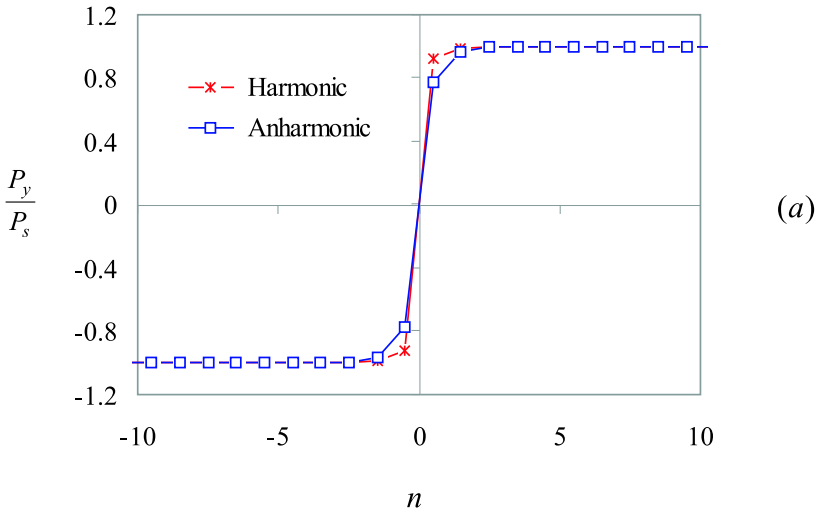

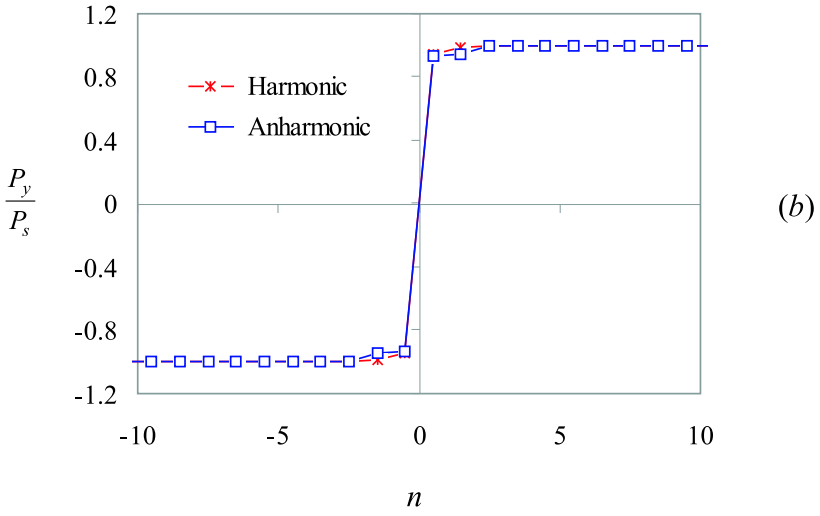

Figure 4.24: Harmonic and anharmonic polarization distributions for Pb and Ti-centered 180° domain walls.

Chapter 5

90° Domain Walls in $BaTiO_3$ and $PbTiO_3$

This chapter presents a lattice statics analysis of 90° domain walls. To our best knowledge, this is the first lattice statics analysis of 90° twins in the literature. The technique developed here can be used in analyzing twin boundaries in similar systems.

5.1 90° Domain Walls in $BaTiO_3$ and $PbTiO_3$

For the 90° domain wall problem, again it is enough to have the displacements only in two planes. Reference configuration in these two planes is shown in Fig. 5.1. It is possible to reduce the governing equations to a 1-D problem, i.e., for each atom type it is enough to have the displacements of cores and shells only on a line perpendicular to the domain wall. In this case the distance between planes of equivalent atoms is

$$\ell = c\sin\theta, \quad \theta = \tan^{-1}\left(\frac{a}{c}\right) \tag{5.1}$$

All the calculations are similar to the 180° problem. The only difference is in the nearest neighbor classes. The solution procedure is also a little different from that of 180° domain walls as will be seen shortly.

Two obvious possibilities for a 90° are A-B-O1-centered and O2-O3-centered domain walls. We consider the A-B-O1-centered 90° domain wall in this work. The reference configuration for A cores and shells is shown in Fig. 5.2. Note that this is a nominal domain wall and we are interested in finding the relaxed configuration starting from this reference configuration. As we will see numerically at the end of this chapter, for a 90° domain wall forces decay to zero very rapidly. It will be seen that the x-components of forces are of the same order as y-components. This means that in the relaxed configuration the 90° domain wall is not centered at an A site. This is consistent with what Meyer and Vanderbilt Meyer and Vanderbilt (2001) observed in their ab initio calculations

for $PbTiO_3$. We will observe in our numerical calculations for $PbTiO_3$ that the anharmonic lattice statics iterations do not converge, i.e., a 90° domain wall cannot be A-B-O-centered. It should be noted that unlike the 180° domain wall problem, there is no symmetry relation between forces and displacements on two sides of the wall. This can be seen in Fig. 5.2. Numerical calculations of the unbalanced forces will also confirm this. This asymmetry implies that we have to solve the governing difference equations for $n \in \mathbb{Z}$. Here we take advantage of the fact that we can partition the problem into two half space problems with constant coefficient matrices in the governing equations. The final solution will be obtained by matching the two solutions. Let us assume that the atoms lying on the domain wall have the index $n = 0$. For range of interaction m we have the following bulk governing equations,

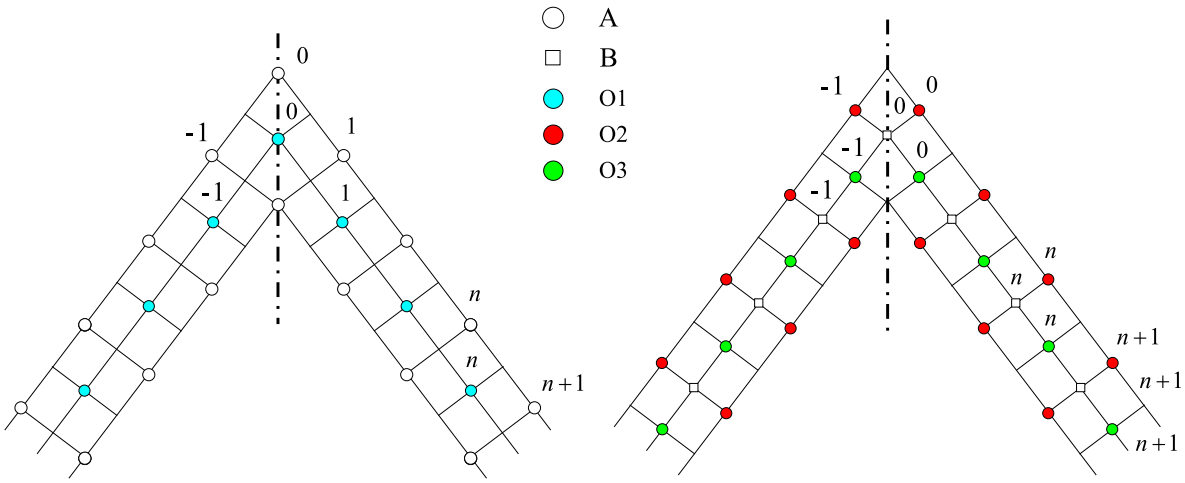

Figure 5.1: Position and numbering of different atoms on the right side of the wall in two parallel planes.

$$\sum_{\alpha=-m}^{\alpha=m} \mathcal{A}_\alpha \mathbf{X}_{n+\alpha} = \mathbf{F}_n \qquad n \geq m+1 \tag{5.2}$$

$$\sum_{\alpha=-m}^{\alpha=m} \bar{\mathcal{A}}_\alpha \mathbf{X}_{n+\alpha} = \mathbf{F}_n \qquad n \leq -m-1 \tag{5.3}$$

where $\mathcal{A}_\alpha$ and $\bar{\mathcal{A}}_\alpha$ are the stiffness matrices of the right and left sides of the domain wall, respectively. There are $2m+1$ indices (unit cells) for which governing equilibrium equations should be written separately. For $m = 1$ and $m = 2$ these are indices $n = -1, 0, 1$ and $n = -2, -1, 0, 1, 2$, respectively. For the sake of clarity we consider the two cases $m = 1$ and $m = 2$ separately and then generalizing the results for an arbitrary range of interaction m would be straightforward.

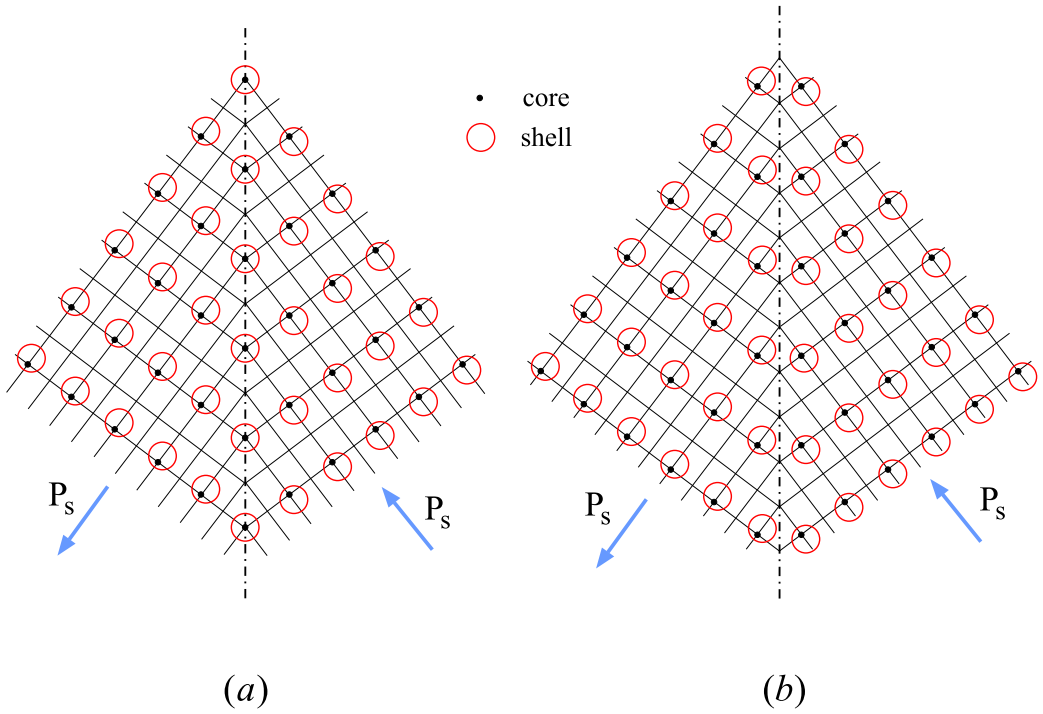

Figure 5.2: Reference configuration of (a) A, B and O1 cores and shells and (b) O2 and O3 cores and shells for a A-B-O1-centered 90° domain wall.

i) ***m=1:*** The bulk governing equations are,

$$\mathcal{A}_{-1}\mathbf{X}_{n-1} + \mathcal{A}_0\mathbf{X}_n + \mathcal{A}_1\mathbf{X}_{n+1} = \mathbf{F}_n \qquad n \geq 2 \tag{5.4}$$

$$\bar{\mathcal{A}}_{-1}\mathbf{X}_{n-1} + \bar{\mathcal{A}}_0\mathbf{X}_n + \bar{\mathcal{A}}_1\mathbf{X}_{n+1} = \mathbf{F}_n \qquad n \leq -2 \tag{5.5}$$

The boundary and transition equations are,

$$n = -1: \quad \mathcal{A}^{(-1)}_{-1}\mathbf{X}_{-2} + \mathcal{A}^{(-1)}_0\mathbf{X}_{-1} + \mathcal{A}^{(-1)}_1\mathbf{X}_0 = \mathbf{F}_{-1} \tag{5.6}$$

$$n = 0: \quad \mathcal{A}^{(0)}_{-1}\mathbf{X}_{-1} + \mathcal{A}^{(0)}_0\mathbf{X}_0 + \mathcal{A}^{(0)}_1\mathbf{X}_1 = \mathbf{F}_0 \tag{5.7}$$

$$n = 1: \quad \mathcal{A}^{(1)}_{-1}\mathbf{X}_0 + \mathcal{A}^{(1)}_0\mathbf{X}_1 + \mathcal{A}^{(1)}_1\mathbf{X}_2 = \mathbf{F}_1 \tag{5.8}$$

Let us define,

$$\mathbf{Y}_n = \begin{pmatrix} \mathbf{X}_{n-1} \\ \mathbf{X}_n \end{pmatrix} \qquad n \geq 2 \tag{5.9}$$

$$\bar{\mathbf{Y}}_n = \begin{pmatrix} \mathbf{X}_{n+1} \\ \mathbf{X}_n \end{pmatrix} \qquad n \leq 2 \tag{5.10}$$

Now the governing equations for $\mathbf{Y}_n$ and $\bar{\mathbf{Y}}_n$ are,

$$\mathbf{Y}_{n+1} = \mathcal{A}\mathbf{Y}_n + \mathbf{G}_n \qquad n \geq 2 \tag{5.11}$$

$$\bar{\mathbf{Y}}_{n-1} = \bar{\mathcal{A}}\bar{\mathbf{Y}}_n + \bar{\mathbf{G}}_n \qquad n \leq -2 \tag{5.12}$$

where

$$\mathcal{A} = \begin{pmatrix} \mathbf{0} & \mathbf{1} \\ -\mathcal{A}_1^{-1}\mathcal{A}_{-1} & -\mathcal{A}_1^{-1}\mathcal{A}_0 \end{pmatrix}, \qquad \mathbf{G}_n = \begin{pmatrix} \mathbf{0} \\ \mathcal{A}_1^{-1}\mathbf{F}_n \end{pmatrix} \tag{5.13}$$

$$\bar{\mathcal{A}} = \begin{pmatrix} \mathbf{0} & \mathbf{1} \\ -\bar{\mathcal{A}}_1^{-1}\bar{\mathcal{A}}_{-1} & -\bar{\mathcal{A}}_1^{-1}\bar{\mathcal{A}}_0 \end{pmatrix}, \qquad \bar{\mathbf{G}}_n = \begin{pmatrix} \mathbf{0} \\ \bar{\mathcal{A}}_{-1}^{-1}\mathbf{F}_n \end{pmatrix} \tag{5.14}$$

Assuming that forces are zero for $|n| > N$, solutions for the bulk unit cells can be written as

$$\begin{aligned}
&\mathbf{Y}_3 = \mathcal{A}\mathbf{c} + \mathbf{G}_2 \\
&\mathbf{Y}_4 = \mathcal{A}^2\mathbf{c} + \mathcal{A}\mathbf{G}_2 + \mathbf{G}_3 \\
&\vdots \\
&\mathbf{Y}_{N+1} = \mathcal{A}^{N-1}\mathbf{c} + \mathcal{A}^{N-2}\mathbf{G}_2 + ... + \mathbf{G}_N = \mathcal{A}^{N-1}\mathbf{c} + \mathbf{d} \\
&\mathbf{Y}_{N+2} = \mathcal{A}\left(\mathcal{A}^{N-1}\mathbf{c} + \mathbf{d}\right) \\
&\vdots \\
&\mathbf{Y}_n = \mathcal{A}^{n-(N+1)}\left(\mathcal{A}^{N-1}\mathbf{c} + \mathbf{d}\right) \qquad n \geq N+1
\end{aligned} \tag{5.15}$$

and,

$$\begin{aligned}
&\bar{\mathbf{Y}}_{-3} = \bar{\mathcal{A}}\bar{\mathbf{c}} + \bar{\mathbf{G}}_{-2} \\
&\bar{\mathbf{Y}}_{-4} = \bar{\mathcal{A}}^2\bar{\mathbf{c}} + \bar{\mathcal{A}}\bar{\mathbf{G}}_{-2} + \bar{\mathbf{G}}_{-3} \\
&\vdots \\
&\bar{\mathbf{Y}}_{-N-1} = \bar{\mathcal{A}}^{N-1}\bar{\mathbf{c}} + \bar{\mathcal{A}}^{N-2}\bar{\mathbf{G}}_{-2} + ... + \bar{\mathbf{G}}_{-N} = \bar{\mathcal{A}}^{N-1}\bar{\mathbf{c}} + \bar{\mathbf{d}} \\
&\bar{\mathbf{Y}}_{-N-2} = \bar{\mathcal{A}}\left(\bar{\mathcal{A}}^{N-1}\bar{\mathbf{c}} + \bar{\mathbf{d}}\right) \\
&\vdots \\
&\bar{\mathbf{Y}}_{-n} = \bar{\mathcal{A}}^{n-(N+1)}\left(\bar{\mathcal{A}}^{N-1}\bar{\mathbf{c}} + \bar{\mathbf{d}}\right) \qquad n \leq -N-1
\end{aligned} \tag{5.16}$$

where

$$\mathbf{c} = \mathbf{Y}_2, \quad \bar{\mathbf{c}} = \bar{\mathbf{Y}}_{-2} \tag{5.17}$$

The boundedness equations are,

$$\left(\mathbf{\Lambda}^{N-1}\mathbf{X}\mathbf{c}\right)_{\{1,\ldots,30\}} = \left(-\mathbf{X}^{-1}\mathbf{d}\right)_{\{1,\ldots,30\}} \tag{5.18}$$

$$\left(\bar{\mathbf{\Lambda}}^{N-1}\bar{\mathbf{X}}\bar{\mathbf{c}}\right)_{\{1,\ldots,30\}} = \left(-\bar{\mathbf{X}}^{-1}\bar{\mathbf{d}}\right)_{\{1,\ldots,30\}} \tag{5.19}$$

Or,

$$\mathbf{D}_{11}\mathbf{X}_{-1} + \mathbf{D}_{12}\mathbf{X}_{-2} = \mathbf{F}_{D1} \tag{5.20}$$

$$\mathbf{D}_{21}\mathbf{X}_{1} + \mathbf{D}_{22}\mathbf{X}_{2} = \mathbf{F}_{D2} \tag{5.21}$$

The vector of unknowns is obtained by solving the following system of linear equations,

$$\begin{pmatrix} \mathbf{D}_{11} & \mathbf{D}_{12} & \mathbf{0} & \mathbf{0} & \mathbf{0} \\ \mathcal{A}_0^{(-1)} & \mathcal{A}_{-1}^{(-1)} & \mathcal{A}_1^{(-1)} & \mathbf{0} & \mathbf{0} \\ \mathcal{A}_{-1}^{(0)} & \mathbf{0} & \mathcal{A}_0^{(0)} & \mathcal{A}_1^{(0)} & \mathbf{0} \\ \mathbf{0} & \mathbf{0} & \mathcal{A}_{-1}^{(1)} & \mathcal{A}_0^{(1)} & \mathcal{A}_1^{(1)} \\ \mathbf{0} & \mathbf{0} & \mathbf{0} & \mathbf{D}_{21} & \mathbf{D}_{22} \end{pmatrix} \begin{pmatrix} \mathbf{X}_{-1} \\ \mathbf{X}_{-2} \\ \mathbf{X}_0 \\ \mathbf{X}_1 \\ \mathbf{X}_2 \end{pmatrix} = \begin{pmatrix} \mathbf{F}_{D1} \\ \mathbf{F}_{-1} \\ \mathbf{F}_0 \\ \mathbf{F}_1 \\ \mathbf{F}_{D2} \end{pmatrix} \tag{5.22}$$

Note that the above system of equations does not have a solution as the nullity of the matrix of coefficients is three (because of translation invariance of the governing equations). In our calculations we fix the position of the Pb core on the domain wall.

ii) ***m=2:*** The bulk equations are,

$$\mathcal{A}_{-3}\mathbf{X}_{n-2} + \mathcal{A}_{-1}\mathbf{X}_{n-1} + \mathcal{A}_0\mathbf{X}_n + \mathcal{A}_1\mathbf{X}_{n+1} + \mathcal{A}_2\mathbf{X}_{n+2} = \mathbf{F}_n \qquad n \geq 3 \tag{5.23}$$

$$\bar{\mathcal{A}}_{-2}\mathbf{X}_{n-2} + \bar{\mathcal{A}}_{-1}\mathbf{X}_{n-1} + \bar{\mathcal{A}}_0\mathbf{X}_n + \bar{\mathcal{A}}_1\mathbf{X}_{n+1} + \bar{\mathcal{A}}_2\mathbf{X}_{n+2} = \mathbf{F}_n \qquad n \leq -3 \tag{5.24}$$

The boundary and transition equations are,

$$\begin{aligned}
n = -2 \quad &: \quad \mathcal{A}_{-2}^{(-2)}\mathbf{X}_{-4} + \mathcal{A}_{-1}^{(-2)}\mathbf{X}_{-3} + \mathcal{A}_0^{(-2)}\mathbf{X}_{-2} + \mathcal{A}_1^{(-2)}\mathbf{X}_{-1} + \mathcal{A}_2^{(-2)}\mathbf{X}_0 = \mathbf{F}_{-2} \\
n = -1 \quad &: \quad \mathcal{A}_{-2}^{(-1)}\mathbf{X}_{-3} + \mathcal{A}_{-1}^{(-1)}\mathbf{X}_{-2} + \mathcal{A}_0^{(-1)}\mathbf{X}_{-1} + \mathcal{A}_1^{(-1)}\mathbf{X}_0 + \mathcal{A}_2^{(-1)}\mathbf{X}_1 = \mathbf{F}_{-1} \\
n = 0 \quad &: \quad \mathcal{A}_{-2}^{(0)}\mathbf{X}_{-2} + \mathcal{A}_{-1}^{(0)}\mathbf{X}_{-1} + \mathcal{A}_0^{(0)}\mathbf{X}_0 + \mathcal{A}_1^{(0)}\mathbf{X}_1 + \mathcal{A}_2^{(0)}\mathbf{X}_2 = \mathbf{F}_0 \\
n = 1 \quad &: \quad \mathcal{A}_{-2}^{(1)}\mathbf{X}_{-1} + \mathcal{A}_{-1}^{(1)}\mathbf{X}_0 + \mathcal{A}_0^{(1)}\mathbf{X}_1 + \mathcal{A}_1^{(1)}\mathbf{X}_2 + \mathcal{A}_2^{(1)}\mathbf{X}_3 = \mathbf{F}_1 \\
n = 2 \quad &: \quad \mathcal{A}_{-2}^{(2)}\mathbf{X}_0 + \mathcal{A}_{-1}^{(2)}\mathbf{X}_1 + \mathcal{A}_0^{(2)}\mathbf{X}_2 + \mathcal{A}_1^{(2)}\mathbf{X}_3 + \mathcal{A}_2^{(2)}\mathbf{X}_4 = \mathbf{F}_2
\end{aligned} \tag{5.25}$$

Let us define,

$$\mathbf{Y}_n = \begin{pmatrix} \mathbf{X}_{n-2} \\ \mathbf{X}_{n-1} \\ \mathbf{X}_n \\ \mathbf{X}_{n+1} \end{pmatrix} \qquad n \geq 3 \tag{5.26}$$

(5.27)

$$\bar{\mathbf{Y}}_n = \begin{pmatrix} \mathbf{X}_{n+2} \\ \mathbf{X}_{n+1} \\ \mathbf{X}_n \\ \mathbf{X}_{n-1} \end{pmatrix} \qquad n \leq -3 \tag{5.28}$$

The bulk equations can be written as

$$\mathbf{Y}_{n+1} = \mathcal{A}\mathbf{Y}_n + \mathbf{G}_n \qquad n \geq 3 \tag{5.29}$$

$$\bar{\mathbf{Y}}_{n-1} = \bar{\mathcal{A}}\bar{\mathbf{Y}}_n + \bar{\mathbf{G}}_n \qquad n \leq -3 \tag{5.30}$$

where

$$\mathcal{A} = \begin{pmatrix} \mathbf{0} & \mathbf{1} & \mathbf{0} & \mathbf{0} \\ \mathbf{0} & \mathbf{0} & \mathbf{1} & \mathbf{0} \\ \mathbf{0} & \mathbf{0} & \mathbf{0} & \mathbf{1} \\ -\mathcal{A}_2^{-1}\mathcal{A}_{-2} & -\mathcal{A}_2^{-1}\mathcal{A}_{-1} & -\mathcal{A}_2^{-1}\mathcal{A}_0 & -\mathcal{A}_2^{-1}\mathcal{A}_1 \end{pmatrix}, \quad \mathbf{G}_n = \begin{pmatrix} \mathbf{0} \\ \mathbf{0} \\ \mathbf{0} \\ \mathcal{A}_2^{-1}\mathbf{F}_n \end{pmatrix} \tag{5.31}$$

(5.32)

$$\bar{\mathcal{A}} = \begin{pmatrix} \mathbf{0} & \mathbf{1} & \mathbf{0} & \mathbf{0} \\ \mathbf{0} & \mathbf{0} & \mathbf{1} & \mathbf{0} \\ \mathbf{0} & \mathbf{0} & \mathbf{0} & \mathbf{1} \\ -\bar{\mathcal{A}}_{-2}^{-1}\bar{\mathcal{A}}_2 & -\bar{\mathcal{A}}_{-2}^{-1}\bar{\mathcal{A}}_1 & -\bar{\mathcal{A}}_{-2}^{-1}\bar{\mathcal{A}}_0 & -\bar{\mathcal{A}}_{-2}^{-1}\bar{\mathcal{A}}_{-1} \end{pmatrix}, \quad \bar{\mathbf{G}}_n = \begin{pmatrix} \mathbf{0} \\ \mathbf{0} \\ \mathbf{0} \\ \bar{\mathcal{A}}_{-2}^{-1}\mathbf{F}_n \end{pmatrix} \tag{5.33}$$

Solutions for the bulk unit cells can be written as

$$\begin{aligned}
&\mathbf{Y}_4 = \mathcal{A}\mathbf{c} + \mathbf{G}_3 \\
&\mathbf{Y}_5 = \mathcal{A}^2\mathbf{c} + \mathcal{A}\mathbf{G}_3 + \mathbf{G}_4 \\
&\vdots \\
&\mathbf{Y}_{N+1} = \mathcal{A}^{N-1}\mathbf{c} + \mathcal{A}^{N-3}\mathbf{G}_3 + ... + \mathbf{G}_N = \mathcal{A}^{N-1}\mathbf{c} + \mathbf{d} \\
&\mathbf{Y}_{N+2} = \mathcal{A}\left(\mathcal{A}^{N-1}\mathbf{c} + \mathbf{d}\right) \\
&\vdots \\
&\mathbf{Y}_n = \mathcal{A}^{n-(N+1)}\left(\mathcal{A}^{N-1}\mathbf{c} + \mathbf{d}\right) \qquad n \geq N+1
\end{aligned} \tag{5.34}$$

and,

$$\begin{aligned}
&\bar{\mathbf{Y}}_{-4} = \bar{\mathcal{A}}\bar{\mathbf{c}} + \bar{\mathbf{G}}_{-3} \\
&\bar{\mathbf{Y}}_{-5} = \bar{\mathcal{A}}^2\bar{\mathbf{c}} + \bar{\mathcal{A}}\bar{\mathbf{G}}_{-3} + \bar{\mathbf{G}}_{-4} \\
&\vdots \\
&\bar{\mathbf{Y}}_{-N-1} = \bar{\mathcal{A}}^{N-1}\bar{\mathbf{c}} + \bar{\mathcal{A}}^{N-3}\bar{\mathbf{G}}_{-3} + ... + \bar{\mathbf{G}}_{-N} = \bar{\mathcal{A}}^{N-1}\bar{\mathbf{c}} + \bar{\mathbf{d}} \\
&\bar{\mathbf{Y}}_{-N-2} = \bar{\mathcal{A}}\left(\bar{\mathcal{A}}^{N-1}\bar{\mathbf{c}} + \bar{\mathbf{d}}\right) \\
&\vdots \\
&\bar{\mathbf{Y}}_{-n} = \bar{\mathcal{A}}^{n-(N+1)}\left(\bar{\mathcal{A}}^{N-1}\bar{\mathbf{c}} + \bar{\mathbf{d}}\right) \qquad n \leq -N-1
\end{aligned} \tag{5.35}$$

where

$$\mathbf{c} = \mathbf{Y}_3, \quad \bar{\mathbf{c}} = \bar{\mathbf{Y}}_{-3} \tag{5.36}$$

The boundedness equations are,

$$\left(\mathbf{\Lambda}^{N-1}\mathbf{X}\mathbf{c}\right)_{\{1,...,60\}} = \left(-\mathbf{X}^{-1}\mathbf{d}\right)_{\{1,...,60\}} \tag{5.37}$$

$$\left(\bar{\mathbf{\Lambda}}^{N-1}\bar{\mathbf{X}}\bar{\mathbf{c}}\right)_{\{1,...,60\}} = \left(-\bar{\mathbf{X}}^{-1}\bar{\mathbf{d}}\right)_{\{1,...,60\}} \tag{5.38}$$

Or,

$$\mathbf{D}_{11}\mathbf{X}_{-1} + \mathbf{D}_{12}\mathbf{X}_{-2} + \mathbf{D}_{13}\mathbf{X}_{-3} + \mathbf{D}_{14}\mathbf{X}_{-4} = \mathbf{F}_{D1} \tag{5.39}$$

$$\mathbf{D}_{21}\mathbf{X}_1 + \mathbf{D}_{22}\mathbf{X}_2 + \mathbf{D}_{23}\mathbf{X}_3 + \mathbf{D}_{24}\mathbf{X}_4 = \mathbf{F}_{D2} \tag{5.40}$$

The vector of unknowns is obtained by solving the following system of linear equations,

$$\begin{pmatrix} \mathbf{D}_{11} & \mathbf{D}_{12} & \mathbf{D}_{13} & \mathbf{D}_{14} & \mathbf{0} & \mathbf{0} & \mathbf{0} & \mathbf{0} & \mathbf{0} \\ \mathcal{A}_1^{(-2)} & \mathcal{A}_0^{(-2)} & \mathcal{A}_{-1}^{(-2)} & \mathcal{A}_{-2}^{(-2)} & \mathcal{A}_2^{(-2)} & \mathbf{0} & \mathbf{0} & \mathbf{0} & \mathbf{0} \\ \mathcal{A}_0^{(-1)} & \mathcal{A}_{-1}^{(-1)} & \mathcal{A}_{-2}^{(-1)} & \mathbf{0} & \mathcal{A}_1^{(-1)} & \mathcal{A}_2^{(-1)} & \mathbf{0} & \mathbf{0} & \mathbf{0} \\ \mathcal{A}_{-1}^{(0)} & \mathcal{A}_{-2}^{(0)} & \mathbf{0} & \mathbf{0} & \mathcal{A}_0^{(0)} & \mathcal{A}_1^{(0)} & \mathcal{A}_2^{(0)} & \mathbf{0} & \mathbf{0} \\ \mathcal{A}_{-2}^{(1)} & \mathbf{0} & \mathbf{0} & \mathbf{0} & \mathcal{A}_{-1}^{(1)} & \mathcal{A}_0^{(1)} & \mathcal{A}_1^{(1)} & \mathcal{A}_2^{(1)} & \mathbf{0} \\ \mathbf{0} & \mathbf{0} & \mathbf{0} & \mathbf{0} & \mathcal{A}_{-2}^{(2)} & \mathcal{A}_{-1}^{(2)} & \mathcal{A}_0^{(2)} & \mathcal{A}_1^{(2)} & \mathcal{A}_2^{(2)} \\ \mathbf{0} & \mathbf{0} & \mathbf{0} & \mathbf{0} & \mathbf{0} & \mathbf{D}_{21} & \mathbf{D}_{22} & \mathbf{D}_{23} & \mathbf{D}_{24} \end{pmatrix} \begin{pmatrix} \mathbf{X}_{-1} \\ \mathbf{X}_{-2} \\ \mathbf{X}_{-3} \\ \mathbf{X}_{-4} \\ \mathbf{X}_0 \\ \mathbf{X}_1 \\ \mathbf{X}_2 \\ \mathbf{X}_3 \\ \mathbf{X}_4 \end{pmatrix} = \begin{pmatrix} \mathbf{F}_{D1} \\ \mathbf{F}_{-2} \\ \mathbf{F}_{-1} \\ \mathbf{F}_0 \\ \mathbf{F}_1 \\ \mathbf{F}_2 \\ \mathbf{F}_{D2} \end{pmatrix} \tag{5.41}$$

Again the matrix of coefficients of the above system of linear equations is not full rank and Pb cores on the domain wall are fixed.

5.1.1 Constraint Solution of 90° Domain Walls

The potential we have for $PbTiO_3$ is stable only under the tetragonal symmetry. Therefore, in order to be able to obtain the fully non-linear solutions (if they exist) we have to impose this constraint. We assume that all the displacements are in the tetragonal c-direction. Let us define two local coordinates (X, Y, Z) and (X', Y', Z') (see Fig. 5.3),

$$\begin{pmatrix} X \\ Y \\ Z \end{pmatrix} = \mathbf{R}_R \begin{pmatrix} x \\ y \\ z \end{pmatrix}, \qquad \begin{pmatrix} X' \\ Y' \\ Z' \end{pmatrix} = \mathbf{R}_L \begin{pmatrix} x \\ y \\ z \end{pmatrix} \tag{5.42}$$

where

$$\mathbf{R}_R = \begin{pmatrix} \cos\theta & -\sin\theta & 0 \\ \sin\theta & \cos\theta & 0 \\ 0 & 0 & 1 \end{pmatrix}, \qquad \mathbf{R}_L = \begin{pmatrix} \cos\theta & \sin\theta & 0 \\ -\sin\theta & \cos\theta & 0 \\ 0 & 0 & 1 \end{pmatrix}, \qquad \theta = \tan^{-1}\left(\frac{c}{a}\right) \tag{5.43}$$

It can be easily shown that the substiffness matrices in coordinates (x, y, z) are related to those in coordinates (X, Y, Z) and (X', Y', Z') as follows,

$$\mathbf{K}_R = \mathbf{R}_R \mathbf{K} \mathbf{R}_R^{\mathsf{T}}, \qquad \mathbf{K}_L = \mathbf{R}_L \mathbf{K} \mathbf{R}_L^{\mathsf{T}} \tag{5.44}$$

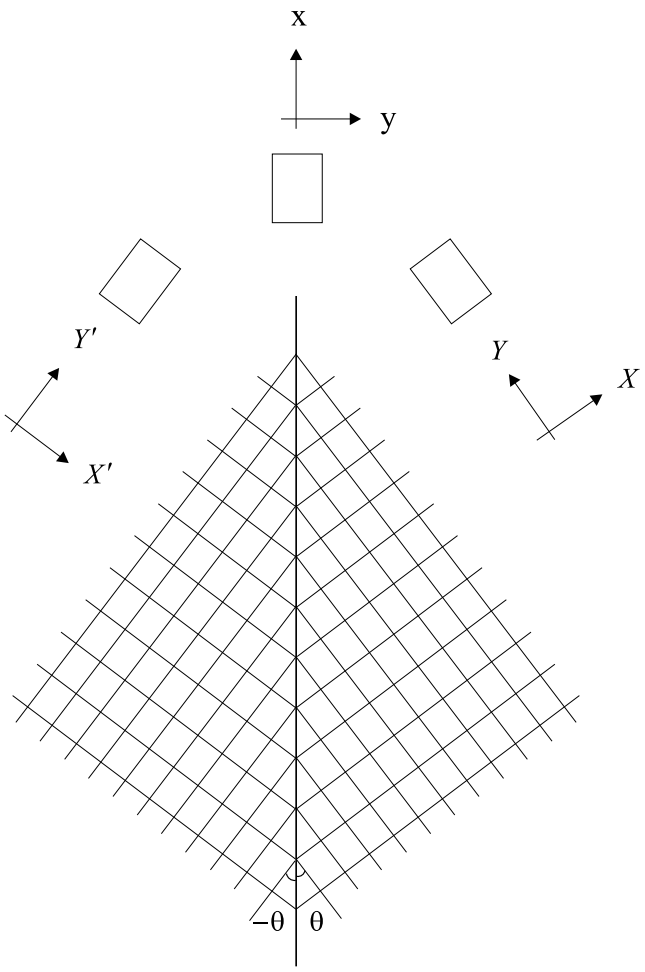

Figure 5.3: Local coordinates of a 90° domain wall.

Forces on the left and right sides of the domain wall can be transformed to the corresponding local coordinates as

$$\mathbf{F}_n^R = \mathbf{R}_R \mathbf{F}_n \qquad n \geq 0 \tag{5.45}$$

$$\mathbf{F}_n^L = \mathbf{R}_L \mathbf{F}_n \qquad n < 0 \tag{5.46}$$

The constrained governing equations are obtained by looking at YY and $Y'Y'$ components of the substiffness matrices and Y and Y' components of forces. This results in the following vector-valued difference equation,

$$\sum_{\alpha=-m}^{m} \mathbf{A}_\alpha(n)\mathbf{x}_n = \mathbf{f}_n \tag{5.47}$$

where for $m = 1$,

$$\mathbf{A}_\alpha(n) \in \mathbb{R}^{10\times 10}, \mathbf{x}_n, \mathbf{f}_n \in \mathbb{R}^{10} \tag{5.48}$$

For example, force vector and bulk stiffness matrix $\mathbf{A}_0$ for the right side of the domain wall have the following forms,

$$\mathbf{f}_n = \left(\mathbf{F}_n^R\right)_{\{2,5,\ldots,29\}}, \quad \mathbf{A}_0 = \begin{pmatrix} (K_{R_{11\ 0}})_{22} & \ldots & (K_{R_{110\ 0}})_{22} \\ \vdots & & \vdots \\ (K_{R_{101\ 0}})_{22} & \ldots & (K_{R_{1010\ 0}})_{22} \end{pmatrix} \tag{5.49}$$

For solving the above reduced difference equations we assume that all the cores and shells lying on the domain wall in the reference configuration remain on the domain wall after relaxation.

5.2 Numerical Results

In this section we present some numerical examples for both $BaTiO_3$ and $PbTiO_3$.

i) ***$BaTiO_3$***: The distribution of unbalanced forces for a BaTiO-centered 90° domain wall is shown in Fig. 5.4. It is seen that forces are nonzero in a highly localized region near the domain wall. Forces parallel and perpendicular to the domain wall are of the same order. This again could lead to a very thin domain wall. It is seen that there is no symmetry relation between forces on two sides of the wall. Displacements of cores and shells are shown in Figs. 5.5 and 5.6. It is seen that the thickness of the 90° domain wall is almost 3 nm. This is in qualitative agreement with ab initio calculations of Meyer and Vanderbilt (2001).

ii) ***$PbTiO_3$***: c-component of unbalanced forces for a Pb-Ti-O1-centered 90° domain wall are shown in Fig. 5.7. It is seen that forces are highly localized. The constrained harmonic displacements are shown in Fig. 5.8. It is seen that the 90° domain wall is almost 3 nm wide. We see that the anharmonic lattice statics iterations do not converge for this configuration. This means that there is no constrained solution for a Pb-Ti-O1-centered 90° domain wall. This could be either because of the tetragonal constraint (artifact of the shell potential) or because the Pb-Ti-O1-centered 90° domain wall configuration is not stable.

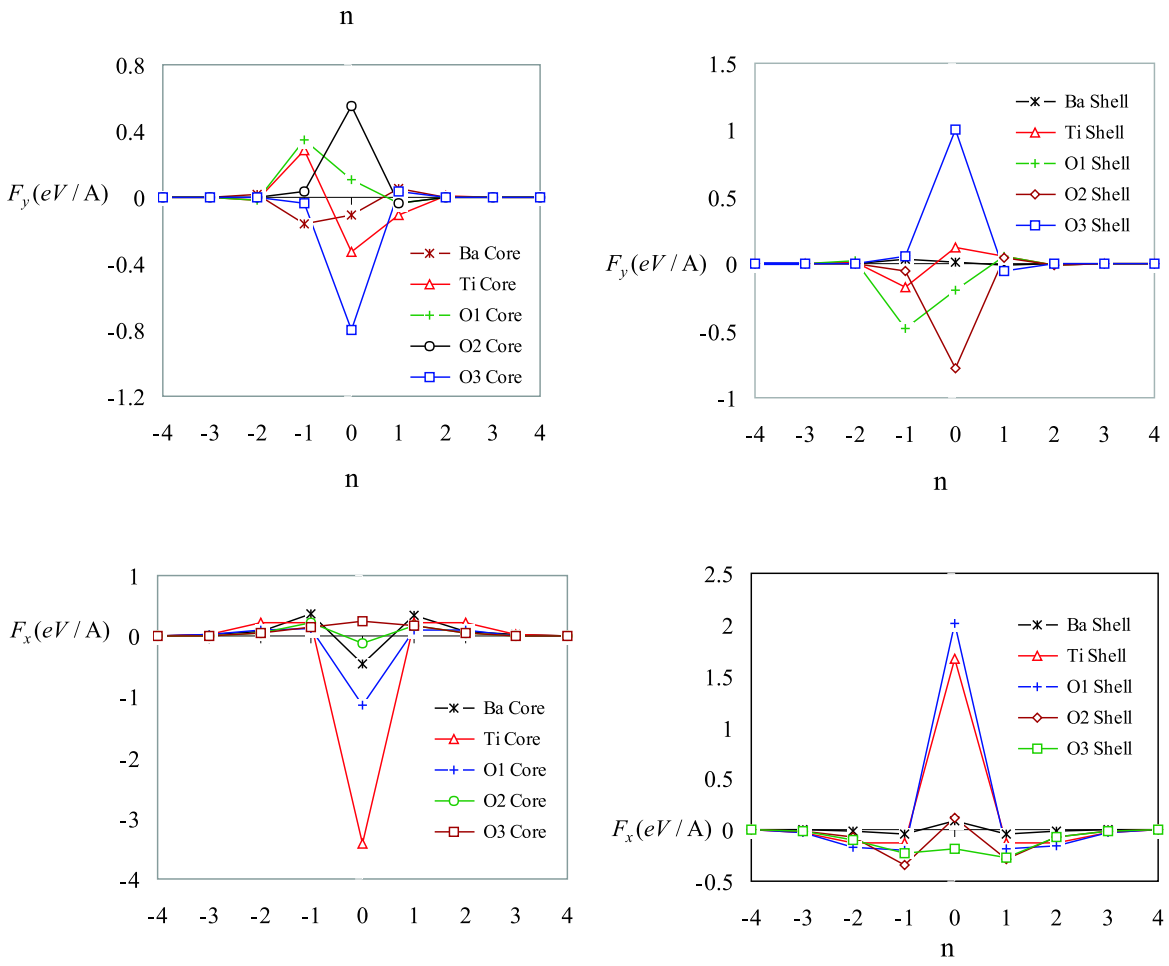

Figure 5.4: y and x components of forces on atoms close to a Ba-Ti-O-centered 90° domain wall. n=0 corresponds to the domain wall. z-components of all the forces are zero.

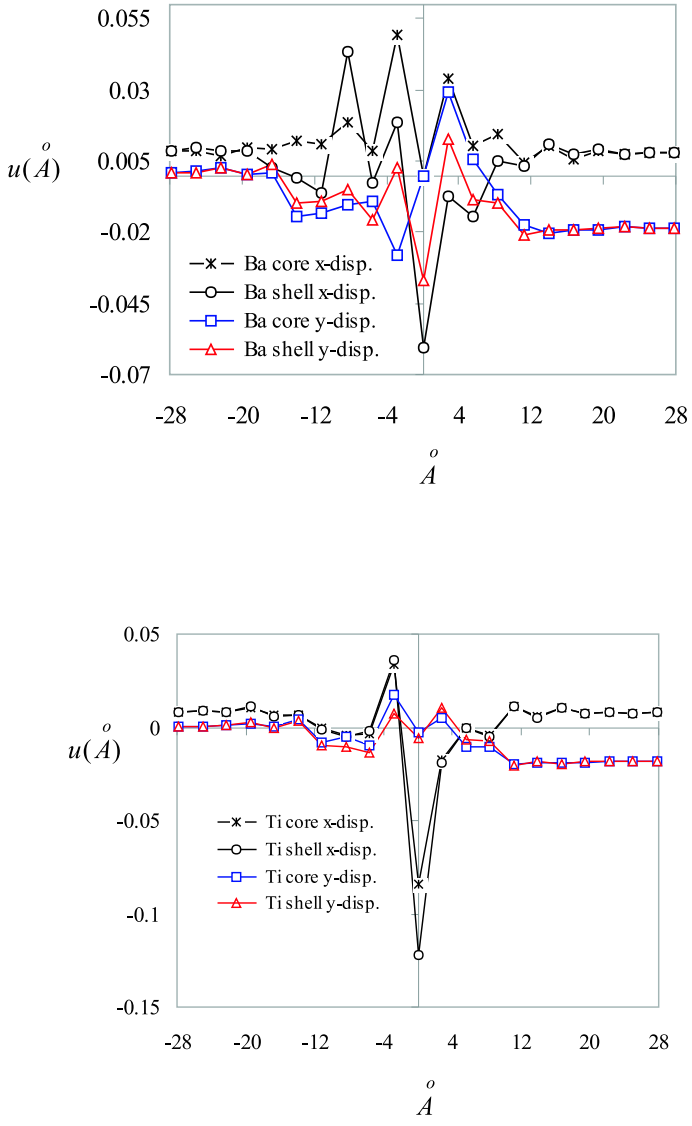

Figure 5.5: Harmonic displacements of Ba and Ti core and shells in a BaTiO-centered 90° domain wall.

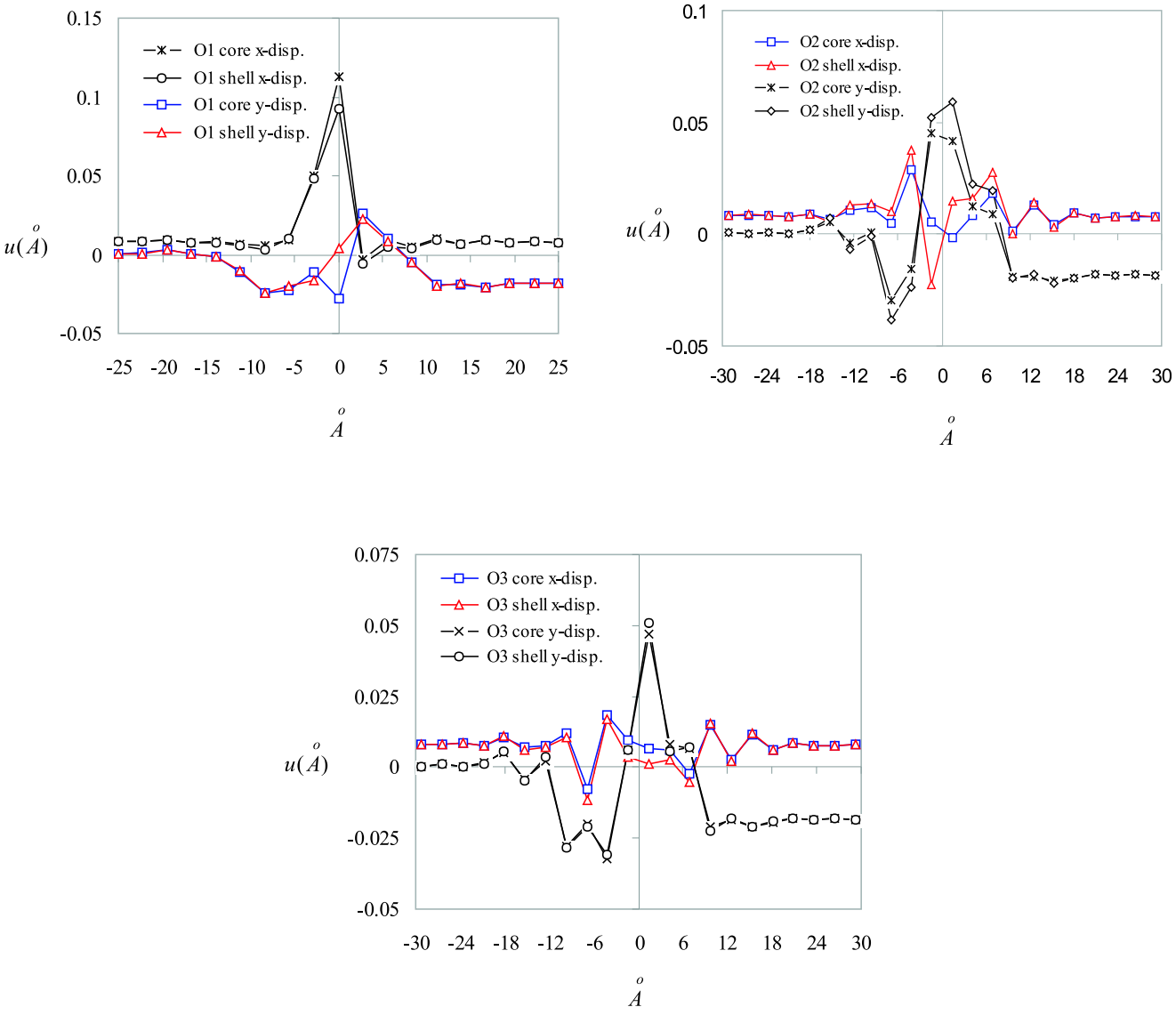

Figure 5.6: Harmonic displacements of O1, O2 and O3 core and shells in a BaTiO-centered 90° domain wall.

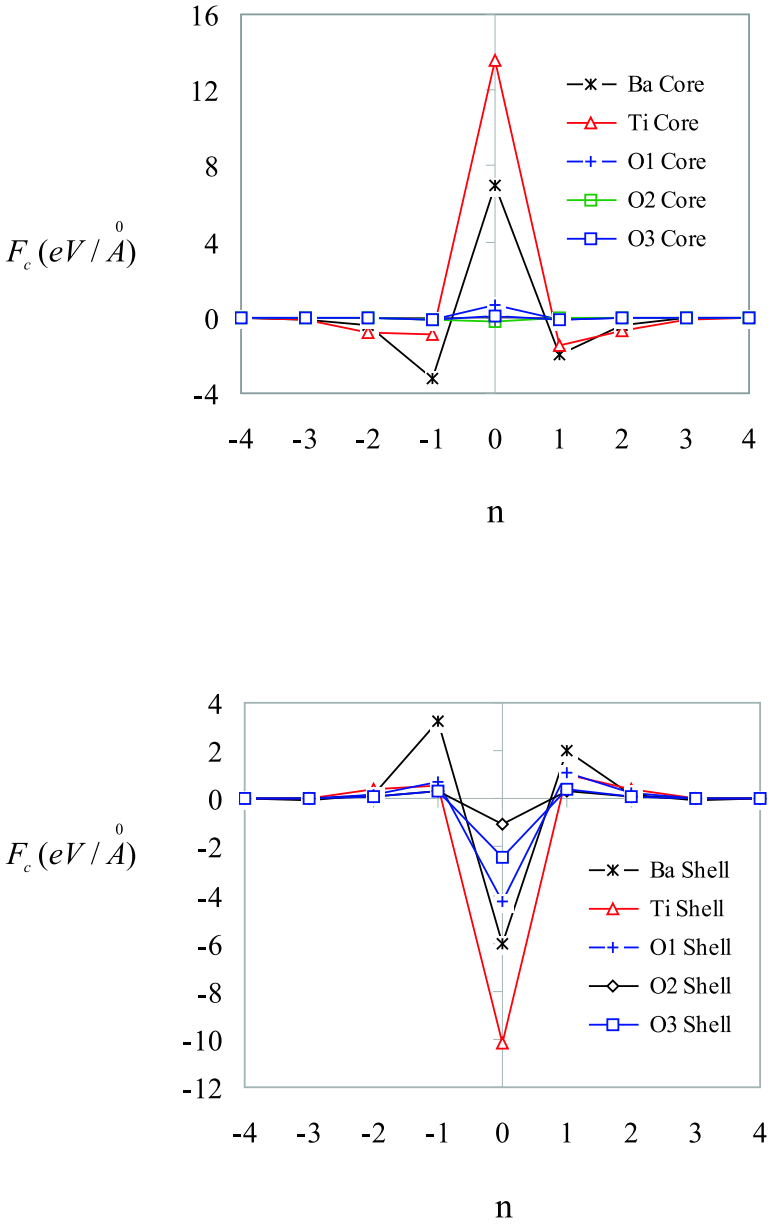

Figure 5.7: c-component of forces on cores and shells close to a Pb-Ti-O-centered 90° domain wall. n=0 corresponds to the domain wall.

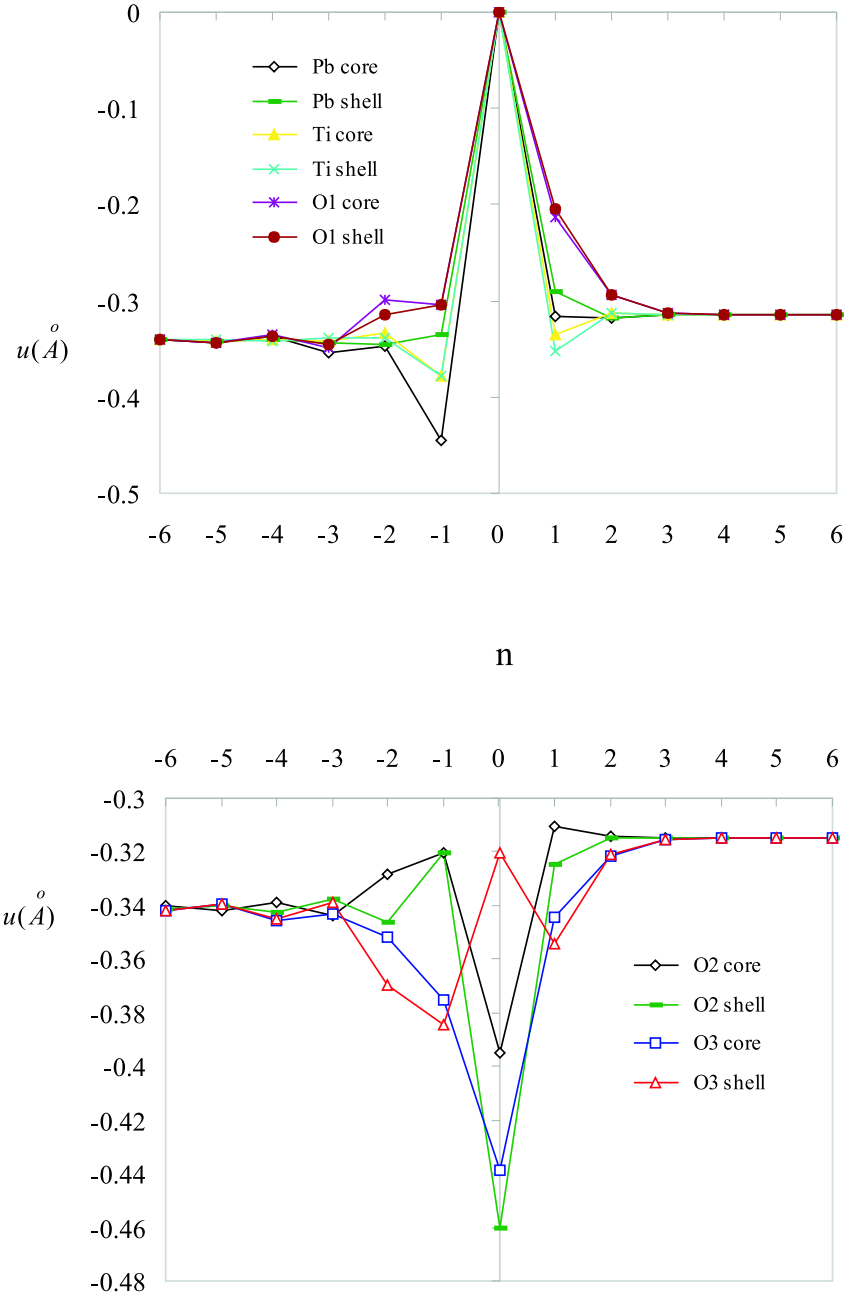

Figure 5.8: Harmonic displacements of cores and shells in a constrained PbTiO1-centered 90° domain wall.

Chapter 6

Free Surfaces in $PbTiO_3$

The second type of defects we study in this work are free surfaces. Lattice statics has been used in the past in studying free surfaces (see Gazis and Wallis (1964), Wallis (1975), Benedek (1978) and references therein). We study the structure of two types of free surfaces: (i) Type c free surfaces in which the polarization direction is parallel to the free surface and (ii) Type a free surfaces in which the polarization direction is perpendicular to the free surface. These are schematically shown in Fig. 6.1. Shell model reference configurations of these free surfaces are shown in Figs. 6.2 and 6.3. Note that here we are looking at PbO-terminated free surfaces. We will see shortly that one can relax the type c free surface under the tetragonal constraint but this is not possible for the Type a free surface. This will indicate that there will be some surface reconstruction in the case of Type a free surfaces.

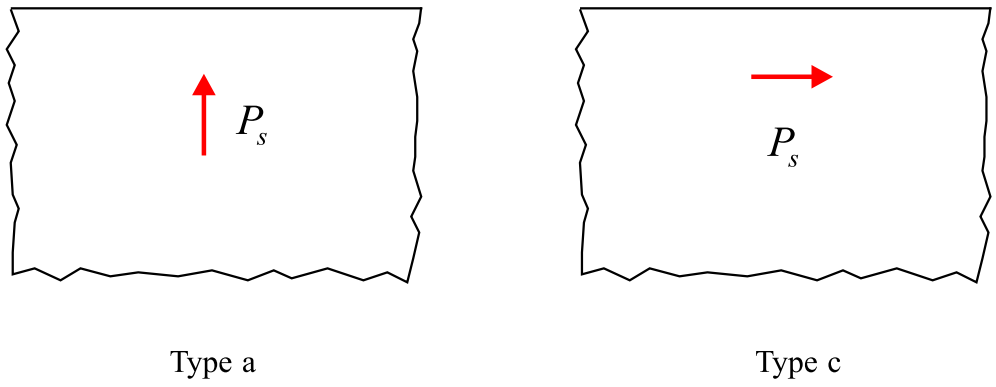

Figure 6.1: Type a and c free surfaces.

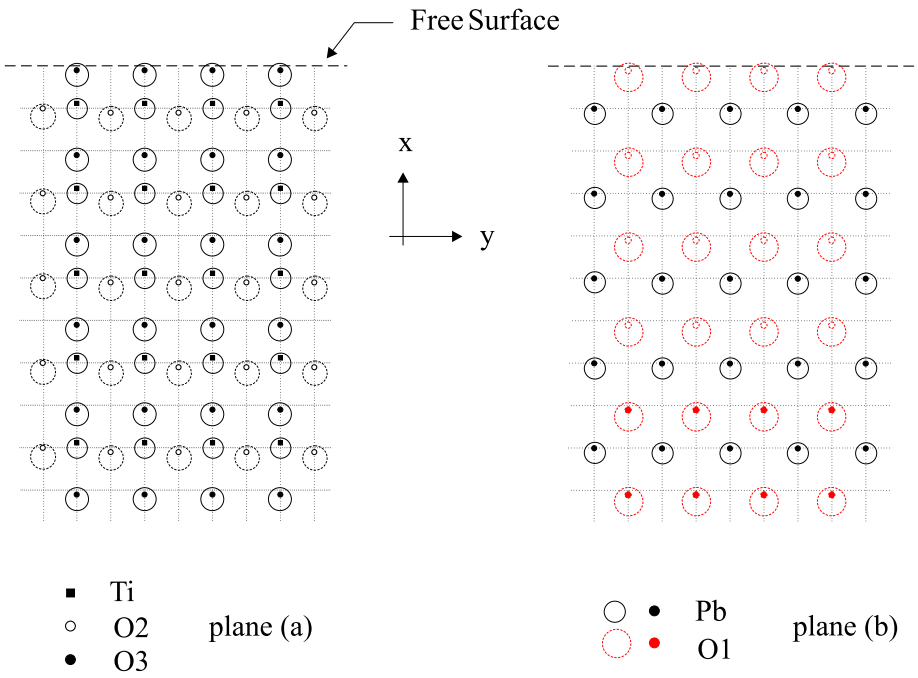

Figure 6.2: Type a free surface reference configuration.

6.1 Type c Free Surfaces

This is very similar to the 180° domain wall problem. Again we partition the half lattice into equivalence classes of atoms of the same type lying on planes parallel to the free surface. Here the unit cell index is $n \in \mathbb{N}$, with $n = 1$ corresponding to the unit cell with some atoms lying on the free surface. The bulk stiffness matrices are the same as those used in the analysis of 180° domain walls. The difference here is in the force distribution, the boundary stiffness matrices and boundary equations. The force distribution is shown in Fig. 6.4. For ranges of interaction $m = 1, 2$ the boundary equations are:

m=1:

$$\begin{aligned} n = 1 \quad &: \quad \mathcal{A}_0^{(1)}\mathbf{X}_1 + \mathcal{A}_1^{(1)}\mathbf{X}_2 = \mathbf{F}_1 \\ n = 2 \quad &: \quad \mathcal{A}_{-1}^{(2)}\mathbf{X}_1 + \mathcal{A}_0^{(2)}\mathbf{X}_2 + \mathcal{A}_1^{(2)}\mathbf{X}_3 = \mathbf{F}_2 \end{aligned} \tag{6.1}$$

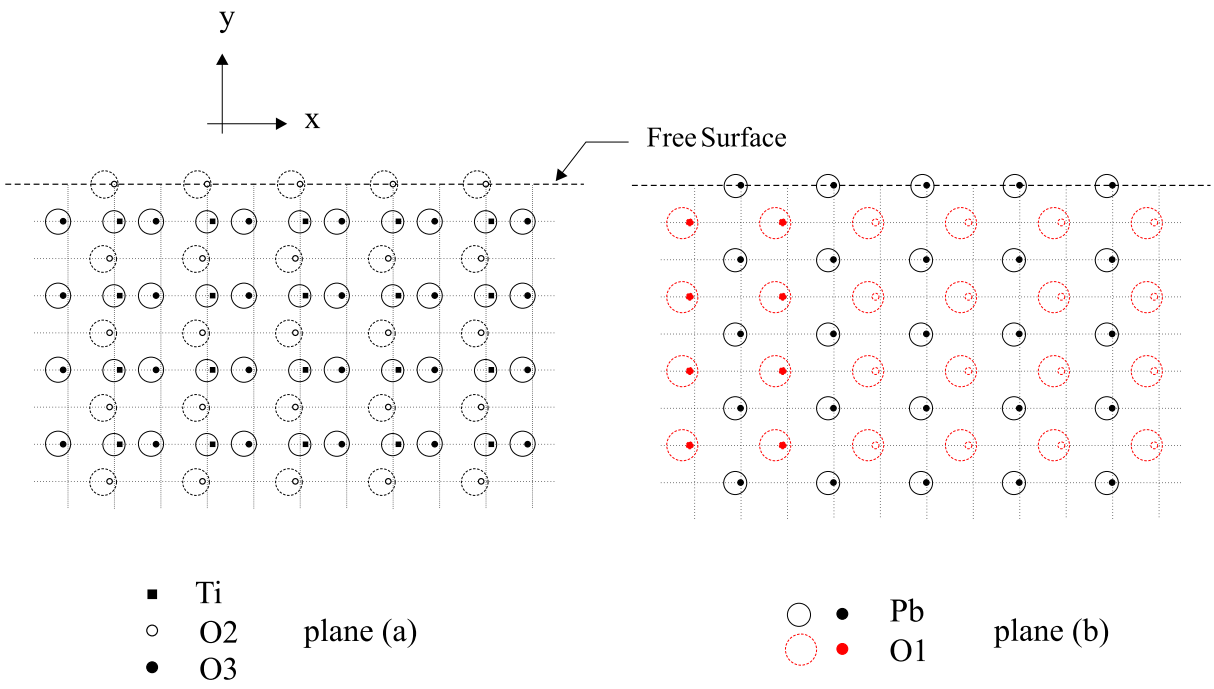

Figure 6.3: Type c free surface reference configuration.

m=2:

$$
\begin{aligned}
n = 1 \quad &: \quad \mathcal{A}_0^{(1)}\mathbf{X}_1 + \mathcal{A}_1^{(1)}\mathbf{X}_2 + \mathcal{A}_2^{(1)}\mathbf{X}_3 = \mathbf{F}_1 \\
n = 2 \quad &: \quad \mathcal{A}_{-1}^{(2)}\mathbf{X}_1 + \mathcal{A}_0^{(2)}\mathbf{X}_2 + \mathcal{A}_1^{(2)}\mathbf{X}_3 + \mathcal{A}_2^{(2)}\mathbf{X}_4 = \mathbf{F}_2 \\
n = 3 \quad &: \quad \mathcal{A}_{-2}^{(3)}\mathbf{X}_1 + \mathcal{A}_{-1}^{(3)}\mathbf{X}_2 + \mathcal{A}_0^{(3)}\mathbf{X}_3 + \mathcal{A}_1^{(3)}\mathbf{X}_4 + \mathcal{A}_2^{(3)}\mathbf{X}_5 = \mathbf{F}_3
\end{aligned} \tag{6.2}
$$

For type c free surface we calculate the displacements under the tetragonal constraint. Unbalanced force distribution for type c free surface is shown in Fig. 6.4. It is seen that the anharmonic lattice statics iterations converge. The harmonic and anharmonic displacements are shown in Figs. 6.5, 6.6, 6.7, 6.8, and 6.9. It is seen the type c free surface is atomically sharp. The polarization distribution is highly localized and is shown in Fig. 6.10.

6.2 Type a Free Surfaces

In this type of free surface the polarization direction is perpendicular to the free surface. The reference configuration of type a free surface is shown in Fig. 6.1 schematically and in more detail for the shell potential in Fig. 6.2. The bulk stiffness matrices are different from those used for the 180° domain wall. The reason is because the equivalence classes now are planes of atoms perpendicular

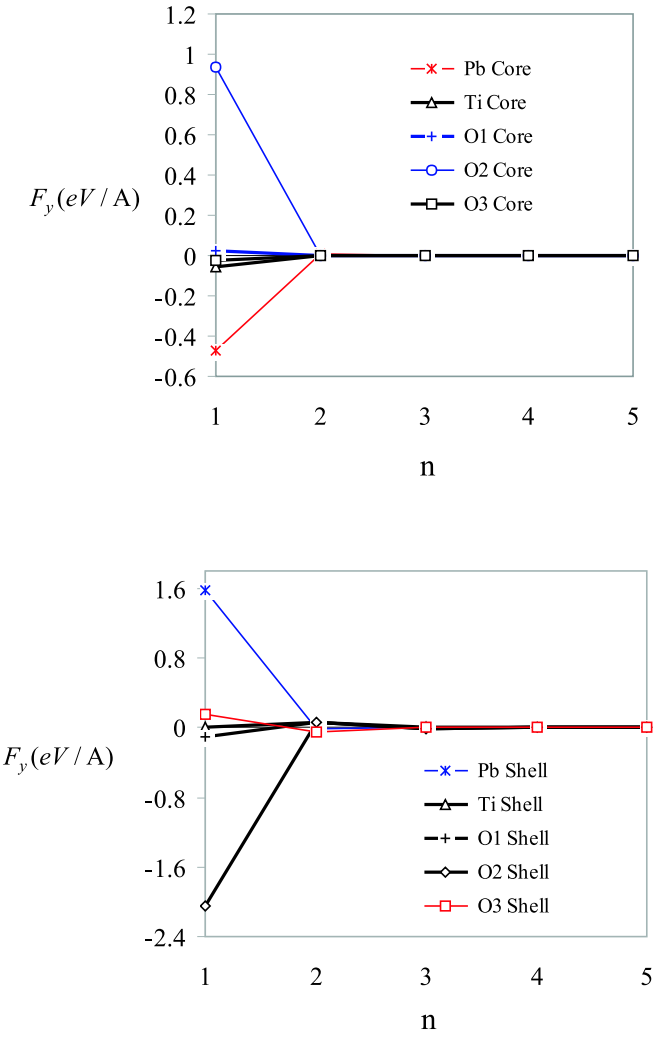

Figure 6.4: Type c free surface force distribution (forces parallel to the tetragonal c-direction).

to the tetragonal c-direction. The dominant unbalanced forces are in the tetragonal c-direction. As it is seen in Fig. 6.11 unbalanced forces have a fairly long tail and vanish only after $n = 7$. It is seen that unbalanced forces are very large compared to that of type c free surface. The harmonic displacements are very large and are given in Fig. 6.12. The anharmonic lattice statics iterations do not converge and this shows that there is no local equilibrium near the reference configuration. This is not surprising as this configuration induces a huge electrostatic field in the empty half space. The lack of convergence of the iterations indicates that there will be a severe surface reconstruction.

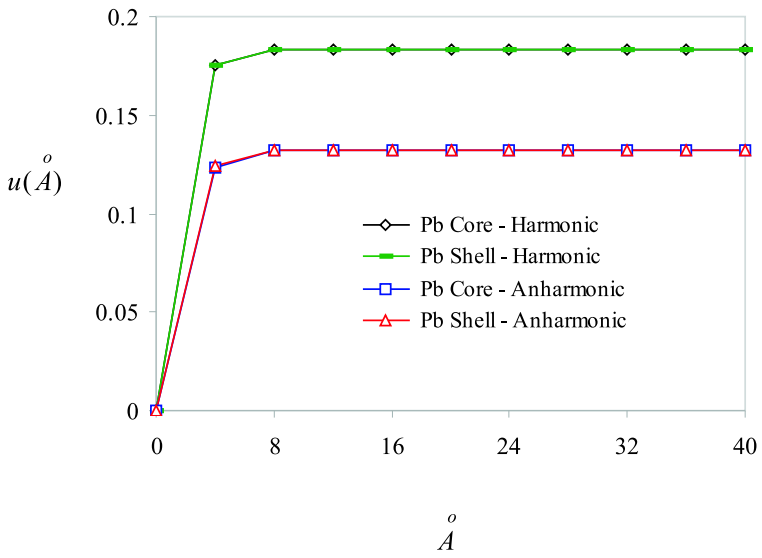

Figure 6.5: Harmonic and anharmonic Pb core and shell displacements in a type c free surface.

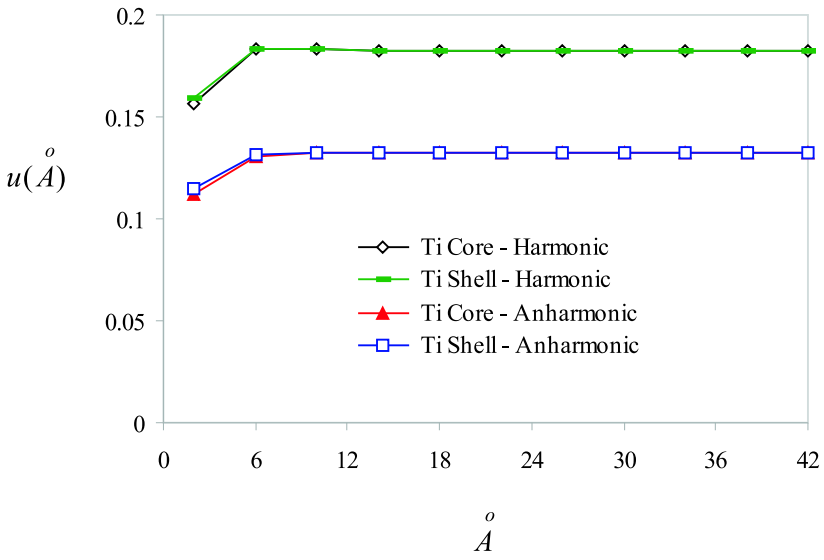

Figure 6.6: Harmonic and anharmonic Ti core and shell displacements in a type c free surface.

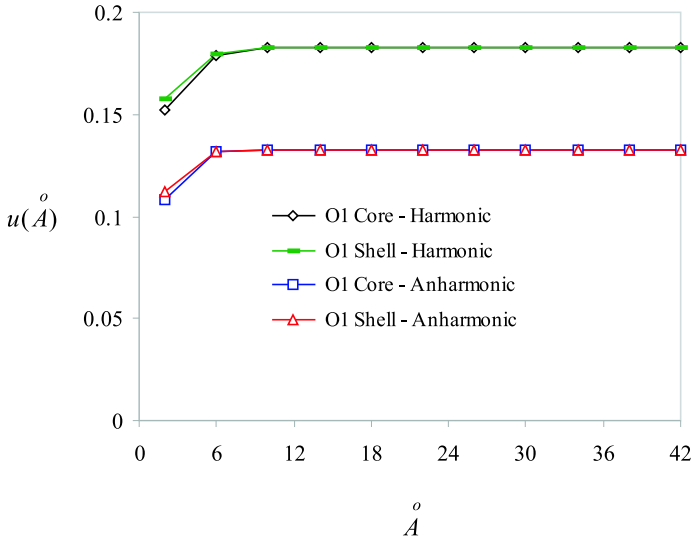

Figure 6.7: Harmonic and anharmonic O1 core and shell displacements in a type c free surface.

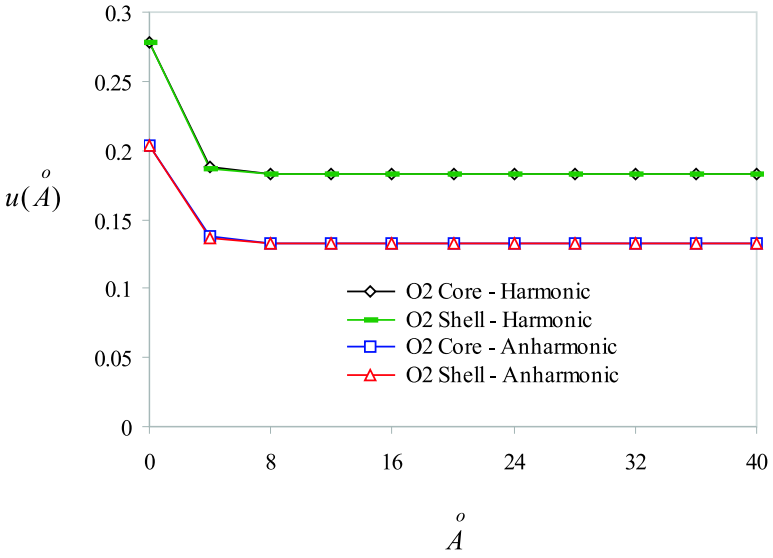

Figure 6.8: Harmonic and anharmonic O2 core and shell displacements in a type c free surface.

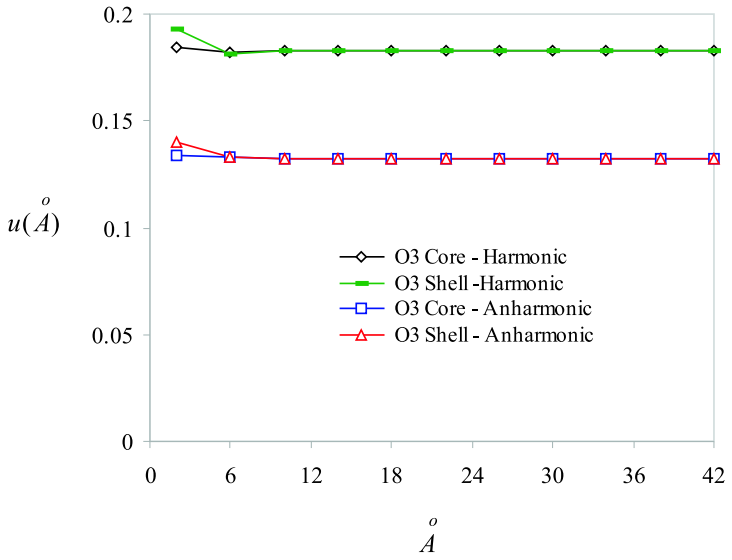

Figure 6.9: Harmonic and anharmonic O3 core and shell displacements in a type c free surface.

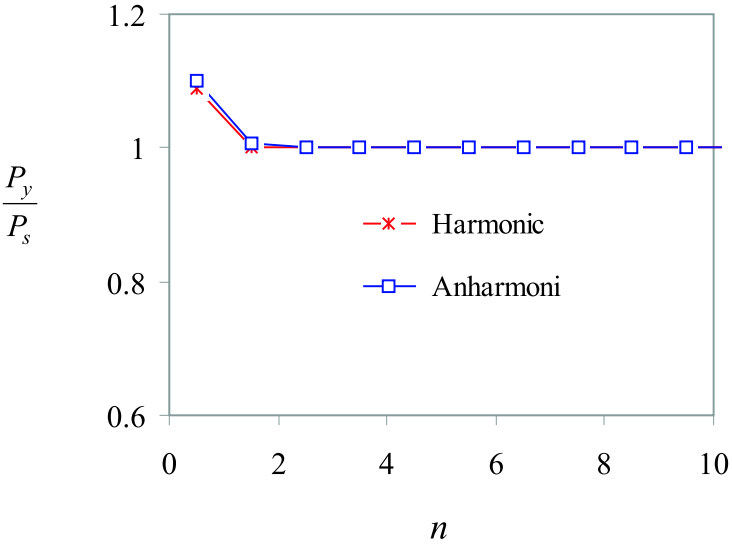

Figure 6.10: Harmonic and anharmonic polarization profile for a type c free surface.

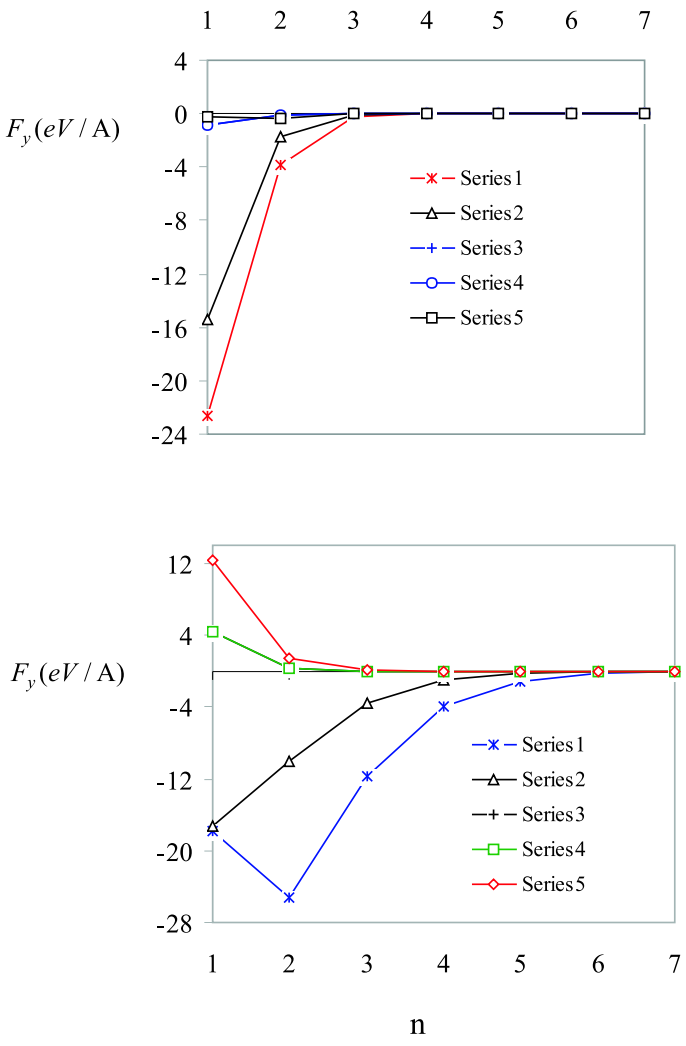

Figure 6.11: Type a free surface force distribution (forces parallel to the tetragonal c-direction).

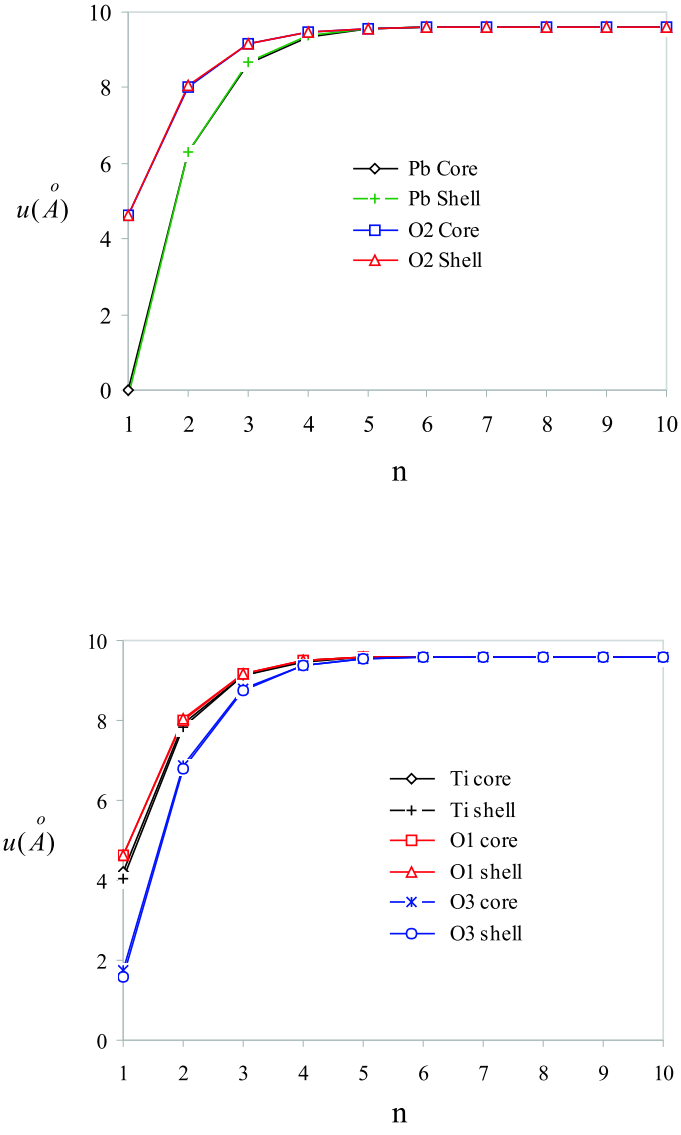

Figure 6.12: Harmonic core and shell displacements in a type a free surface.

Chapter 7

Steps in 180° Domain Walls in $PbTiO_3$

In this chapter we investigate the structure of a 180° step in tetragonal $PbTiO_3$. Assuming that the step is centered on two planes passing through some atoms, there are three possibility for the step: (i) Pb/Pb centered, (ii) Ti/Ti centered and (iii) Pb/Ti (or Ti/Pb) centered. In the first two cases the distance between the two planes of the step is a and in the third case it is $a/2$. Here we study only the first case as the other two would be very similar. The reference configuration of a Pb/O3/Pb 180° step is shown in Fig. 7.1. Clearly, for the step problem there is still translation invariance in the z-direction. For a 180° step the collection of cores and shells can be partitioned into ten pairwise disjoint sublattices,

$$\mathcal{L} = \bigcup_{I=1}^{10} \mathcal{L}_I \tag{7.1}$$

Now each $\mathcal{L}_I$ can be further partitioned into equivalence classes according to their position relative to the step core.

$$\mathcal{L}_I = \bigcup_{\alpha,\beta=-\infty}^{\infty} \mathcal{S}_{I\alpha\beta} \tag{7.2}$$

where

$$\mathcal{S}_{I\alpha\beta} = \{\mathbf{x} \in \mathcal{L}_I | (\mathbf{x} - \mathbf{p}_I) \cdot \hat{\mathbf{e}}_x = \alpha a, (\mathbf{x} - \mathbf{p}_I) \cdot \hat{\mathbf{e}}_y = \beta c, \alpha, \beta \in \mathbb{Z}\} \tag{7.3}$$

Linearizing the governing equations about a reference configuration $\mathcal{B}_0$ we obtain,

$$\frac{\partial^2 \mathcal{E}^i}{\partial \mathbf{x}^i \partial \mathbf{x}^i}(\mathcal{B}_0)\left(\mathbf{x}^i - \mathbf{x}_0^i\right) + \sum_{j \in \mathcal{S}_i} \frac{\partial^2 \mathcal{E}^i}{\partial \mathbf{x}^i \partial \mathbf{x}^j}(\mathcal{B}_0)\left(\mathbf{x}^j - \mathbf{x}_0^j\right) = -\frac{\partial \mathcal{E}}{\partial \mathbf{x}^i}(\mathcal{B}_0) \qquad \forall\ i \in \mathcal{L} \tag{7.4}$$

Thus

$$\frac{\partial^2 \mathcal{E}}{\partial \mathbf{x}^i \partial \mathbf{x}^i}(\mathcal{B}_0)\mathbf{u}^i + \sum_{J=1}^{10} \sum_{\alpha=-m}^{\alpha=m}{}' \sum_{\beta=-m}^{\beta=m} \mathbf{K}_{iJ\alpha\beta}\mathbf{u}^{J\alpha\beta} = \mathbf{f}^i \tag{7.5}$$

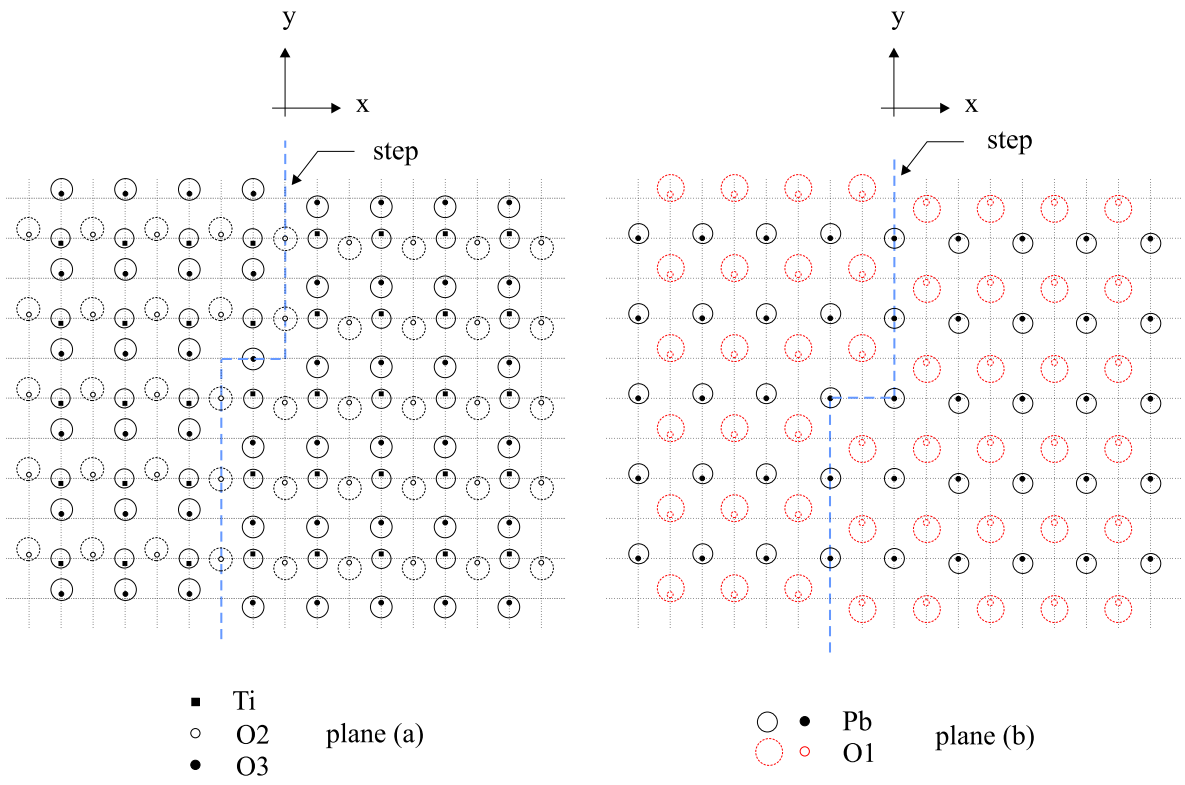

Figure 7.1: Reference configuration for a Pb/O3/Pb centered 180° step.

where

$$\mathbf{K}_{iJ\alpha\beta} = \sum_{j \in \mathcal{S}_{J\alpha\beta}} \frac{\partial^2 \mathcal{E}^i}{\partial \mathbf{x}^i \partial \mathbf{x}^j}(\mathcal{B}_0), \qquad \mathbf{f}^i = -\frac{\partial \mathcal{E}}{\partial \mathbf{x}^i}(\mathcal{B}_0) \tag{7.6}$$

and prime on the summation means that the term $\alpha = \beta = 0, I = i$ is excluded. Note that $\mathbf{K}_{iJ\alpha\beta}$ is defined in terms of an absolutely convergent lattice sum because $\frac{\partial^2 \mathcal{E}^i}{\partial \mathbf{x}^i \partial \mathbf{x}^j}(\mathcal{B}_0) = O\left(\frac{1}{r^3}\right)$ and these are summed on a one-dimensional manifold. These substiffness matrices are less sensitive to the number of atoms taken from equivalence classes compared to those of the domain walls. Note that a finite range of interaction m in both x and y directions has been assumed.

For pairwise interactions we know that

$$\frac{\partial^2 \mathcal{E}^i}{\partial \mathbf{x}^i \partial \mathbf{x}^i}(\mathcal{B}_0) = -\sum_{J=1}^{10} \sum_{\alpha=-m}^{\alpha=m} {}' \sum_{\beta=-m}^{\beta=m} \mathbf{K}_{iJ\alpha\beta} \tag{7.7}$$

Therefore the linearized governing equations are,

$$-\left(\sum_{J=1}^{10} \sum_{\alpha=-m}^{\alpha=m} {}' \sum_{\beta=-m}^{\beta=m} \mathbf{K}_{iJ\alpha\beta} \right) \mathbf{u}^i + \sum_{J=1}^{10} \sum_{\alpha=-m}^{\alpha=m} {}' \sum_{\beta=-m}^{\beta=m} \mathbf{K}_{iJ\alpha\beta} \mathbf{u}^{J\alpha\beta} = \mathbf{f}^i \tag{7.8}$$

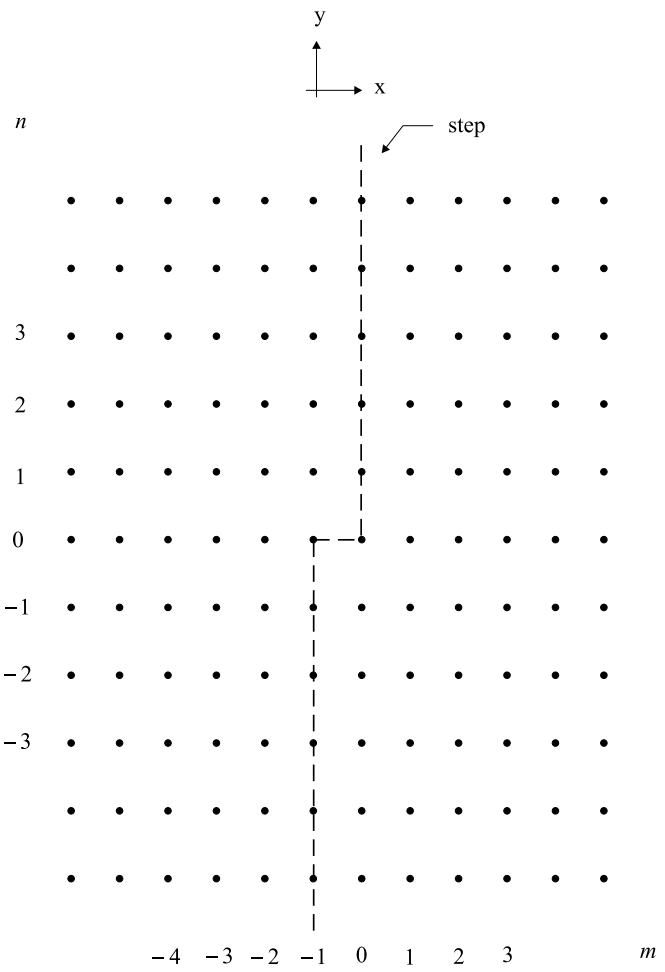

Figure 7.2: Unit cell numbering for a 180° step.

Denoting $\mathbf{X}_{m,n} \in \mathbb{R}^{30}$ the vector of displacements for the representative unit cell (m, n), the linearized governing equations can be written more compactly as

$$\sum_{\alpha=-r}^{\alpha=r} \sum_{\beta=-s}^{\beta=s} \mathcal{A}_{\alpha\beta}(m,n)\mathbf{X}_{m+\alpha,n+\beta} = \mathbf{F}_{m,n} \qquad m,n \in \mathbb{Z} \tag{7.9}$$

where ranges of interaction r and s in the respective directions m and n have been assumed. Note that stiffness matrices explicitly depend on m, n. Far from the step we have

$$\mathcal{A}_{\alpha\beta}(m,n) = \mathcal{A}^{+}_{\alpha\beta} \qquad m > m_0 \tag{7.10}$$

$$\mathcal{A}_{\alpha\beta}(m,n) = \mathcal{A}^{-}_{\alpha\beta} \qquad m < -m_0 \tag{7.11}$$

For $-m_0 \leq m \leq m_0$ stiffness matrices vary (boundary stiffnesses). Similar to what we discussed

for the problem of a 180° domain wall, $\mathcal{A}^{+}_{\alpha\beta}$ and $\mathcal{A}^{-}_{\alpha\beta}$ are not equal, in general. To be able to solve the governing equations (7.9) we make the following two simplifying assumptions: (i) Stiffness matrices are assumed to be uniform everywhere, i.e., the fact that close to the step stiffnesses vary and stiffnesses far from the step on the right and left sides are unequal is ignored. (ii) The average stiffnesses are uses, i.e.,

$$\mathcal{A}_{\alpha\beta} = \frac{1}{2}\left(\mathcal{A}^{+}_{\alpha\beta} + \mathcal{A}^{-}_{\alpha\beta}\right) \tag{7.12}$$

Thus it is assumed that the following are the governing equations,

$$\sum_{\alpha=-r}^{\alpha=r}\sum_{\beta=-s}^{\beta=s} \mathcal{A}_{\alpha\beta}\mathbf{X}_{m+\alpha,n+\beta} = \mathbf{F}_{m,n} \qquad m,n \in \mathbb{Z} \tag{7.13}$$

We know from our numerical studies of the 180° problem that averaging the stiffnesses is a very good approximation. The less accurate assumption is assuming that stiffnesses do not vary close to the step. Note that because of translation invariance,

$$\text{Nullity}\left(\sum_{\alpha=-r}^{\alpha=r}\sum_{\beta=-s}^{\beta=s} \mathcal{A}_{\alpha\beta}\right) = 3 \tag{7.14}$$

Also note that $\mathcal{A}_{\alpha\beta}$'s are not symmetric.

Because of the symmetry of the reference configuration, the unbalanced forces in a Pb/O3/Pb-centered step have the following symmetries for $m \geq 2, n \in \mathbb{Z}$,

$$Pb \;:\; \mathbf{F}_{-m,-n} = -\mathbf{F}_{m-1,n} \tag{7.15}$$

$$Ti \;:\; \mathbf{F}_{-m,-n} = -\mathbf{F}_{m-2,n-1} \tag{7.16}$$

$$O1 \;:\; \mathbf{F}_{-m,-n} = -\mathbf{F}_{m-2,n-1} \tag{7.17}$$

$$O2 \;:\; \mathbf{F}_{-m,-n} = -\mathbf{F}_{m-1,n-1} \tag{7.18}$$

$$O3 \;:\; \mathbf{F}_{-m,-n} = -\mathbf{F}_{m-2,n} \tag{7.19}$$

and for $m = 1$,

$$Pb \;:\; \mathbf{F}_{-1,-n} = -\mathbf{F}_{0,n} \qquad \forall n \in \mathbb{Z} \tag{7.20}$$

$$Ti \;:\; \mathbf{F}_{-1,-n} = -\mathbf{F}_{-1,n-1} \qquad \forall n \geq 1 \tag{7.21}$$

$$O1 \;:\; \mathbf{F}_{-1,-n} = -\mathbf{F}_{-1,n-1} \qquad \forall n \geq 1 \tag{7.22}$$

$$O2 \;:\; \mathbf{F}_{-1,-n} = -\mathbf{F}_{0,n-1} \qquad \forall n \in \mathbb{Z} \tag{7.23}$$

$$O3 \;:\; \mathbf{F}_{-1,-n} = -\mathbf{F}_{-1,n} \qquad \forall n \geq 1 \quad \text{and} \quad \mathbf{F}_{-1,0} = \mathbf{0} \tag{7.24}$$

Our numerical calculations verify these symmetries. We also observe that away from the core of the step ($|n| \geq 3$) the unbalanced forces are exactly the same as those of a Pb-centered 180° domain wall.

Applying discrete Fourier transform to the simplified governing equations (7.12) we obtain,

$$\left(\sum_{\alpha=-r}^{\alpha=r} \sum_{\beta=-s}^{\beta=s} \mathcal{A}_{\alpha\beta} e^{-i(\alpha k_1 + \beta k_2)} \right) \widehat{\mathbf{X}_{m,n}}(k_1, k_2) = \widehat{\mathbf{F}_{m,n}}(k_1, k_2) \tag{7.25}$$

Thus

$$\widehat{\mathbf{X}_{m,n}}(k_1, k_2) = \mathbf{B}^{-1}(k_1, k_2) \widehat{\mathbf{F}_{m,n}}(k_1, k_2) \tag{7.26}$$

where

$$\mathbf{B}(k_1, k_2) = \sum_{\alpha=-r}^{\alpha=r} \sum_{\beta=-s}^{\beta=s} e^{-i(\alpha k_1 + \beta k_2)} \mathcal{A}_{\alpha\beta} \tag{7.27}$$

Therefore the solution can be expressed as

$$\mathbf{X}_{m,n} = \frac{1}{(2\pi)^2} \int_{-\pi}^{\pi} \int_{-\pi}^{\pi} e^{-i(mk_1 + nk_2)} \mathbf{B}^{-1}(k_1, k_2) \widehat{\mathbf{F}_{m,n}}(k_1, k_2) dk_1 dk_2 \tag{7.28}$$

Note that this would be the solution if the matrix $\mathbf{B}$ is invertible for all $(k_1, k_2) \in B = [-\pi, \pi] \times [-\pi, \pi]$. Here we know that the governing discrete equations are translation invariant, i.e., $\mathbf{B}$ is not full rank at $(k_1, k_2) = (0, 0)$. This is not necessarily the only such point. Our numerical study of $\mathbf{B}$ shows that indeed $(0, 0)$ is the only point at which $\mathbf{B}$ is not full rank. This means that there is a singularity at $(0, 0)$ and the inverse Fourier transform as written above is not a convergent double integral in general. One way of removing the singularity is to impose a suitable rigid translation. Of course, not every rigid translation is a suitable choice. The following is a suitable choice,*

$$\mathbf{X}_{m,n} = \frac{1}{(2\pi)^2} \int_{-\pi}^{\pi} \int_{-\pi}^{\pi} e^{-imk_1 - ink_2} \left[\mathbf{B}^{-1}(k_1, k_2) - e^{imk_1 + ink_2} \mathbf{D}(k_1, k_2) \right] \widehat{\mathbf{F}_{n,m}}(k_1, k_2) dk_1 dk_2 \tag{7.31}$$

*An alternative approach to remove the singularity is as follows. Let us first introduce the following change of variables,

$$\bar{\mathbf{X}}_{m,n} = (-1)^n \mathbf{X}_{m,n}, \quad \bar{\mathbf{F}}_{mn} = (-1)^n \mathbf{F}_{mn}, \quad \overline{\mathcal{A}}_{\alpha\beta} = (-1)^n \mathcal{A}_{\alpha\beta} \tag{7.29}$$

The governing equations in terms of the new variables are,

$$\sum_{\alpha=-r}^{\alpha=r} \sum_{\beta=-s}^{\beta=s} \overline{\mathcal{A}}_{\alpha\beta} \bar{\mathbf{X}}_{m+\alpha, n+\beta} = \bar{\mathbf{F}}_{m,n} \qquad m, n \in \mathbb{Z} \tag{7.30}$$

The above system of difference equations are not translation invariant.

where

$$\mathbf{D}(k_1,k_2)=\begin{pmatrix}\mathbf{U}(k_1,k_2) & \dots & \mathbf{U}(k_1,k_2)\\ \vdots & & \vdots \\ \mathbf{U}(k_1,k_2) & \dots & \mathbf{U}(k_1,k_2)\end{pmatrix},\qquad \mathbf{U}(k_1,k_2)=\begin{pmatrix}d_1(k_1,k_2) & 0 & 0\\ 0 & d_2(k_1,k_2) & 0\\ 0 & 0 & d_3(k_1,k_2)\end{pmatrix},$$

$$d_1(k_1,k_2)=\left(\mathbf{B}^{-1}(k_1,k_2)\right)_{11},d_2(k_1,k_2)=\left(\mathbf{B}^{-1}(k_1,k_2)\right)_{22},d_3(k_1,k_2)=\left(\mathbf{B}^{-1}(k_1,k_2)\right)_{33}$$

In the step problem practically there is no problem in calculating the inverse DFT as the loads are symmetric and kill the singularity. This will be explained in some detail in Appendix B.

For the sake of completeness let us look at the discrete Green's functions, which are solutions of the following equations,

$$\sum_{\alpha=-r}^{\alpha=r}\sum_{\beta=-s}^{\beta=s}\mathcal{A}_{\alpha\beta}\mathbf{g}^{(j)}_{m+\alpha,n+\beta}=\delta_{mn}\mathbf{e}_j\qquad m,n\in\mathbb{Z}\ ,\ j=1,...,p \tag{7.32}$$

where

$$\delta_{mn}=1\quad\text{if}\quad m=n=0\quad\text{and}\quad\delta_{mn}=0\quad\text{otherwise} \tag{7.33}$$

and,

$$\mathbf{e}_j=\begin{pmatrix}0\\ \vdots\\ 0\\ 1\\ 0\\ \vdots\\ 0\end{pmatrix}\in\mathbb{R}^p \tag{7.34}$$

where the nonzero entry is the jth component. The discrete Green's functions can be expressed as

$$\mathbf{g}^{(j)}_{m,n}=\frac{1}{(2\pi)^2}\int_{-\pi}^{\pi}\int_{-\pi}^{\pi}e^{-i(mk_1+nk_2)}\left[\mathbf{B}^{-1}(k_1,k_2)-e^{i(mk_1+nk_2)}\left(\mathbf{B}^{-1}(k_1,k_2)\right)_{11}\mathbf{1}\otimes\mathbf{1}\right]\mathbf{e}_j dk_1dk_2 \tag{7.35}$$

where $\mathbf{1}\otimes\mathbf{1}\in\mathbb{R}^{p\times p}$ is a matrix with all entries equal to 1. Note that the rigid translation,

$$-\frac{1}{(2\pi)^2}\int_{-\pi}^{\pi}\int_{-\pi}^{\pi}\left(\mathbf{B}^{-1}(k_1,k_2)\right)_{11}(\mathbf{1}\otimes\mathbf{1})\mathbf{e}_j\ dk_1dk_2 \tag{7.36}$$

removes the singularity at $(k_1, k_2) = (0, 0)$. Also note that

$$(\mathbf{1} \otimes \mathbf{1})\mathbf{e}_j = \begin{pmatrix} 1 \\ \vdots \\ 1 \end{pmatrix} \qquad \forall j = 1, ..., p \tag{7.37}$$

This means that the same rigid translation is used for all j. Now the solution can be written as

$$\mathbf{X}_{m,n} = \sum_{j=1}^{p} \sum_{l_1=-\infty}^{\infty} \sum_{l_2=-\infty}^{\infty} (\mathbf{F}_{l_1,l_2} \cdot \mathbf{e}_j)\mathbf{g}^{(j)}_{m-l_1,n-l_2} = \sum_{j=1}^{p} \sum_{l_1=-\infty}^{\infty} \sum_{l_2=-\infty}^{\infty} (\mathbf{F}_{m-l_1,n-l_2} \cdot \mathbf{e}_j)\mathbf{g}^{(j)}_{l_1,l_2} \tag{7.38}$$

Or in terms of discrete convolution,

$$\mathbf{X}_{m,n} = \sum_{j=1}^{p} \Big((\mathbf{F} \cdot \mathbf{e}_j) * \mathbf{g}^{(j)} \Big)_{mn} \tag{7.39}$$

In our problem $p = 10$ and forces are nonzero only in the infinite band,[†]

$$\{(l_1, l_2) : l_1 \in \{-3, -2, -1, 0, 1, 2\}, l_2 \in \mathbb{Z}\} \tag{7.40}$$

In the step problem forces are not concentrated and there are non-zero forces along the step half planes all the way to $\pm\infty$. This makes the direct application of DFT hopeless because the integrands would be extremely oscillatory. Usually the advantage of using discrete Green's functions is that one solves for displacements for a set of unit forces and then solution for an arbitrary force vector can be reduced to some simple summations. In calculating the discrete Green's functions one has a nonzero force only at $(m, n) = (0, 0)$ and using a 100×100 Gaussian quadrature gives displacements accurate to within $10^{-4}\mathring{A}$ in the region $|m|, |n| \leq 10$. This is a good accuracy as we expect the displacements to be localized around the step. However, considering the support of unbalanced forces one needs to calculate the discrete Green's functions for very large unit cell indices. This makes the calculations inaccurate and not practical. We will resolve this issue by making an approximation, which will be explained in the sequel.

There are several numerical integration schemes for evaluating highly oscillatory integrals in the literature (see Evans and Webster (1999) and references therein). Our numerical tests show that the standard Gaussian quadrature is efficient enough for calculating the inverse DFT's in this work.

For a Pb/O3/Pb centered 180° step we have the following symmetries for displacements of cores

[†]Note that $m = 0$ and $m = -1$ are symmetry related.

and shells for $p \geq 2, q \in \mathbb{Z}$,

$$Pb \quad : \quad \mathbf{X}_{-p,-q} = -\mathbf{X}_{p-1,q} \tag{7.41}$$

$$Ti \quad : \quad \mathbf{X}_{-p,-q} = -\mathbf{X}_{p-2,q-1} \tag{7.42}$$

$$O1 \quad : \quad \mathbf{X}_{-p,-q} = -\mathbf{X}_{p-2,q-1} \tag{7.43}$$

$$O2 \quad : \quad \mathbf{X}_{-p,-q} = -\mathbf{X}_{p-1,q-1} \tag{7.44}$$

$$O3 \quad : \quad \mathbf{X}_{-p,-q} = -\mathbf{X}_{p-2,q} \tag{7.45}$$

which can be rewritten as

$$\mathbf{X}_{-p,-q} = \mathcal{R}_1\mathbf{X}_{p-1,q} + \mathcal{R}_2\mathbf{X}_{p-2,q-1} + \mathcal{R}_3\mathbf{X}_{p-1,q-1} + \mathcal{R}_4\mathbf{X}_{p-2,q} \qquad p \geq 2 \tag{7.46}$$

where

$$\mathcal{R}_1 = \begin{pmatrix} \mathbf{-1} & & & & \\ & \mathbf{0} & & & \\ & & \mathbf{0} & & \\ & & & \mathbf{0} & \\ & & & & \mathbf{0} \end{pmatrix}, \quad \mathcal{R}_2 = \begin{pmatrix} \mathbf{0} & & & & \\ & \mathbf{-1} & & & \\ & & \mathbf{-1} & & \\ & & & \mathbf{0} & \\ & & & & \mathbf{0} \end{pmatrix} \tag{7.47}$$

$$\mathcal{R}_3 = \begin{pmatrix} \mathbf{0} & & & & \\ & \mathbf{0} & & & \\ & & \mathbf{0} & & \\ & & & \mathbf{-1} & \\ & & & & \mathbf{0} \end{pmatrix}, \quad \mathcal{R}_4 = \begin{pmatrix} \mathbf{0} & & & & \\ & \mathbf{0} & & & \\ & & \mathbf{0} & & \\ & & & \mathbf{0} & \\ & & & & \mathbf{-1} \end{pmatrix} \tag{7.48}$$

For $p = -1$ we have the following symmetries,

$$Pb \quad : \quad \mathbf{X}_{-1,-q} = -\mathbf{X}_{0,q} \qquad \forall q \in \mathbb{Z} \tag{7.49}$$

$$Ti \quad : \quad \mathbf{X}_{-1,-q} = -\mathbf{X}_{-1,q-1} \qquad \forall q \geq 1 \tag{7.50}$$

$$O1 \quad : \quad \mathbf{X}_{-1,-q} = -\mathbf{X}_{-1,q-1} \qquad \forall q \geq 1 \tag{7.51}$$

$$O2 \quad : \quad \mathbf{X}_{-1,-q} = -\mathbf{X}_{0,q-1} \qquad \forall q \in \mathbb{Z} \tag{7.52}$$

$$O3 \quad : \quad \mathbf{X}_{-1,-q} = -\mathbf{X}_{-1,q} \qquad \forall q \geq 1 \quad \text{and} \quad \mathbf{X}_{-1,0} = \mathbf{0} \tag{7.53}$$

We make use of the above symmetries and reduce the number of calculations.

It turns out that using any of the abovementioned methods for solving the partial difference equations, the solutions are not accurate because forces are nonzero on an infinite band along the

step. Here we make an approximation and use the solutions of the Pb-centered 180° domain wall. We know that away from the step core the relaxed configuration should be the same as that of a Pb-centered 180° domain wall. The force localization idea is schematically shown in Fig. 7.4. Our calculations show that unbalanced forces have the following property,

$$\mathbf{F}_{mn} = \mathbf{F}_{DW}(m) \qquad n \geq 3 \tag{7.54}$$

$$\mathbf{F}_{mn} = \mathbf{F}_{DW}(m+1) \qquad n \leq -3 \tag{7.55}$$

where $\mathbf{F}_{DW}(m)$ is the domain wall displacement (assuming that atoms lying on the domain wall have index $m = 0$). Thus we consider the step forces in the range $(m, n) \in \{-3, -2, -1, 0, 1, 2\} \times \{-2, -1, 0, 1, 2\}$.[‡] The solutions obtained from this localized system of forces can be accurately obtained using DFT. The approximate harmonic solution is then obtained by superposing the domain wall solution to this. This would be a reference configuration with the nice property that its unbalanced forces are localized.

The construction of the localized forces is not trivial and one should be careful with symmetries. For Ti, O1 and O2 (the atom types that do not lie on the step) we construct the localized force system as follows.

$$n \geq 0 \quad : \quad \mathbf{F}^{\text{localized}}_{mn} = \mathbf{F}_{mn} - \mathbf{F}_{DW}(m) \tag{7.56}$$

$$n \leq -1 \quad : \quad \mathbf{F}^{\text{localized}}_{mn} = \mathbf{F}_{mn} - \mathbf{F}_{DW}(m+1) \tag{7.57}$$

and,

$$\mathbf{F}^{\text{localized}}_{mn} = \mathbf{0} \qquad |n| \geq 2 \tag{7.58}$$

Let us first check the symmetry of the localized forces.

- *Ti and O1:*

  i) $m \geq 2$

$$\mathbf{F}^{\text{localized}}_{-m,-n} = \begin{cases} \mathbf{F}_{-m,-n} - \mathbf{F}_{DW}(-m) & n \leq 0 \\ \mathbf{F}_{-m,-n} - \mathbf{F}_{DW}(-m+1) & n \geq 1 \end{cases}$$

$$= \begin{cases} -\mathbf{F}_{m-2,n-1} + \mathbf{F}_{DW}(m-1) & n \leq 0 \\ \mathbf{F}_{m-2,n-1} - \mathbf{F}_{DW}(m-2) & n \geq 1 \end{cases} \tag{7.59}$$

$$= \begin{cases} -\mathbf{F}^{\text{localized}}_{m-2,n-1} & n \leq 0 \\ -\mathbf{F}^{\text{localized}}_{m-2,n-1} & n \geq 1 \end{cases} \tag{7.60}$$

[‡]Note that the indices $m = -1$ and $m = 0$ are symmetry related.

Thus

$$\mathbf{F}^{\text{localized}}_{-m,-n} = -\mathbf{F}^{\text{localized}}_{m-2,n-1} \qquad \square \tag{7.61}$$

ii) $m = 1$

$$\mathbf{F}^{\text{localized}}_{-1,-n} = \mathbf{F}_{-1,-n} - \mathbf{F}_{DW}(0) = -\mathbf{F}_{-1,n-1} + \mathbf{F}_{DW}(-1) = -\mathbf{F}^{\text{localized}}_{-1,n-1}, n \geq 1 \qquad \square \tag{7.62}$$

- *O2:*

$$\begin{aligned}
\mathbf{F}^{\text{localized}}_{-m,-n} &= \begin{cases} \mathbf{F}_{-m,-n} - \mathbf{F}_{DW}(-m) & n \leq 0 \\ \mathbf{F}_{-m,-n} - \mathbf{F}_{DW}(-m+1) & n \geq 1 \end{cases} \\
&= \begin{cases} -\mathbf{F}_{m-1,n-1} + \mathbf{F}_{DW}(m) & n \leq 0 \\ \mathbf{F}_{m-1,n-1} - \mathbf{F}_{DW}(m-1) & n \geq 1 \end{cases} \qquad (7.63) \\
&= \begin{cases} -\mathbf{F}^{\text{localized}}_{m-1,n-1} & n \leq 0 \\ -\mathbf{F}^{\text{localized}}_{m-1,n-1} & n \geq 1 \end{cases} \qquad (7.64)
\end{aligned}$$

Thus

$$\mathbf{F}^{\text{localized}}_{-m,-n} = -\mathbf{F}^{\text{localized}}_{m-1,n-1} \qquad \square \tag{7.65}$$

For Pb and O3 one should be more careful because these atoms lie on the step for $n = 0$.

- *Pb:* For $n \neq 0$ the localized force system is constructed as follows,

$$\mathbf{F}^{\text{localized}}_{m,n} = \begin{cases} \mathbf{F}_{m,n} - \mathbf{F}_{DW}(m) & n > 0 \\ \mathbf{F}_{m,n} - \mathbf{F}_{DW}(m+1) & n < 0 \end{cases} \tag{7.66}$$

For $n = 0$ the localized forces are,

$$\mathbf{F}^{\text{localized}}_{m,0} = \mathbf{F}_{m,0} - \mathbf{F}_{DW}(m) \qquad m \geq 0 \tag{7.67}$$

and,

$$\mathbf{F}^{\text{localized}}_{-m,0} = -\left(\mathbf{F}_{m-1,0} - \mathbf{F}_{DW}(m-1)\right) \qquad m \geq 1 \tag{7.68}$$

This means that the symmetry $\mathbf{F}^{\text{localized}}_{-m,0} = -\mathbf{F}^{\text{localized}}_{m-1,0}$ is automatically satisfied. The other

symmetries can be easily checked as follows,

$$\begin{aligned}
\mathbf{F}^{\text{localized}}_{-m,-n} &= \begin{cases} \mathbf{F}_{-m,-n} - \mathbf{F}_{DW}(-m) & n < 0 \\ \mathbf{F}_{-m,-n} - \mathbf{F}_{DW}(-m+1) & n > 0 \end{cases} \\
&= \begin{cases} -\mathbf{F}_{m-1,n} + \mathbf{F}_{DW}(m) & n < 0 \\ \mathbf{F}_{m-1,n} - \mathbf{F}_{DW}(m-1) & n > 0 \end{cases} \qquad (7.69) \\
&= \begin{cases} -\mathbf{F}^{\text{localized}}_{m-1,n} & n < 0 \\ -\mathbf{F}^{\text{localized}}_{m-1,n} & n > 0 \end{cases} = -\mathbf{F}^{\text{localized}}_{m-1,n} \qquad \square \qquad (7.70)
\end{aligned}$$

- *O3:*

i) $m \geq 2$: For $n \neq 0$ the localized force system is constructed as follows,

$$\mathbf{F}^{\text{localized}}_{m,n} = \begin{cases} \mathbf{F}_{m,n} - \mathbf{F}_{DW}(m) & n > 0 \\ \mathbf{F}_{m,n} - \mathbf{F}_{DW}(m+1) & n < 0 \end{cases} \qquad (7.71)$$

For $n = 0$ the localized forces are,

$$\mathbf{F}^{\text{localized}}_{m,0} = \mathbf{F}_{m,0} - \mathbf{F}_{DW}(m) \qquad m \geq 0 \qquad (7.72)$$

and,

$$\mathbf{F}^{\text{localized}}_{-m,0} = -\left(\mathbf{F}_{m-2,0} - \mathbf{F}_{DW}(m-2)\right) \qquad m \geq 2 \qquad (7.73)$$

This would mean that the symmetry $\mathbf{F}^{\text{localized}}_{-m,0} = -\mathbf{F}^{\text{localized}}_{m-2,0}$ is automatically satisfied. The other symmetries can be easily checked as follows,

$$\begin{aligned}
\mathbf{F}^{\text{localized}}_{-m,-n} &= \begin{cases} \mathbf{F}_{-m,-n} - \mathbf{F}_{DW}(-m) & n < 0 \\ \mathbf{F}_{-m,-n} - \mathbf{F}_{DW}(-m+1) & n > 0 \end{cases} \\
&= \begin{cases} -\mathbf{F}_{m-1,n} + \mathbf{F}_{DW}(m-1) & n < 0 \\ \mathbf{F}_{m-1,n} - \mathbf{F}_{DW}(m-2) & n > 0 \end{cases} \qquad (7.74) \\
&= \begin{cases} -\mathbf{F}^{\text{localized}}_{m-2,n} & n < 0 \\ -\mathbf{F}^{\text{localized}}_{m-2,n} & n > 0 \end{cases} = -\mathbf{F}^{\text{localized}}_{m-2,n} \qquad \square \qquad (7.75)
\end{aligned}$$

ii) $m = 1$:

$$\mathbf{F}^{\text{localized}}_{-1,n} = \mathbf{F}_{-1,n} - \mathbf{F}_{DW}(-1) \qquad n > 0 \qquad (7.76)$$

and,

$$\mathbf{F}^{\text{localized}}_{-1,n} = -\mathbf{F}^{\text{localized}}_{-1,-n} \qquad n < 0 \qquad (7.77)$$

The discrete displacement field due to localized forces are denoted by $\mathbf{X}_{mn}^{\text{localized}}$. Our numerical results show that for $|m| > 5$ or $|n| > 25$ the displacement components are less than $10^{-3}\mathring{A}$. Thus we assume that the localized displacements are zero outside the square $\{(m,n) : |m| \leq 5, |n| \leq 25\}$. By 'harmonic step displacement field' we mean the following discrete displacement field,

- *Pb:*

$$\mathbf{X}_{mn}^{\text{harmonic}} = \begin{cases} \mathbf{X}_{mn}^{\text{localized}} + \mathbf{X}_{m}^{\text{DW}} & n > 0 \\ \mathbf{X}_{mn}^{\text{localized}} + \mathbf{X}_{m+1}^{\text{DW}} & n < 0 \end{cases}$$

  and,

$$m \geq 0 \quad : \quad \mathbf{X}_{m,0}^{\text{harmonic}} = \mathbf{X}_{m,0}^{\text{localized}} + \mathbf{X}_{m}^{\text{DW}} \tag{7.78}$$

$$m < 0 \quad : \quad \mathbf{X}_{m,0}^{\text{harmonic}} = -\mathbf{X}_{-m-1,0}^{\text{harmonic}} \tag{7.79}$$

  where $\mathbf{X}_{m}^{\text{DW}}$ is the anharmonic domain wall displacement field.

- *Ti,O1,O2:*

$$\mathbf{X}_{mn}^{\text{harmonic}} = \begin{cases} \mathbf{X}_{mn}^{\text{localized}} + \mathbf{X}_{m}^{\text{DW}} & n \geq 0 \\ \mathbf{X}_{mn}^{\text{localized}} + \mathbf{X}_{m+1}^{\text{DW}} & n < 0 \end{cases}$$

- *O3:*

$$\mathbf{X}_{mn}^{\text{harmonic}} = \begin{cases} \mathbf{X}_{mn}^{\text{localized}} + \mathbf{X}_{m}^{\text{DW}} & n > 0 \\ \mathbf{X}_{mn}^{\text{localized}} + \mathbf{X}_{m+1}^{\text{DW}} & n < 0 \end{cases}$$

  and,

$$m \geq 0 \quad : \quad \mathbf{X}_{m,0}^{\text{harmonic}} = \mathbf{X}_{m,0}^{\text{localized}} + \mathbf{X}_{m}^{\text{DW}} \tag{7.80}$$

$$m < -1 \quad : \quad \mathbf{X}_{m,0}^{\text{harmonic}} = -\mathbf{X}_{-m-2,0}^{\text{harmonic}} \tag{7.81}$$

  and,

$$\mathbf{X}_{-1,-n}^{\text{harmonic}} = -\mathbf{X}_{-1,n}^{\text{harmonic}} \qquad n > 0 \tag{7.82}$$

7.1 Anharmonic Lattice Statics of steps in 180° domain walls

The idea of anharmonic lattice statics for a step is very similar to that of domain walls. The discrete boundary-value problem (DBVP) is

$$\begin{cases} \sum_{\alpha=-r}^{r} \sum_{\beta=-s}^{s} \mathcal{A}_{\alpha\beta} \mathbf{X}_{m+\alpha,n+\beta} = \mathbf{F}_{m,n} & (m,n) \in \mathbb{Z}^2 \\ \|\mathbf{X}_{m,n}\| < \infty \quad \text{as } |m||n| \to \infty \end{cases}$$

The difference between anharmonic lattice statics of step and domain walls is in the first step. We start from the reference configuration $\mathcal{B}_0'$ and localize the unbalanced forces, calculate the harmonic localized displacements and superpose it to the domain wall anharmonic solutions as was explained in the previous section. The resulting configuration is denoted by $\mathcal{B}_0$. In the second iteration, one finds $\mathbf{X}^1 = \{\mathbf{X}^1_{m,n}\}$ by solving the following DBVP,

$$\begin{cases} \sum_{\alpha=-r}^{r}\sum_{\beta=-s}^{s}\mathcal{A}_{\alpha\beta}\mathbf{X}^1_{m+\alpha,n+\beta} = \mathbf{F}^0_{m,n} & (m,n)\in\mathbb{Z}^2 \\ \|\mathbf{X}^1_{m,n}\| < \infty \quad \text{as } |m||n| \to \infty \end{cases} \tag{7.83}$$

where, $\mathbf{F}^0_{m,n} = \mathbf{F}_{m,n}(\mathcal{B}_0)$. In the next step,

$$\mathcal{B}_1 = \mathcal{B}_0 + \{\mathbf{X}^1_{m,n}\}, \qquad \mathbf{F}^1_{m,n} = \mathbf{F}_{m,n}(\mathcal{B}_0) \tag{7.84}$$

The governing DBVP for determining $\mathbf{X}^{k+1} = \{\mathbf{X}^{k+1}_{m,n}\}$ is

$$\begin{cases} \sum_{\alpha=-r}^{r}\sum_{\beta=-s}^{s}\mathcal{A}_{\alpha\beta}\mathbf{X}^{k+1}_{m+\alpha,n+\beta} = \mathbf{F}^k_{m,n} & (m,n)\in\mathbb{Z}^2 \\ \|\mathbf{X}^{k+1}_{m,n}\| < \infty \quad \text{as } |m||n| \to \infty \end{cases} \tag{7.85}$$

where

$$\mathcal{B}_k = \mathcal{B}_{k-1} + \{\mathbf{X}^k_{m,n}\}, \qquad \mathbf{F}^k_{m,n} = \mathbf{F}_{m,n}(\mathcal{B}_k) \tag{7.86}$$

It will be seen that away from the step core displacements are small and one can clearly see the decay of displacement norm as $\sqrt{m^2+n^2}$ increases.

7.2 Numerical Results

Unbalanced forces for Pb, Ti and O3 cores are shown in Fig. 7.3 for different values of m as functions of n. It is seen that for a given m, as n increases forces approach to constant values, which are equal to Pb-centered 180° domain wall unbalanced forces. Localized unbalanced forces for Pb and O3 cores and shells are given in Fig. 7.5. Convergence of displacements for the ranges of interaction $r = s = 1$ and $r = s = 2$ in terms of the number of Gauss points is shown in Fig. 7.6. It is seen that for $r = s = 2$ a larger number of Gauss points is necessary as the integrands are more oscillatory than those of $r = s = 1$. Fig. 7.7 compares the displacement norms for $r = s = 1$ and $r = s = 2$ and it is seen that the displacement norms are very close. The displacement decay in the multi-lattice under the localized forces is shown in Fig. 7.8 for Pb and Ti cores and shells. It is seen that for a fixed m (here $m = 0$) displacements in n direction are long-tailed. However, for a fixed n (here for $n = 0$) displacements in m direction are fairly localized. Harmonic displacements for Pb, Ti, O1,

O2 and O3 cores are given in Figs.7.9, 7.10, 7.11, 7.12, and 7.13. These displacements are given for different values of n as functions of m. It is seen that for large n the displacements approach those of a Pb-centered 180° domain wall. The anharmonic solutions are given in Figs. 7.14–7.18.

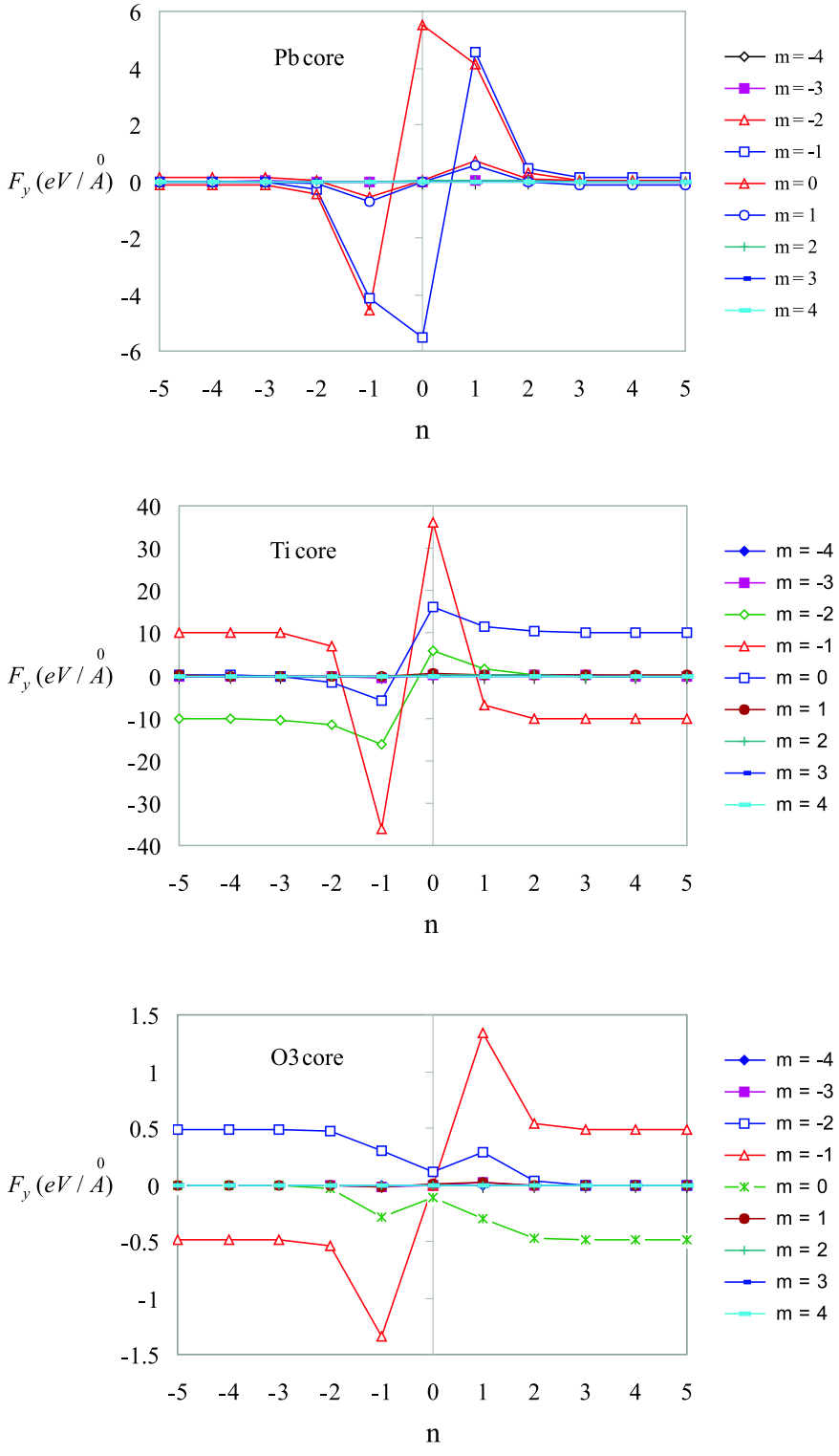

Figure 7.3: Force distribution in a Pb/O3/Pb-centered 180° step. (a) Pb cores, (b) Ti cores and (c) O3 cores.

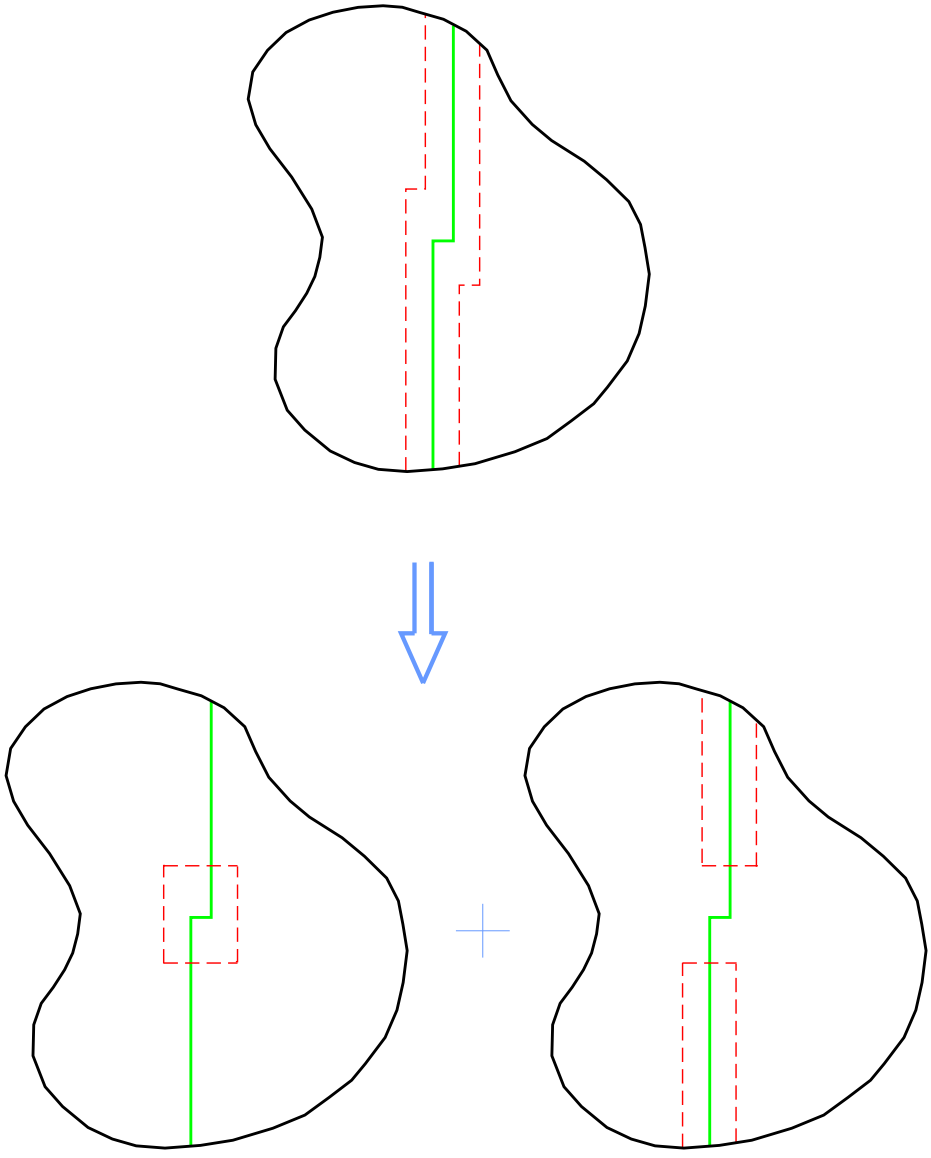

Figure 7.4: Localization of the unbalanced forces in a 180° step.

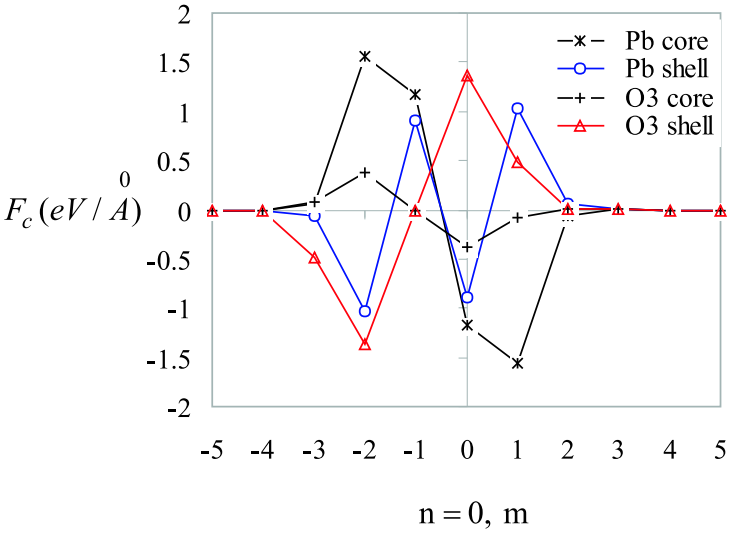

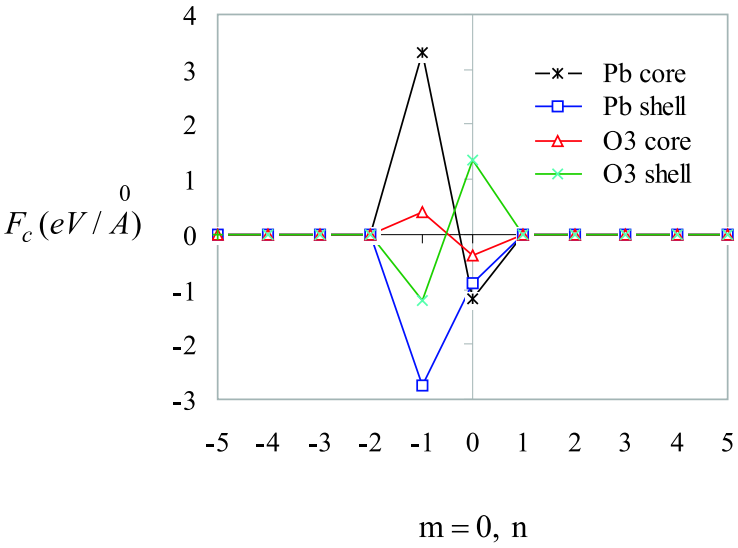

Figure 7.5: Unbalanced forces in the localized reference configuration.

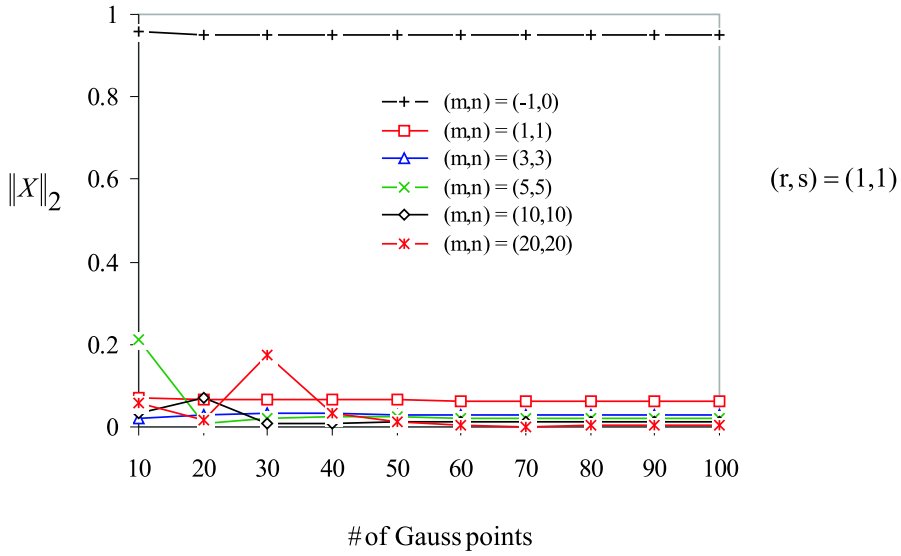

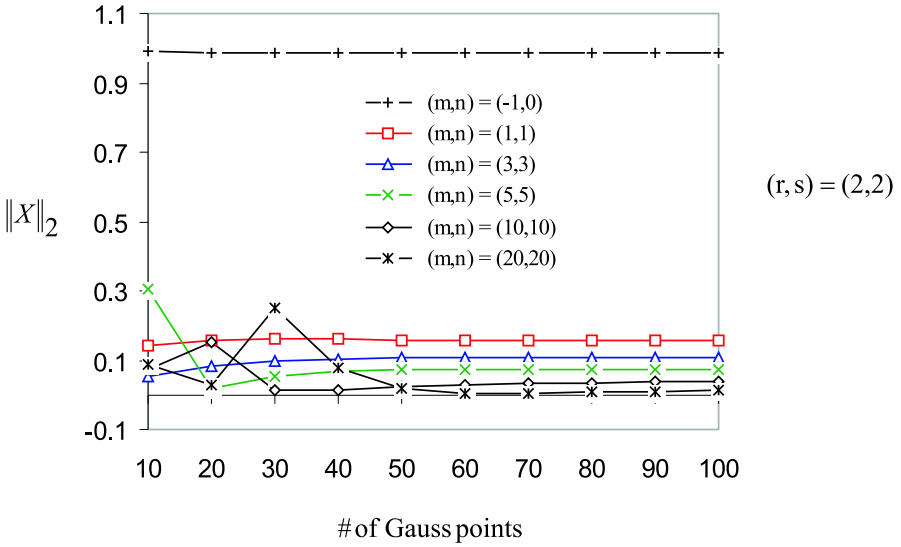

Figure 7.6: Convergence of displacements due to localized forces in terms of the number of Gaussian points.

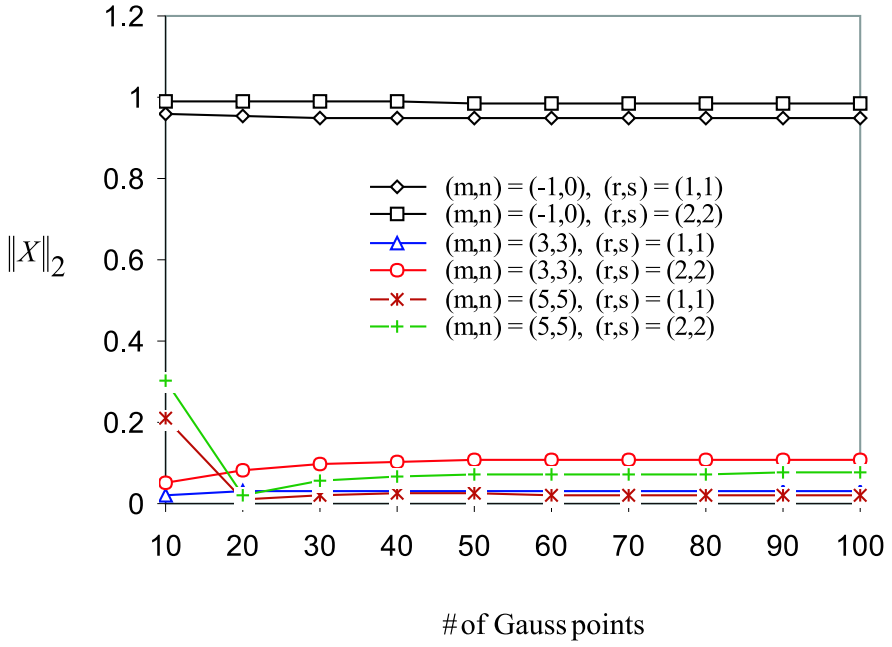

Figure 7.7: Range of interaction comparison for $(r, s) = (1, 1)$ and $(r, s) = (2, 2)$.

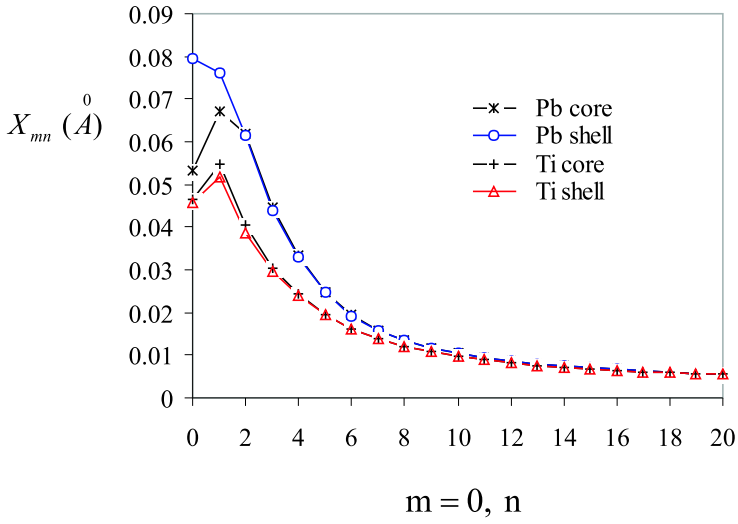

(a)

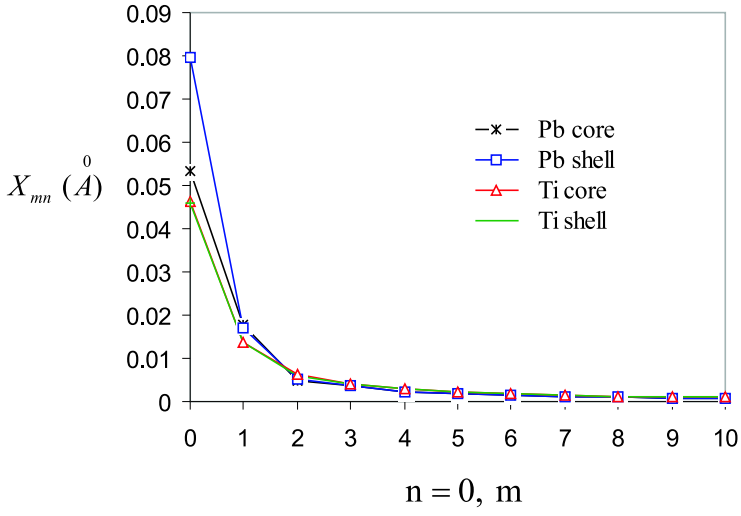

(b)

Figure 7.8: (a) Pb and Ti core and shell displacements for $m = 0$ as a function of n. (b) Pb and Ti core and shell displacements for $n = 0$ as a function of m.

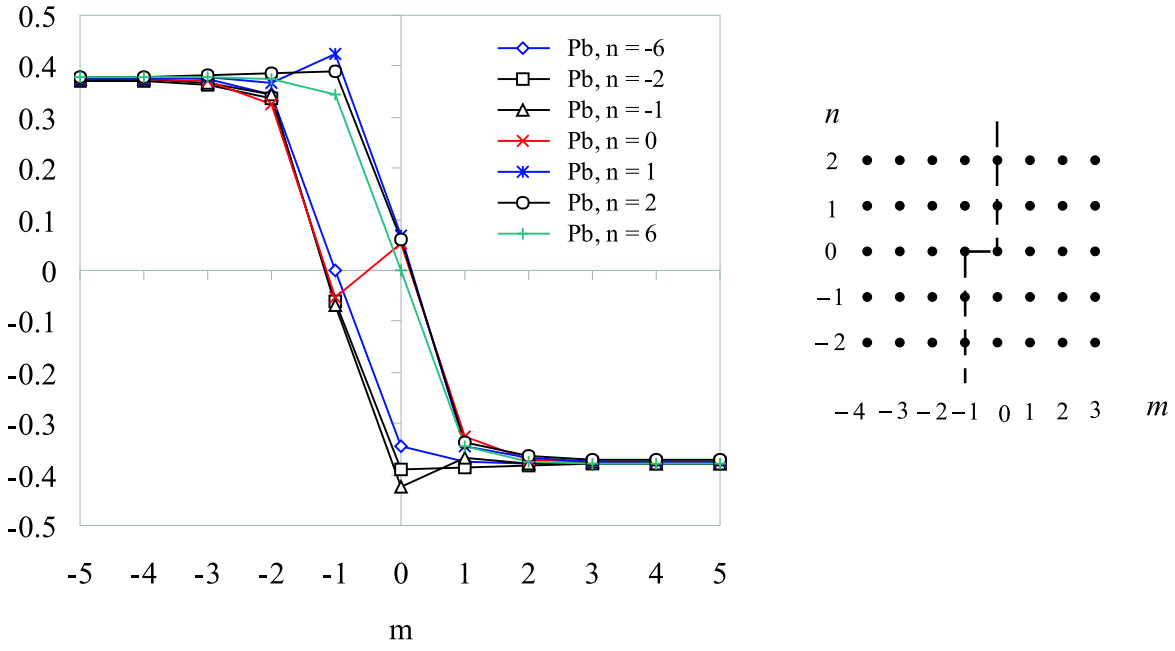

Figure 7.9: Pb core harmonic displacements of the step.

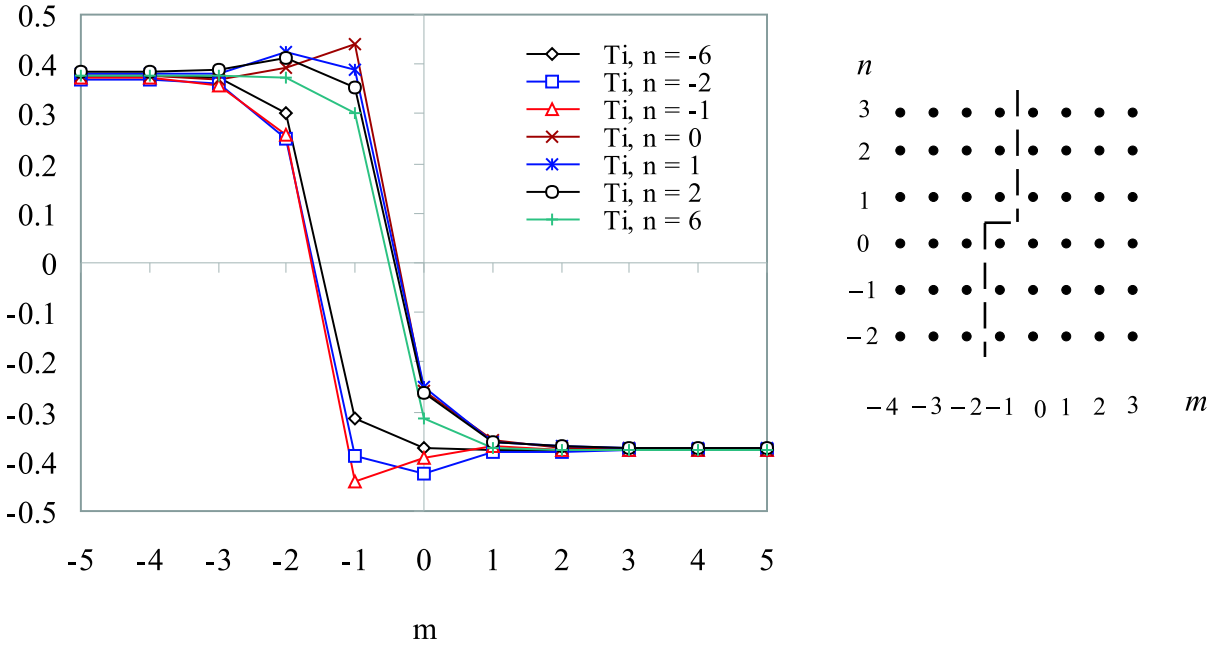

Figure 7.10: Ti core harmonic displacements of the step.

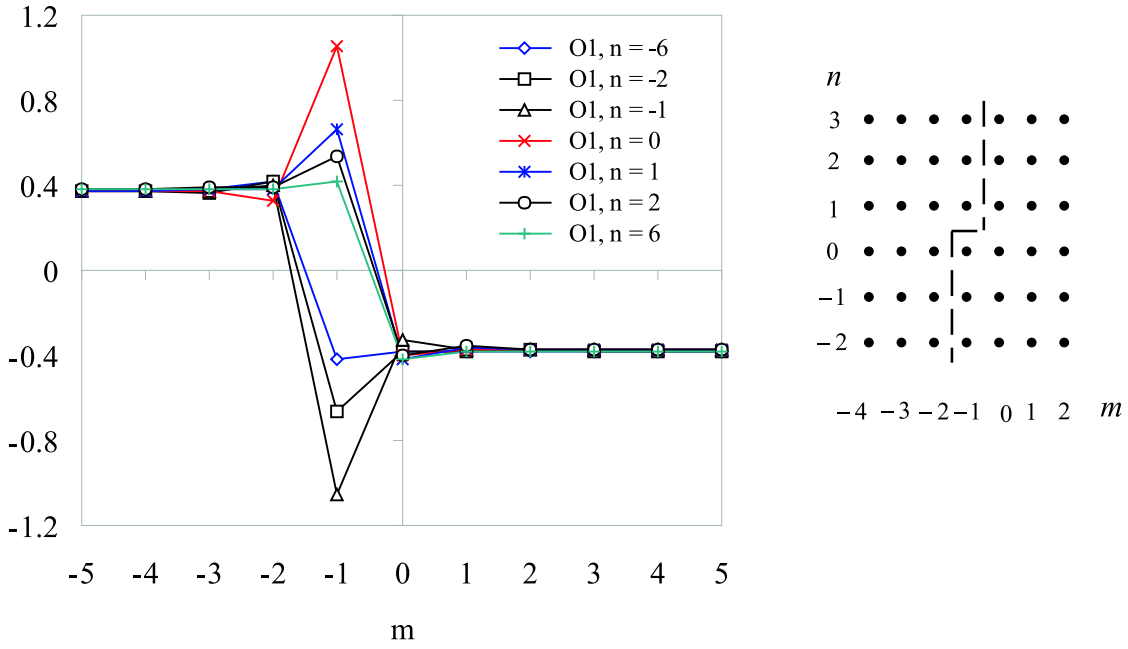

Figure 7.11: O1 core harmonic displacements of the step.

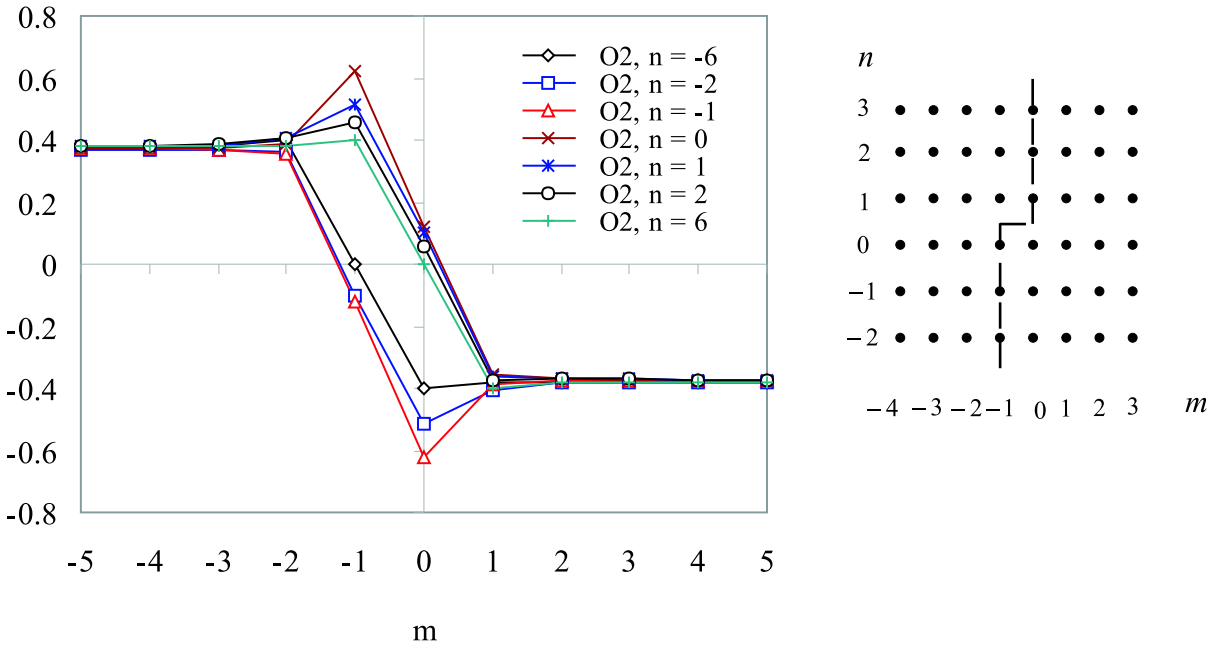

Figure 7.12: O2 core harmonic displacements of the step.

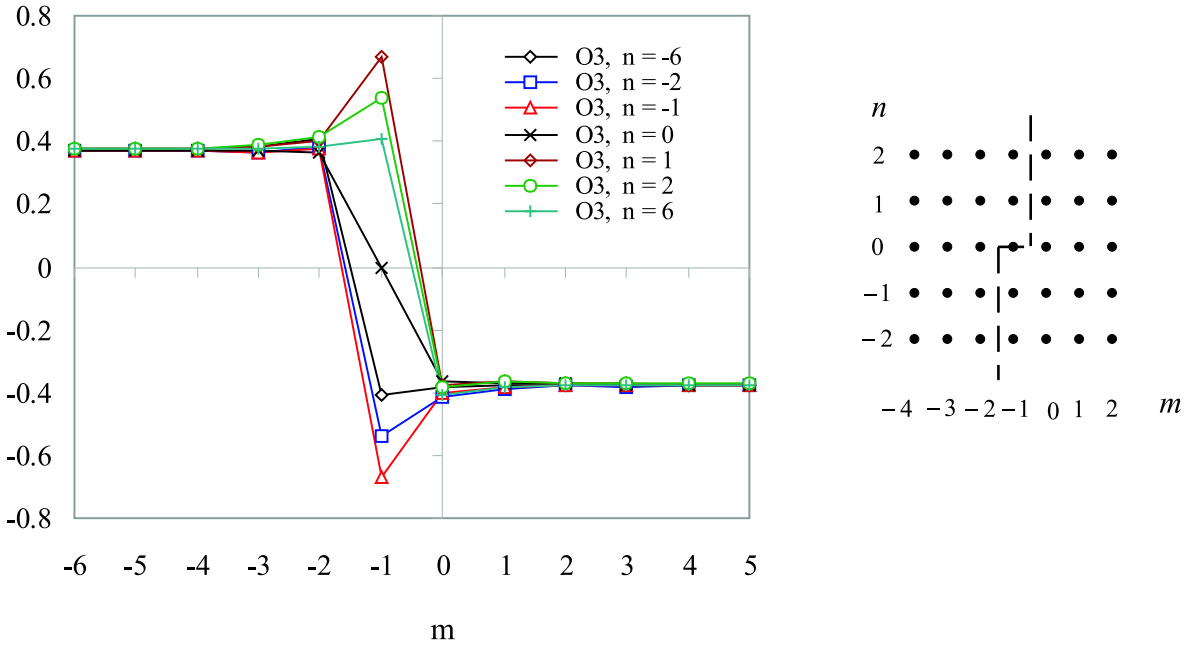

Figure 7.13: O3 core harmonic displacements of the step.

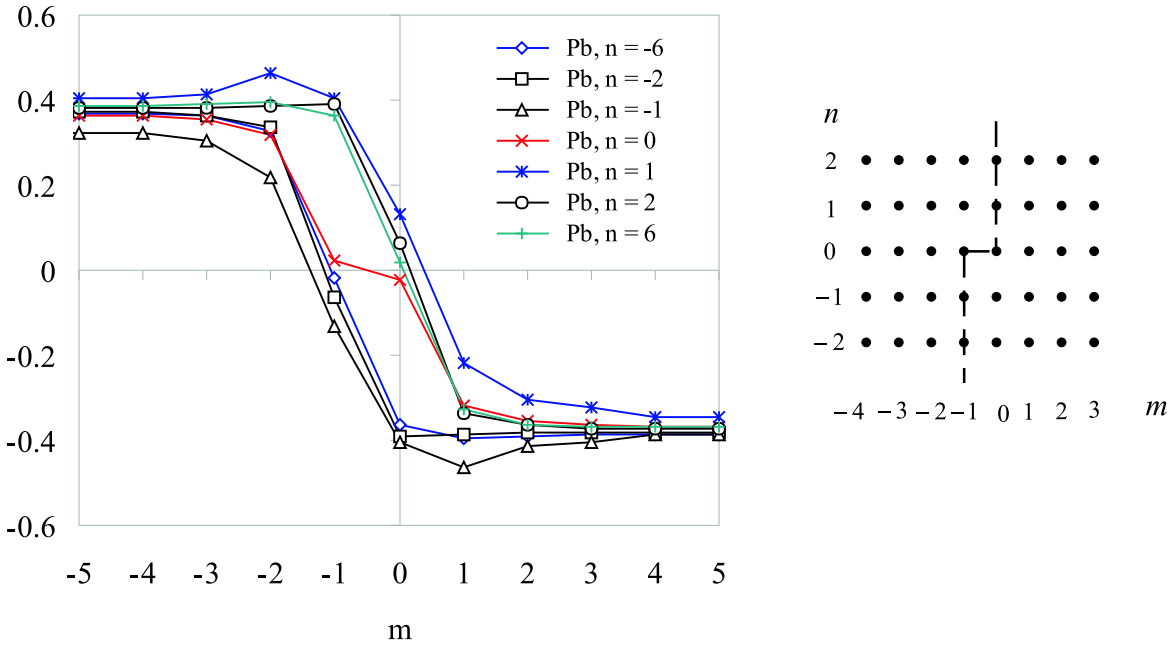

Figure 7.14: Pb core anharmonic displacements of the step.

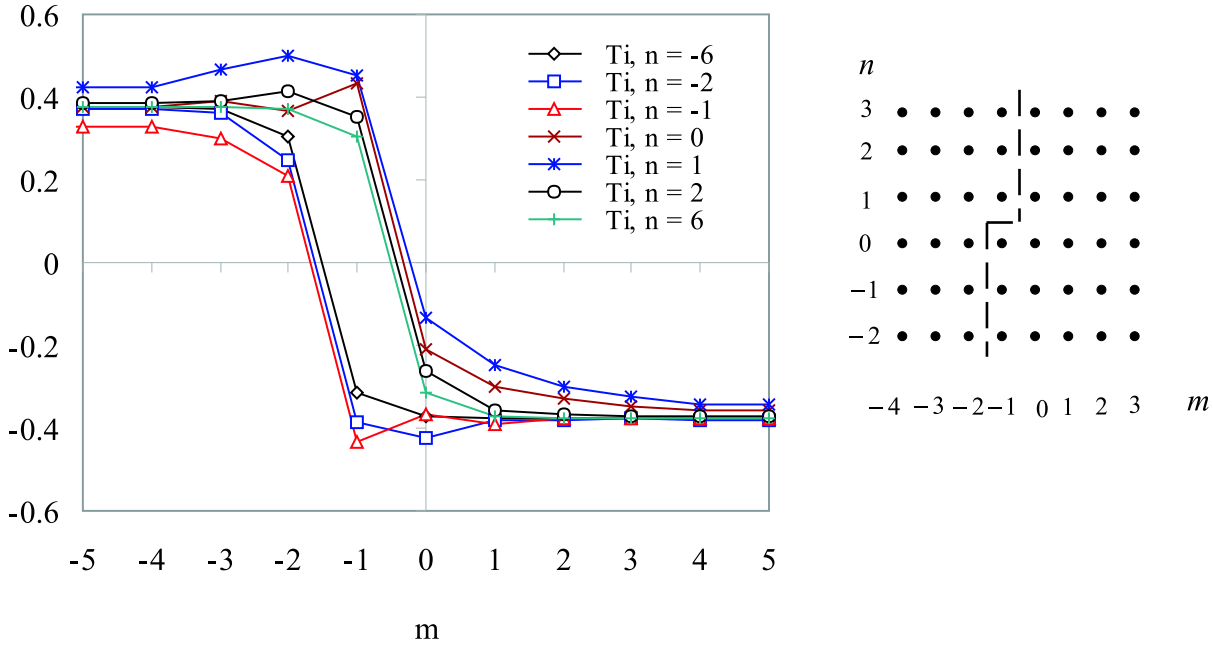

Figure 7.15: Ti core anharmonic displacements of the step.

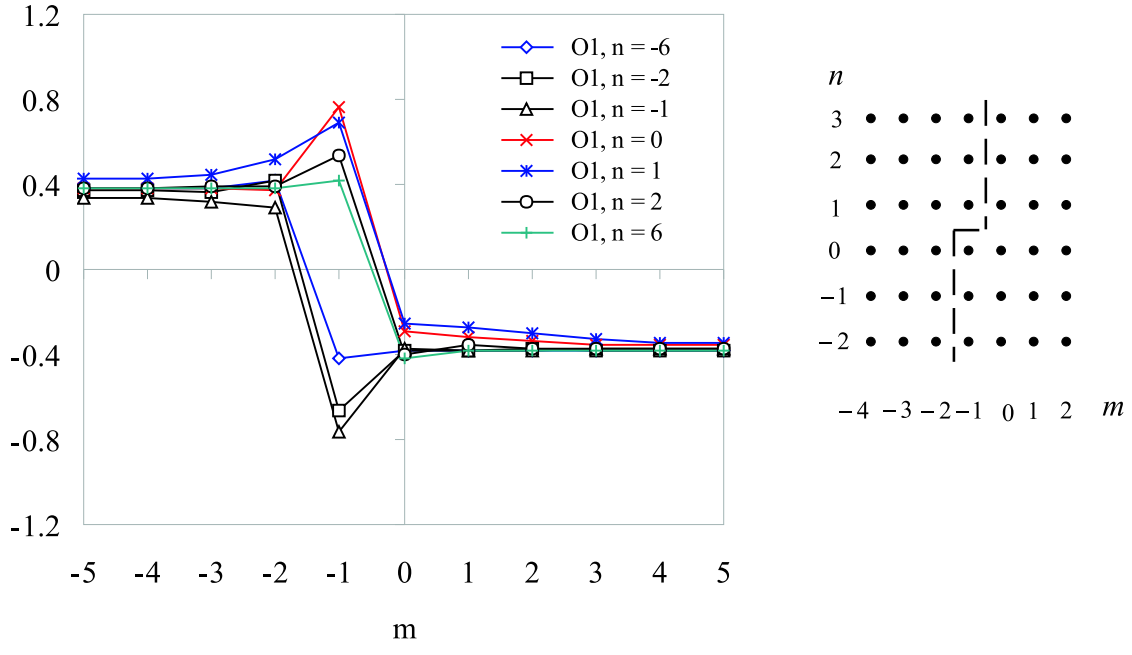

Figure 7.16: O1 core anharmonic displacements of the step.

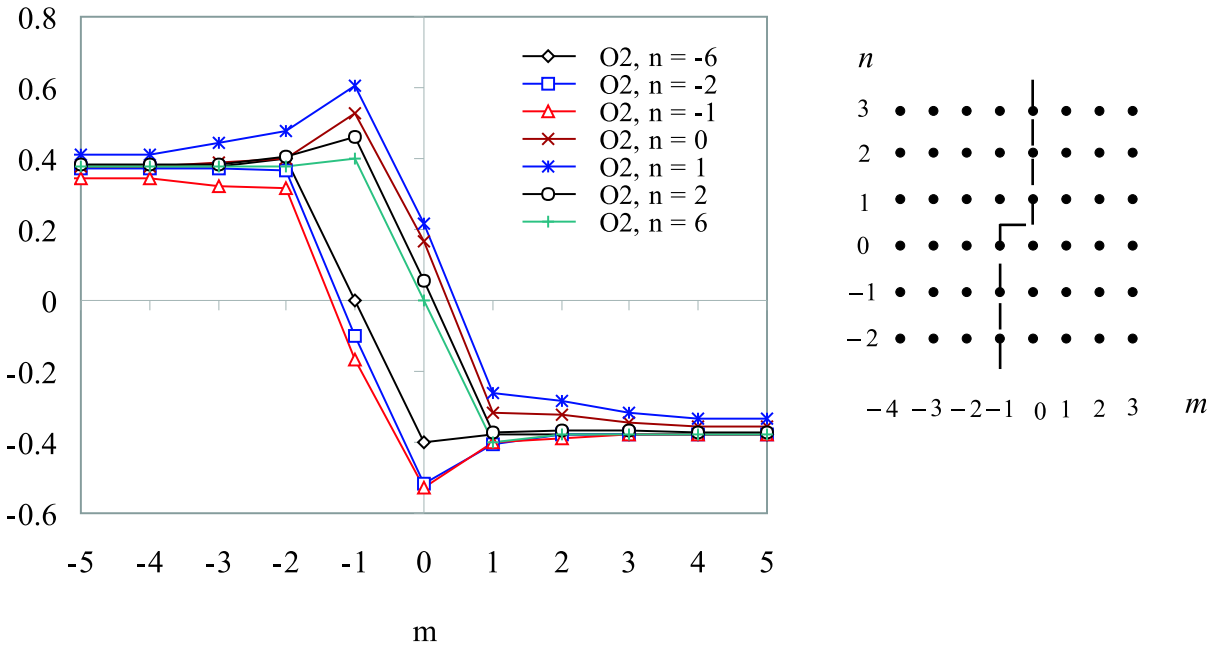

Figure 7.17: O2 core anharmonic displacements of the step.

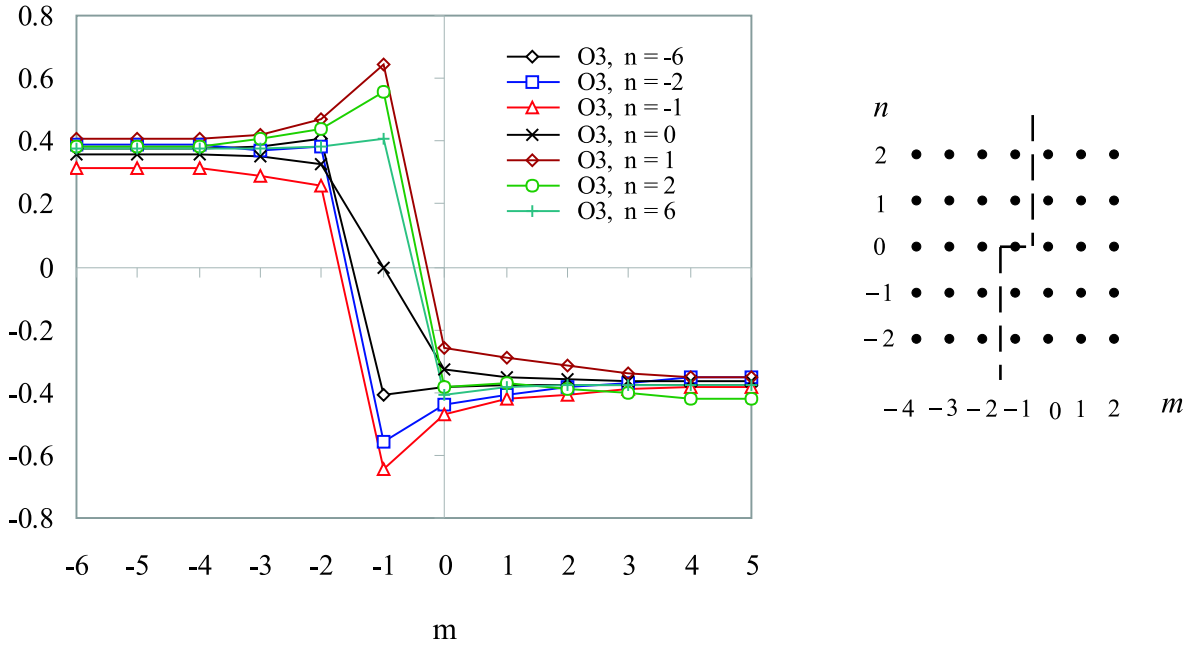

Figure 7.18: O3 core anharmonic displacements of the step.

Chapter 8

Conclusions

In this thesis we started by looking at interatomic potentials describing two technologically important ferroelectrics, namely $BaTiO_3$ and $PbTiO_3$. We optimized the tetragonal structure of these two materials using the corresponding shell potentials. It turns out that all these potentials predict a stable ground state (rhombohedral for $BaTiO_3$ and tetragonal for $PbTiO_3$) only under some symmetry constraints. Therefore, we had to perform all the numerical calculations in the stable submanifold. However, all the developments and implementations are general and can be repeated for any potential.

We developed a systematic method of lattice statics more general than the available classical lattice statics. We call this reformulation 'inhomogeneous lattice statics'. This differs from all the existing treatments in that it does not apply only to Bravais lattices and does not rely on the knowledge of force constants. Instead, it can be used for defective lattices and all is needed is an interatomic potential describing the interaction of atoms. The idea of our inhomogeneous lattice statics is to start from a reference configuration that is not necessarily in equilibrium and perhaps not translation invariant. This reference configuration is arbitrary and problem dependent. A desirable choice could be some nominal defect, i.e., a configuration that resembles the real defect but is not necessarily relaxed. The discrete (nonlinear) governing equations are linearized about the reference configuration. This leads to a nonhomogeneous system of linear difference equations with variable coefficient matrices. The forcing terms are a result of the fact that the reference configuration is not a local minimum of the energy, in general. We call these forces the unbalanced forces. Our formulation of lattice statics is more general than other formulations in the literature in the sense that we base the formulation on an interatomic potential and calculate the force constants using the potential and geometry of the problem. The idea of symmetry reduction for one and two-dimensional defects presented in this thesis is novel. Our formulation mimics continuum mechanics and in that sense is close to what continuum mechanicians are used to. This can be very useful for the solid mechanics community and can be a base of a rigorous theory of discrete mechanics for crystalline solids.

Three different types of defects in ferroelectrics are considered: (i) 180° and 90° domain walls, (ii) free surfaces and (iii) steps in 180° domain walls. For domain walls the reference configuration is decomposed into equivalence classes, which are infinite sets of atoms of the same type lying on a plane parallel to the domain wall. The governing equations are written in terms of interactions of these equivalence classes and this leads to substiffness matrices defined in terms of lattice sums. We carefully studied convergence of all these lattice sums. The resulting one-dimensional system of difference equations is directly solved using a novel method developed here. Our numerical studies show that shell potentials are extremely localized and this is consistent with the previous theoretical and experimental studies of ferroelectric domain walls that had suggested atomically sharp domain walls.

Our next step was to calculate the fully nonlinear solutions using modified Newton-Raphson iterations. We call this treatment of defects, 'inhomogeneous anharmonic lattice statics'. The idea is to keep the initial stiffness matrices and update forces by modifying the reference configuration. In other words, having the first harmonic solution, one modifies the reference configuration by superimposing the discrete harmonic displacement field. Then new forces are calculated and this scheme is repeated until convergence is accomplished. Convergence of this scheme requires a stable reference configuration. Our reference configurations for both Pb-centered and Ti-centered 180° domain walls seem to be stable as the iterations converged. However the anharmonic lattice statics for constrained 90° domain wall did not converge. For $BaTiO_3$, our three-dimensional harmonic solutions show that the displacements perpendicular to the domain wall are not zero. However, polarization vector has zero components perpendicular to the tetragonal c-direction. We were not able to verify this for the nonlinear solutions as the shell potential was not stable.

We studied stiffness matrices in the reference configurations of 180° and 90° domain walls and observed that substiffness matrices on the right and left sides of the domain walls are different. This makes the application of discrete Fourier transformation very difficult. We have also explained the differences and similarities of our inhomogeneous lattice statics with the method of discrete eigendistortions. It turns out that the harmonic solutions of a homogenized lattice, i.e., those obtained using the average stiffness matrices differ from those of the nonhomogeneous lattice by about forty percent. However, the final nonlinear solutions are exactly the same. This shows that using the homogenized lattice is a good approximation. We observe very sharp domain walls in the order of $2-3$ nm. This is in agreement with the ab initio calculations of domain walls in $PbTiO_3$ and also with the recent experimental observations.

We studied two types of free surfaces, one with polarization parallel to the free surface and one with polarization perpendicular to the free surface. For the former free surface we were able to relax the reference configuration in the constraint manifold. The latter free surface has very large unbalanced forces and the anharmonic lattice statics does not converge. This suggests that one

would expect to see some severe surface reconstruction for this configuration.

The other defect that we studied in this work was a 180° step in $PbTiO_3$. There are several types of steps and we considered a Pb/O3/Pb centered 180° step. The symmetry relation on two sides of the step is more complicated than that of a Pb-centered 180° domain wall. Here the equivalence classes are infinite sets of atoms (cores or shells) of the same type lying on a line parallel to the z-axis. This is somewhat a perturbation of a Pb-centered 180° domain wall. Away from the core of the step, forces are equal to forces in a Pb-centered 180° domain wall. The linearized discrete governing equations are a set of partial difference equations. A straightforward solution technique would be to apply DFT to the homogenized reference configuration. The problem with this method is that the integrands appearing in the inverse of DFT are extremely oscillatory and a large number of Gauss points is needed, say $200 - 400$ points in each direction. This makes the solution very inefficient and extremely slow. We used a novel method for solving the partial difference equations. We applied DFT in the direction parallel to the half planes of the step and obtained a system of ordinary difference equations for the partial DFT's. This system can be solved analytically on the whole $\mathbb{Z}$ (similar to the 90° domain wall problem). Then one needs to apply inverse DFT in one direction. This semidirect method of solving partial difference equations accelerates the calculations tremendously. The more practical method is to use the anharmonic 180° displacement field away from the step core and localized the unbalanced forces. We explained in detail how one should do the force localization consistently. We observed that the deviation from the domain wall displacements is long-tailed along the half domain walls and is localized perpendicular to the half domain walls.

The lattice statics model presented here can be used as an analytical tool to compare different interatomic potentials. Unfortunately, at this time we cannot use it for $BaTiO_3$ or $PbTiO_3$ as we are not aware of second interatomic potentials. However, we believe that lattice statics can be a good analytic tool to compare interatomic potentials in terms of different mechanical quantities they predict. This would be of particular interest for mechanical design of small devices. Our lattice statics model can also be an analytical verification tool for numerical techniques like quasi-continuum method. They idea would be to run a quasi-continuum code for some simple geometries and compare the results with those from lattice statics.

8.1 Contributions of The Thesis

Contributions of this thesis can be summarized as follows.

- We have reformulated lattice statics in a form similar to continuum mechanics. This formulation is a generalization of the classical lattice statics, which is only applicable to perfect crystals. Our inhomogeneous lattice statics formulation is a step forward in developing a theory

of discrete elasticity. For example, we studied the restriction that material-frame-indifference puts on the form of an interatomic potential. We have also looked at a discrete balance of energy. We studied the consequences of invariance of balance of energy under isometries of $\mathbb{R}^3$. This is the discrete version of Green-Rivilin-Naghdi theorem. We believe the techniques presented in this thesis can be used in studying other defective crystals as well.

- To our best knowledge this is the first lattice statics modelling of Perovskites using shell potentials.
- We have numerically studied Wolf's method for shell potentials and have discovered that this method should be used very carefully. Wolf et al.'s conclusions for NaCl do not seem to be generic. We have observed that, for example, unit cell energy convergence for $PbTiO_3$ is not oscillatory.
- We introduced the idea of 1-D and 2-D symmetry reduction for defective crystals. Symmetry reduction is an old idea in mechanics but to our best knowledge this is the first time it is being used in the lattice statics calculations.
- We have analyzed defects in an infinite lattice without the periodicity assumption. Starting from a reference configuration, we relax the infinite lattice and the localization of atomic distortions would come as part of the solution. This is more general than the usual techniques in the literature in which a finite number of unit cells are relaxed and the rest are assumed to be rigid. The advantage and superiority of our formulation over the existing treatments is in the fact that we have treated the problem of a defective crystal as a discrete boundary-value problem.
- To our best knowledge this is the first lattice statics analysis of ferroelectric defects. For defective ferroelectric crystals with 1-D symmetry reduction, e.g., domain walls and free surfaces, we were able to solve the governing vector-valued ordinary difference equations directly on $\mathbb{Z}$. Our solution method is simple but yet original.
- During the course of this research we discovered that all the shell potentials that we worked with have stability issues. All these potentials predict a stable ground state only under some constraints. This issue of stability forced us to perform all the numerical calculations under the relevant constraints.

8.2 Future Directions

We can summarize the future directions as follows.

- Our inhomogeneous lattice statics can be applied to other systems and one direction would be to analyze defective crystals of materials with better understood interatomic potentials. Applying this technique to dislocations and cracks would be of interest. This can be a motivation for developing techniques for solving vector-valued Wiener-Hopf difference equations.

- Understanding surface effects and their relation to conditional convergence of lattice sums that define some physical quantities is of interest. Our experience with this literature indicates that still there are open problems that should be solved for a better understanding of the behavior of ferroelectric devices.

- We believe the solid mechanics community can use the experience with continuum mechanics and contribute to small-scale mechanics by rationalizing the existing theories and techniques and developing a structured theory of discrete mechanics.

- Including inertial and finite temperature effects would be of great interest.

- Our lattice calculation were done for a physical system. Most of the existing theoretical lattice-scale studies are for highly idealized systems. One open problem is derivation of a continuum kinetic equation using atomistic information.

Appendix A

Summing Conditionally Convergent Lattice Sums

In this appendix we review Ewald's (Ewald, 1921) technique and explain the mathematics behind it. This is important as we have Coulombic interactions and our system is not periodic.

Definition 8. *Fourier transform of $f \in L^2(\mathbb{R}^n)$ is defined as*

$$\hat{f}(\mathbf{k}) = \int_{\mathbb{R}^n} f(\mathbf{x})\ e^{-2\pi i \mathbf{k}\cdot\mathbf{x}} d\mathbf{x} \tag{A.1}$$

and,

$$\sum_{\mathbf{k}\in\mathbb{Z}^n} \hat{f}(\mathbf{k})\ e^{2\pi i \mathbf{k}\cdot\mathbf{x}} \tag{A.2}$$

is called the Fourier series of f.

Theorem 9. ***(The Poisson's Summation Formula)*** *If $f \in C(\mathbb{R}^n)$, $|f(\mathbf{x})| \leq C(1+|\mathbf{x}|)^{-n-\varepsilon}$, $|\hat{f}(\mathbf{k})| \leq C(1+|\mathbf{k}|)^{-n-\varepsilon}$ for some C and $\varepsilon > 0$, then,*

$$\sum_{\mathbf{n}\in\mathbb{Z}^n} f(\mathbf{x}+\mathbf{n}) = \sum_{\mathbf{k}\in\mathbb{Z}^n} \hat{f}(\mathbf{k})\ e^{2\pi i \mathbf{k}\cdot\mathbf{x}} \tag{A.3}$$

In particular, for $\mathbf{x} = \mathbf{0}$,

$$\sum_{\mathbf{n}\in\mathbb{Z}^n} f(\mathbf{n}) = \sum_{\mathbf{k}\in\mathbb{Z}^n} \hat{f}(\mathbf{k}) \tag{A.4}$$

Lemma 10. ***(Riemann-Lebesgue Lemma)*** *For $f \in L^1(\mathbb{R})$,*

$$\lim_{|\mathbf{k}|\to 0} \hat{f}(\mathbf{k}) = 0$$

Theorem 11. *If f is n-times differentiable and $f^{(k-1)}$ is absolutely continuous then,*

$$\hat{f}(\mathbf{k}) = o(|\mathbf{k}|^{-n}) \quad \text{as } |\mathbf{k}| \to \infty \tag{A.5}$$

For more details the reader can refer to Katznelson (2003). We now review some definitions and results on convergence of a series in $\mathbb{R}$.

Definition 12. *A convergent series $\sum a_n$ is called absolutely convergent if the series $\sum |a_n|$ is also convergent.*

Definition 13. *A convergent but not absolutely convergent series is called a conditionally convergent series.*

Definition 14. *If $\sum a_n$ is absolutely convergent then $\sum a_n = \sum a_{\sigma(n)}$, where $\sigma(n)$ is any rearrangement (permutation) of natural numbers.*

Theorem 15. *If $\sum a_n$ is conditionally convergent, then there are rearrangements $\sum a_{\sigma(n)}$ of it that diverge.*

Theorem 16. ***(Riemann's Theorem)*** *Consider a conditionally convergent series $\sum a_n$. Given any real number x, there is a rearrangement $\sigma(n)$ of natural numbers such that $\sum a_{\sigma(n)} = x$.*

In dimension d, potentials that decay to zero slower than $o(r^{-d})$ are called long-range potentials. Coulombic potential is an example. For the sake of simplicity, we first consider a simple series,

$$l = \sum_{n=1}^{\infty} f(n) \tag{A.6}$$

We assume that this series converges slowly and conditionally to the limit l. This means that we have to be specific about the order of summation. This is not a problem in 1-D and the above representation tells us all we need to calculate the series. However, for lattice sums in dimensions two and three we have to be careful and specify a way of adding up the terms if the sum is conditionally convergent. For the above simple series we make the following assumptions on the function f,

(i) $\lim_{x\to\infty} f(x) = 0$ slowly

(ii) $\lim_{x\to 0} f(x) = \infty$

Now consider an auxiliary function $\xi(x)$ with the following properties:

(i) $\lim_{x\to\infty} \xi(x) = 0$ rapidly

(ii) $\lim_{x\to 0} \xi(x) < \infty$

(iii) $f(x)[1 - \xi(x)]$ is smooth at $x = 0$.

Eq. (A.6) may be written as

$$l = \sum_{n=1}^{\infty} f(n)\xi(n) + \sum_{n=1}^{\infty} f(n)[1 - \xi(n)] \tag{A.7}$$

The first term converges rapidly. The second term is a slowly varying (smooth) function of x. Therefore, its Fourier transform converges rapidly in the reciprocal (Fourier) space. Hence, using Poisson's summation formula, (A.7) can be rewritten as

$$l = \sum_{n=1}^{\infty} f(n)\xi(n) + \sum_{k=1}^{\infty}[f(1-\xi)]\hat{}(k) \tag{A.8}$$

This idea is schematically shown in Fig. A.1. In our lattice statics model, we have to calculate

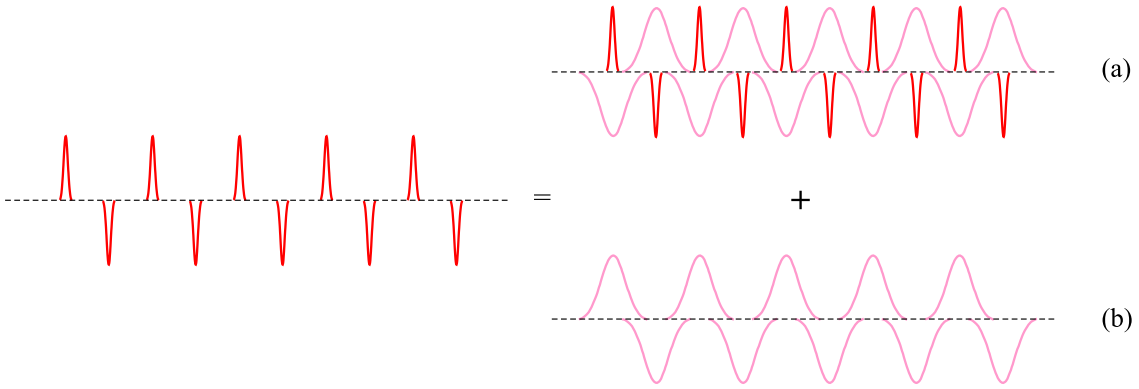

Figure A.1: An interpretation of Ewald summation using screening charges. (a) Summation in the direct space, (b) Summation in the Fourier space.

stiffness matrices that are defined in terms of lattice sums of square matrices. Thus, understanding convergence properties of lattice sums in $\mathbb{R}^n$ is crucial. Let us consider a series $\sum x_n$ in a Banach space $(X, \|.\|)$.

Definition 17. *A series $\sum x_n$ is absolutely convergent if $\sum \|x_n\| < \infty$.*

Theorem 18. *An absolutely convergent series in a Banach space is convergent.*

Definition 19. *A series $\sum x_n$ is unconditionally convergent if it converges for any rearrangements of its terms.*

In general, absolute convergence implies unconditional convergence but the converse in not true. If $X = \mathbb{R}$, the absolute and unconditional convergence are equivalent.

Definition 20. *A series is conditionally convergent if it converges but not unconditionally.*

Theorem 21. *If $\sum x_n$ converges unconditionally in a Banach space X, then all its rearrangements converge to the same sum.*

Definition 22. *A series $\sum x_n$ converges perfectly if the series $\sum \alpha_n x_n$ converges for any choice of $\alpha_n \in \{-1, 1\}$.*

Theorem 23. *In a Banach space a series converges perfectly if and only if it converges unconditionally.*

Theorem 24. *In a finite-dimensional normed space every unconditionally convergent series is absolutely convergent.*

Definition 25. *Suppose $\sum x_n$ is a series in the Banach space X. The domain of sums of this series is defined as*

$$\mathcal{DS}\big(\sum_{n=1}^{\infty} x_n\big) = \Big\{x \in X : \sum_{n=1}^{\infty} x_{\pi(n)} = x \text{ for some } \pi : \mathbb{N} \to \mathbb{N}\Big\} \tag{A.9}$$

It is known (as a consequence of Steinitz's theorem (Kadets and Kadets, 1985)) that in a finite dimensional Banach space, domain of sums of any conditionally convergent series is at least one-dimensional. This means that any conditionally convergent series in $\mathbb{R}^n$ can converge to infinitely many points in $\mathbb{R}^n$ depending on the summation scheme.

Here we briefly review the mathematical foundation of Ewald and related methods. Ewald summation is heavily based on transformation properties of theta functions. For details on theta functions see Bellman (1961). Consider the following improper integral,

$$h(y,t) = \int_{-\infty}^{\infty} e^{-tx^2+2xy} dx \qquad t, y \in \mathbb{C} \tag{A.10}$$

This is an entire function of y and an analytic function of t for $Re(t) > 0$ (this can be easily proved using Morera's theorem). If y and t lie on the real axis,

$$h(y,t) = \frac{e^{\frac{y^2}{t}}}{\sqrt{t}} \int_{-\infty}^{\infty} e^{\left(x-\frac{y}{\sqrt{t}}\right)^2} dx = \frac{e^{\frac{y^2}{t}}}{\sqrt{t}} \int_{-\infty}^{\infty} e^{-x^2} dx = \sqrt{\frac{\pi}{t}} e^{\frac{y^2}{t}} \tag{A.11}$$

Uniqueness theorem for analytic functions implies that the above representation is valid for all y and t such that $Re(t) > 0$. Now consider the function $f(x) = e^{-tx^2}, Re(t) > 0$. The Poisson's summation formula can be applied for this function. Thus

$$\sum_{n=-\infty}^{\infty} e^{-t(x+n)^2} = \sum_{n=-\infty}^{\infty} e^{2\pi i k x} \int_{-\infty}^{\infty} e^{-tx_1^2 - 2\pi i k x_1} dx_1 = \sqrt{\frac{\pi}{t}} \sum_{k=-\infty}^{\infty} e^{2\pi i k x - \frac{\pi^2 k^2}{t}} \tag{A.12}$$

where in arriving at the second line use was made of Eq. (A.11). When $x = 0$,

$$\sum_{n=-\infty}^{\infty} e^{-tn^2} = \sqrt{\frac{\pi}{t}} \sum_{k=-\infty}^{\infty} e^{-\frac{\pi^2 k^2}{t}} \tag{A.13}$$

Similarly, it can be shown that

$$\sum_{\mathbf{n}\in\mathbb{Z}^3} e^{-t|\mathbf{x}+\mathbf{n}|^2} = \left(\frac{\pi}{t}\right)^{\frac{3}{2}} \sum_{\mathbf{k}\in\mathbb{Z}^3} e^{-\frac{\pi^2|\mathbf{k}|^2}{t}+2\pi i\mathbf{k}\cdot\mathbf{r}} \tag{A.14}$$

Consider an atomic potential ϕ with the following property,

$$|\phi(\mathbf{r})| \leq C|\mathbf{r}|^{-3-\epsilon} \qquad C, \epsilon > 0 \tag{A.15}$$

Consider the following lattice sum that represents the energy per atom in a crystal,

$$\mathcal{E}_i = \frac{1}{2} \sum_{\mathbf{x}_j\in\mathcal{L}} \phi(\mathbf{r}_{ij})$$

where $\mathbf{r}_{ij} = \mathbf{x}_j - \mathbf{x}_i$. Note that

$$\Big|\sum \phi(\mathbf{r})\Big| \leq \sum\ |\phi(\mathbf{r})| \leq C \sum\ |\mathbf{r}|^{-3-\epsilon} \tag{A.16}$$

Convergence of the last series can be shown using Cauchy's integral test that says the series and the following integral have the same convergence properties, i.e., they both converge or both diverge.

$$\int_{\mathbb{R}^3} |\mathbf{r}|^{-3-\epsilon} dV \sim \int_a^\infty r^{1-\epsilon} dr < \infty \tag{A.17}$$

Thus the lattice sum converges absolutely and hence can be summed in an arbitrary order.

Definition 26. ***(Transformation of a lattice sum into a simple sum)*** *Consider the following lattice sum,*

$$\sum_{\mathbf{k}\in\mathbb{Z}^3} a_{\mathbf{k}} \tag{A.18}$$

Note that the above sum is meaningless, in general, unless the order of summation is specified. Now consider a sequence $\{\Omega_n\} \subset \mathbb{R}^3$ such that

$$\Omega_n \subset \Omega_{n+1}, \quad \bigcup_{n=1}^{\infty} \Omega_n = \mathbb{R}^3 \tag{A.19}$$

This sequence induces a transformation $\mathcal{F}$ that transforms the lattice sum (A.18) into a simple series as shown below,

$$\mathcal{F} : \sum_{\mathbf{k}\in\mathbb{Z}^3} a_{\mathbf{k}} \mapsto \sum_{n=1}^{\infty} b_n$$

where

$$b_n := \sum_{a_{\mathbf{k}} \in \Omega_{n+1} \setminus \Omega_n} a_{\mathbf{k}}$$

Note that, in general, depending on the sequence chosen different values will be obtained for the lattice sum (A.18). For a conditionally convergent lattice sum that represents a well-defined physical quantity, the sequence(s) corresponding to the right value of the quantity somehow shows the structure of the system.

A.1 Ewald Summation Technique

We now explain how one should calculate the electrostatic energy per unit cell in a periodic system using the celebrated Ewald method (Ewald, 1921). Consider a tetragonal lattice $\mathcal{L}$ with lattice spacings a and c. Suppose there are N charges in each unit cell. In our model N=10. It is assumed that each cell is charge neutral, i.e.,

$$\sum_{i=1}^{N} Q_i = 0 \tag{A.20}$$

Within the unit cell centered at lattice site $\mathbf{n}$, charge Q_i has position vector $\mathbf{r}_i$. The total electrostatic energy of the cell centered at $\mathbf{n} = \mathbf{0}$ is

$$\mathcal{E}_{\text{cell}} = \frac{1}{2} {\sum_{\mathbf{n}\in\mathcal{L}}}' \Big(\sum_{i,j=1}^{N} \frac{Q_i Q_j}{|\mathbf{r}_{ij} + \mathbf{n}|} \Big) \tag{A.21}$$

where $\mathbf{r}_{ij} = \mathbf{r}_i - \mathbf{r}_j$. The prime on the first sum indicates that when $\mathbf{n} = \mathbf{0}$ the terms $i = j$ are omitted, i.e., self-energy is not included. It should be noted that the cell energy is defined in terms of a conditionally convergent lattice sum. We follow de Leeuw et al. (1980) and use a convergence factor to extract the electrostatic energy from the lattice sum. Define,

$$E(s) = \frac{1}{2} {\sum_{\mathbf{n}\in\mathcal{L}}}' e^{-s|\mathbf{n}|^2} \left(\sum_{i,j=1}^{N} \frac{Q_i Q_j}{|\mathbf{r}_{ij} + \mathbf{n}|} \right) \tag{A.22}$$

The convergence factor makes the lattice sum uniformly convergent in s and also Fobini's theorem can be used in interchanging the double sums. Now we can write,

$$E(s) = \frac{1}{2} \sum_{i,j=1}^{N} Q_i Q_j {\sum_{\mathbf{n}\in\mathcal{L}}}' \frac{e^{-s|\mathbf{n}|^2}}{|\mathbf{r}_{ij} + \mathbf{n}|} = \frac{1}{2} \sum_{i,j=1}^{N} Q_i Q_j \Big(\Psi(\mathbf{r}_{ij}, s) - \sum_{\substack{\mathbf{n}\in\mathcal{L} \\ \mathbf{n}\neq\mathbf{0}}} \frac{e^{-s|\mathbf{n}|^2}}{|\mathbf{n}|} \Big) \tag{A.23}$$

where

$$\Psi(\mathbf{r},s)=\sum_{\mathbf{n}\in\mathcal{L}}\frac{e^{-s|\mathbf{n}|^2}}{|\mathbf{r}+\mathbf{n}|}=\sum_{\mathbf{n}\in\mathcal{L}}\frac{e^{-s|\mathbf{n}|^2}\mathrm{erfc}(\alpha|\mathbf{r}+\mathbf{n}|)}{|\mathbf{r}+\mathbf{n}|}+\frac{1}{\sqrt{\pi}}\sum_{\mathbf{n}\in\mathcal{L}}\int_0^{\alpha^2}t^{-\frac{1}{2}}e^{-s|\mathbf{n}|^2-t|\mathbf{r}+\mathbf{n}|^2}dt \tag{A.24}$$

The first lattice sum converges very rapidly in the direct space. We now need to understand the structure of the singularity of the second lattice sum, which we call I, for $s\to 0$. This lattice sum can be rewritten as

$$I=\sum_{\substack{\mathbf{n}\in\mathcal{L}\\ \mathbf{n}\neq\mathbf{0}}}\pi\int_0^{\alpha^2}\frac{1}{\sqrt{t(s+t)^3}}e^{-\frac{st|\mathbf{r}|^2}{s+t}+\frac{2\pi\mathbf{n}\cdot t\mathbf{r}}{s+t}-\frac{\pi^2|\mathbf{n}|^2}{s+t}}dt+\pi\int_0^{\alpha^2}\frac{1}{\sqrt{t(s+t)^3}}e^{-\frac{st|\mathbf{r}|^2}{s+t}}dt=I_1+I_2 \tag{A.25}$$

It can be shown that

$$I_1=\sum_{\substack{\mathbf{n}\in\mathcal{L}\\ \mathbf{n}\neq\mathbf{0}}}\pi\int_0^{\alpha^2}\frac{1}{\sqrt{t(s+t)^3}}e^{\frac{t}{s(s+t)}|\pi\mathbf{n}+is\mathbf{r}|^2}e^{\frac{-\pi^2|\mathbf{n}|^2}{s}}dt \tag{A.26}$$

Using Poisson's summation formula, it can be shown that for small s, I_1 simplifies to,*

$$I_1=\sum_{\substack{\mathbf{n}\in\mathcal{L}\\ \mathbf{n}\neq\mathbf{0}}}\frac{1}{\pi|\mathbf{n}|^2}e^{-\frac{\pi^2|\mathbf{n}|^2}{\alpha^2}+2\pi i\mathbf{n}\cdot\mathbf{r}}[1+O(s)] \tag{A.27}$$

Asymptotic analysis of I_2 for small s yields

$$I_2=\frac{2\pi}{s}\big(1+\frac{s}{\alpha^2}\big)^{-\frac{1}{2}}-\frac{2\pi}{3}|\mathbf{r}|^2+O(s) \tag{A.28}$$

This means that for small s, $\Psi(\mathbf{r},s)$ can be written as

$$\Psi(\mathbf{r},s)=\sum_{\mathbf{n}\in\mathcal{L}}\frac{e^{-s|\mathbf{n}|^2}\mathrm{erfc}(\alpha|\mathbf{r}+\mathbf{n}|)}{|\mathbf{r}+\mathbf{n}|}+\sum_{\substack{\mathbf{n}\in\mathcal{L}\\ \mathbf{n}\neq\mathbf{0}}}\frac{1}{\pi|\mathbf{n}|^2}e^{-\frac{\pi^2|\mathbf{n}|^2}{\alpha^2}+2\pi i\mathbf{n}\cdot\mathbf{r}}[1+O(s)]+\frac{2\pi}{s}\big(1+\frac{s}{\alpha^2}\big)^{-\frac{1}{2}}-\frac{2\pi}{3}|\mathbf{r}|^2+O(s) \tag{A.29}$$

Similarly, it can be shown that

$$\sum_{\substack{\mathbf{n}\in\mathcal{L}\\ \mathbf{n}\neq\mathbf{0}}}\frac{e^{-s|\mathbf{n}|^2}}{|\mathbf{n}|}=\sum_{\substack{\mathbf{n}\in\mathcal{L}\\ \mathbf{n}\neq\mathbf{0}}}\left(\frac{\mathrm{erfc}(\alpha|\mathbf{n}|)}{|\mathbf{n}|}+\frac{e^{-\frac{\pi^2|\mathbf{n}|^2}{\alpha^2}}}{\pi|\mathbf{n}|^2}\right)-\frac{2\alpha}{\sqrt{\pi}}+\frac{2\pi}{s}\big(1+\frac{s}{\alpha^2}\big)^{-\frac{1}{2}}+O(s) \tag{A.30}$$

*Note that we are considering a cubic lattice with lattice parameter $a=1$. For this special lattice the lattice and reciprocal lattice coincide.

Note that this was derived for a cubic lattice of unit lattice parameter. For our tetragonal lattice with lattice vectors Eq. (2.42) we have

$$\mathbf{n} = n_1\mathbf{e}_1 + n_2\mathbf{e}_2 + n_3\mathbf{e}_3 = (an_1, cn_2, an_3) \tag{A.31}$$

It can be easily shown that for this lattice Eq. (A.14) has the following form,

$$\sum_{\mathbf{n}\in\mathcal{L}} e^{-t|\mathbf{r}+\mathbf{n}|^2} = \frac{1}{a^2c}\left(\frac{\pi}{t}\right)^{\frac{3}{2}} \sum_{\mathbf{k}\in\widehat{\mathcal{L}}} \exp\Big(-\frac{|\mathbf{k}|^2}{4t} + i\mathbf{k}\cdot\mathbf{r}\Big) \tag{A.32}$$

where $\mathbf{k} = 2\pi\big(\frac{k_1}{a}, \frac{k_2}{c}, \frac{k_3}{a}\big)$, $k_1, k_2, k_3 \in \mathbb{Z}$ and $\widehat{\mathcal{L}}$ is the reciprocal lattice. Therefore,

$$\frac{1}{\sqrt{\pi}}\int_0^{\alpha^2} \sum_{\mathbf{n}\in\mathcal{L}} t^{-\frac{1}{2}}\, \exp\big(-|\mathbf{r}+\mathbf{n}|^2 t\big)\, dt = \frac{\pi}{a^2c}\sum_{\mathbf{k}\in\widehat{\mathcal{L}}}\int_0^{\alpha^2} t^{-2}\, \exp\Big(-\frac{|\mathbf{k}|^2}{4t} + i\mathbf{k}\cdot\mathbf{r}\Big)\, dt \tag{A.33}$$

Note that here $\mathbf{r}$ cannot be a function of $\mathbf{n}$. Our reference configuration for a 180° can be transformed into a periodic tetragonal lattice. However, the internal coordinates of the unit cells depend on the position of the unit cell, i.e., $\mathbf{r}_{ij} = \mathbf{r}_{ij}(\mathbf{n})$. The above analysis shows that if we can somehow ignore the reciprocal lattice sum, then the usual Ewald summation technique can be used to find the forces. It is known that the reciprocal lattice sum can be ignored for an appropriate choice of the parameter α.[†]

Now the above sum can be simplified as

$$\begin{aligned}\frac{\pi}{a^2c}\sum_{\mathbf{k}\in\widehat{\mathcal{L}}}\int_0^{\alpha^2} t^{-2}\, \exp\Big(-\frac{|\mathbf{k}|^2}{4t} + i\mathbf{k}\cdot\mathbf{r}\Big)\, dt &= \frac{\pi}{a^2c}\sum_{\mathbf{k}\in\widehat{\mathcal{L}}} e^{i\mathbf{k}\cdot\mathbf{r}}\int_0^{\alpha^2} t^{-2}\, \exp\Big(-\frac{|\mathbf{k}|^2}{4t}\Big)\, dt \\ &= \frac{1}{\pi a^2 c}\sum_{\substack{\mathbf{k}\in\widehat{\mathcal{L}}\\ \mathbf{k}\neq\mathbf{0}}} \frac{1}{|\mathbf{k}|^2}\exp\Big(-\frac{|\mathbf{k}|^2}{4\alpha^2} + i\mathbf{k}\cdot\mathbf{r}\Big) + J(\mathbf{M},\mathcal{P})\end{aligned}$$

where $\mathbf{M} = \sum_{i=1}^{N} Q_i\mathbf{r}_i$ is the unit cell polarization and $J(\mathbf{M},\mathcal{P})$ is a shape dependent term and depends on the summation geometry $\mathcal{P}$ (Smith, 1981) and is the contribution of the term $\mathbf{k} = \mathbf{0}$ (Deem et al., 1990). The direct space lattice sum would be identical to the previous case. For spherical geometry, i.e., when the energy lattice sum is transformed to a simple series using spherical shells and the convergence factor $e^{-sN(\mathbf{n})^2}$ is used (and there is no surrounding medium) the shape dependent term has the following form (de Leeuw et al., 1980),

$$J(\mathbf{M},\mathcal{S}) = \frac{2\pi}{3}|\mathbf{M}|^2 \tag{A.34}$$

[†]This has been shown for large N in Rycerz and Jacobs (1992) but it does not mean that the same conclusions are valid for small N.

For an interesting discussion on this term and some other issues in Ewald technique see Fraser et al. (1996). Note also that for spherical shells $N(\mathbf{n}) = |\mathbf{n}|$. The term Ψ_0[‡] can be similarly simplified to,

$$\Psi_0 = \sum_{\substack{\mathbf{n}\in\mathcal{L}\\ \mathbf{n}\neq\mathbf{0}}} \frac{\mathrm{erfc}(\alpha|\mathbf{n}|)}{|\mathbf{n}|} + \frac{4\pi}{V}\sum_{\substack{\mathbf{k}\in\hat{\mathcal{L}}\\ \mathbf{k}\neq\mathbf{0}}} \frac{e^{-\frac{|\mathbf{k}|^2}{4\alpha^2}}}{|\mathbf{k}|^2} - \frac{2\alpha}{\sqrt{\pi}} \tag{A.36}$$

Note that here we have again assumed spherical summation with the convergence factor $e^{-sN(\mathbf{n})^2}$. Now the cell energy can be written as

$$\begin{aligned}\mathcal{E}_{\mathrm{cell}} \quad = \quad & \sum_{1\le i<j\le N} Q_iQ_j \sum_{\mathbf{n}\in\mathcal{L}} \frac{\mathrm{erfc}(\alpha|\mathbf{r}_{ij}+\mathbf{n}|)}{|\mathbf{r}_{ij}+\mathbf{n}|} + \frac{1}{\pi V}\sum_{1\le i<j\le N}^{N} Q_iQ_j \sum_{\substack{\mathbf{k}\in\hat{\mathcal{L}}\\ \mathbf{k}\neq\mathbf{0}}} \frac{4\pi^2}{|\mathbf{k}|^2}\, e^{-\frac{|\mathbf{k}|^2}{4\alpha^2}}\, \cos(\mathbf{k}\cdot\mathbf{r}_{ij}) \\ & + \frac{1}{2}\Psi_0\sum_{i=1}^{N} Q_i^2 + J(\mathbf{M},\mathcal{P}) \end{aligned} \tag{A.37}$$

where $V = a^2c$ is the volume of the unit cell. The cell energy can be written as

$$\mathcal{E}_{\mathrm{cell}} = \mathcal{E}_{\mathrm{cell}}^{(r)} + \mathcal{E}_{\mathrm{cell}}^{(k)} + \mathcal{E}_{\mathrm{cell}}^{(s)} + \mathcal{E}_{\mathrm{cell}}^{(d)} \tag{A.38}$$

where

$$\begin{aligned}\mathcal{E}_{\mathrm{cell}}^{(r)} &= \frac{1}{2}\sum_{i,j=1}^{N} Q_iQ_j {\sum_{\mathbf{n}\in\mathcal{L}}}' \frac{\mathrm{erfc}(\alpha|\mathbf{r}_{ij}+\mathbf{n}|)}{|\mathbf{r}_{ij}+\mathbf{n}|} \\ \mathcal{E}_{\mathrm{cell}}^{(k)} &= \frac{1}{2\pi V}\sum_{\substack{\mathbf{k}\in\hat{\mathcal{L}}\\ \mathbf{k}\neq\mathbf{0}}} \frac{4\pi^2}{|\mathbf{k}|^2}\, e^{-\frac{|\mathbf{k}|^2}{4\alpha^2}} |\rho(\mathbf{k})|^2 \\ \mathcal{E}_{\mathrm{cell}}^{(s)} &= \frac{1}{2}\sum_{i=1}^{N} Q_i^2\Psi_0 \\ \mathcal{E}_{\mathrm{cell}}^{(d)} &= J(\mathbf{M},\mathcal{P}) \end{aligned}$$

where

$$\rho(\mathbf{k}) = \sum_{j=1}^{N} Q_j e^{-i\mathbf{k}\cdot\mathbf{r}_j}$$

Force on ion i can be calculated as

$$\mathbf{F}_i = -\frac{\partial\mathcal{E}_{\mathrm{cell}}}{\partial\mathbf{r}_i} = \mathbf{F}_i^{(r)} + \mathbf{F}_i^{(k)} + \mathbf{F}_i^{(d)} \tag{A.39}$$

[‡]We can formally define,

$$\Psi_0 = \sum_{\mathbf{n}\in\mathcal{L}\setminus\{\mathbf{0}\}} \frac{1}{|\mathbf{n}|} \tag{A.35}$$

It can be easily shown that

$$\mathbf{F}_i^{(r)} = Q_i \sum_{j=1}^{N} Q_j \sum_{\mathbf{n}\in\mathcal{L}}{}' \Big[\frac{2\alpha\ e^{-\alpha^2|\mathbf{r}_{ij}+\mathbf{n}|^2}}{\sqrt{\pi}} + \frac{\operatorname{erfc}(\alpha|\mathbf{r}_{ij}+\mathbf{n}|)}{|\mathbf{r}_{ij}+\mathbf{n}|} \Big] \frac{\mathbf{r}_{ij}+\mathbf{n}}{|\mathbf{r}_{ij}+\mathbf{n}|^2} \tag{A.40}$$

$$\mathbf{F}_i^{(k)} = \frac{Q_i}{\pi V} \sum_{j=1}^{N} Q_j \sum_{\substack{\mathbf{k}\in\hat{\mathcal{L}} \\ \mathbf{k}\neq\mathbf{0}}} \frac{4\pi^2\mathbf{k}}{|\mathbf{k}|^2}\ e^{-\frac{|\mathbf{k}|^2}{4\alpha^2}} \sin(\mathbf{k}\cdot\mathbf{r}_{ij}) \tag{A.41}$$

$$\mathbf{F}_i^{(d)} = -\frac{4\pi Q_i}{3V}\Big(\sum_{j=1}^{N} Q_j\mathbf{r}_j\Big) \tag{A.42}$$

Note that because of symmetry of a Bravais lattice the real and reciprocal forces can be simplified to,

$$\mathbf{F}_i^{(r)} = Q_i \sum_{\substack{j=1 \\ j\neq i}}^{N} Q_j \sum_{\mathbf{n}\in\mathcal{L}} \left[\frac{2\alpha\ e^{-\alpha^2|\mathbf{r}_{ij}+\mathbf{n}|^2}}{\sqrt{\pi}} + \frac{\operatorname{erfc}(\alpha|\mathbf{r}_{ij}+\mathbf{n}|)}{|\mathbf{r}_{ij}+\mathbf{n}|} \right] \frac{\mathbf{r}_{ij}+\mathbf{n}}{|\mathbf{r}_{ij}+\mathbf{n}|^2} \tag{A.43}$$

$$\mathbf{F}_i^{(k)} = \frac{Q_i}{\pi V} \sum_{\substack{j=1 \\ j\neq i}}^{N} Q_j \sum_{\substack{\mathbf{k}\in\hat{\mathcal{L}} \\ \mathbf{k}\neq\mathbf{0}}} \frac{4\pi^2\mathbf{k}}{|\mathbf{k}|^2}\ e^{-\frac{|\mathbf{k}|^2}{4\alpha^2}} \sin(\mathbf{k}\cdot\mathbf{r}_{ij}) \tag{A.44}$$

Let us now calculate the Hessian of the electrostatic interactions.

A.1.1 Ewald Summation for a Periodic Collection of Distributed Charges

It can be shown that the Ewald-type techniques implicitly introduce a convergence function $\phi(r)$ (Deem et al., 1990) and write the cell energy as

$$\mathcal{E}_{\text{cell}} = \frac{1}{2}\sum_{\mathbf{n}\in\mathcal{L}}{}' \sum_{i,j=1}^{N} Q_iQ_j \frac{\phi(|\mathbf{r}_{ij}+\mathbf{n}|)}{|\mathbf{r}_{ij}+\mathbf{n}|} + \frac{1}{2}\sum_{\mathbf{n}\in\mathcal{L}}{}' \sum_{i,j=1}^{N} Q_iQ_j \frac{1-\phi(|\mathbf{r}_{ij}+\mathbf{n}|)}{|\mathbf{r}_{ij}+\mathbf{n}|} \tag{A.45}$$

ϕ has the same properties of f mentioned earlier. For Coulombic energy, ϕ is the complementary error function,

$$\phi(r) = \operatorname{erfc}(\alpha r) = 1 - \operatorname{erf}(\alpha r) \tag{A.46}$$

where α determines what fraction of the lattice sum should be evaluated in the real (direct) space. This parameter has a nice physical interpretation (Toukmaji and Board Jr., 1996). See Lee et al. (1997) for a discussion on finding an optimal partition function. Suppose each point charge is surrounded by a Gaussian charge distribution of equal magnitude and opposite sign (see Fig. A.1). The charge distribution has the following form,

$$\rho(r) = Q\Big(\frac{\alpha}{\sqrt{\pi}}\Big)^3 e^{-\alpha^2r^2} \tag{A.47}$$

Note that this is the same charge distribution used in the PCEFF-potential with $\alpha = \sqrt{\eta}$. This charge distribution screens the interactions and makes them short range. The resulting lattice sum can be evaluated in the direct space. To recover the original lattice sum, for each point charge, another Gaussian charge distribution with the same magnitude and sign is added. This second lattice sum is very smooth and can be efficiently computed in the Fourier space.

In PCEFF shell potential charges are assumed to have Gaussian distributions. But still we can calculate part of the energy and forces in the direct space and part of it in the reciprocal space. The cell energy can be rewritten as

$$\begin{aligned}
\mathcal{E}_{\text{cell}} &= \frac{1}{2}\sum_{i,j=1}^{N} Q_i Q_j \sum_{\mathbf{n}\in\mathcal{L}}{}' \frac{\text{erf}(\beta_{ij}|\mathbf{r}_{ij}+\mathbf{n}|)}{|\mathbf{r}_{ij}+\mathbf{n}|} \\
&= \frac{1}{2}\sum_{i,j=1}^{N} Q_i Q_j \sum_{\mathbf{n}\in\mathcal{L}}{}' \frac{\text{erfc}(\alpha|\mathbf{r}_{ij}+\mathbf{n}|)-\text{erfc}(\beta_{ij}|\mathbf{r}_{ij}+\mathbf{n}|)}{|\mathbf{r}_{ij}+\mathbf{n}|} + \frac{1}{2}\sum_{i,j=1}^{N} Q_i Q_j \sum_{\mathbf{n}\in\mathcal{L}}{}' \frac{\text{erf}(\alpha|\mathbf{r}_{ij}+\mathbf{n}|)}{|\mathbf{r}_{ij}+\mathbf{n}|}
\end{aligned}$$

where

$$\beta_{ij} = \sqrt{\frac{\eta_i \eta_j}{\eta_i + \eta_j}} \tag{A.48}$$

The first lattice sum can be efficiently calculated in the direct space. The second lattice sum simplifies to,

$$\frac{1}{\pi V}\sum_{1\le i<j\le N}^{N} Q_i Q_j \sum_{\substack{\mathbf{k}\in\hat{\mathcal{L}}\\ \mathbf{k}\neq\mathbf{0}}} \frac{4\pi^2}{|\mathbf{k}|^2}\, e^{-\frac{|\mathbf{k}|^2}{4\alpha^2}}\, \cos(\mathbf{k}\cdot\mathbf{r}_{ij}) + \frac{1}{2}\sum_{i=1}^{N} Q_i^2 \Psi_0^i + J(\mathbf{M},\mathcal{P}) \tag{A.49}$$

where

$$\Psi_0^i = \sum_{\substack{\mathbf{n}\in\mathcal{L}\\ \mathbf{n}\neq\mathbf{0}}} \frac{\text{erfc}(\alpha|\mathbf{n}|)}{|\mathbf{n}|} + \frac{4\pi}{V}\sum_{\substack{\mathbf{k}\in\hat{\mathcal{L}}\\ \mathbf{k}\neq\mathbf{0}}} \frac{e^{-\frac{|\mathbf{k}|^2}{4\alpha^2}}}{|\mathbf{k}|^2} - \frac{2\alpha}{\sqrt{\pi}} \qquad \text{(no summation on } i\text{)} \tag{A.50}$$

Therefore, the cell energy can be written as

$$\begin{aligned}
\mathcal{E}_{\text{cell}} &= \frac{1}{2}\sum_{i,j=1}^{N} Q_i Q_j \sum_{\mathbf{n}\in\mathcal{L}}{}' \frac{\text{erfc}(\alpha|\mathbf{r}_{ij}+\mathbf{n}|)-\text{erfc}(\beta_{ij}|\mathbf{r}_{ij}+\mathbf{n}|)}{|\mathbf{r}_{ij}+\mathbf{n}|} \\
&+ \frac{1}{\pi V}\sum_{1\le i<j\le N}^{N} Q_i Q_j \sum_{\substack{\mathbf{k}\in\hat{\mathcal{L}}\\ \mathbf{k}\neq\mathbf{0}}} \frac{4\pi^2}{|\mathbf{k}|^2}\, e^{-\frac{|\mathbf{k}|^2}{4\alpha^2}}\, \cos(\mathbf{k}\cdot\mathbf{r}_{ij}) + \frac{1}{2}\sum_{i=1}^{N} Q_i^2 \Psi_0^i + J(\mathbf{M},\mathcal{P})
\end{aligned} \tag{A.51}$$

Similar to the classical Coulombic potential, force on the ion i can be written as

$$\mathbf{F}_i = -\frac{\partial \mathcal{E}_{\text{cell}}}{\partial \mathbf{r}_i} = \mathbf{F}_i^{(r)} + \mathbf{F}_i^{(k)} + \mathbf{F}_i^{(d)} \tag{A.52}$$

where

$$\mathbf{F}_i^{(r)} = Q_i \sum_{j=1}^{N} Q_j \sum_{\mathbf{n}\in\mathcal{L}}{}' \Big[\frac{2(\alpha\ e^{-\alpha^2|\mathbf{r}_{ij}+\mathbf{n}|^2} - \beta_{ij}\ e^{-\beta_{ij}^2|\mathbf{r}_{ij}+\mathbf{n}|^2})}{\sqrt{\pi}} \tag{A.53}$$

$$+ \frac{\mathrm{erfc}(\alpha|\mathbf{r}_{ij}+\mathbf{n}|) - \mathrm{erfc}(\beta_{ij}|\mathbf{r}_{ij}+\mathbf{n}|)}{|\mathbf{r}_{ij}+\mathbf{n}|}\Big]\ \frac{\mathbf{r}_{ij}+\mathbf{n}}{|\mathbf{r}_{ij}+\mathbf{n}|^2} \tag{A.54}$$

$$\mathbf{F}_i^{(k)} = \frac{Q_i}{\pi V} \sum_{j=1}^{N} Q_j \sum_{\substack{\mathbf{k}\in\hat{\mathcal{L}} \\ \mathbf{k}\neq\mathbf{0}}} \frac{4\pi^2\mathbf{k}}{|\mathbf{k}|^2}\ e^{-\frac{|\mathbf{k}|^2}{4\alpha^2}} \sin(\mathbf{k}\cdot\mathbf{r}_{ij}) \tag{A.55}$$

$$\mathbf{F}_i^{(d)} = -\frac{4\pi Q_i}{3V}\Big(\sum_{j=1}^{N} Q_j\mathbf{r}_j\Big) \tag{A.56}$$

In PCEFF potential shell charges can change and there is a force corresponding to that. The charge force can be written as

$$f_i = \frac{\partial\mathcal{E}_{\mathrm{cell}}}{\partial Q_i^s} = f_i^{(r)} + f_i^{(k)} + f_i^{(s)} + f_i^{(d)} \tag{A.57}$$

where

$$\begin{aligned} f_i^{(r)} &= \sum_{j=1}^{N} Q_j \sum_{\mathbf{n}\in\mathcal{L}} \frac{\mathrm{erfc}(\alpha|\mathbf{r}_{ij}+\mathbf{n}|) - \mathrm{erfc}(\beta_{ij}|\mathbf{r}_{ij}+\mathbf{n}|)}{|\mathbf{r}_{ij}+\mathbf{n}|} \\ f_i^{(k)} &= \frac{1}{\pi V}\sum_{j=1}^{N} Q_j \sum_{\mathbf{k}\neq\mathbf{0}} \frac{4\pi^2}{|\mathbf{k}|^2} e^{-\frac{|\mathbf{k}|^2}{4\alpha^2}} \cos(\mathbf{k}\cdot\mathbf{r}_{ij}) \\ f_i^{(s)} &= \Psi_0 Q_i \\ f_i^{(d)} &= \frac{4\pi}{3}\mathbf{r}_i\cdot\mathbf{M} \end{aligned} \tag{A.58}$$

A.1.2 Electrostatic Hessian Matrix

Let us first calculate the real part of the Hessian. The real energy is

$$\mathcal{E}^{(r)} = \frac{1}{2}\sum_{I,J=1}^{N} Q_I Q_J \sum_{\mathbf{n}\in\mathcal{L}}{}' \Phi(\mathbf{r}_{IJ}+\mathbf{n}) \tag{A.59}$$

where

$$\Phi(\mathbf{x}) = \frac{\mathrm{erfc}(\alpha|\mathbf{x}|)}{|\mathbf{x}|} \tag{A.60}$$

Thus

$$\frac{\partial\mathcal{E}}{\partial\mathbf{r}_I} = \sum_{\substack{K=1 \\ K\neq I}} \sum_{\mathbf{n}\in\mathcal{L}} \Phi'(\mathbf{r}_{IK}+\mathbf{n})\ \frac{\mathbf{r}_{IK}+\mathbf{n}}{|\mathbf{r}_{IK}+\mathbf{n}|} \tag{A.61}$$

Now for $J \neq I$,

$$\frac{\partial^2\mathcal{E}}{\partial\mathbf{r}_I\partial\mathbf{r}_J} = \sum_{\substack{K=1 \\ K\neq I}} \sum_{\mathbf{n}\in\mathcal{L}} \frac{\partial}{\partial\mathbf{r}_J}\left(\Phi'(\mathbf{r}_{IK}+\mathbf{n})\ \frac{\mathbf{r}_{IK}+\mathbf{n}}{|\mathbf{r}_{IK}+\mathbf{n}|}\right) \tag{A.62}$$

But,

$$\frac{\partial}{\partial \mathbf{r}_J}\left(\Phi'(\mathbf{r}_{IK}+\mathbf{n})\frac{\mathbf{r}_{IK}+\mathbf{n}}{|\mathbf{r}_{IK}+\mathbf{n}|}\right) = -\Phi''(\mathbf{r}_{IK}+\mathbf{n})\frac{(\mathbf{r}_{IK}+\mathbf{n})\otimes(\mathbf{r}_{IK}+\mathbf{n})}{|\mathbf{r}_{IK}+\mathbf{n}|^2}\delta_{JK} - \Phi'(\mathbf{r}_{IK}+\mathbf{n})\frac{\mathbf{1}}{|\mathbf{r}_{IK}+\mathbf{n}|}\delta_{JK} + \Phi'(\mathbf{r}_{IK}+\mathbf{n})\frac{(\mathbf{r}_{IK}+\mathbf{n})\otimes(\mathbf{r}_{IK}+\mathbf{n})}{|\mathbf{r}_{IK}+\mathbf{n}|^3}\delta_{JK} \tag{A.63}$$

Therefore, for $J \neq I$,

$$\mathbf{K}_{IJ}^{(r)} = \sum_{\mathbf{n}\in\mathcal{L}} \mathbf{k}_{IJ}(\mathbf{n}) \tag{A.64}$$

where

$$\mathbf{k}_{IJ}(\mathbf{n}) = -\Phi''(\mathbf{r}_{IJ}+\mathbf{n})\frac{(\mathbf{r}_{IJ}+\mathbf{n})\otimes(\mathbf{r}_{IJ}+\mathbf{n})}{|\mathbf{r}_{IJ}+\mathbf{n}|^2} - \Phi'(\mathbf{r}_{IJ}+\mathbf{n})\ \frac{\mathbf{1}}{|\mathbf{r}_{IJ}+\mathbf{n}|} + \Phi'(\mathbf{r}_{IJ}+\mathbf{n})\frac{(\mathbf{r}_{IJ}+\mathbf{n})\otimes(\mathbf{r}_{IJ}+\mathbf{n})}{|\mathbf{r}_{IJ}+\mathbf{n}|^3} \tag{A.65}$$

And,

$$\mathbf{K}_{II}^{(r)} = -\sum_{\substack{J=1\\J\neq I}} \mathbf{K}_{IJ}^{(r)} \tag{A.66}$$

The reciprocal energy is

$$\mathcal{E}^{(k)} = \sum_{I,J=1}^{N} \frac{Q_I Q_J}{2\pi V} \sum_{\substack{\mathbf{k}\in\mathcal{L}\\\mathbf{k}\neq\mathbf{0}}} \frac{4\pi^2}{|\mathbf{k}|^2} e^{-\frac{|\mathbf{k}|^2}{4\alpha^2}} \cos(\mathbf{k}\cdot\mathbf{r_{IJ}}) \tag{A.67}$$

Thus

$$\frac{\partial}{\partial \mathbf{r}_I}\mathcal{E}^{(k)} = -\sum_{J=1}^{N} \frac{Q_I Q_J}{\pi V} \sum_{\substack{\mathbf{k}\in\mathcal{L}\\\mathbf{k}\neq\mathbf{0}}} \frac{4\pi^2}{|\mathbf{k}|^2} e^{-\frac{|\mathbf{k}|^2}{4\alpha^2}} \sin(\mathbf{k}\cdot\mathbf{r_{IJ}})\ \mathbf{k} \tag{A.68}$$

Hence for $J \neq I$,

$$\mathbf{K}_{IJ}^{(k)} = \frac{\partial^2}{\partial \mathbf{r}_I \partial \mathbf{r}_J}\mathcal{E}^{(k)} = \frac{Q_I Q_J}{\pi V} \sum_{\substack{\mathbf{k}\in\mathcal{L}\\\mathbf{k}\neq\mathbf{0}}} \frac{4\pi^2}{|\mathbf{k}|^2} e^{-\frac{|\mathbf{k}|^2}{4\alpha^2}} \cos(\mathbf{k}\cdot\mathbf{r_{IJ}})\ \mathbf{k}\otimes\mathbf{k} \tag{A.69}$$

And,

$$\mathbf{K}_{II}^{(k)} = -\sum_{\substack{J=1\\J\neq I}} \mathbf{K}_{IJ}^{(k)} \tag{A.70}$$

The total stiffness matrices are defined as

$$\mathbf{K}_{IJ} = \mathbf{K}_{IJ}^{(r)} + \mathbf{K}_{IJ}^{(k)} \tag{A.71}$$

A.2 Direct Summation Methods

Evjen (1932) proposed an interesting direct summation method for calculating the Madelung energy. For cubic crystals, he considered cubic shells and calculated a weighted electrostatic potential. In each cubic shell each charge has a weight w. For charges inside the shell $w = 1$, for charges on a face of the cube, $w = \frac{1}{2}$, for charges on an edge $w = \frac{1}{4}$ and for charges on corners $w = \frac{1}{8}$.

In a macroscopically neutral ionic crystal the divergent long-range fields cancel. However, the details of this cancellation depends strongly on the method used for evaluating the electrostatic interactions and different methods can lead to different values. The lattice sum defining electrostatic energy of unit cell in an ionic crystal, like any other conditionally convergent lattice sum, is composed of two divergent sums with different signs (Knopp, 1956). Harris (1975) gives a simple and interesting example of a one-dimensional chain of charges and gives several possibilities for defining the unit cell. In general, for a bulk crystal, any charge-neutral unit cell is acceptable but different unit cells characterize the crystal surfaces differently. As Harris (1975) explains, Ewald summation method assumes that all moments of the unit cell (in direct space) up to the second order are zero. This means that using any unit cell which has a nonzero first or second moment, in general, leads to a cell energy that is different from that obtained by Ewald technique. The reader may refer to Tosi (1964) for an interesting review of different direct lattice summation methods.

As a real crystal is finite, the conditional convergence of electrostatic energy implies a shape and size dependence of energy and forces. One way of direct summation is to group ions of the system into cells with zero leading multipoles (of orders zero, one and two). As Young (1987) explains the ambiguity in conditionally convergent lattice sums comes from the surface charges on the boundary of these cells.

Appendix B

Theory of Difference Equations

Difference equations arise in many problems of mathematical physics. They also appear in discretization of boundary value problems and also in combinatorics. In this appendix we mention a few facts and theorems from theory of difference equations. For more details see Agarwal (2000); Elaydi (1996); Lakshmikantham and Trigiante (1988). There are two contributions in this appendix. One is a discussion on direct solution of a degenerate difference equation. The other one is a semidirect solution method for a class of linear partial difference equations. At the end of this appendix we study a simple 2-D lattice under two loading systems and develop some intuition.

B.1 Ordinary Difference Equations

An ordinary difference equation is the discrete analogue of an ordinary differential equation. Difference equations can be defined on bounded or unbounded discrete domains. For us all difference equations are defined on unbounded domains. Consider a sequence $\{u_n\}_{n\in\mathbb{N}} \subset \mathbb{R}$. A difference equation in the independent variable n is an equation of the form,

$$f(n, u_n, ..., u_{n+p}) = 0 \tag{B.1}$$

The order of a difference equation is the difference between the largest and smallest arguments explicitly involved in the equation. For example, the following (nonlinear) difference equation is of order five.

$$u_{n+2} + nu_{n-1} + 3u_n u_{n-3} = f_n \tag{B.2}$$

A linear difference equation has the following form,

$$\sum_{j=0}^{p} K_j(n) u_{n+j} = b_n \qquad n \in \mathbb{N} \tag{B.3}$$

Here, we are interested in linear difference equations with constant coefficients. These equations show up in discrete systems with uniform physical properties. Consider a pth order difference equation with constant coefficients,

$$u_{n+p} + a_1 u_{n+p-1} + a_2 u_{n+p-2} + ... + a_p u_n = b_n \tag{B.4}$$

First, we solve the corresponding homogeneous equation. Suppose solutions are of the form $\lambda^n,\ \lambda \in \mathbb{C}$. Then,

$$\lambda^p + a_1 \lambda^{p-1} + ... + a_p = 0 \tag{B.5}$$

This is the characteristic equation of difference equation (B.4). There are several possibilities for characteristic roots. If all the roots are real and distinct the general solution is of the form,

$$u_n^c = c_1 \lambda_1^n + c_2 \lambda_2^n + ... + c_1 \lambda_p^n \tag{B.6}$$

For details on other possibilities see Elaydi (1996). The general solution of Eq. (B.4) can be written as

$$u_n = u_n^c + u_n^p \tag{B.7}$$

where u_n^p is a particular solution of the nonhomogeneous equation.

A system of linear difference equations of first order has the following form,*

$$\mathbf{u}_{n+1} = \mathcal{A}(n)\mathbf{u}_n + \mathbf{b}_n, \quad \mathbf{u}_n, \mathbf{b}_n \in \mathbb{R}^p,\ \mathcal{A}(n) \in \mathbb{R}^{p \times p} \tag{B.8}$$

If $\mathcal{A}$ does not depend on n the system (B.8) is called a system with constant coefficients.

$$\mathbf{u}_{n+1} = \mathcal{A}\mathbf{u}_n + \mathbf{b}_n \tag{B.9}$$

For the homogeneous system with constant coefficients corresponding to (B.9), i.e.,

$$\mathbf{u}_{n+1} = \mathcal{A}\mathbf{u}_n \tag{B.10}$$

the general solution is

$$\mathbf{u}_n = \mathcal{A}^n \mathbf{c}, \quad \mathbf{c} \in \mathbb{R}^p, \quad \forall n \in \mathbb{N} \tag{B.11}$$

Here, $\mathcal{A}^n$ is called the fundamental matrix of the system (B.9). This is the analogue of $e^{\mathcal{A}t}$ in a linear system of differential equations.

Theorem 27. *System of difference equations (B.9) has p linearly independent solutions and the*

*It will be seen in the next section that this is not the most general form of a first order difference equation.

general solution can be written as

$$\mathbf{u}_n = \mathcal{A}^n \mathbf{c} + \mathbf{u}_n^p \tag{B.12}$$

where $\mathbf{u}_n^p$ *is a particular solution. Using the method of variation of constants the general solution can be expressed as*

$$\mathbf{u}_n = \mathcal{A}^n \mathbf{c} + \sum_{j=0}^{n-1} \mathcal{A}^{n-j-1} \mathbf{b}_j \tag{B.13}$$

A system of difference equations can be thought of as an ordinary difference equation for a vector-valued discrete function. Let $\mathbf{X} : \mathbb{K} \to \mathbb{R}^p$, where $\mathbb{K} \subset \mathbb{Z}$.

Definition 28. *The shift operator* E *is defined as*

$$E\mathbf{X}(n) = \mathbf{X}(n+1) \tag{B.14}$$

provided that $n, n+1 \in \mathbb{K}$. *If* $n, n+k \in \mathbb{K}$, *then,*

$$E^k\mathbf{X}(n) = \mathbf{X}(n+k) \tag{B.15}$$

Inverse of the shift operator is defined as

$$E^{-1}\mathbf{X}(n) = \mathbf{X}(n-1) \tag{B.16}$$

assuming that $n, n-1 \in \mathbb{K}$.

Example 29. *The ordinary difference equation,*

$$\mathbf{X}(n+1) - 5\mathbf{X}(n) + 2\mathbf{X}(n-1) = \mathbf{F}(n) \qquad n \in \mathbb{Z} \tag{B.17}$$

can be rewritten as

$$\left(E - 5I + 2E^{-1}\right)\mathbf{X}(n) = \mathbf{F}(n) \qquad n \in \mathbb{Z} \tag{B.18}$$

The solution can be formally written as

$$\mathbf{X}(n) = \left(E - 5I + 2E^{-1}\right)^{-1}\mathbf{F}(n) \tag{B.19}$$

There are methods for calculating inverse of such simple operators but these are not useful for the applications we have in mind.

B.2 Degenerate Systems of Difference Equations and Their Solution

Consider the following first-order system of difference equations for a sequence $\{\mathbf{X}_n\} \subset \mathbb{R}^N$,

$$\mathbf{A}\mathbf{X}_{n+1} + \mathbf{B}\mathbf{X}_n = \mathbf{F}_n \qquad n \geq 1 \tag{B.20}$$

and assume that $\det \mathbf{A} = 0$. This means that this system cannot be transformed to a canonical system of first-order equations,

$$\mathbf{X}_{n+1} = \mathcal{A}\mathbf{X}_n + \mathbf{G}_n \tag{B.21}$$

We call the system (B.20) degenerate. Here we present a direct method for solving such a degenerate difference equation.[†] The matrix $\mathbf{A}$ can be diagonalized (it is assumed to be symmetric),

$$\mathbf{X}^{-1}\mathbf{A}\mathbf{X} = \mathbf{\Lambda} = \mathrm{diag}(\lambda_1, ..., \lambda_p, \underbrace{0, ..., 0}_{N-p \text{ copies}}) = \begin{pmatrix} \overline{\mathbf{\Lambda}} & \mathbf{0} \\ \mathbf{0} & \mathbf{0} \end{pmatrix} \tag{B.22}$$

where $\mathbf{X}$ is the orthogonal matrix of eigenvectors. Thus (B.20) can be written as

$$\mathbf{\Lambda}\mathbf{X}^{-1}\mathbf{X}_{n+1} + \mathbf{C}\mathbf{X}_n = \mathbf{G}_n \tag{B.23}$$

where $\mathbf{C} = \mathbf{X}^{-1}\mathbf{B}$ and $\mathbf{G}_n = \mathbf{X}^{-1}\mathbf{F}_n$. We use the following notations,

$$\mathbf{Z} = \begin{pmatrix} \overline{\mathbf{Z}} \\ \overline{\overline{\mathbf{Z}}} \end{pmatrix} \in \mathbb{R}^N \quad \text{and} \quad \overline{\mathbf{Z}} \in \mathbb{R}^p,\ \overline{\overline{\mathbf{Z}}} \in \mathbb{R}^{N-p}, \quad \mathbf{A} = \begin{pmatrix} \mathbf{A}_{11} & \mathbf{A}_{12} \\ \mathbf{A}_{21} & \mathbf{A}_{22} \end{pmatrix}, \quad \mathbf{C} = \begin{pmatrix} \mathbf{C}_{11} & \mathbf{C}_{12} \\ \mathbf{C}_{21} & \mathbf{C}_{22} \end{pmatrix} \tag{B.24}$$

Now Eq. (B.23) can be written as the following two sets of equations,

$$\begin{cases} \overline{\mathbf{\Lambda}\ \overline{\mathbf{X}^{-1}X_{n+1}}} + \overline{\mathbf{C}X_n} = \overline{G_n} \\ \\ \overline{\overline{\mathbf{C}X_n}} = \overline{\overline{G_n}} \end{cases} \tag{B.25}$$

The second equation gives,

$$\overline{\overline{\mathbf{X}_n}} = \mathbf{T}\overline{\mathbf{X}_n} + \mathbf{H}_n \tag{B.26}$$

[†]We have not seen such an explicit solution for such a degenerate difference equation in the literature.

where $\mathbf{T} = -\mathbf{C}_{22}^{-1}\mathbf{C}_{21}$ and $\mathbf{H}_n = \mathbf{C}_{22}^{-1}\overline{\overline{\mathbf{G}_n}}$. Finally we will have the following nondegenerate system of equations for the sequence $\{\overline{\mathbf{X}_n}\} \subset \mathbb{R}^p$,

$$\overline{\mathbf{X}_{n+1}} = \overline{\mathbf{A}}\ \overline{\mathbf{X}_n} + \overline{\mathbf{F}_n} \tag{B.27}$$

where

$$\overline{\mathbf{A}} = -\Big[\overline{\mathbf{\Lambda}}\big((\mathbf{X}^{-1})_{11} + (\mathbf{X}^{-1})_{12}\mathbf{T}\big)\Big]^{-1}(\mathbf{C}_{11} + \mathbf{C}_{12}\mathbf{T})$$

and

$$\overline{\mathbf{F}_n} = \Big[\overline{\mathbf{\Lambda}}\big((\mathbf{X}^{-1})_{11} + (\mathbf{X}^{-1})_{12}\mathbf{T}\big)\Big]^{-1}\big(\ \overline{\mathbf{G}_n} - \overline{\mathbf{\Lambda}}(\mathbf{X}^{-1})_{12}\mathbf{H}_{n+1} - \mathbf{C}_{12}\mathbf{H}_n\big)$$

Example 30. *Consider the following degenerate system,*

$$\mathbf{A} = \begin{pmatrix} 2 & -2 \\ -1 & 1 \end{pmatrix}, \quad \mathbf{B} = \begin{pmatrix} 1 & 0 \\ 2 & 3 \end{pmatrix}, \quad \mathbf{F}_n = \begin{pmatrix} 0 \\ 0 \end{pmatrix}, \quad \mathbf{X}_n = \begin{pmatrix} u_n \\ v_n \end{pmatrix}$$

It can be easily shown that

$$\mathbf{T} = \begin{pmatrix} -\frac{5}{6} \end{pmatrix}, \quad \overline{\mathbf{A}} = \begin{pmatrix} -\frac{3}{11} \end{pmatrix}$$

Thus

$$v_n = -\frac{5}{6}u_n, \quad u_n = \Big(-\frac{3}{11}\Big)^n\ c \qquad n \geq 1$$

This derivation for a first-order equation should be enough to convince the reader that the situation would become much more complicated for higher-order degenerate difference equations. A more practical solution would be to avoid degenerate systems of equations, especially for a large problem like our lattice statics model of ferroelectrics. At the end of this chapter we will show an example of a physical system that leads to a degenerate ordinary difference equation.

B.3 Partial Difference Equations

Partial difference equations are discrete analogues of partial differential equations. Let $\mathbb{Z}^p$ be the set of all p-tuples of integers ($p \geq 2$). A linear partial difference equation has the following form,

$$L\mathbf{X}_\alpha = \sum_{\beta \in \Omega} \mathbf{A}(\beta)\mathbf{X}_{\alpha+\beta} = \mathbf{F}_\alpha \tag{B.28}$$

where $\Omega \subset \mathbb{Z}^p$, $\alpha, \beta \in \mathbb{Z}^p$ and,

$$\mathbf{X}, \mathbf{F} : \Omega \to \mathbb{R}^q, \qquad \mathbf{A} : \Omega \to \mathbb{R}^q \times \mathbb{R}^q \tag{B.29}$$

For $p = 2$, a linear partial difference equation has the following form,

$$\sum_{(r,s)\in\mathbb{Z}^2} \mathbf{A}_{rs}\mathbf{X}_{m+r,n+s} = \mathbf{F}_{mn} \qquad (m,n) \in \Omega \tag{B.30}$$

Let $\mathbf{X} : \mathbb{L} \to \mathbb{R}^p$, where $\mathbb{L} \subset \mathbb{Z} \times \mathbb{Z}$. partial shift operators E_1 and E_2 are defined as

$$E_1\mathbf{X}(m,n) = \mathbf{X}(m+1,n) \tag{B.31}$$

$$E_2\mathbf{X}(m,n) = \mathbf{X}(m,n+1) \tag{B.32}$$

provided that $(m,n),(m+1,n),(m,n+1) \in \mathbb{L}$. The inverse partial shift operators are defined as

$$E_1^{-1}\mathbf{X}(m,n) = \mathbf{X}(m-1,n) \tag{B.33}$$

$$E_2^{-1}\mathbf{X}(m,n) = \mathbf{X}(m,n-1) \tag{B.34}$$

provided that $(m,n),(m-1,n),(m,n-1) \in \mathbb{L}$.

Example 31. *The partial difference equation,*

$$\sum_{\alpha=-1}^{1}\sum_{\beta=-2}^{2} \mathcal{A}_{\alpha\beta}\mathbf{X}(m+\alpha,n+\beta) = \mathbf{F}(m,n) \tag{B.35}$$

can be written as

$$\sum_{\alpha=-1}^{1}\sum_{\beta=-2}^{2} \mathcal{A}_{\alpha\beta}E_1^{\alpha}E_2^{\beta}\mathbf{X}(m,n) = \mathbf{F}(m,n) \tag{B.36}$$

Formally, the solution can be written as

$$\mathbf{X}(m,n) = \left(\sum_{\alpha=-1}^{1}\sum_{\beta=-2}^{2} \mathcal{A}_{\alpha\beta}E_1^{\alpha}E_2^{\beta}\right)^{-1}\mathbf{F}(m,n) \tag{B.37}$$

A powerful technique for solving partial difference equations is discrete Fourier transform, which will be briefly reviewed in the next section. Applying DFT to the above partial difference equation one gets,

$$\left(\sum_{(r,s)\in\mathbb{Z}^2} e^{i(-rk_1-sk_2)}\mathbf{A}_{rs}\right)\widehat{\mathbf{X}_{m,n}}(k_1,k_2) = \widehat{\mathbf{F}_{mn}}(k_1,k_2) \qquad (k_1,k_2) \in B = [-\pi,\pi]\times[-\pi,\pi] \tag{B.38}$$

The behavior of the partial difference equation strongly depends on the characteristic matrix,

$$\mathbf{B}(k_1,k_2) = \sum_{(r,s)\in\mathbb{Z}^2} e^{i(-rk_1-sk_2)}\mathbf{A}_{rs} \tag{B.39}$$

The matrix $\mathbf{B}$ may not be invertible at some points in the first Brillouin zone. An example would be the singularity at the origin for translation invariant partial difference equations.

For solving partial difference equations on bounded rectangular domains there are direct methods using matrix tensor product methods (Lynch et al., 1964). However, these methods are not applicable to the problems we are dealing with in this thesis. There are also some direct methods for solving simple partial difference equations (see Mickens (1990)). However, these methods are not applicable for general vector-valued partial difference equations.

B.4 Discrete Fourier Transform

Discrete Fourier Transform (DFT) is a powerful technique for solving system of linear difference equations. In the literature there are two different types of discrete Fourier transform both known as DFT. The first type, which is the one we use in this thesis, transforms a sequence (or more precisely a lattice function) to a function of a continuous variable(s). This is sometimes called *continuous discrete Fourier transform* (CDFT). Theory of CDFT was developed in (Babŭska, 1959; Babŭska et al., 1960; Vitásek, 1959). The other type of DFT, which we call *discrete DFT* (DDFT), transforms a sequence to another sequence (Briggs and Hendon, 1995), (Benedetto, 1997) and is usually useful for solving periodic difference equations or difference equations on bounded domains. In this work by DFT we mean CDFT, i.e., the one that maps a mesh function to a continuous function in k-space.

Consider a lattice $\mathcal{L}$ and a lattice function $f : \mathcal{L} \to \mathbb{R}^3$. The discrete Fourier transform of f is defined formally as

$$\hat{f}(\mathbf{k}) = V \sum_{\mathbf{j} \in \mathcal{L}} f(\mathbf{j}) e^{i\mathbf{k}\cdot\mathbf{x}^{\mathbf{j}}} \qquad \mathbf{k} \in B \tag{B.40}$$

where V is the volume of the unit cell and B is the first Brillouin zone. For a chain of atoms of unit lattice spacing this definition reduces to the usual definition of DFT of a sequence in $\mathbb{R}$, where $V = 1$, $B = [-\pi, \pi]$. Let us denote by $\mathcal{U}$ the set of all discrete Fourier transformable lattice functions. Let us also denote by $\mathcal{R}$ the set of those lattice functions such that

$$|f(\mathbf{x})| \leq C \prod_{i=1}^{3} \left(1 + |x_i|^p\right) \qquad \forall\ \mathbf{x} = (x_1, x_2, x_3) \in \mathcal{L} \tag{B.41}$$

for some integer $p \geq 0$ and constant $C \geq 0$. It can be shown (Vitásek, 1959) that there is a one-to-one correspondence between the spaces $\mathcal{R}$ and $\mathcal{U}$. It should be noted that in the definition of DFT the convergence should be understood in the sense of distributions.

Inverse DFT is defined as

$$f(\mathbf{j}) = \frac{1}{(2\pi)^3} \int_B \hat{f}(\mathbf{k}) e^{-i\mathbf{k}\cdot\mathbf{x}^{\mathbf{j}}} d^3k \tag{B.42}$$

DFT has many nice properties and here we mention a few of them. DFT is a linear operator, i.e.,

$$(\alpha f + \beta g)^{\wedge} = \alpha \hat{f} + \beta \hat{g} \qquad \forall \alpha, \beta \in \mathbb{R},\ \forall\ f, g \in \mathcal{U} \tag{B.43}$$

Shifting property of DFT is essential in solving difference equations. Suppose,

$$\widehat{\mathbf{X}_\mathbf{n}} = \mathbf{Y}(\mathbf{k}) \tag{B.44}$$

Then,

$$\widehat{\mathbf{X}_{\mathbf{n}+\mathbf{m}}} = e^{-i\mathbf{m}\cdot\mathbf{k}}\ \mathbf{Y}(\mathbf{k}) \tag{B.45}$$

Definition 32. *Discrete convolution of two lattice functions f and g is defined as*

$$(f * g)(\mathbf{i}) = V \sum_{\mathbf{j}\in\mathcal{L}} f(\mathbf{i}-\mathbf{j}) g(\mathbf{j}) \tag{B.46}$$

Note that the multiplication $f(\mathbf{i}-\mathbf{j})g(\mathbf{j})$ is defined componentwise.

Theorem 33. *If $f, g \in \mathcal{U}$, then*

$$\widehat{(f * g)}(\mathbf{k}) = \hat{f}(\mathbf{k})\hat{g}(\mathbf{k}) \tag{B.47}$$

Discrete Fourier Transform is a powerful tool in solving partial difference equations but should be used carefully in numerical calculations.

B.4.1 DFT and Difference Equations

Consider the following ordinary difference equation.

$$x_{p+1} - 2x_p + x_{p-1} = f_p \qquad p \in \mathbb{Z} \tag{B.48}$$

Note that this difference equation is translation invariant, i.e., if the sequence $\{x_p\}$ is a solution so is the sequence $\{x_p + c\},\ \forall\ c \in \mathbb{R}$. Applying DFT to this difference equation we get,

$$\left(e^{-ik} - 2 + e^{ik}\right) \widehat{x_p}(k) = \widehat{f_p}(k) \tag{B.49}$$

Or,

$$\widehat{x_p}(k) = \frac{1}{2(\cos k - 1)} \widehat{f_p}(k) \tag{B.50}$$

Thus

$$x_p = \frac{1}{2\pi}\int_{-\pi}^{\pi} e^{-ipk}\frac{1}{2(\cos k - 1)}\widehat{f}_p(k)dk \tag{B.51}$$

Note that this integral is not convergent in general because there is a singularity at $k = 0$,

$$\frac{1}{2(\cos k - 1)} = -\frac{1}{k^2} + O(1) \tag{B.52}$$

This is a consequence of translation invariance of the difference equation. In other words for this difference equation the solution can be obtained up to a rigid translation and this shows up in the inverse discrete Fourier transform as a singularity. One could make the integral convergent by adding a suitable rigid translation. The following would be a rigid translation that removes the singularity,

$$x_p = \frac{1}{2\pi}\int_{-\pi}^{\pi} e^{-ipk}\left[\frac{1}{2(\cos k - 1)}\widehat{f}_p(k) - \frac{e^{ipk}}{2(\cos k - 1)}\right]dk \tag{B.53}$$

For $\mathbb{R}$-valued difference equations there are rigorous treatments of this problem in the literature (see De Boor et al. (1989) and Veit (2003)). In a special case when the loading sequence is symmetric about $p = 0$ the inverse DFT is convergent. An example would be the following,

$$f_{-p} = f_p \qquad \forall\ p \in \mathbb{N}, \quad f_0 = 0 \tag{B.54}$$

In this case $\widehat{f}_p(0) = 0$ and the inverse DFT is convergent.

B.5 A Semidirect Method for Solving a Class of Linear Partial Difference Equations

In this section we present an efficient method for solving a class of linear partial difference equations. The idea of this method is similar to that of reducing a partial differential equation to an ordinary differential equation by applying Laplace or Fourier transform in one direction. Our semidirect method can be useful in problems where a very large number of Gauss points in necessary in evaluating the two-dimensional (or three-dimensional) DFT. Here we present the method for a two-dimensional partial difference equation but generalizing it to higher order partial difference equations would be straightforward.

Consider the following partial difference equation,

$$\sum_{\alpha=-r}^{\alpha=r}\sum_{\beta=-s}^{\beta=s}\mathcal{A}_{\alpha\beta}\mathbf{X}_{m+\alpha,n+\beta} = \mathbf{F}_{m,n} \qquad m, n \in \mathbb{Z} \tag{B.55}$$

Let us assume that

$$\mathbf{F}_{m,n} = \mathbf{0} \qquad |m| > M \tag{B.56}$$

Applying DFT in $n-$direction for the above partial difference equation we obtain,

$$\sum_{n=-\infty}^{\infty} e^{ink} \sum_{\alpha=-r}^{\alpha=r} \sum_{\beta=-s}^{\beta=s} \mathcal{A}_{\alpha\beta} \mathbf{X}_{m+\alpha,n+\beta} = \sum_{n=-\infty}^{\infty} e^{ink} \mathbf{F}_{m,n} \qquad m \in \mathbb{Z} \tag{B.57}$$

Or,

$$\sum_{\alpha=-r}^{\alpha=r} \sum_{\beta=-s}^{\beta=s} e^{-i\beta k} \mathcal{A}_{\alpha\beta} \hat{\mathbf{Y}}_{m+\alpha}(k) = \hat{\mathbf{f}}_m(k) \qquad m \in \mathbb{Z} \tag{B.58}$$

where

$$\hat{\mathbf{Y}}_{m+\alpha}(k) = \sum_{n=-\infty}^{\infty} e^{ink} \mathbf{X}_{m+\alpha,n}, \qquad \hat{\mathbf{f}}_m(k) = \sum_{n=-\infty}^{\infty} e^{ink} \mathbf{F}_{m,n} \tag{B.59}$$

This can be rewritten as

$$\sum_{\alpha=-r}^{\alpha=r} \mathcal{A}_{\alpha}(k) \hat{\mathbf{Y}}_{m+\alpha}(k) = \hat{\mathbf{f}}_m(k) \qquad m \in \mathbb{Z} \tag{B.60}$$

where

$$\mathcal{A}_{\alpha}(k) = \sum_{\beta=-s}^{\beta=s} e^{-i\beta k} \mathcal{A}_{\alpha\beta} \tag{B.61}$$

Note that for a given value of k Eq. (B.60) is an ordinary system of difference equations. Let us write the solution explicitly for $r = 1$ and $r = 2$ as generalizing it for an arbitrary r would be straightforward.

i) ***r=1:*** The governing ordinary difference equations are,

$$\mathcal{A}_{-1}(k) \hat{\mathbf{Y}}_{m-1}(k) + \mathcal{A}_0(k) \hat{\mathbf{Y}}_m(k) + \mathcal{A}_1(k) \hat{\mathbf{Y}}_{m+1}(k) = \hat{\mathbf{f}}_m(k) \qquad m \in \mathbb{Z} \tag{B.62}$$

Let us define,

$$\mathbf{Z}_m = \begin{pmatrix} \hat{\mathbf{Y}}_{m-1} \\ \hat{\mathbf{Y}}_m \end{pmatrix} \qquad m \geq 1 \tag{B.63}$$

The governing equations can be rewritten as

$$\mathbf{Z}_{m+1} = \mathbf{A}\mathbf{Z}_m + \mathbf{G}_m \qquad m \geq 1 \tag{B.64}$$

where

$$\mathbf{A} = \begin{pmatrix} \mathbf{0} & \mathbf{1} \\ -\mathcal{A}_1^{-1}\mathcal{A}_{-1} & -\mathcal{A}_1^{-1}\mathcal{A}_0 \end{pmatrix}, \qquad \mathbf{G}_m = \begin{pmatrix} \mathbf{0} \\ \mathcal{A}_1^{-1}\hat{\mathbf{f}}_m \end{pmatrix} \tag{B.65}$$

Let us assume that

$$\mathbf{F}_{m,n} = \mathbf{0} \qquad m > M \tag{B.66}$$

Thus

$$\hat{\mathbf{f}}_m(k) = \mathbf{0} \qquad m > M \tag{B.67}$$

Therefore the solution of (B.64) for large m ($m \geq M+1$ can be expressed as

$$\mathbf{Z}_m = \mathbf{A}^{m-M-1}\left(\mathbf{A}^M\mathbf{c} + \mathbf{d}\right) \qquad m \geq M+1 \tag{B.68}$$

where

$$\mathbf{c} = \mathbf{Z}_1 = \begin{pmatrix} \hat{\mathbf{Y}}_0 \\ \hat{\mathbf{Y}}_1 \end{pmatrix}, \qquad \mathbf{d} = \mathbf{A}^{M-1}\mathbf{G}_1 + \mathbf{A}^{M-2}\mathbf{G}_2 + ... + \mathbf{A}\mathbf{G}_{M-1} + \mathbf{G}_M \tag{B.69}$$

The boundary equations are the governing equations for $m = 0$,

$$\mathcal{A}_{-1}(k)\hat{\mathbf{Y}}_{-1}(k) + \mathcal{A}_0(k)\hat{\mathbf{Y}}_0(k) + \mathcal{A}_1(k)\hat{\mathbf{Y}}_1(k) = \hat{\mathbf{f}}_0(k) \tag{B.70}$$

The boundedness equations at infinity guarantee the following,

$$\|\hat{\mathbf{Y}}_m\| < \infty \qquad \text{as} \qquad m \to \infty \tag{B.71}$$

The matrix $\mathbf{A}$ has the following Jordan decomposition,

$$\mathbf{A} = \mathbf{X}\mathbf{\Lambda}\mathbf{X}^{-1} \tag{B.72}$$

where $\mathbf{X}$ is the matrix of generalized eigenvectors. The solution can be rewritten as

$$\mathbf{Z}_m = \mathbf{X}\mathbf{\Lambda}^{m-M-1}\left(\mathbf{X}^{-1}\mathbf{A}^M\mathbf{c} + \mathbf{X}^{-1}\mathbf{d}\right) = \mathbf{X}\mathbf{\Lambda}^{m-M-1}\left(\mathbf{\Lambda}^M\mathbf{X}^{-1}\mathbf{c} + \mathbf{X}^{-1}\mathbf{d}\right) \qquad m \geq M+1 \tag{B.73}$$

Boundedness of solutions at infinity requires that

$$\left(\mathbf{\Lambda}^M\mathbf{X}^{-1}\mathbf{c}\right)_\star = -\left(\mathbf{X}^{-1}\mathbf{d}\right)_\star \tag{B.74}$$

The boundedness equations can be rewritten as follows,

$$\mathcal{D}_1(k)\hat{\mathbf{Y}}_0(k) + \mathcal{D}_2(k)\hat{\mathbf{Y}}_1(k) = \mathbf{F}_D \tag{B.75}$$

For SC shell potential it turns out that $M = 2$. Thus, after calculating the integration constants

c the solution can be expressed as

$$\mathbf{Z}_2 = \mathbf{A}\mathbf{c} + \mathbf{G}_1 \tag{B.76}$$

$$\mathbf{Z}_3 = \mathbf{A}^2\mathbf{c} + \mathbf{A}\mathbf{G}_1 + \mathbf{G}_2 \tag{B.77}$$

$$\mathbf{Z}_m = \mathbf{X}\mathbf{\Lambda}^{m-3}\left(\mathbf{\Lambda}^2\mathbf{X}^{-1}c + \mathbf{X}^{-1}\mathbf{d}\right) \qquad m \geq 4 \tag{B.78}$$

where

$$\mathbf{d} = \mathbf{A}\mathbf{G}_1 + \mathbf{G}_2 \tag{B.79}$$

If the matrix $\mathbf{A}(k)$ is ill-conditioned, the solution for large m should be rewritten as follows,

$$\mathbf{Z}_m = \mathbf{X}\mathbf{\Lambda}^{m-M-1}\mathbf{e} \tag{B.80}$$

where

$$\mathbf{e} = \begin{pmatrix} \mathbf{0} \\ \mathbf{E} \end{pmatrix}, \qquad \mathbf{E} = \left(\mathbf{\Lambda}^M\mathbf{X}^{-1}\mathbf{c} + \mathbf{X}^{-1}\mathbf{d}\right)_* \tag{B.81}$$

The subscript $*$ refers to those rows that were not in the boundedness equations.

Looking at the symmetry relations (7.46) carefully, one can see that there is no simple relation between the values of $\hat{\mathbf{Y}}_m$ for positive and negative values of m and one has to solve the complete governing equations (B.62). Let us define,

$$\bar{\mathbf{Z}}_m = \begin{pmatrix} \hat{\mathbf{Y}}_{m+1} \\ \hat{\mathbf{Y}}_m \end{pmatrix} \qquad m \leq -1 \tag{B.82}$$

Now the governing equations (B.62) can be rewritten as

$$\bar{\mathbf{Z}}_{m-1} = \bar{\mathbf{A}}\bar{\mathbf{Z}}_m + \bar{\mathbf{G}}_m \qquad m \leq -1 \tag{B.83}$$

where

$$\bar{\mathbf{A}}(k) = \begin{pmatrix} \mathbf{0} & \mathbf{1} \\ -\mathcal{A}_{-1}^{-1}\mathcal{A}_1 & -\mathcal{A}_{-1}^{-1}\mathcal{A}_0 \end{pmatrix}, \qquad \bar{\mathbf{G}}_m = \begin{pmatrix} \mathbf{0} \\ \mathcal{A}_{-1}^{-1}\hat{\mathbf{f}}_m \end{pmatrix} \tag{B.84}$$

We know that for the step problem and the given potential for $PbTiO_3$,

$$\bar{\mathbf{G}}_m = \mathbf{0} \qquad m < -\bar{M} \tag{B.85}$$

For $m \leq -\bar{M} - 1$,

$$\bar{\mathbf{Z}}_m = \bar{\mathbf{A}}^{-m-\bar{M}-1}\left(\bar{\mathbf{A}}^{\bar{M}}\bar{\mathbf{c}} + \bar{\mathbf{d}}\right) \tag{B.86}$$

where

$$\bar{\mathbf{c}} = \bar{\mathbf{Z}}_{-1} = \begin{pmatrix} \hat{\mathbf{Y}}_0(k) \\ \hat{\mathbf{Y}}_{-1}(k) \end{pmatrix}, \qquad \bar{\mathbf{d}} = \bar{\mathbf{A}}^{\bar{M}-1}\bar{\mathbf{G}}_{-1} + ... + \bar{\mathbf{G}}_{-\bar{M}} \tag{B.87}$$

Using the Jordan decomposition of $\bar{\mathbf{A}}$, i.e., $\bar{\mathbf{A}} = \bar{\mathbf{X}}\bar{\mathbf{\Lambda}}\bar{\mathbf{X}}^{-1}$ the above relation can be rewritten as

$$\bar{\mathbf{Z}}_m = \bar{\mathbf{X}}\bar{\mathbf{\Lambda}}^{-\bar{M}-1-m}\left(\bar{\mathbf{\Lambda}}^{\bar{M}}\bar{\mathbf{X}}^{-1}\bar{\mathbf{c}} + \bar{\mathbf{X}}^{-1}\bar{\mathbf{d}}\right) \tag{B.88}$$

where $\bar{\mathbf{X}}$ is the matrix of generalized eigenvectors. For SC potential it turns out that $\bar{M} = 2$ and hence,

$$\bar{\mathbf{Z}}_m = \bar{\mathbf{X}}\bar{\mathbf{\Lambda}}^{-m-3}\left(\bar{\mathbf{\Lambda}}^{2}\bar{\mathbf{X}}^{-1}\bar{\mathbf{c}} + \bar{\mathbf{X}}^{-1}\bar{\mathbf{d}}\right) \tag{B.89}$$

Boundedness equations ensure the following,

$$\|\hat{\mathbf{Y}}_m\| < \infty \qquad \text{as} \qquad m \to -\infty \tag{B.90}$$

and read,

$$\left(\bar{\mathbf{\Lambda}}^{2}\bar{\mathbf{X}}^{-1}\bar{\mathbf{c}}\right)_\star = -\left(\bar{\mathbf{X}}^{-1}\bar{\mathbf{d}}\right)_\star \tag{B.91}$$

These can be rewritten as

$$\bar{\mathcal{D}}_1(k)\hat{\mathbf{Y}}_{-1}(k) + \bar{\mathcal{D}}_2(k)\hat{\mathbf{Y}}_0(k) = \bar{\mathbf{F}}_D \tag{B.92}$$

Boundary equations are governing equations for $m = 0$,

$$\mathcal{A}_{-1}(k)\hat{\mathbf{Y}}_{-1}(k) + \mathcal{A}_0(k)\hat{\mathbf{Y}}_0(k) + \mathcal{A}_1(k)\hat{\mathbf{Y}}_1(k) = \hat{\mathbf{f}}_0(k) \tag{B.93}$$

The unknowns are $\hat{\mathbf{Y}}_{-1}(k)$, $\hat{\mathbf{Y}}_0(k)$ and $\hat{\mathbf{Y}}_1(k)$, which are determined using the boundary equations and boundedness equations at $\pm\infty$,

$$\begin{pmatrix} \mathbf{0} & \mathcal{D}_1(k) & \mathcal{D}_2(k) \\ \mathcal{A}_{-1}(k) & \mathcal{A}_0(k) & \mathcal{A}_1(k) \\ \bar{\mathcal{D}}_1(k) & \bar{\mathcal{D}}_2(k) & \mathbf{0} \end{pmatrix} \begin{pmatrix} \hat{\mathbf{Y}}_{-1}(k) \\ \hat{\mathbf{Y}}_0(k) \\ \hat{\mathbf{Y}}_1(k) \end{pmatrix} = \begin{pmatrix} \mathbf{F}_D \\ \hat{\mathbf{f}}_0(k) \\ \bar{\mathbf{F}}_D \end{pmatrix} \tag{B.94}$$

Solving the above system of linear equations gives us $\mathbf{c}$ and $\bar{\mathbf{c}}$. Thus the solution can be written

as

$$\bar{\mathbf{Z}}_m = \bar{\mathbf{X}}\bar{\mathbf{\Lambda}}^{-\bar{M}-m-1}\left(\bar{\mathbf{\Lambda}}^{\bar{M}}\bar{\mathbf{X}}^{-1}\bar{\mathbf{c}} + \bar{\mathbf{X}}^{-1}\bar{\mathbf{d}}\right) \qquad m \leq -3 \tag{B.95}$$

$$\bar{\mathbf{Z}}_{-2} = \bar{\mathbf{A}}\bar{\mathbf{c}} + \bar{\mathbf{G}}_{-1} \tag{B.96}$$

$$\mathbf{Z}_2 = \mathbf{A}\mathbf{c} + \mathbf{G}_1 \tag{B.97}$$

$$\mathbf{Z}_m = \mathbf{X}\mathbf{\Lambda}^{m-3}\left(\mathbf{\Lambda}^2\mathbf{X}^{-1}\mathbf{c} + \mathbf{X}^{-1}\mathbf{d}\right) \qquad m \geq 3 \tag{B.98}$$

ii) ***r=2:*** The governing ordinary difference equations are,

$$\mathcal{A}_{-2}(k)\hat{\mathbf{Y}}_{m-2}(k)+\mathcal{A}_{-1}(k)\hat{\mathbf{Y}}_{m-1}(k)+\mathcal{A}_0(k)\hat{\mathbf{Y}}_m(k)+\mathcal{A}_1(k)\hat{\mathbf{Y}}_{m+1}(k)+\mathcal{A}_2(k)\hat{\mathbf{Y}}_{m+2}(k) = \hat{\mathbf{f}}_m(k) \qquad m \in \mathbb{Z} \tag{B.99}$$

Define,

$$\mathbf{Z}_m = \begin{pmatrix} \hat{\mathbf{Y}}_{m-2}(k) \\ \hat{\mathbf{Y}}_{m-1}(k) \\ \hat{\mathbf{Y}}_m(k) \\ \hat{\mathbf{Y}}_{m+1}(k) \end{pmatrix}, \qquad \bar{\mathbf{Z}}_m = \begin{pmatrix} \hat{\mathbf{Y}}_{m+2}(k) \\ \hat{\mathbf{Y}}_{m+1}(k) \\ \hat{\mathbf{Y}}_m(k) \\ \hat{\mathbf{Y}}_{m-1}(k) \end{pmatrix} \tag{B.100}$$

Thus

$$\mathbf{Z}_{m+1} = \mathbf{A}\mathbf{Z}_m + \mathbf{G}_m \qquad m \geq 2 \tag{B.101}$$

$$\mathbf{Z}_{m-1} = \bar{\mathbf{A}}\bar{\mathbf{Z}}_m + \bar{\mathbf{G}}_m \qquad m \leq -2 \tag{B.102}$$

where

$$\mathbf{A}(k) = \begin{pmatrix} \mathbf{0} & \mathbf{1} & \mathbf{0} & \mathbf{0} \\ \mathbf{0} & \mathbf{0} & \mathbf{1} & \mathbf{0} \\ \mathbf{0} & \mathbf{0} & \mathbf{0} & \mathbf{1} \\ -\mathcal{A}_2(k)^{-1}\mathcal{A}_{-2}(k) & -\mathcal{A}_2(k)^{-1}\mathcal{A}_{-1}(k) & -\mathcal{A}_2(k)^{-1}\mathcal{A}_0(k) & -\mathcal{A}_2(k)^{-1}\mathcal{A}_1(k) \end{pmatrix},$$

$$\bar{\mathbf{A}}(k) = \begin{pmatrix} \mathbf{0} & \mathbf{1} & \mathbf{0} & \mathbf{0} \\ \mathbf{0} & \mathbf{0} & \mathbf{1} & \mathbf{0} \\ \mathbf{0} & \mathbf{0} & \mathbf{0} & \mathbf{1} \\ -\mathcal{A}_{-2}(k)^{-1}\mathcal{A}_2(k) & -\mathcal{A}_{-2}(k)^{-1}\mathcal{A}_1(k) & -\mathcal{A}_{-2}(k)^{-1}\mathcal{A}_0(k) & -\mathcal{A}_{-2}(k)^{-1}\mathcal{A}_{-1}(k) \end{pmatrix},$$

$$\mathbf{G}_m = \begin{pmatrix} \mathbf{0} \\ \mathbf{0} \\ \mathbf{0} \\ \mathcal{A}_2(k)^{-1}\hat{\mathbf{f}}_m(k) \end{pmatrix}, \qquad \bar{\mathbf{G}}_m = \begin{pmatrix} \mathbf{0} \\ \mathbf{0} \\ \mathbf{0} \\ \mathcal{A}_{-2}(k)^{-1}\hat{\mathbf{f}}_m(k) \end{pmatrix}$$

It can be easily shown that

$$\mathbf{Z}_m = \mathbf{A}^{m-M-1}\left(\mathbf{A}^{M-1}\mathbf{c}+\mathbf{d}\right) = \mathbf{X}\mathbf{\Lambda}^{m-M-1}\left(\mathbf{\Lambda}^{M-1}\mathbf{X}^{-1}\mathbf{c}+\mathbf{X}^{-1}\mathbf{d}\right) \qquad m \geq M+1$$
$$\bar{\mathbf{Z}}_m = \bar{\mathbf{A}}^{-m-\bar{M}-1}\left(\bar{\mathbf{A}}^{\bar{M}-1}\bar{\mathbf{c}}+\bar{\mathbf{d}}\right) = \bar{\mathbf{X}}\bar{\mathbf{\Lambda}}^{m-\bar{M}-1}\left(\bar{\mathbf{\Lambda}}^{\bar{M}-1}\bar{\mathbf{X}}^{-1}\bar{\mathbf{c}}+\bar{\mathbf{X}}^{-1}\bar{\mathbf{d}}\right) \qquad m \leq -\bar{M}-1$$

where

$$\mathbf{c} = \mathbf{Z}_2 = \begin{pmatrix} \hat{\mathbf{Y}}_0(k) \\ \hat{\mathbf{Y}}_1(k) \\ \hat{\mathbf{Y}}_2(k) \\ \hat{\mathbf{Y}}_3(k) \end{pmatrix}, \qquad \mathbf{d} = \mathbf{A}^{M-2}\mathbf{G}_2 + ... + \mathbf{G}_M \tag{B.103}$$

$$\bar{\mathbf{c}} = \bar{\mathbf{Z}}_{-2} = \begin{pmatrix} \hat{\mathbf{Y}}_0(k) \\ \hat{\mathbf{Y}}_{-1}(k) \\ \hat{\mathbf{Y}}_{-2}(k) \\ \hat{\mathbf{Y}}_{-3}(k) \end{pmatrix}, \qquad \bar{\mathbf{d}} = \bar{\mathbf{A}}^{\bar{M}-2}\bar{\mathbf{G}}_{-2} + ... + \bar{\mathbf{G}}_{-\bar{M}} \tag{B.104}$$

Boundedness equations are,

$$\left(\mathbf{\Lambda}^{M-1}\mathbf{X}^{-1}\mathbf{c}\right)_\star = -\left(\mathbf{X}^{-1}\mathbf{d}\right)_\star \tag{B.105}$$
$$\left(\bar{\mathbf{\Lambda}}^{\bar{M}-1}\bar{\mathbf{X}}^{-1}\bar{\mathbf{c}}\right)_\star = -\left(\bar{\mathbf{X}}^{-1}\bar{\mathbf{d}}\right)_\star \tag{B.106}$$

Or,

$$\mathcal{D}_1(k)\hat{\mathbf{Y}}_0(k) + \mathcal{D}_2(k)\hat{\mathbf{Y}}_1(k) + \mathcal{D}_3(k)\hat{\mathbf{Y}}_2(k) + \mathcal{D}_4(k)\hat{\mathbf{Y}}_3(k) = \mathbf{F}_D \tag{B.107}$$
$$\bar{\mathcal{D}}_1(k)\hat{\mathbf{Y}}_{-3}(k) + \bar{\mathcal{D}}_2(k)\hat{\mathbf{Y}}_{-2}(k) + \bar{\mathcal{D}}_3(k)\hat{\mathbf{Y}}_{-1}(k) + \bar{\mathcal{D}}_4(k)\hat{\mathbf{Y}}_0(k) = \bar{\mathbf{F}}_D \tag{B.108}$$

Boundary equations are the governing equations for unit cells $m = -1, 0, 1$,

$$m=-1: \quad \mathcal{A}_{-2}(k)\hat{\mathbf{Y}}_{-3}(k) + \mathcal{A}_{-1}(k)\hat{\mathbf{Y}}_{-2}(k) + \mathcal{A}_0(k)\hat{\mathbf{Y}}_{-1}(k) + \mathcal{A}_1(k)\hat{\mathbf{Y}}_0(k) + \mathcal{A}_2(k)\hat{\mathbf{Y}}_1(k) = \hat{\mathbf{f}}_{-1}(k)$$
$$m=0: \quad \mathcal{A}_{-2}(k)\hat{\mathbf{Y}}_{-2}(k) + \mathcal{A}_{-1}(k)\hat{\mathbf{Y}}_{-1}(k) + \mathcal{A}_0(k)\hat{\mathbf{Y}}_0(k) + \mathcal{A}_1(k)\hat{\mathbf{Y}}_1(k) + \mathcal{A}_2(k)\hat{\mathbf{Y}}_2(k) = \hat{\mathbf{f}}_0(k)$$
$$m=1: \quad \mathcal{A}_{-2}(k)\hat{\mathbf{Y}}_{-1}(k) + \mathcal{A}_{-1}(k)\hat{\mathbf{Y}}_0(k) + \mathcal{A}_0(k)\hat{\mathbf{Y}}_1(k) + \mathcal{A}_1(k)\hat{\mathbf{Y}}_2(k) + \mathcal{A}_2(k)\hat{\mathbf{Y}}_3(k) = \hat{\mathbf{f}}_1(k)$$

Thus

$$\begin{pmatrix} \mathbf{0} & \mathbf{0} & \mathbf{0} & \mathcal{D}_1(k) & \mathcal{D}_2(k) & \mathcal{D}_3(k) & \mathcal{D}_4(k) \\ \mathcal{A}_{-2}(k) & \mathcal{A}_{-1}(k) & \mathcal{A}_0(k) & \mathcal{A}_1(k) & \mathcal{A}_2(k) & \mathbf{0} & \mathbf{0} \\ \mathbf{0} & \mathcal{A}_{-2}(k) & \mathcal{A}_{-1}(k) & \mathcal{A}_0(k) & \mathcal{A}_1(k) & \mathcal{A}_2(k) & \mathbf{0} \\ \mathbf{0} & \mathbf{0} & \mathcal{A}_{-2}(k) & \mathcal{A}_{-1}(k) & \mathcal{A}_0(k) & \mathcal{A}_1(k) & \mathcal{A}_2(k) \\ \bar{\mathcal{D}}_1(k) & \bar{\mathcal{D}}_2(k) & \bar{\mathcal{D}}_3(k) & \bar{\mathcal{D}}_4(k) & \mathbf{0} & \mathbf{0} & \mathbf{0} \end{pmatrix} \begin{pmatrix} \hat{\mathbf{Y}}_{-3}(k) \\ \hat{\mathbf{Y}}_{-2}(k) \\ \hat{\mathbf{Y}}_{-1}(k) \\ \hat{\mathbf{Y}}_0(k) \\ \hat{\mathbf{Y}}_1(k) \\ \hat{\mathbf{Y}}_2(k) \\ \hat{\mathbf{Y}}_3(k) \end{pmatrix} = \begin{pmatrix} \mathbf{F}_D \\ \hat{\mathbf{f}}_{-1}(k) \\ \hat{\mathbf{f}}_0(k) \\ \hat{\mathbf{f}}_1(k) \\ \bar{\mathbf{F}}_D \end{pmatrix} \tag{B.109}$$

Solving the above system of equations gives us $\mathbf{c}$ and $\bar{\mathbf{c}}$. For $M = \bar{M} = 2$ the solution can be written as

$$\bar{\mathbf{Z}}_m = \bar{\mathbf{X}}\bar{\mathbf{\Lambda}}^{m-3}\left(\bar{\mathbf{\Lambda}}\bar{\mathbf{X}}^{-1}\bar{\mathbf{c}} + \bar{\mathbf{X}}^{-1}\bar{\mathbf{d}}\right) \qquad m \leq -3 \tag{B.110}$$

$$\mathbf{Z}_m = \mathbf{X}\mathbf{\Lambda}^{m-3}\left(\mathbf{\Lambda}\mathbf{X}^{-1}\mathbf{c} + \mathbf{X}^{-1}\mathbf{d}\right) \qquad m \geq 3 \tag{B.111}$$

After having $\hat{\mathbf{Y}}_m(k)$, the solution $\mathbf{X}_{mn}$ can be recovered by applying the inverse DFT in n-direction,

$$\mathbf{X}_{mn} = \frac{1}{2\pi}\int_{-\pi}^{\pi} e^{-ink}\hat{\mathbf{Y}}_m(k)dk \tag{B.112}$$

B.6 Ill-Conditioned Problems

A problem is well-posed in the sense of Hadamard if a solution exists, it is unique and depends continuously on the data of the problem. However, this is not enough in numerical problems when one would like to see small errors in the solution due to small errors in the parameters of the problem. In a *well-conditioned* problem, small errors in the data cause small errors in the solution. If small errors of the data causes large errors in the solution the problem is called *ill-conditioned*.

Definition 34. *Let X and Y be normed spaces with the norm $\|.\|$ and $L : X \to Y$ a bounded linear transformation with a bounded inverse $L^{-1} : Y \to X$. The condition number of L is defined by*

$$\kappa(L) = \|L\|\|L^{-1}\| \tag{B.113}$$

Note that $\kappa(L) \geq 1$. Ill-conditioned problems are those with very large condition numbers, i.e., $\kappa(L) \gg 1$. Equivalently, an ill-conditioned problem has a wide spectrum.

In our lattice statics model, we need to calculate matrix powers of a highly ill-conditioned matrix $\mathcal{A}$. $\mathcal{A}$ is full-rank but multiplying it by itself a few times, it loses rank due to numerical round-off

errors. Here we explain how $\mathcal{A}^n$ should be calculated. We know that

$$\mathcal{A} = \mathbf{X}\mathbf{\Lambda}\mathbf{X}^{-1}, \qquad \mathbf{\Lambda} = \begin{pmatrix} \mathbf{\Lambda}_1 & \mathbf{0} \\ \mathbf{0} & \mathbf{\Lambda}_2 \end{pmatrix} \tag{B.114}$$

where $\mathbf{\Lambda}_1$ and $\mathbf{\Lambda}_2$ are the diagonal matrices of eigenvalues with modulus greater than or equal to one and less that one, respectively. We also know that

$$\mathcal{A}^n = \mathbf{X}\mathbf{\Lambda}^n\mathbf{X}^{-1} = \begin{pmatrix} \mathbf{X}_{11} & \mathbf{X}_{12} \\ \mathbf{X}_{21} & \mathbf{X}_{22} \end{pmatrix} \begin{pmatrix} \mathbf{\Lambda}_1 & \mathbf{0} \\ \mathbf{0} & \mathbf{\Lambda}_2 \end{pmatrix} \begin{pmatrix} \widetilde{\mathbf{X}}_{11} & \widetilde{\mathbf{X}}_{12} \\ \widetilde{\mathbf{X}}_{21} & \widetilde{\mathbf{X}}_{22} \end{pmatrix} \tag{B.115}$$

This can be rewritten as

$$\begin{aligned} \mathcal{A}^n &= \begin{pmatrix} \mathbf{X}_{11}\mathbf{\Lambda}_1^n\widetilde{\mathbf{X}}_{11} & \mathbf{X}_{11}\mathbf{\Lambda}_1^n\widetilde{\mathbf{X}}_{12} \\ \mathbf{X}_{21}\mathbf{\Lambda}_1^n\widetilde{\mathbf{X}}_{11} & \mathbf{X}_{21}\mathbf{\Lambda}_1^n\widetilde{\mathbf{X}}_{12} \end{pmatrix} + \frac{1}{s^n} \begin{pmatrix} \mathbf{X}_{12}(s\mathbf{\Lambda}_2)^n\widetilde{\mathbf{X}}_{21} & \mathbf{X}_{12}(s\mathbf{\Lambda}_2)^n\widetilde{\mathbf{X}}_{22} \\ \mathbf{X}_{22}(s\mathbf{\Lambda}_2)^n\widetilde{\mathbf{X}}_{21} & \mathbf{X}_{22}(s\mathbf{\Lambda}_2)^n\widetilde{\mathbf{X}}_{22} \end{pmatrix} \\ &= \mathcal{A}n1 + \frac{1}{s^n}\mathcal{A}n2(s) \end{aligned} \tag{B.116}$$

where $s = \frac{1}{|\lambda_{\min}|}$ is a scaling factor.

B.7 A 2-D Lattice Problem

In order to develop some intuition, we have studied a two-dimensional lattice under different loading conditions. This would give us an idea on what one should expect in the complex lattice of ABO_3. This example also helps us to check and compare different methods of solving the governing ordinary or partial difference equations.

Let us consider a two-dimensional lattice with lattice parameters a and c and look at the governing equilibrium equations for different ranges of interactions. The simplicity of this 2-D model will allow us to see the reason for degeneracy of a system of difference equations representing a discrete physical system very clearly. We assume interactions of up to fifth nearest neighbors and the linear spring connecting the jth nearest neighbors has stiffness k_j. The simple lattice is indexed by $(m, n) \in \mathbb{Z}\times\mathbb{Z}$. Consider two system of forces I and II. In system I we consider a boundary line ℓ (wall) in such a tetragonal lattice and assume that forces of magnitude 1 are applied to atoms which are one lattice parameter away from the wall ℓ as shown Fig. B.1. Note that this problem has translational symmetry in y-direction. This means that all the atoms lying on the same line parallel to the wall have the same displacements. Here n is the atomic index of the line which is na away from ℓ. We assume that the atoms on the wall are fixed, i.e., $u_0 = v_0 = 0$. The boundary equations are the equations governing atoms with index $n = 1$ (two equations). The associated matrix of the auxiliary

first-order equation has two eigenvalues $\lambda_1,\ \lambda_2$ with modulus larger than one and two eigenvalues $\lambda_7,\ \lambda_8$ with modulus less than one. The other eigenvalue is $\lambda = 1$ with multiplicity four. The following are the global (interior) equilibrium equations,

$$\mathbf{A}_{-2}\mathbf{X}_{n-2} + \mathbf{A}_{-1}\mathbf{X}_{n-1} + \mathbf{A}_0\mathbf{X}_n + \mathbf{A}_1\mathbf{X}_{n+1} + \mathbf{A}_2\mathbf{X}_{n+2} = \mathbf{F}_n \qquad n \geq 2 \tag{B.117}$$

where

$$\mathbf{X}_n = \begin{pmatrix} u_n \\ v_n \end{pmatrix} \in \mathbb{R}^2$$

and $u_n,\ v_n$ are displacements in the direction of x and y axes, respectively. The matrices $\mathbf{A}_i,\ i = -2, ..., 2$ have the following form,

$$\begin{aligned}
\mathbf{A}_{-2} = \mathbf{A}_2 &= \begin{pmatrix} k_3 + 2(\cos\alpha)^2 k_4 + 2(\cos\theta)^2 k_5 & 0 \\ 0 & 2(\sin\alpha)^2 k_4 + 2(\sin\theta)^2 k_5 \end{pmatrix} \\
\mathbf{A}_{-1} = \mathbf{A}_1 &= \begin{pmatrix} k_1 + 2(\cos\theta)^2 k_2 + 2(\sin\alpha)^2 k_4 & 0 \\ 0 & 2(\sin\theta)^2 k_2 + 2(\cos\alpha)^2 k_4 \end{pmatrix} \\
\mathbf{A}_0 &= \begin{pmatrix} -2\big[k_1 + 2(\cos\theta)^2 k_2 + k_3 + 2k_4 + 2(\cos\theta)^2 k_5\big] & 0 \\ 0 & -2\big[2(\sin\theta)^2 k_2 + 2k_4 + 2(\sin\theta)^2 k_5\big] \end{pmatrix}
\end{aligned}$$

where $\theta = \tan^{-1}\left(\frac{c}{a}\right)$ and $\alpha = \tan^{-1}\left(\frac{c}{2a}\right)$. Note that $\det(\mathbf{A}_2) = 0$ if $k_4 = 0$. This means that if we consider only the first three nearest neighbors then the resulting system of difference equations cannot be transformed into an auxiliary first-order system. Singularity of $\mathbf{A}_5$ (and $\mathbf{A}_1$) physically means that there are zero-energy modes involved in the problem. Obviously, it would be more convenient to work with systems of difference equations that are transformable to a first-order system. This means that for a given order of governing difference equations we should choose the maximum range of interaction.[‡] Note also that

$$\mathbf{A}_{-2} + \mathbf{A}_{-1} + \mathbf{A}_0 + \mathbf{A}_1 + \mathbf{A}_2 = \mathbf{0} \tag{B.118}$$

which reflects the translation invariance of the governing equations.

The solution can be written as

$$\mathbf{Y}_n = \mathbf{A}^n\mathbf{c} \tag{B.119}$$

[‡]For ABO_3 multi-lattice we studied defects with 1-D and 2-D symmetry reductions. In the step problem we used DFT and did not need to worry about degeneracy. For domain walls we considered interaction of a representative unit cell n with representative unit cells $n-m, ..., n+m$. Interaction of the unit cell n with representative unit cell $n+m$ is interaction of a unit cell n with all the members of the equivalence class $n+m$ and this is why the matrix $\mathcal{A}_{n+m}$ was not singular. The numerical tests confirmed this.

where

$$\mathbf{c} = \mathbf{Y}_2 = \begin{pmatrix} c_1 \\ c_2 \\ c_3 \\ c_4 \\ c_5 \\ c_6 \\ c_7 \\ c_8 \end{pmatrix} = \begin{pmatrix} u_0 \\ v_0 \\ u_1 \\ v_1 \\ u_2 \\ v_2 \\ u_3 \\ v_3 \end{pmatrix} \tag{B.120}$$

We now require the solutions to be bounded at infinity.

We assume that $u_0 = v_0 = 0$. The other two equations come from equilibrium equations of atoms $n = 1$ (boundary equations), which have the only nonzero forcing term. It is seen that the number of equations and unknowns are equal and this problem is well-posed.

One should note that in this specific problem the governing equations of u_n and v_n are uncoupled and it would be instructive to solve the two equations separately and see the difference in the solution technique with the matrix method. The governing equations for u_n and v_n are,

$$u_{n+2} + \alpha u_{n+1} - 2(1+\alpha)u_n + \alpha u_{n-1} + u_{n-2} = 0 \qquad |n| \geq 2 \tag{B.121}$$

$$v_{n+2} + \beta u_{n+1} - 2(1+\beta)v_n + \beta v_{n-1} + v_{n-2} = 0 \qquad |n| \geq 2 \tag{B.122}$$

where

$$\alpha = \frac{k_1 + 2(\cos\theta)^2 k_2 + 2(\sin\alpha)^2 k_4}{k_3 + 2(\cos\alpha)^2 k_4 + 2(\cos\theta)^2 k_5}, \quad \beta = \frac{2(\sin\theta)^2 k_2 + 2(\cos\alpha)^2 k_4}{2(\sin\alpha)^2 k_4 + 2(\sin\theta)^2 k_5} \tag{B.123}$$

The solutions for u_n and v_n have the following form,

$$u_n = c_1 + c_2 n + c_3 \lambda_1^n + c_4 \lambda_2^n \qquad n \geq 0, \quad |\lambda_1| < 1, |\lambda_2| > 1 \tag{B.124}$$

$$u_n = c_1' + c_2' n + c_3' \mu_1^n + c_4' \mu_2^n \qquad n \geq 0, \quad |\mu_1| < 1, |\mu_2| > 1 \tag{B.125}$$

Boundedness at infinity implies that

$$c_2 = c_4 = c_2' = c_4' = 0 \tag{B.126}$$

The condition $u_0 = v_0 = 0$ yields

$$u_n = c_1\big(1 - \lambda_1^n\big), \quad v_n = c_1'\big(1 - \mu_1^n\big) \tag{B.127}$$

There is no loading in y-direction and hence $c_1' = 0$, i.e., $v_n = 0, \ \forall n$. The boundary equation for u_n

(assumping that $u_0 = 0$ and $u_{-n} = -u_n$) gives us

$$c_1' = \frac{1}{1 - \lambda_1^3 + \alpha(1 - \lambda_1^2) - (3 + 2\alpha)(1 - \lambda_1)} \tag{B.128}$$

Suppose $k_1 = 1.0,\ k_2 = \frac{1}{2}k_1,\ k_3 = \frac{1}{3}k_1,\ k_4 = \frac{1}{4}k_1,\ k_5 = \frac{1}{5}K_1,\ a = c = 1.0$. The solution is shown in Fig. B.1.a.

Discrete Fourier Transform Method. For the sake of illustration, we first solve the governing equation of u_n using DFT. The one-dimensional discrete Fourier transform is a transformation between sequences in $\mathbb{R}$ and functions defined on $\mathbb{R}$. Given a sequence $\{u_n\}_{n=-\infty}^{\infty}$, its DFT is defined as

$$\widehat{u_n}(k) = \sum_{n=-\infty}^{\infty} u_n e^{ink} \tag{B.129}$$

Having the DFT of a sequence the inverse transform is

$$u_n = \frac{1}{2\pi} \int_{-\pi}^{\pi} \widehat{u_n}(k) e^{ink} dk \qquad \forall n \in \mathbb{Z} \tag{B.130}$$

To be able to use DFT the governing equations should be written for the whole reduced chain of atoms. The governing equation for u_n reads,

$$u_{n+2} + \alpha u_{n+1} - 2(1 + \alpha)u_n + \alpha u_{n-1} + u_{n-2} = f_n \qquad n \in \mathbb{Z} \tag{B.131}$$

where

$$f_1 = -f_{-1} = f, f_n = 0 \quad \forall n \notin \{-1, 1\} \tag{B.132}$$

This means that, $\widehat{f_n}(k) = f(e^{ik} - e^{-ik}) = 2if \sin k$. Taking DFT from both sides of Eq. (B.131) and using the shifting property of DFT we have

$$\left[e^{2ik} + \alpha e^{ik} - 2(1 + \alpha) + \alpha e^{-ik} + e^{-2ik}\right] \widehat{u_n}(k) = 2if \sin k \tag{B.133}$$

Thus

$$u_n = \frac{f}{2\pi} \int_{-\pi}^{\pi} \frac{i \sin k e^{-ink}}{\cos(2k) + \alpha \cos k - (1 + \alpha)} dk \tag{B.134}$$

Note that $u_0 = 0$. It may happen that for convergence one has to add a rigid translation to the solution (Gallego and Ortiz, 1993). However, here because of the symmetry of forces there is no singularity. For the matrix equations one should similarly consider the governing equations for the whole space. Taking the DFT from the matrix equations (note that DFT of a vector is the vector

of the DFT of the components) one gets,

$$\mathcal{A}(k)\widehat{\mathbf{X}_n}(k) = \widehat{\mathbf{F}_n}(k) \tag{B.135}$$

where

$$\mathcal{A}(k) = e^{2ink}\mathbf{A}_{-2} + e^{ink}\mathbf{A}_{-1} + \mathbf{A}_0 + e^{-ink}\mathbf{A}_1 + e^{-2ink}\mathbf{A}_2, \qquad \widehat{\mathbf{F}_n}(k) = \begin{pmatrix} 2if\sin k \\ 0 \end{pmatrix} \tag{B.136}$$

Thus

$$\mathbf{X}_n = \frac{f}{2\pi}\int_{-\pi}^{\pi} \mathcal{A}^{-1}(k)\widehat{\mathbf{F}_n}(k)e^{-ink}dk \tag{B.137}$$

For the same lattice let us consider only the first and second nearest neighbor interactions. But this time let us not assume any symmetry along the y-axis. The governing system of partial difference equations has the following form,

$$\sum_{\alpha=-1}^{\alpha=1}\sum_{\beta=-1}^{\beta=1} \mathbf{A}_{\alpha\beta}\mathbf{X}_{m+\alpha,n+\beta} = \mathbf{F}_{mn} \tag{B.138}$$

where

$$\mathbf{A}_{-1,-1} = \begin{pmatrix} k_2C^2 & k_2CS \\ k_2CS & k_2S^2 \end{pmatrix}, \quad \mathbf{A}_{-1,0} = \begin{pmatrix} k_1 & 0 \\ 0 & 0 \end{pmatrix}, \quad \mathbf{A}_{-1,1} = \begin{pmatrix} k_2C^2 & -k_2CS \\ -k_2CS & k_2S^2 \end{pmatrix}$$

$$\mathbf{A}_{0,-1} = \begin{pmatrix} 0 & 0 \\ 0 & k_1 \end{pmatrix}, \quad \mathbf{A}_{0,0} = \begin{pmatrix} -2k_1 - 4k_2C^2 & 0 \\ 0 & -2k_1 - 4k_2S^2 \end{pmatrix}, \quad \mathbf{A}_{0,1} = \begin{pmatrix} k_2C^2 & -k_2CS \\ -k_2CS & k_2S^2 \end{pmatrix}$$

$$\mathbf{A}_{1,-1} = \begin{pmatrix} k_2C^2 & -k_2CS \\ -k_2CS & k_2S^2 \end{pmatrix}, \quad \mathbf{A}_{1,0} = \begin{pmatrix} k_1 & 0 \\ 0 & 0 \end{pmatrix}, \quad \mathbf{A}_{1,1} = \begin{pmatrix} k_2C^2 & k_2CS \\ k_2CS & k_2S^2 \end{pmatrix}$$

Consider loading system II, which is a discrete dipole. One would expect to see a localized discrete displacement field. Because of symmetry only the quadrant $\{(m,n) : m,n \geq 0\}$ needs to be considered. The solutions are shown in Fig. B.1.b. It is seen that the discrete displacement field is localized, though with a fairly long tail. This is the qualitative behavior we expect to see in the step problem with localized forces.

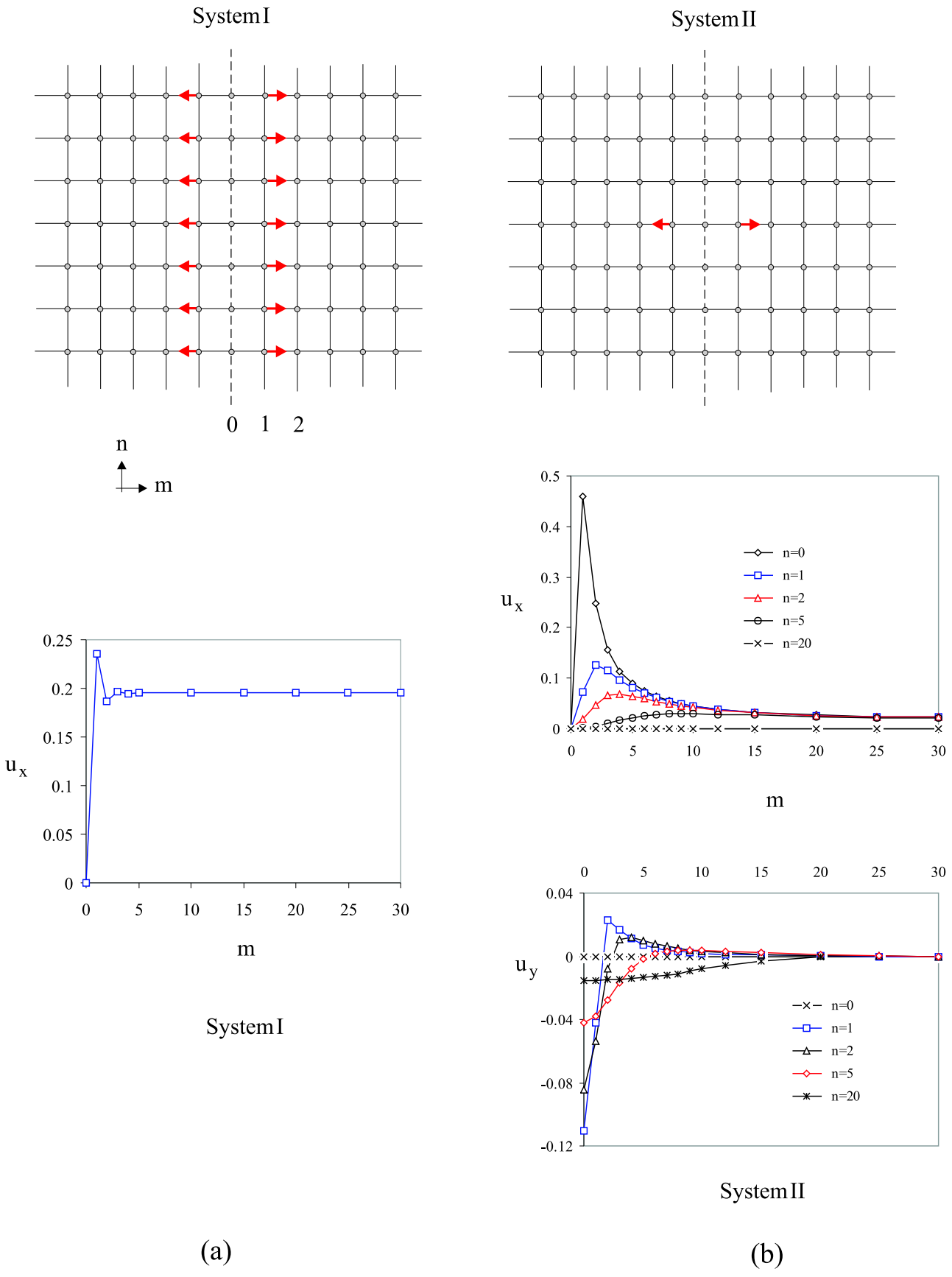

Figure B.1: (a) Discrete displacement field of the 2-D lattice under loading system I., (b) Discrete displacement field of the 2-D lattice under the discrete dipole.

Bibliography

Agarwal, R. P. (2000). *Difference Equations and Inequalities*. Marcel Dekker.

Arlt, G. and Sasko, P. (1980). Domain configuration and equilibrium size of domains in $BaTiO_3$ ceramics. *Journal of Applied Physics*, 51(9):4956–4960.

Babŭska, I. (1959). The Fourier transform in the theory of difference equations and its applications. *Archiwum Mechaniki Stosowanej*, 11(4):349–381.

Babŭska, I., Vitásek, E., and Kroupa, F. (1960). Some applications of the discrete Fourier transform to problems of crystal lattice deformation, i,ii. *Czechoslovak Journal of Physics B*, 10:419–427, 488–504.

Bellman, R. (1961). *A Brief Introduction to Theta Functions*. Holt, Rinehart and Winston.

Benedek, R. (1978). Lattice statics calculation of surface relaxation in metals. *Journal of Physics F: Metal Physics*, 8(6):1119–1129.

Benedetto, J. J. (1997). *Harmonic Analysis and Applications*. CRC Press.

Born, M. and Huang, K. (1988). *Dynamical Theory of Crystal Lattices*. Oxford.

Boyer, L. L. and Hardy, J. R. (1971). Lattice statics applied to screw dislocations in cubic metals. *Philosophical Magazine*, 24:647–671.

Briggs, W. L. and Hendon, V. E. (1995). *The DFT An Owner's Manual for the Discrete Fourier Transform*. SIAM.

Bullough, R. and Tewary, V. K. (1979). Lattice theory of dislocations. In *Dislocations in Solids, ed. F. R. N. Nabarro, North-Holland, Amsterdam*, volume 2.

Burcsu, E., Ravichandran, G., and Bhattacharya, K. (2000). Large strain electrostrictive actuation in Barium Titanate. *Applied Physics Letters*, 77(11):1698–1700.

Burcsu, E., Ravichandran, G., and Bhattacharya, K. (2004). Large electrostrictive actuation of Barium Titanate single crystals. *Journal of the Mechanics and Physics of Solids*, 52:823–846.

Burkert, U. and Allinger, N. L. (1982). *Molecular Mechanics*. American Chemical Society.

Cao, W. and Cross, L. E. (1991). Theory of tetragonal twin structures in ferroelectric perovskites with a first-order phase transition. *Physical Review B*, 44(1):5–12.

Carlsson, A. E. (1990). Beyond pair potentials in elemental transition metals and semiconductors. *Solid State Physics*, 43:1–91.

Cohen, R. and Krakauer, H. (1992). Electronic structure studies of the differences in ferroelectric behavior of $BaTiO_3$ and $PbTiO_3$. *Ferroelectrics*, 136:65–83.

Damjanovic, D. (1998). Ferroelectric, dielectric and piezoelectric properties of ferroelectric thin films and ceramics. *Reports on Progress in Physics*, 61(4):1267–1324.

De Boor, C., Holling, K., and Riemenschneider, S. (1989). Fundamental solutions of multivariate difference equations. *Journal of American Mathematical Society*, 111:403–415.

de Leeuw, S. W., Perram, J. W., and Smith, E. R. (1980). Simulation of electrostatic systems in periodic boundary conditions. i. Lattice sums and dielectric constants. *Procedeengs of the Royal Society of London A*, 373:27–56.

Deem, M. W., Newsam, J. M., and Sinha, S. K. (1990). The $h = 0$ term in Coulomb sums by the Ewald transformation. *Journal of Physical Chemistry*, 94:8356–8359.

Dennis, J. E. and Schnabel, R. B. (1996). *Numerical Methods for Unconstrained Optimization and Nonlinear Equations*. SIAM.

Devonshire, A. F. (1949a). Theory of Barium Titanate: Part 1. *Phylosophical Magazine*, 40(309):1040–1063.

Devonshire, A. F. (1949b). Theory of Barium Titanate: Part 2. *Phylosophical Magazine*, 42(333):1065–1079.

Devonshire, A. F. (1954). Theory of ferroelectrics. *Advances in Physics*, 3(10):85–130.

Dick, B. G. and Overhauser, A. W. (1964). Theory of the dielectric constants of alkali halide crystals. *Physical Review*, 112:90–103.

Elaydi, S. N. (1996). *An Introduction to Difference Equations*. Springer.

Eshelby, J. D. (1951). The force on an elstic singularity. *Philosophical Transactions*, A244:87–112.

Eshelby, J. D. (1975). The elstic energy-momentum tensor. *Journal of Elasticity*, 5(3-4):321–335.

Esterling, D. M. (1978). Modified lattice-statics approach to dislocation calculations i. Formalism. *Journal of Applied Physics*, 49(7):3954–3959.

Esterling, D. M. and Moriarty, J. A. (1978). Modified lattice-statics approach to dislocation calculations ii. Application. *Journal of Applied Physics*, 49(7):3960–3966.

Evans, G. A. and Webster, J. R. (1999). A comparison of some methods for the evaluation of highly oscillatory integrals. *Journal of Computational and Applied Mathematics*, 112:55–69.

Evjen, H. M. (1932). On the stability of certain heteropolar crystals. *Physical Review*, 39:675–687.

Ewald, P. P. (1921). Die berechnung optischer gitterpotentiale. *Annalen der Physik*, 64:253–287.

Flocken, J. W. (1972). Modified lattice-statics approach to point defect calculations. *Physical Review B*, 6(4):1176–1181.

Flocken, J. W. and Hardy, J. R. (1969). Application of the method of lattice statics to vacancies in Na, K, Rb, and Cs. *Physical Review*, 117(3):1054–1062.

Flocken, J. W. and Hardy, J. R. (1970). The Method of Lattice Statics. In Eyring, H. and Henderson, D., editors, *Fundamental Aspects of Dislocation Theory*, volume 1 of *J. A. Simmons and R. de Wit and R. Bullough*, pages 219–245.

Floquet, N., Valot, C. M., Mesnier, M. T., Niepce, J. C., Normand, L., T. A., and Kilaas, R. (1997). Ferroelectric domain walls in $BaTiO_3$: fingerprints in XRPD diagrams and quantitative HRTEM image analysis. *Journal of Physics III France*, 7:1105–1128.

Foeth, M., Sfera, A., Stadelmann, P., and Buffat, P.-A. (1999). A comparison of hrem and weak beam transmission electron microscopy for the quantitative measurement of the thickness of ferroelectric domain walls. *Japanese Society of Electron Microscopy*, 48(6):717–723.

Fraser, L. M., Foulkes, W. M., Rajagopal, G., Needs, R. J., Kenny, S. D., and Williamson, A. J. (1996). Finite-size effects and coulombic interactions in quantum Monte Carlo calculations for homogeneous systems with periodic boundary conditions. *Physical Review B*, 53(4):1814–1832.

Gale, J. D. (1996). Empirical potential derivation for ionic materials. *Philosophical Magazine B*, 73(1):3–19.

Gale, J. D. (1997). GULP: A computer program for the symmetry-adapted simulation of solids. *Journal of Chemical Society, Faraday Transactions*, 93(4):629–637.

Gale, J. D. and Rohl, A. L. (2003). The general utility lattice program (GULP). *Molecular Simmulation*, 29(5):291–341.

Gallego, R. and Ortiz, M. (1993). A harmonic/anharmonic energy partition method for lattice statics computations. *Modelling and Simulation in Materials Sceince and Engineering*, 1:417–436.

Gazis, D. C. and Wallis, R. F. (1964). Surface tension and surface modes in semi-infinite lattices. *Surface Science*, 3:19–32.

Goddard, W. A., Zhang, Q., Uludogan, M., Strachan, A., and Cagin, T. (2003). The ReaxFF polarizable reactive force fields for molecular dynamics simulation of ferroelectrics. *Physical Review B*.

Green, A. E. and Rivilin, R. S. (1964). On cauchy's equations of motion. *ZAMP*, 15:290–293.

Harris, F. E. (1975). Hartree-Fock Studies of Electronic Structures of Crystalline Solids. In Eyring, H. and Henderson, D., editors, *Theoretical Chemistry Advances and Perspectives*.

Hsieh, C. and Thomson, J. (1973). Lattice theory of fracture and crack creep. *Journal of Applied Physics*, 44:2051–2063.

Hu, X.-L. and Chen, L.-Q. (1997). Computer simulations of 90^0 ferroelectric domain formation in two-dimensions. *Materials Science and Engineering*, A238:182–191.

Hu, X.-L. and Chen, L.-Q. (1998). Three-dimensional computer simulations of ferroelectric domain formation. *Journal of American Ceramics Society*, 81(3):492–500.

Hu, Y. H., Chan, H. M., Wen, Z. X., and Harmer, M. P. (1986). Scanning electron microscopy and transmission electron microscopy study of ferroelectric domains in doped $BaTiO_3$. *Journal of American Ceramic Society*, 69(8):594–602.

Huang, X. R., Hu, X. B., Jiang, S. S., and Feng, D. (1997). Theoretical model of 180^0 domain-wall structures and their transformation in ferroelectric perovskites. *Physical Review B*, 55(9):5534–5537.

James, R. D. (2002). Configurational forces in magnetism with application to the dynamics of a small-scale ferromagnetic shape memory cantilever. *Continuum Mechanics and Thermodynamics*, 14:55–86.

Jona, F. and Shirane, G. (1993). *Ferroelectric Crystals*. Dover.

Kadets, V. M. and Kadets, M. I. (1985). *Rearrangements of Series in Banach Spaces*. American Mathematical Society.

Kamlah, M. (2001). Ferroelectric and ferroelastic piezoceramics – modeling of electromechanical hysteresis phenomena. *Continuum Mechanics and Thermodynamics*, 13:219–268.

Kanazaki, H. (1957). Point defects in face-centered cubic lattice-i distortion around defects. *Journal of Physics and Chemistry of Solids*, 2:24–36.

Kanzig, W. (1957). Ferroelectrics and antiferroelectrics. *Solid State Physics-Advances in Research and Applications*, 4:1–197.

Katznelson, Y. (2003). *An Introduction to Harmonic Analysis*. Dover.

Kinase, W. (1955). On interactions among ions of a $BaTiO_3$ crystal and on its 180° and 90° type domain boundaries. *Progress of Theoretical Physics*, 13(5):529–539.

King, K. C. and Mura, T. (1991a). The eigenstrain method for small defects in a lattice. *Journal of the Physics and Chemistry of Solids*, 52(8):1019–1030.

King, K. C. and Mura, T. (1991b). The eigenstrain method for small defects in a lattice. *Journal of Physics and Chemistry of Solids*, 52(8):1019–1030.

King-Smith, R. D. and Vanderbilt, D. (1989). Theory of polarization of crystalline solids. *Physical Review B*, 47:1651–1654.

Knopp, K. (1956). *Infinite Series and Sequences*. Dover.

Krishnan, A., Treacy, M. M., and Bisher, M. E. (2000). Maxwellian charge on domain walls. *Fundamental Physics of Ferroelectrics*, pages 191–200.

Lakshmikantham, V. and Trigiante, D. (1988). *Theory of Difference Equations: Numerical Methods and Applications*. Academic Press.

Lawless, W. N. (1968). 180° domain-wall energies in $BaTiO_3$. *Physical Review*, 175:619–624.

Lee, A. M., Taylor, S. W., Dombroski, J. P., and Gill, P. M. W. (1997). Optimal partition of the Coulomb operator. *Physical Review A*, 55(4):3233–3235.

Li, Z., Foster, C. M., Dai, X. H., Xu, X. Z., Chan, S. K., and Lam, D. J. (1992). Piezoelectrically-induced switching of 90° domains in tetragonal $BaTiO_3$ and $PbTiO_3$ investigated by micro-raman spectroscopy. *Journal of Applied Physics*, 71(9):4481–4486.

Little, E. A. (1955). Dynamic behavior of domain walls in Barium Titanate. *Physical Review*, 98(4):978–984.

Lynch, R. E., Rice, J. R., and Thomas, D. H. (1964). Direct solution of partial difference equations by tensor product methods. *Numerische Mathematik*, 6:185–199.

Maradudin, A. A. (1958). *Journal of the Physics and Chemistry of Solids*, 9:1–.

Maradudin, A. A., Montroll, E. W., and Weiss, G. H. (1971). *Theory of Lattice Dynamics in The Harmonic Approximation*. Academic Press.

Marsden, J. E. and Hughes, J. R. (1983). *Mathematical Foundations of Elasticity*. Dover.

Matsubara, T. J. (1952). Theory of diffuse scattering of x-rays by local lattice distortions. *Journal of Physical Society of Japan*, 7:270–274.

Merz, W. J. (1952). Domain properties of $BaTiO_3$. *Physical Review*, 88:421–422.

Merz, W. J. (1954). Domain formation and domain wall motions in ferroelectric $BaTiO_3$ single crystals. *Physical Review*, 95(3):690–698.

Meyer, B. and Vanderbilt, D. (2001). Ab initio study of ferroelectric domain walls in $PbTiO_3$. *Physical Review B*, 65:1–11.

Mickens, R. E. (1990). *Difference Equations Theory and Applications*. Chapman & Hall.

Mura, T. (1977). Eigenstrains in lattice theory. In *Continuum Models of Discrete Systems*, pages 503–519.

Mura, T. (1982). *Micromechanics of Defects in Solids*. Martinus Nijhoff.

Ortiz, M. and Phillips, R. (1999). Nanomechanics of defects in solids. *Advances in Applied Mechanics*, 59(1):1217–1233.

Padilla, J., Zhong, W., and Vanderbilt, D. (1996). First-principles investigation of 180° domain walls in $BaTiO_3$. *Physical Review B*, 53(10):R5969–R5973.

Pöykkö, S. and Chadi, D. J. (1999). Ab initio study of 180° domain wall energy and structure in $PbTiO_3$. *Applied Physics Letters*, 75(18):2830–2832.

Pöykkö, S. and Chadi, D. J. (2000). Ab initio study of dipolar defects and 180° domain walls in $PbTiO_3$. *Journal of Physics and Chemistry of Solids*, 61:291–294.

Resta, R. (1994). Macroscopic polarization in crystalline dielectrics: the geometric phase approach. *Reviews of Modern Physics*, 66(3):899–915.

Resta, R. (2003). Ab initio simulation of the properties of ferroelectric materials. *Modelling and Simulation in Materials Science and Engineering*, 11:R69–R96.

Rycerz, Z. A. and Jacobs, P. W. M. (1992). Ewald summation in the molecular dynamics simulation of large ionic systems: The cohesive energy. *Molecular Simulation*, 8:197–213.

Sepliarsky, M. and Cohen, R. E. (2002). Development of a shell model potential for molecular dynamics for $PbTiO_3$ by fitting first principles results. In Cohen, R. E., editor, *Fundamental Physics of Ferroelectrics*, pages 36–44.

Sepliarsky, M., Wu, Z., Asthagiri, and Cohen, R. E. (2004). Atomistic model potential for $PbTiO_3$ and PMN by fitting first principles results. *Ferroelectrics*, 301:55–59.

Shenoy, V. B., Ortiz, M., and Phillips, R. (1999). The atomistic structure and energy of nascent dislocation loops. *Modelling and Simulation in Materials Science and Engineering*, 7:603–619.

Shilo, D., Ravichandran, G., and Bhattacharya, K. (2004). Investigation of twin wall structure at the nanometer scale using atomic force microscopy. *Nature Materials*, 3:453–457.

Shu, Y. C. and Bhattacharya, K. (2001). Domain patterns and macroscopic behavior of ferroelectric materials. *Phylosophical Magazine B*, 81(12):2021–2054.

Smith, E. R. (1981). Electrostatic energy in ionic crystals. *Procedeengs of the Royal Society of London A*, 375:475–505.

Stemmer, S., Streiffer, S. K., and Rühle, M. (1995). Atomic structure of 90° domain walls in ferroelectric $PbTiO_3$ thin films. *Philosophical Magazine A*, 71(3):713–724.

Tewary, V. K. (1973). Green-function method for lattice statics. *Advances in Physics*, 22:757–810.

Tewary, V. K. (2000). Lattice-statics model for edge dislocations in crystals. *Philosophical Magazine A*, 80(6):1445–1452.

Tosi, M. P. (1964). Cohesion of ionic solids in the Born model. *Solid State Physics*, 16:1–120.

Toukmaji, A. Y. and Board Jr., J. A. (1996). Ewald summation techniques in perspective: a survay. *Computer Physics Communications*, 95:73–92.

Valasek, J. (1921). Piezo-electric and allied phenomena in rochelle salt. *Physical Review*, 17:475–481.

Veit, J. (2003). Fundamental solutions of partial difference equations. *ZAMM*, 83(1):51–59.

Vitásek, E. (1959). The n-dimensional fourier transform in the theory of difference equations. *Archiwum Mechaniki Stosowanej*, 12(2):185–202,488–504.

Wales, D. J. (2003). *Energy Landscapes*. Cambridge University Press.

Wallis, R. F. (1975). Effects of Surfaces in Lattice Dynamics. In Horton, G. K. and Maradudin, A. A., editors, *Dynamical Properties of Solids*, volume 2, pages 441–507.

Wolf, D. (1992). Reconstruction of NaCl surfaces from a dipolar solution to the Madelung Problem. *Physical Review Letters*, 68(22):3315–3318.

Wolf, D. (1995). Simulation of ionic surfaces from an absolutely convergent solution of the Madelung problem. *Springer Proceedings in Physics*, 80:57–68.

Wolf, D., Keblinski, P., Phillpot, S. R., and Eggebrecht, J. (1999). Exact method for the simulation of coulombic systems by spherically truncated, pairwise r^{-1} summation. *Journal of Chemical Physics*, 110:8254–8282.

Yang, W. and Chen, L.-Q. (1995). Computer simulation of the dynamics of 180° ferroelectric domains. *Journal of American Ceramics Society*, 78(9):4.

Young, K. (1987). Physical condition for elimination of ambiguity in conditionally convergent lattice sums. *Journal of Mathematical Physics*, 28(2):425–427.

Zhirnov, V. A. (1959). A contribution to the theory of domain walls in ferroelectrics. *Soviet Physics JETP*, 35(8):825–832.